

KAUNAS UNIVERSITY OF TECHNOLOGY

KAROLIS LEITONAS

**DEVELOPMENT OF EFFICIENT
ELECTROLUMINESCENT DEVICES
EXPLOITING CROSSING FROM TRIPLET TO
SINGLET STATE IN ORGANIC EMITTERS**

Doctoral dissertation
Technological Sciences, Materials Engineering (T 008)

2025, Kaunas

The dissertation has been prepared at the Faculty of Chemical Technology of the Department of Polymer Chemistry and Technology of Kaunas University of Technology, in 2020–2024. The research has been sponsored by the Research Council of Lithuania.

Research supervisor:

Chief Researcher Dr. Hab. Dmytro VOLYNIUK (Kaunas University of Technology, Technological Sciences, Materials Engineering, T 008).

Research consultant:

Senior Researcher Dr. Asta DABULIENĖ (Kaunas University of Technology, Technological Sciences, Chemical Engineering, T 005).

Edited by: English language editor Dr. Armandas Rumšas (Publishing House *Technologija*), Lithuanian language editor Aurelija Gražina Rukšaitė (Publishing House *Technologija*).

Dissertation Defence Board of Materials Engineering Science Field:

Prof. Dr. Hab. Sigitas TAMULEVIČIUS (Kaunas University of Technology, Technological Sciences, Materials Engineering, T 008) – **chairperson**;

Prof. Dr. Hab. Arvidas GALDIKAS (Kaunas University of Technology, Technological Sciences, Materials Engineering, T 008);

Prof. Dr. Saulius GRIGALEVIČIUS (Kaunas University of Technology, Technological Sciences, Materials Engineering, T 008);

Prof. Dr. Törmä PÄIVI (Aalto University, Finland, Natural Sciences, Physics, N 002);

Chief Researcher Dr. Gediminas RAČIUKAITIS (State Research Institute Center for Physical Sciences and Technology, Natural Sciences, Physics, N 002).

The dissertation defence will be held on 7 February 2025, at 11 a.m. in a public meeting of the Dissertation Defence Board of the Materials Engineering Science Field at the Rectorate Hall of Kaunas University of Technology.

Address: K. Donelaičio 73-402, LT-44249 Kaunas, Lithuania.

Phone (+370) 608 28 527; email doktorantura@ktu.lt

The dissertation was sent out on 7 January 2025.

The dissertation is available on <http://ktu.edu> and at the Library of Kaunas University of Technology (Gedimino 50, LT-44239 Kaunas, Lithuania).

KAUNO TECHNOLOGIJOS UNIVERSITETAS

KAROLIS LEITONAS

EFEKTYVIŲ ELEKTROLIUMINESCENCINIŲ
PRIETAISŲ KŪRIMAS PANAUDOJANT
ORGANINIŲ SPINDUOLIŲ EKSITONŲ
VIRSMUS IŠ TRIPLETINĖS Į SINGLETINĘ
BŪSENĄ

Daktaro disertacija
Technologijos mokslai, medžiagų inžinerija (T 008)

2025, Kaunas

Disertacija rengta 2020–2024 metais Kauno technologijos universiteto Cheminės technologijos fakultete Polimerų chemijos ir technologijos katedroje. Mokslinius tyrimus rėmė Lietuvos mokslo taryba.

Mokslinis vadovas:

Vyriausiasis mokslo darbuotojas habil. dr. Dmytro VOLYNIUK (Kauno technologijos universitetas, technologijos mokslai, medžiagų inžinerija, T 008).

Mokslinis konsultantas:

Vyresnioji mokslo darbuotoja dr. Asta DABULIENĖ (Kauno technologijos universitetas, technologijos mokslai, chemijos inžinerija, T 005).

Redagavo: lietuvių kalbos redaktorė Aurelija Gražina Rukšaitė (leidykla „Technologija“) ir anglų kalbos redaktorius dr. Armandas Rumšas (leidykla „Technologija“).

Prof. habil. dr. Sigitas TAMULEVIČIUS (Kauno technologijos universitetas, technologijos mokslai, medžiagų inžinerija, T 008) – **pirmininkas**;

Prof. habil. dr. Arvidas GALDIKAS (Kauno technologijos universitetas, technologijos mokslai, medžiagų inžinerija, T 008);

Prof. dr. Saulius GRIGALEVIČIUS (Kauno technologijos universitetas, technologijos mokslai, medžiagų inžinerija, T 008);

Prof. dr. Törmä PÄIVI (Alto universitetas, Suomija, gamtos mokslai, fizika, N 002);

Vyr. m. d. dr. Gediminas RAČIUKAITIS (Valstybinis mokslinių tyrimų institutas Fizinių ir technologijos mokslų centras, gamtos mokslai, fizika, N 002).

Disertacija bus ginama viešame Medžiagų inžinerijos mokslo krypties disertacijos gynimo tarybos posėdyje 2025 m. vasario 7 d. 11 val. Kauno technologijos universiteto Rektorato salėje.

Adresas: K. Donelaičio g. 73-402, LT-44249 Kaunas, Lietuva.

Tel: (+370) 608 28 527; el. paštas doktorantura@ktu.lt

Disertacija išsiųsta 2025 m. sausio 7 d.

Su disertacija galima susipažinti interneto svetainėje <http://ktu.edu> ir Kauno technologijos universiteto bibliotekoje (Gedimino g. 50, LT-44239 Kaunas, Lietuva).

CONTENTS

LIST OF FIGURES	8
LIST OF ABBREVIATIONS AND DEFINITIONS	11
1. INTRODUCTION.....	13
2. BRIEF REVIEW OF SCIENTIFIC LITERATURE.....	17
3. REVIEW OF THE PUBLISHED ARTICLES	20
3.1. White Vertical Organic Permeable-Base Light-Emitting Transistors Obtained by Mixing of Blue Exciton and Orange Interface Exciplex Emissions (scientific publication No. 1, Q1, 5 quotations)	20
3.2. TADF versus TTA Emission Mechanisms in Acridan and Carbazole- Substituted Dibenzo[a,c]phenazines: towards Triplet Harvesting Emitters and Hosts Emissions (scientific publication No. 2, Q1, 25 quotations).....	25
3.3. Dual versus Normal TADF of Pyridines Ornamented with Multiple Donor Moieties and their Performance in OLEDs (scientific publication No. 3, Q1, 10 quotations).....	32
3.4. 3,5-Dicyanopyridine Motifs for Electron-Transporting Semiconductors: from Design and Synthesis to Efficient Organic Light-Emitting Diodes (scientific publication No. 4, Q1, 5 quotations).....	41
4. CONCLUSIONS.....	50
5. SANTRAUKA	53
5.1. Įvadas	53
5.2. Paskelbtų publikacijų apžvalga.....	55
5.2.1. Baltieji vertikalūs organiniai pralaidžiosios bazės šviesą skleidžiantys tranzistoriai, gauti maišant mėlynojo eksitono ir oranžinio eksiplekso emisijas .	55
5.2.2. TADF ir TTA emisijos mechanizmai akridano ir karbazolo pakaitų dibenzo[a,c]fenazino pagrindo molekulėse: tripletus išnaudojantys spinduoliai ir matricos	58
5.2.3. Dvigubo ir įprastinio TADF mechanizmų priklausomybė nuo donoro pakaitų pirimidino junginiuose.....	62
5.2.4. 3,5-Dicianopiridino pagrindo elektronus transportuojantys puslaidininkiams: nuo dizaino ir sintezės iki efektyvių organinių šviesos diodų	66
5.3. Išvados	71
6. LITERATURE	74

7.	COPIES OF AUTHOR'S PUBLICATIONS	83
8.	CURRICULUM VITAE	129
9.	LIST OF AUTHOR'S PUBLICATIONS AND CONFERENCES	132
10.	ACKNOWLEDGEMENTS	139

LIST OF TABLES

Table 1. EL parameters of orange, blue and white OPB-LETs.....	23
Table 2. IP, EA and charge mobility values for AcDbp and CzDbp	27
Table 3. Photophysical properties of AcDbp and CzDbp	28
Table 4. EL parameters of devices A–J	31
Table 5. Photophysical data for 5a and 5b^a	34
Table 6. Electroluminescence parameters of the OLEDs	39
Table 7. Electrochemical and photoelectrical parameters of compounds.....	42
Table 8. EL characteristics of OLEDs A–C	48
9 lentelė. Tirtų OPB-LET prietaisų elektroliuminescencijos parametrai	57
10 lentelė. Prietaisų A–J EL charakteristikos.....	61
11 lentelė. OLED prietaisų EL parametrai.....	64
12 lentelė. Elektrocheminiai ir fotoelektriniai junginių PPDD , FPDD ir CzPDD parametrai	67
13 lentelė. OLED prietaisų A–C EL charakteristikos	70

LIST OF FIGURES

Fig. 1. Overview of mechanisms for harvesting triplet excitons to achieve electroluminescence in OLED devices. a) conventional fluorescence; b) thermally activated delayed fluorescence (TADF); c) triplet-triplet annihilation (TTA); d) hybridised local and charge transfer (HLCT).....	18
Fig. 2. a) Chemical structures of the utilised compounds; b) Device configuration illustration for white (blue) OPB-LETs; c) and d) Energy level diagrams at equilibrium for blue (orange) and white OPB-LETs. HOMO/LUMO values in eV. Insets: Photographs of blue and white OPB-LETs under zero and applied bias	21
Fig. 3. a) EL spectrum at 12 V; b) Transfer; c) Output characteristics (current density-voltage); d) Current density-voltage and brightness-voltage at $V_{EB} = 4$ V; e) Current density and brightness under ‘on’ and ‘off’ states; f) Current, power, and EQE vs. collector current density J_{EC} for the orange exciplex-based OPB-LET.....	22
Fig. 4. a) EL spectrum at 12 V; b) Transfer; c) Output characteristics (current density-voltage); d) Current density-voltage and brightness-voltage at $V_{EB} = 4$ V; e) Current density and brightness under ‘on’ and ‘off’ states; f) Current, power, and EQE vs. collector current density J_{EC} for the blue exciplex OPB-LET.....	23
Fig. 5. a) EL spectra; and b) the corresponding CIE colour coordinates obtained at various voltages. c) Transfer characteristics for the white exciplex-based OPB-LET. d) Normalized PL spectra of the CzPm , CzPm:PO-T2T , and CzPm:TAPC films. e) Current density and brightness as a function of voltage at $V_{EB} = 5$ V. f) Efficiency metrics (current, power, EQE) versus collector current density. The CIE colour diagram b) is supplemented with the colour coordinates of CzPm exciton and CzPm:TAPC exciplex emissions	24
Fig. 6. Time-resolved EL response of the CzPm:TAPC -based device.....	25
Fig. 7. Chemical structures of investigated compounds AcDbp and CzDbp	26
Fig. 8. UV-Vis absorption profiles of a) AcDbp and b) CzDbp in toluene and THF solutions.....	27
Fig. 9. Room-temperature a) fluorescence and b) PL spectra as well as c), d) PH spectra recorded at 77 K of THF solutions of AcDbp and CzDbp (PH spectrum of the solution of Dbp in THF recorded at 77 K is presented as the yellow line).....	28
Fig. 10. a), c) PL spectra and b), d) the corresponding PL decay curves for air-equilibrated and deoxygenated toluene solutions of a), b) AcDbp and c), d) CzDbp	29
Fig. 11. a), c) PL spectra and b), d) corresponding PL decay curves acquired at various temperatures for neat layers of a), b) AcDbp and c), d) CzDbp	30
Fig. 12. a) EL spectra; b) and c) EQE as a function of brightness, for devices D–J employing AcDbp and CzDbp as either host or emitter materials	32
Fig. 13. Chemical structures of investigated compounds 5a and 5b	33
Fig. 14. a) CV and PE spectra of compounds 5a and 5b . b) UV-Vis and PL spectra (ex. 350 nm) of 5a , 5b , and I in toluene solution, as well as neat and doped films (mCP host). c) and d) Solvent effects on the UV-Vis and PL spectra of 5a and 5b ,	

respectively, in dilute solutions (ca. 10^{-4} mg/mL). e) Time-resolved PL spectra of 5b in toluene solution at different time delays after excitation. f) PL decay curves of 5b in toluene solution recorded at various emission wavelengths.....	35
Fig. 15. a) PL decay curves and b) corresponding PL spectra recorded at various temperatures for films of compounds 5a and 5b doped in mCP	37
Fig. 16. a) EL spectra at 8 V; b) Current density and brightness as a function of voltage; c) EQE versus current density; and d) Operational lifetimes of non-passivated devices under ambient air conditions at a constant voltage of 5 V.....	38
Fig. 17. a) and c) EL spectra recorded at various voltages; b) Current density and luminescence as a function of applied voltage; and d) EQE plotted against luminescence, all for the optimised devices o-5a and o-5b	40
Fig. 18. Chemical structures of compounds PPDD , FPDD and CzPDD	42
Fig. 19. a) Normalized UV-Vis and PL spectra comparing solid-state, toluene, and THF solutions (1×10^{-5} M) of PPDD , FPDD , and CzPDD . b) PL decay kinetics in toluene solutions. Inset: Sample images under UV illumination. c) Low-temperature (77 K) PL and PH spectra in THF (ex. 300 nm for PPDD , FPDD ; 340 nm for CzPDD)	43
Fig. 20. Normalised PL spectra of the solutions (1×10^{-5} M) of a) PPDD , b) FPDD , and c) CzPDD in the solvents of the different polarity and the corresponding Lippert–Mataga plots d), e) and f) of dependencies of the Stokes shifts $\Delta(v)$ on solvent orientation polarizability function $\Delta(f)$	45
Fig. 21. a) PL spectra and b) corresponding PL decay curves recorded in vacuum for solid solutions of DAcIPN (10 wt.%) in various hosts (PPDD , FPDD , CzPDD , and mCBP). c) PL spectra and d) PL decay curves of the DAcIPN (10 wt.%) solid solution in FPDD host, measured at different temperatures	46
Fig. 22. a) Energy level diagram of devices A–C and b) molecular structures of the compounds used for the preparation of light-emitting layers of the devices.....	47
Fig. 23. a) Normalised EL spectra and b) corresponding decay curves for devices A–C . c) Current density and luminescence as a function of applied voltage, and d) EQE plotted against luminescence for devices A–C	49
24 pav. Naudojamų junginių molekulinės struktūros a), balto OPB-LET prietaiso principinė struktūros schema b).....	56
25 pav. a) Baltos spalvos eksiplekso pagrindu veikiančio OPB-LET EL spektras ir b) CIE spalvinės koordinatės esant skirtingoms įtampoms; c) perdavimo srovės tankio ir įtampos charakteristikos; d) normalizuotas CzPm:PO-T2T, CzPm ir CzPm:TAPC plėvelių PL spektras; e) srovės tankio ir įtampos santykio bei ryškumo ir įtampos santykio grafikai, kai bazinė įtampa V_{EB} yra 5 V; f) srovės, galios ir išorinis kvantinis efektyvumas, palyginti su srovės tankiu kolektoriuje J_{EC} . CzPm eksitonų emisijos ir eksiplekso CzPm :TAPC emisijos spalvų koordinatės pridamos prie CIE spalvų diagramos b)	57
26 pav. Junginių AcDbp ir CzDbp cheminės struktūros.....	58
27 pav. AcDbp ir CzDbp UV-Vis sugertis a), d), tirpalų ir plėvelių fluorescencijos spektrai kambario temperatūroje b), c), THF tirpalų fosforescencijos spektrai 77 K temperatūroje e), f)	59

28 pav. PL spektrai a), c) ir PL gesimo kreivės b), d) nelegiruotų AcDBp ir CzDBp sluoksnių, kurie buvo išmatuoti skirtingose temperatūrose nuo 77 iki 300 K.....	60
29 pav. Prietaisų D-J EL spektrai a); EQE priklausomybė nuo ryškumo, kai AcDBp ir CzDBp naudojami kaip matricos b) ir kai naudojami kaip spinduoliai c)	61
30 pav. Cheminės junginių 5a ir 5b struktūros	62
31 pav. 5a ir 5b CV ir fotoelektronų emisijos spektrai a); 5a , 5b junginių tolueno tirpalų ir grynų bei legiruotų plėvelių absorbcijos ir emisijos spektrai (sužadinant bangos ilgiu 350 nm b); tirpiklio poliškumo poveikis 5a c) ir 5b d) junginių optinei sugerčiai ir PL spektrui tirpaluose, kurių koncentracija yra apie 10–4 mg/ml; 5b tolueno tirpalo spektrai laike skirtinguose laiko intervaluose po sužadinimo, užregistruoti su skirtingais laiko uždelsimais e); 5b tolueno tirpalo PL gesimo kreivė, užregistruota esant skirtingiems emisijos bangos ilgiams f)	63
32 pav. EL spektrai esant skirtingoms įtampoms a) ir b); srovės tankio ir ryškumo priklausomybė nuo įtampos c); efektyvumo priklausomybė nuo srovės tankio d) optimizuotuose OLED.....	65
33 pav. Cheminės junginių PPDD , FPDD ir CzPDD struktūros	66
34 pav. Normalizuoti UV-VIS ir PL a) spektrai plėvelių, tolueno ir THF tirpalų PPDD , FPDD ir CzPDD su 1×10^{-5} M koncentracija; tolueno tirpalų PL gesimo kreivės b); intarpas rodo mėginius UV šviesoje. THF tirpalų PPDD , FPDD ir CzPDD esant 77 K PL ir PH PH spektrai c); PPDD ir FPDD sužadinimo bangos ilgis (λ_{ex}) buvo 300 nm, o CzPDD – 340 nm	68
35 pav. Normalizuoti praskiestų PPDD , FPDD ir CzPDD skirtingų poliškumų tirpalų spektrai a), b), c) ir atitinkami Lippert-Mataga grafikai d), e), f), kuriuose pavaizduota Stokso poslinkio $\Delta(\nu)$ priklausomybė nuo tirpiklio orientacijos poliarizuotumo funkcijos $\Delta(f)$	69
36 pav. OLED prietaisų sluoksnių ir energetinių lygmenų diagrama a) bei emisiniame sluoksnyje naudotų medžiagų cheminės struktūros b)	70

LIST OF ABBREVIATIONS AND DEFINITIONS

Abbreviations:

(piq) ₂ Ir(acac).....	Bis(1-phenylisoquinoline)(acetylacetonate)iridium(III).
5a	2,6-Bis-(3,6-di-tert-butyl-carbazol-9-yl)-4-[4-(3,6-di-tert-butyl-carbazol-9-yl)-phenyl]-pyridine-3,5-dicarbonitrile.
5b	2,6-Bis(3,6-di-tert-butyl-9H-carbazol-9-yl)-4-(4-(3,7-dibromo-10H-phenothiazin-10-yl)phenyl)pyridine-3,5-dicarbonitrile.
AcDbp	2,7-bis(9,9-dimethylacridin-10(9H)-yl)dibenzo[a,c]phenazine.
Al	aluminium.
C70	(C ₇₀ -D _{5h(6)})[5,6]fullerene.
Compound I	2,6-bis-(3,6-di-tert-butylcarbazol-9-yl)-4-(4-fluorophenyl)-pyridine-3,5-carbonitrile.
CT	charge-transfer.
CV	cyclic voltammetry.
CzDbp.....	2,7-bis(3,6-di-tert-butyl-9H-carbazol-9-yl)dibenzo[a,c]phenazine.
CzPDD.....	4,40-(5-((4-9H-Carbazol-9-yl)phenyl)ethynyl)-1,3-phenylene)bis(2,6-dimethylpyridine-3,5-dicarbonitrile).
CzPm	4,6-bis(4-(9H-carbazol-9yl)phenyl)pyrimidine-5-carbonitrile.
D-A	donor-acceptor.
DAcIPN	4,6-di(9,9-dimethylacridan-10-yl)isophthalonitrile.
EA.....	electron affinity.
EL	electroluminescence.
EQE	external quantum efficiency.
FET	Förster energy transfer.
FPDD.....	4,4'-(5-((4-fluorophenyl)ethynyl)-1,3-phenylene)bis(2,6-dimethylpyridine-3,5-dicarbonitrile).
FWHM.....	full width at half-maxima.
HAT-CN	1,4,5,8,9,11-Hexaazatriphenylenehexacarbonitrile.
HLCT.....	hybridised local and charge transfer.
HOMO.....	highest occupied molecular orbital.
IC	internal conversion.
IP	ionisation potential.
IQE	internal quantum efficiency.
ITO	indium tin oxide.
J _{EB}	emitter-base current density.
J _{EC}	emitter-collector current density.
LE	locally-excited.
LiF	lithium fluoride.
Liq	8-Hydroxyquinolinolato-lithium.
LUMO	lowest unoccupied molecular orbital.
mCBP	3,3'-Di(9H-carbazol-9-yl)-1,1'-biphenyl.
mCP	1,3-Bis(N-carbazolyl)benzene.

MoO₃ molybdenum trioxide.
 nBPhen 2,9-Dinaphthalen-2-yl-4,7-diphenyl-1,10-phenanthroline.
 NPB N,N'-Di(1-naphthyl)-N,N'-diphenyl-(1,1'-biphenyl)-4,4'-diamine.
 OLED organic light emitting diode.
 OLET organic light emitting transistor.
 OPB-LET organic permeable-base light-emitting transistor.
 PH phosphorescence.
 PHOLED phosphorescent-based organic light emitting diode.
 PL photoluminescence.
 PLQY photoluminescence quantum yield.
 PO-T2T 2,4,6-tris[3-(diphenylphosphinyl)phenyl]-1,3,5-triazine.
 PPDD 4,40-(5-Phenylethynyl)-1,3-phenylene)bis(2,6-dimethylpyridine3,5-dicarbonitrile).
 RISC reverse intersystem crossing.
 TADF thermally activated delayed fluorescence.
 TAPC 1,1-Bis[(di-4-tolylamino)phenyl]cyclohexane.
 THF tetrahydrofuran.
 ToF time-of-flight.
 TPBi 2,2',2''-(1,3,5-Benzinetriyl)-tris(1-phenyl-1-H-benzimidazole).
 TSPO1 diphenyl[4-(triphenylsilyl)phenyl]phosphine oxide.
 TTA triplet-triplet annihilation.
 V_{driving} voltage at 10 mA/cm².
 V_{EB} emitter-base voltage.
 V_{EC} emitter-collector voltage.
 V_{ON} turn-on voltage.
 ΔE_{ST} singlet-triplet energy gap.

1. INTRODUCTION

I vividly remember starting our organic chemistry course at high school. It was a significant shift from the simple balancing of chemical equations to analysing complex, carbon-based chains, and hexagon-shaped rings, not to mention the drawing of 'balloon-shaped' orbitals. Back then, none of us, myself included, could have imagined actually using this knowledge in the future. Yet, here I am, more than a decade later, writing a thesis on organic semiconductors...

Little did I know that those initial lessons in organic chemistry were the foundation for understanding a field that is now at the cutting edge of modern technology. The exploration of organic semiconductors is driven by their potential and the challenges they present. These materials, primarily composed of carbon-based small molecules or polymers, offer distinct advantages over the traditional inorganic semiconductors. They are inherently flexible, potentially cheaper to produce, and can be processed in solutions.¹ This makes them ideal for innovative applications such as flexible displays, wearable electronics, and even biodegradable sensors, marking them as pivotal in the evolution of electronic devices towards more sustainable and versatile technologies.^{2,3,4}

While organic semiconductors offer promising advantages, they also face significant challenges that hinder their widespread adoption.^{5,6} One of the primary issues is their relatively short operational lifetime, which is often attributed to factors such as device degradation, exciton quenching, and charge carrier imbalance.^{7,8} Additionally, an efficient triplet-to-singlet energy transfer, a crucial process for achieving high performance organic light-emitting diodes (OLEDs), remains a complex and ongoing research area. In OLEDs, the majority of excited states generated are triplets, which are usually non-radiative. To overcome this limitation, efficient triplet-to-singlet energy transfer mechanisms are essential to convert these non-radiative triplets into radiative singlets, thereby enhancing the overall efficiency of devices.⁹ The development of new materials and device architectures that promote the triplet-to-singlet energy transfer is a key focus of research in the field of organic semiconductors.

In response to these challenges, **this work aims** to advance the development of efficient electroluminescent devices by exploring and optimizing triplet-to-singlet energy crossing mechanisms in organic emitters, with a focus on innovative materials and processes that enhance the device performance.

The following **objectives** were outlined in order to achieve the aim of the dissertation:

- Explore the application of exciplex emitters that display TADF in white organic permeable-base light-emitting transistors (OPB-LETs).
- Characterise novel dibenzo[a,c]phenazine-based TADF and TTA exhibiting materials and evaluate their performance in yellow-orange-red OLED applications.

- Assess the impact of different donor types on the efficiency of dicyanopyridine-based TADF compounds in OLEDs, particularly focussing on device lifetime and optimisation.
- Investigate the effectiveness of novel host materials in enhancing the performance of TADF OLEDs compared to that of a commercial host.

The scientific novelty of the work

In the first study, significant breakthroughs were achieved in the development of white organic light-emitting transistors (OPB-LETs) by introducing a novel vertical device structure. The initial efforts using known exciplex emitters faced challenges due to inefficient electron injection, which prevented the achievement of white electroluminescence (EL). This issue was addressed by using a new emitter, 4,6-bis(4-(9H-carbazol-9yl)phenyl)pyrimidine-5-carbonitrile (**CzPm**), which uniquely features orange exciplex forming capabilities. This innovative approach allowed us to successfully combine blue exciton and orange exciplex emissions, producing white light with an enhanced brightness and efficiency. The resulting OPB-LETs not only demonstrated the capacity for white EL but also showed improvements in external quantum efficiency and a remarkable colour rendering index of 93.

The second study marks significant advancements in the OLED technology through the exploration of carbazole or acridan-substituted dibenzo[a,c]phenazines (**CzDbp** and **AcDbp**) employing a donor-acceptor-donor architecture aimed at inducing TADF. Both compounds were characterised by media-dependent combinations of TADF and TTA. While **AcDbp** demonstrated microsecond-lived fluorescence, whereas **CzDbp** showcased a distinct nanosecond-lived fluorescence. The OLED using **CzDbp** as the host for the red phosphorescent emitter (piq)₂Ir(acac) demonstrated enhanced EL parameters, achieving a higher external quantum efficiency (EQE) of 15.9% and a reduced efficiency roll-off compared to devices using the commonly employed hosts mCP, mCBP, NPB, and nBPhen. When utilised as TADF/TTA emitters, the compounds **CzDbp** and **AcDbp** enabled the yellow and orange host-guest system-based devices to reach EQE of 19.4% and 22.1%, respectively. This approach not only refines our understanding of TADF/TTA triplet harvesting mechanisms but also pushes the boundaries of the OLED performance, thereby promising more efficient and durable OLED applications.

The third study introduces an innovative approach to the design of OLEDs using two newly developed multiple donor-substituted dicyanopyridines. These compounds, of which one consists of three donors of the same type (3,6-di-tert-butyl-carbazole) (**5a**) and the other involves a combination of two types (3,6-di-tert-butyl-carbazole and 3,7-dibromophenothiazine) (**5b**), exhibit efficient green and orange TADF emission. When tested in OLEDs, compound **5b** displayed low device lifetimes and limited maximum external efficiencies of 3.1% for devices without a host and 5% for emitter-in-matrix devices. In contrast, OLEDs based on the **5a** showed significantly better performance. These devices achieved high device lifetimes and impressive maximum EQE of 8.1% for devices without an additional host and

impressive 25% for host-guest system-based and optimised devices. This effort represents a significant step forward in the functional design of TADF OLEDs, while utilising perspective dicyanopyridine-based emitters.

The fourth study introduces the use of 3,5-dicyanopyridine motifs in the design of electroactive materials for optoelectronic devices, highlighting three electron-transporting semiconductors with promising properties. These materials exhibit high triplet energies ranging from 2.68 to 2.79 eV and ionisation potentials around 6 eV. Notably, two of these compounds produce deep blue emissions through relaxation of HLCT states, while the third, incorporating an additional carbazole donor unit, shows pure charge-transfer (CT) emission. These compounds demonstrate varied hosting capabilities, significantly influencing the efficiency of the TADF emitter 4,6-di(9,9-dimethylacridan-10-yl)isophthalonitrile (DAcIPN). The standout performer was an OLED which used 4,4'-(5-((4-fluorophenyl)ethynyl)-1,3-phenylene)bis(2,6-dimethylpyridine-3,5-dicarbonitrile) (**FPDD**) as a host. The device with **FPDD** achieved a maximum EQE of 21.9%, thus significantly outperforming the 12.2% efficiency of the device based on the conventional host mCBP. This exceptional efficiency underscores the potential of these materials to advance the OLED technology, while offering significant improvements in the device performance and durability.

Contribution of the author

The author of the dissertation conducted a series of experiments and analyses to advance the research presented. This included all steady-state and time-resolved photophysical, photoelectrical, electroluminescent, and stability measurements. Additionally, the author analysed the resulting data and personally fabricated all electroluminescent devices using vacuum deposition techniques. Dr. Viktorija Andrulevičienė (Department of Polymer Chemistry and Technology, Kaunas University of Technology (KTU)) synthesised carbazole or acridan-substituted dibenzo[a,c]phenazines derivatives and provided theoretical calculations. Mr. Matas Gužauskas (Department of Polymer Chemistry and Technology, KTU) provided expertise and assistance in the work on exciplexes. Dr. Uliana Tsiko (Department of Polymer Chemistry and Technology, KTU) synthesised 4,6-Bis(4-(9H-carbazol-9-yl)phenyl)pyrimidine-5carbonitrile (CzPm). Dr. Audrius Bučinskas and Dr. Levani Skhirtladze (Department of Polymer Chemistry and Technology, KTU) aided with the purification of compounds. Prof. Dr. Gjergji Sini (Laboratory of Physicochemistry of Polymers and Interfaces, CY Cergy Paris University) contributed to the computational simulations. Dr. Jūratė Simokaitienė (Department of Polymer Chemistry and Technology, KTU) measured the thermal properties of the compounds. Dr. Pavel Arsenyan, Dr. Brigita Vigante, Dr. Sergey Belyakov and Dr. Pavels Dimitrijevs (Latvian Institute of Organic Synthesis) synthesised 3,5-Dicyanopyridine derivatives. Prof. Dr. Tien-Lung Chiu (Department of Electrical Engineering, Yuan Ze University, Taiwan) assisted with the device optimisation process. Dr. Hab. Dmytro Volyniuk (Department of Polymer Chemistry and Technology, KTU) as the supervisor significantly contributed to the success of the research by conducting charge

transporting properties measurements, as well as analysis, and preparation of the manuscripts. Prof. Dr. Juozas Vidas Gražulevičius (Department of Polymer Chemistry and Technology, KTU), as the research group leader, ensured that the research would be meaningful and provided opportunities to gain experience in the best laboratories of foreign partners.

List of scientific publications on the topic of the dissertation

1. **Leitonas, Karolis**; Gužauskas, Matas; Tsiko, Uliana; Simokaitienė, Jūratė; Volyniuk, Dmytro; Gražulevičius, Juozas Vidas. White vertical organic permeable-base light-emitting transistors obtained by mixing of blue exciton and orange interface exciplex emissions // *Journal of Materials Chemistry C*. Cambridge: Royal Society of Chemistry. ISSN 2050-7534. eISSN 2050-7526. 2022, Vol. 10, iss. 26, p. 9786–9793. (Web of Science); DOI: 10.1039/d2tc01326f. [IF: 6.400; Q1]
2. Andrulevičienė, Viktorija; **Leitonas, Karolis**; Volyniuk, Dmytro; Sini, Gjergji; Gražulevičius, Juozas Vidas; Getautis, Vytautas. TADF versus TTA emission mechanisms in acridan and carbazole-substituted dibenzo[a,c]phenazines: towards triplet harvesting emitters and hosts // *Chemical Engineering Journal*. Amsterdam: Elsevier. ISSN 1385-8947. eISSN 1873-3212. 2021, Vol. 417, art. No. 127902, p. 1–14. (Web of Science); DOI: 10.1016/j.cej.2020.127902. [IF: 16.744; Q1]
3. Arsenyan, Pavel; Vigante, Brigita; **Leitonas, Karolis**; Volyniuk, Dmytro; Andrulevičienė, Viktorija; Skhirtladze, Levani; Belyakov, Sergey; Gražulevičius, Juozas Vidas. Dual versus normal TADF of pyridines ornamented with multiple donor moieties and their performance in OLEDs // *Journal of Materials Chemistry C*. Cambridge: Royal Society of Chemistry. ISSN 2050-7526. eISSN 2050-7534. 2021, Vol. 9, iss. 11, p. 3928–3938. (Web of Science); DOI: 10.1039/d0tc05745b. [IF: 8.067; Q1]
4. **Leitonas, Karolis**; Vigante, Brigita; Volyniuk, Dmytro; Bučinskis, Audrius; Keruckienė, Rasa; Dimitrijevs, Pavels; Chiu, Tien-Lung; Gražulevičius, Juozas Vidas; Arsenyan, Pavel. 3,5-Dicyanopyridine motifs for electron-transporting semiconductors: from design and synthesis to efficient organic light-emitting diodes // *Journal of Materials Chemistry C*. Cambridge: Royal Society of Chemistry. ISSN 2050-7526. eISSN 2050-7534. 2023, Vol. 11, iss. 28, p. 9514–9526. (Web of Science); DOI: 10.1039/d3tc00841j [IF: 6.400; Q1]

2. BRIEF REVIEW OF SCIENTIFIC LITERATURE

Organic semiconductors have not only advantages, but also their limitations. Historically, their electronic and optical properties lagged behind those of their inorganic counterparts, often exhibiting lower charge carrier mobilities and operational stabilities as well as difficulties in large area defect-free applications.^{3,8,10,11,12} These shortcomings present significant hurdles, but also propel the field forward as researchers strive to harness and enhance the intrinsic properties of these organic materials.

One of the most promising avenues of research involves the efficient management of excitons – bound states of electrons and holes within a semiconductor. Organic materials naturally facilitate robust exciton formation due to their strong exciton binding energies, making them excellent candidates for optoelectronic applications.^{13,14} Yet, efficiently harnessing singlet and triplet excitons for light emission still remains a challenge. To address this, phenomena such as *thermally activated delayed fluorescence* (TADF), *triplet-triplet annihilation* (TTA), and *hybridised local charge transfer* (HLCT) are being explored.^{15,16,17,18,19} These mechanisms allow the conversion of triplet excitons, which typically do not contribute to light emission, into singlet excitons that emit photons, thereby enhancing the efficiency and performance of devices such as OLED and *organic light emitting transistors* (OLET).

This dynamic interplay of the potential benefits and challenges highlights why organic semiconductors are at the forefront of scientific inquiry. Researchers are not merely trying to replicate the functionalities of inorganic semiconductors but are actually aiming to surpass them, exploiting the unique properties of organic materials to develop technologies that were previously unattainable.²⁰

Currently, one of the most popular approaches for developing high efficiency organic-based electroluminescent devices is triplet harvesting.^{15,17,18} Based on spin statistics, during electrical excitation, singlet excitons constitute only 25% of the total population of charges, while the remaining 75% consist of triplet excitons.²¹ This distribution makes triplet harvesting essential for achieving efficient OLEDs because, in conventional fully organic fluorescent devices, only singlet excitons can be used to generate photons.¹⁵ Triplet harvesting is based on converting triplet excitons (Fig. 1), which usually do not emit light, into singlet excitons that *do* emit photons, thus increasing the theoretical internal quantum efficiency (IQE) from as little as 25% up to 100%.^{22,23,24}

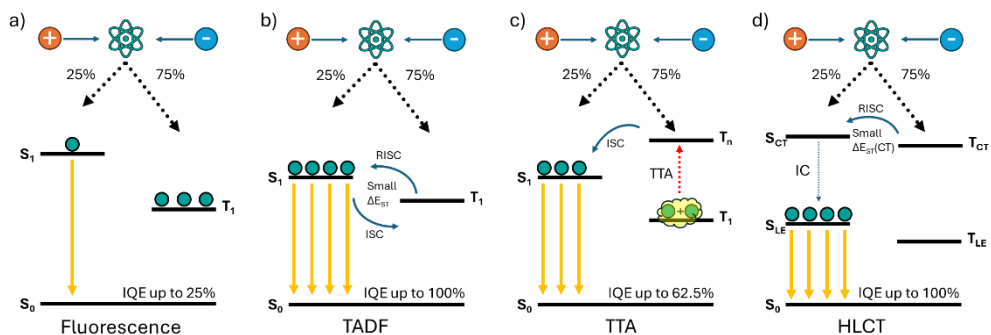


Fig. 1. Overview of mechanisms for harvesting triplet excitons to achieve electroluminescence in OLED devices. a) conventional fluorescence; b) thermally activated delayed fluorescence (TADF); c) triplet-triplet annihilation (TTA); d) hybridised local and charge transfer (HLCT)

One effective method for this conversion is called *thermally activated delayed fluorescence* (TADF), alongside *reverse intersystem crossing* (RISC). A phenomenon initially reported by Perrin nearly a century ago remained merely a spectroscopic curiosity until 2011.²⁵ It was then that Adachi suggested its use in harvesting triplets in OLEDs, potentially bringing their theoretical internal quantum efficiency to 100%.^{26,27,28} TADF materials use thermal energy and a very small energy gap between singlet and triplet levels (ΔE_{ST}) to convert triplet excitons into a singlet state via RISC, allowing for efficient light emission.^{22,26,28} This is particularly important for creating high-efficiency electroluminescent devices without using toxic heavy metals, which are common in phosphorescent materials. An example of the impact of TADF is seen in the development of blue OLEDs, which now nearly match the performance of phosphorescent alternatives, marking a significant achievement in the OLED technology.^{8,18}

Another method, TTA, is manifested when two triplet excitons interact, and one transfers energy to the other, forming a higher energy singlet state that emits light. This mechanism is useful in devices that achieve high triplet exciton concentrations, enhancing the light output. Usually, TTA emitters are used in conjunction with sensitizers, which absorb photon energy, generating a singlet excited state before undergoing *intersystem crossing* (ISC) to transition into its triplet state. Subsequently, triplet energy transfer populates the triplet state of the TTA emitter.^{29,30,31} Upon the encounter of two triplet excitons, TTA facilitates an up-conversion process resulting in the formation of one singlet exciton that can undergo radiative decay via fluorescence.³² Unfortunately, since two triplet excitons are needed to generate one singlet exciton, only half of the generated triplet excitons can theoretically contribute to emission. This limitation means that the maximum IQE can reach only up to 62.5%.²²

HLCT involves a novel arrangement where the molecular structure encourages interaction between *localised excited* (LE) states and *charge-transfer* (CT) states. The LE state supports high-efficiency fluorescence through rapid radiative decay, while the CT state facilitates the generation of singlet excitons in a high yield. This occurs via RISC, where excitons transition from a high-lying CT-based triplet excited state back to the CT-based singlet excited state.²² This interaction boosts both the charge and the energy transfer within the molecule, enhancing the stability and efficiency of light-emitting devices.³³ HLCT has proven especially beneficial in harvesting nearly all electrically generated excitons in OLEDs without any delayed fluorescence, demonstrating a significant potential in the development of low-cost, fully organic emissive materials.^{34,35,36}

Despite these advances, challenges in triplet harvesting remain. Managing triplet exciton dynamics to prevent their energy from being lost (quenching) and maximizing the light emission efficiency are ongoing concerns.²² Moreover, developing materials that can harness these mechanisms without losing the colour quality or stability under operational stress continues to be a key research area. The advancements in triplet harvesting techniques not only push the field of organic electronics forward, but also support broader goals of making electronic devices more sustainable and versatile. By reducing the dependence on rare or toxic metals and enhancing the energy efficiency of displays and lighting, these technologies help promote environmental sustainability and economic efficiency, aligning with the future needs of organic electronics.

3. REVIEW OF THE PUBLISHED ARTICLES

3.1. White Vertical Organic Permeable-Base Light-Emitting Transistors Obtained by Mixing of Blue Exciton and Orange Interface Exciplex Emissions (scientific publication No. 1, Q1, 5 quotations)

This sub-chapter is based on the paper published in *Journal of Materials Chemistry C*, **2022**, 10, 9786 by K. Leitonas, M. Gužauskas, U. Tsiko, J. Simokaitienė, D. Volyniuk, J. V. Gražulevičius.³⁷

In this work, exciplex emitters displaying TADF were used to build white *organic permeable-base light-emitting transistors* (OPB-LETs). Since the initial report,³⁸ TADF materials have been an uncommon find for single-colour OLETs^{39,40} despite their high potential as heavy-metal-free emitters for OLEDs. As far as we are aware, white OLETs have not yet employed TADF emitters. The newly synthesised bipolar chemical 4,6-bis(4-(9H-carbazol-9-yl)phenyl)pyrimidine-5-carbonitrile⁴¹ (**CzPm**) was used in this work to produce OPB-LETs. They demonstrated a maximum external quantum efficiency of 2.4% and white electroluminescence (EL) with CIE colour coordinates of (0.34; 0.36) and a *colour rendering index* (CRI) of 93. These OPB-LETs have an entire active area that emits light, which is the crossing area between the three electrodes.

The designed OPB-LETs comprised a three-electrode structure, which was derived from two parts of organic multilayers (Fig. 2 b, c, d). The first (between the top electrode (emitter) and the middle electrode (base)) had only C₇₀ electron-transporting and LiF electron-injecting layers which were selected according to previously published articles.^{42,43} The second part (placed between the middle electrode (base) and the bottom electrode (collector)) played the role of an OLED structure and was expected to produce efficient EL. The structures of the devices were the following:

- ITO/MoO₃ [3 nm]/TAPC [80 nm]/PO-T2T [40 nm]/Al [10 nm]/C₇₀ [120 nm]/LiF [2 nm]/Al (**orange** OPB-LET)
- ITO/MoO₃ [1 nm]/TAPC [60 nm]/mCP [20 nm]/PO-T2T [40 nm]/Al [15 nm]/C₇₀ [120 nm]/LiF [1 nm]/Al (**blue** OPB-LET)
- ITO/MoO₃ [1 nm]/TAPC [60 nm]/**CzPm** [20 nm]/PO-T2T [40 nm]/Al [15 nm]/C₇₀ [120 nm]/LiF [1 nm]/Al (**white** OPB-LET)

The presence of MoO₃ and TAPC layers facilitated the effective injection and transportation of holes from the ITO electrode to the light-emitting, exciplex-capable,⁴⁴ interface TAPC/PO-T2T which indeed resulted in the orange colour EL peaking at 558 nm (Fig. 3 a).

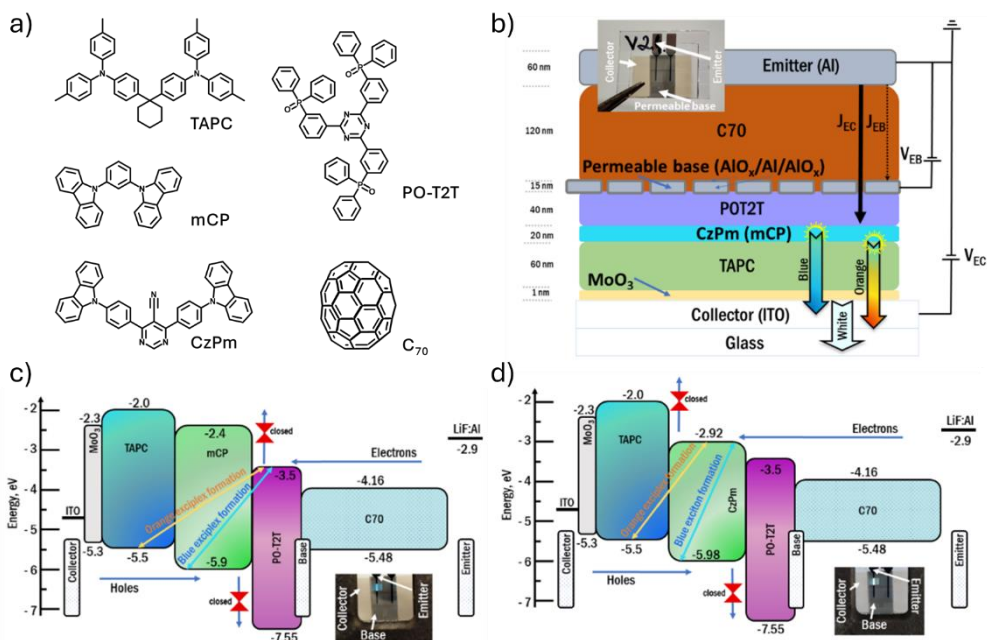


Fig. 2. a) Chemical structures of the utilised compounds; b) Device configuration illustration for white (blue) OPB-LETs; c) and d) Energy level diagrams at equilibrium for blue (orange) and white OPB-LETs. HOMO/LUMO values in eV. Insets: Photographs of blue and white OPB-LETs under zero and applied bias

The observed EL spectrum demonstrated the ability of electrons to pass through the permeable base. A comparison of collector current densities (J_{EC}) and base current densities (J_{EB}) (Fig. 3 b, Table 1) indicated that the amount of current leaking to the permeable base was relatively minimal. The base leakage current density J_{EB} is significantly lower than that of J_{EC} by more than three orders of magnitude at the same external voltages, suggesting that the self-passivating AlO_x layer (Fig. 2 b) has a high insulating efficiency.

In order to demonstrate the current and EL modulation effect, we measured the variations of the current density (J_{EC}) and brightness in relation to the collector voltage (V_{EC}) (Fig. 3 e). The V_{EC} was adjusted within a very narrow range of 7.00 to 7.08 V, with small increments. The photodiode recorded the brightness in *arbitrary units* (a.u.). The choice of these parameters enabled the recording of these characteristics for approximately 10 seconds. During the measurements, the base voltage V_{EB} was alternated between two states: ‘on’ ($V_{EB}=4$ V) and ‘off’ ($V_{EB}=0$ V). Consequently, distinct disparities were noted in the collector current density J_{EC} and the output brightness at various V_{EB} states. When the device is in the ‘on’ state, electrons that are injected from the emitter electrode can flow through the base electrode and then undergo radiative hole-electron recombination via EL at the interface between TAPC and PO-T2T (Fig. 2 c). The efficiency of electron injection from the emitter electrode increased as the voltage V_{EB} increased, suggesting that the base voltage V_{EB} can

regulate the passage of electrons through the permeable base containing pinholes (Fig. 3 c). However, the low maximum EQE of 0.17% of the **orange** OPB-LET suggested the replacement of exciplex TAPC:PO-T2T by a more efficient one.

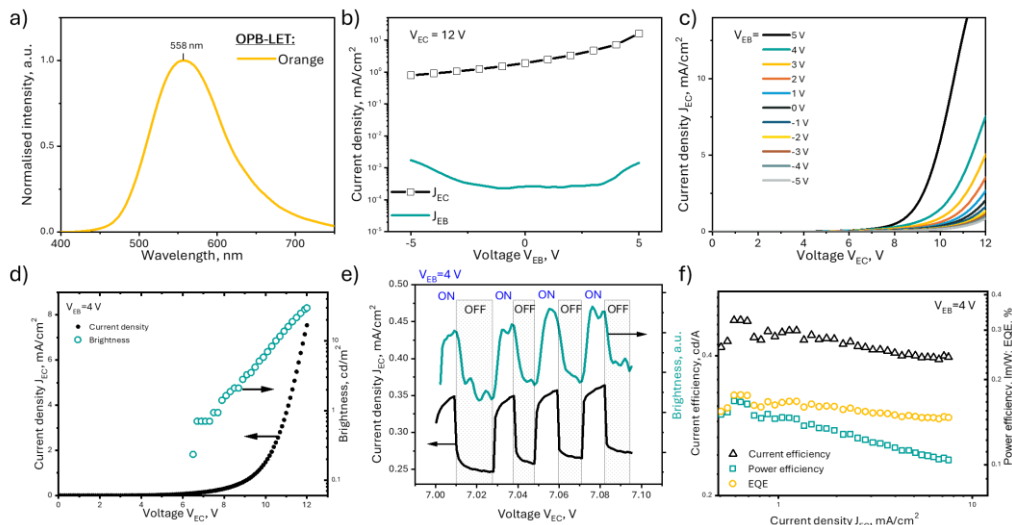


Fig. 3. a) EL spectrum at 12 V; b) Transfer; c) Output characteristics (current density-voltage); d) Current density-voltage and brightness-voltage at $V_{EB} = 4$ V; e) Current density and brightness under ‘on’ and ‘off’ states; f) Current, power, and EQE vs. collector current density J_{EC} for the orange exciplex-based OPB-LET

In search of a more efficient exciplex system, the structure was supplemented with an mCP interlayer between the layers of TAPC and PO-T2T (Fig. 2 b, c) which indeed resulted in **blue** EL with a peak intensity of 478 nm⁴⁵ (Fig. 4 a). The recombination zone between holes and electrons was located at the interface between the mCP and PO-T2T layers (Fig. 2 c). There was no injection of electrons from PO-T2T to mCP because of the significant energy barrier of 1.1 eV between their respective lowest unoccupied molecular orbitals (LUMO) at the mCP/PO-T2T interface. The voltage-dependent transfer current density plots (Fig. 4 b) indicate that the **blue** OPB-LET does not exhibit significant current leakages through the base.

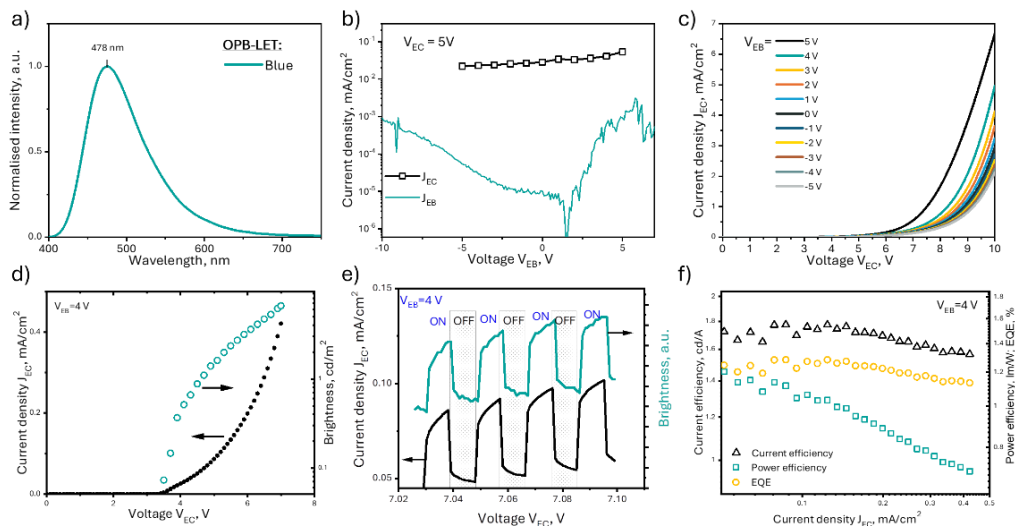


Fig. 4. a) EL spectrum at 12 V; b) Transfer; c) Output characteristics (current density-voltage); d) Current density-voltage and brightness-voltage at $V_{EB} = 4$ V; e) Current density and brightness under ‘on’ and ‘off’ states; f) Current, power, and EQE vs. collector current density J_{EC} for the **blue** exciplex OPB-LET

However, increasing the voltage applied to the base results in a higher collector current J_{EC} of the **blue** OPB-LET. Fig. 4 e illustrates the current and brightness modulation effect that is obtained by switching V_{EB} between the ‘on’ and ‘off’ states. Although the **blue** OPB-LET exhibited a brightness of only 7 cd/m^2 (Fig. 4 d) due to low sensitivity of the human eye to the blue light, the maximum EQE was estimated at 1.2% (Fig. 4 f, Table 1). Once more, searching for an enhancement of efficiency, the newly synthesised emitter **CzPm** (Fig. 2 a, b, d) was used in place of mCP, and **white** EL was observed for OPB-LET (Fig. 5 a).

Table 1. EL parameters of **orange**, **blue** and **white** OPB-LETs

OPB-LETs	V_{on} , V at 0.1 cd/m^2	Max brightness, cd/m^2	EQE, %	EL maximum*, nm	CIE 1931 coordinates (x, y)*	CRI*
Orange	6.7	30	0.17	558		-
Blue	3.6	7	1.2	478	(0.22, 0.31)	-
White	3.3	300	2.4	478, 556	(0.34; 0.36)	93

* at turn-on voltages

In the EL spectra of **white** OPB-LET, one can observe a high-energy emission band centred at 478 nm and a low-energy band with the highest intensity at 556 nm (Fig. 5 a). The band reaching its highest intensity at a wavelength of 478 nm is

associated with the emission of blue excitons from **CzPm**. On the other hand, the band with a lower energy is seemingly linked to the emission of orange exciplexes at the interfaces of **CzPm**/PO-T2T or **CzPm**/TAPC. After a thorough photophysical investigation, it was observed that the blue shift in the photoluminescence (PL) spectrum of the **CzPm**:PO-T2T mixture, compared to the PL spectrum of the **CzPm** film, is caused by a solid-state solvatochromism-like process. The observed red shift in the PL spectrum of the **CzPm** and TAPC mixture, compared to the PL spectrum of the **CzPm** film, can be explained by the formation of exciplexes (Fig. 5 d).

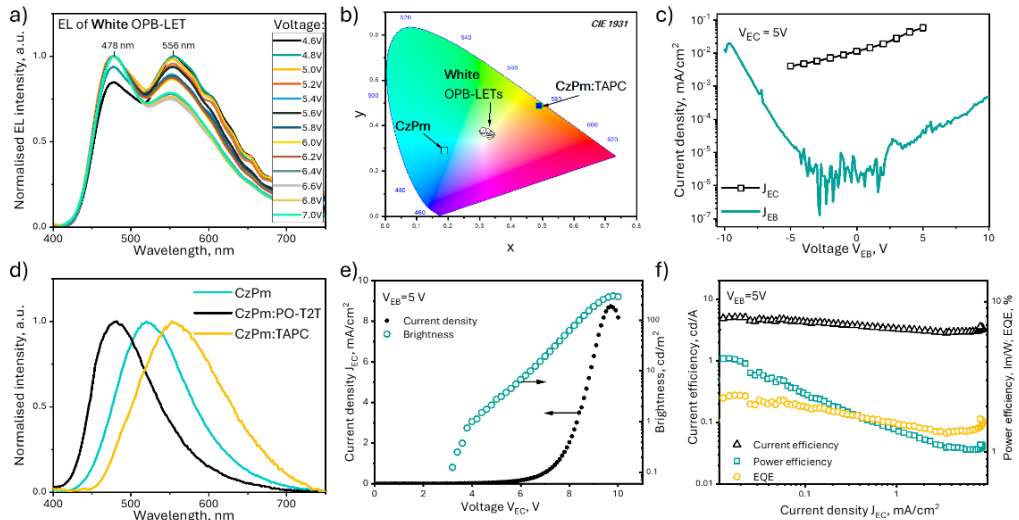


Fig. 5. a) EL spectra; and b) the corresponding CIE colour coordinates obtained at various voltages. c) Transfer characteristics for the **white** exciplex-based OPB-LET. d) Normalized PL spectra of the **CzPm**, **CzPm**:PO-T2T, and **CzPm**:TAPC films. e) Current density and brightness as a function of voltage at $V_{EB} = 5V$. f) Efficiency metrics (current, power, EQE) versus collector current density. The CIE colour diagram b) is supplemented with the colour coordinates of **CzPm** exciton and **CzPm**:TAPC exciplex emissions

The TADF properties of the exciplex-forming molecular mixture **CzPm**:TAPC were investigated and proven by recording its PL spectra and PL decay curves at temperatures from 77 K to 300 K. Transient EL curves were recorded to verify the contribution of TADF to the exciplex emission of the molecular mixture **CzPm**:TAPC exciplex.

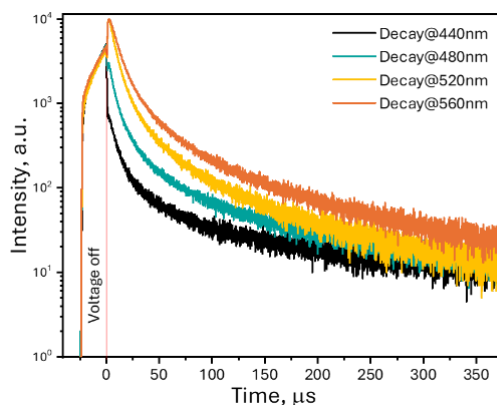


Fig. 6. Time-resolved EL response of the **CzPm:TAPC**-based device

The blue and orange components of the EL from the **CzPm:TAPC**-based device were specifically analysed (Fig. 6); thus the contribution of TADF to the orange component was supported by long-lived EL decay curves. Due to the mixing of blue exciton emission from **CzPm** and the orange exciplex emission from **CzPm:TAPC**, **white** OPB-LET was characterised by pure white EL with the colour coordinates of (0.33, 0.33) close to natural white (Fig. 5 b) and exhibited a colour rendering index (CRI) ranging from 77 to 93. The transfer and output current density-voltage characteristics of the **white** OPB-LET were found to be similar to those of the **orange** and **blue** OPB-LETs described above, thereby indicating a similar working mechanism of the **white** OPB-LET. Compared to the **orange** and **blue** OPB-LETs, the **white** OPB-LET was characterised by the lowest turn-on voltage of 3.3 V, the highest maximum brightness of 300 cd/m², and the highest EQE of 2.4%. These results can be explained by the TADF properties of the newly observed exciplex **CzPm:TAPC** together with good charge-injection and charge-transporting properties of the film of **CzPm**. Overall, the OPB-LETs with a three-electrode-containing structure exhibited effective EL together with the active current modulation ability, giving promising prospects for future use across diverse domains.

3.2. TADF versus TTA Emission Mechanisms in Acridan and Carbazole-Substituted Dibenzo[a,c]phenazines: towards Triplet Harvesting Emitters and Hosts Emissions (scientific publication No. 2, Q1, 25 quotations)

This sub-chapter is based on the paper published in the *Chemical Engineering Journal*, **2021**, 417, 127902 by V. Andrulėvičienė, K. Leitonas, D. Volyniuk, G. Sini, J. V. Gražulevičius, V. Getautis.⁴⁶

TADF materials have attracted considerable attention in the field of organic optoelectronics because they have the potential to achieve 100% IQE by capturing triplet excitons through RISC.^{47,48,49} TADF hosts are capable of efficiently transferring energy to the guest molecules through the Förster energy transfer (FET), while achieving a utilisation rate of 100%. A minimal energy difference between the singlet and triplet states (ΔE_{ST}) is crucial for achieving efficient TADF through RISC.⁵⁰

Organic materials that possess a high ΔE_{ST} can be utilised in the OLED technology if they demonstrate the phenomenon of TTA ‘hot excitons’ or upper-level triplet-singlet intersystem crossing.^{51,52}

Both TADF and TTA materials can serve as hosts in OLEDs if they fulfil certain criteria. These criteria include possessing high and balanced charge mobilities, a wide transporting band gap with suitable HOMO and LUMO energy levels for charge injection, and exhibiting high optical, thermal, and electrochemical stability.^{53,54,55} These hosts serve multiple purposes, including mitigating the negative effects of aggregation-induced quenching on OLED emitters in the solid state, facilitating the recombination of holes and electrons within the light-emitting layer, and enabling additional triplet harvesting within the host.⁵⁶

The objective of this study is to concentrate on the advancement of effective TADF and TTA hosts which are known for their highly twisted molecular structures that typically result in inadequate charge transport properties. The study presents new compounds with dibenzo[a,c]phenazine acceptor that have been substituted at either the C-2 or C-7 positions with electron-donating carbazole (CzDbp) or acridan (AcDbp) groups (Fig. 7). Surprisingly, the developed dibenzo[a,c]phenazine derivatives exhibited TTA, contrary to what had been expected. These derivatives also showed conventional TADF, which is advantageous for creating highly efficient orange-red OLEDs.

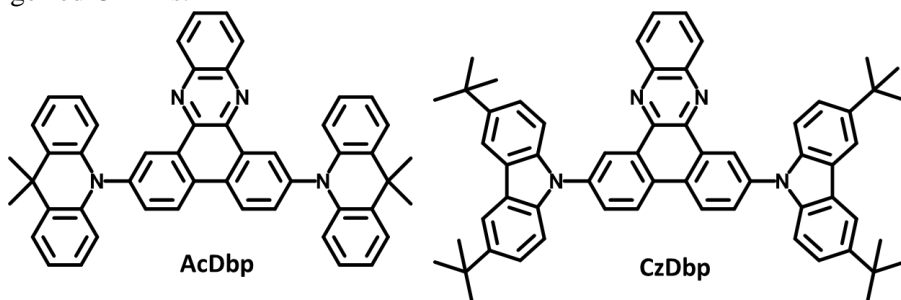


Fig. 7. Chemical structures of investigated compounds **AcDbp** and **CzDbp**

The study started from the investigation of the *ionisation potentials* (IP) of materials **AcDbp** and **CzDbp**, through the use of *photoelectron emission* (PE) and *cyclic voltammetry* (CV). The IP values determined by PE were found to be the same for both materials at 5.5 eV, while the values measured by CV were slightly lower – 5.25 and 5.44 eV for **AcDbp** and **CzDbp**, respectively (Table 2). The discrepancy arises from the heightened polarisation effects observed in the solid state. The energy of the lowest unoccupied molecular orbital (EA^{PE}) for **AcDbp** was 0.24 eV greater than that of **CzDbp** (Table 2).

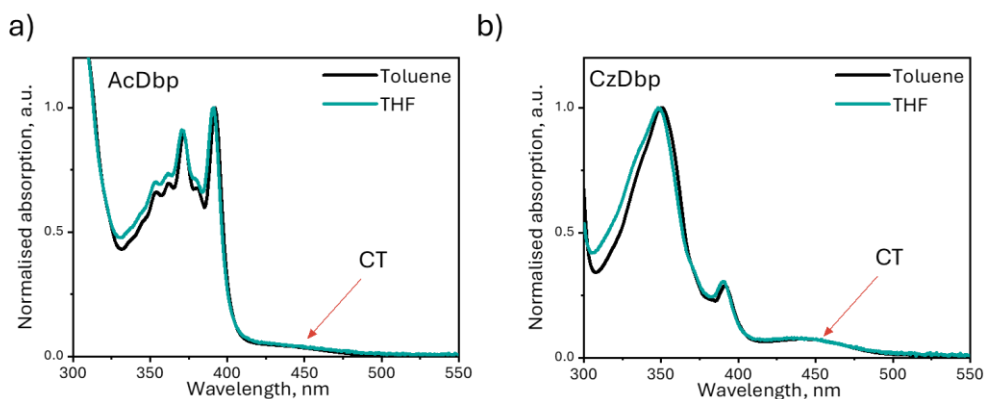
Table 2. IP, EA and charge mobility values for **AcDbp** and **CzDbp**

	IP^{PE} , eV	E_g^{opt} , eV	EA^{PE} , eV	IP^{CV} , eV	EA^{CV} , eV	μ_h^* , cm^2/Vs	μ_e^* , cm^2/Vs
AcDbp	5.50	2.73	2.77	5.25	3.12	$2.4 \cdot 10^{-3}$	$1.2 \cdot 10^{-3}$
CzDbp	5.50	2.97	2.53	5.44	3.11	$3.8 \cdot 10^{-3}$	$1.0 \cdot 10^{-4}$

* charge mobility at 2.02×10^5 V/cm

The charge transport properties of vacuum-deposited layers of **AcDbp** and **CzDbp** were analysed by using the *time-of-flight* (ToF) technique. The findings indicated that the solid layers of **AcDbp** and **CzDbp** have the ability to transport both holes and electrons, with charge-drift mobilities exceeding 10^{-3} cm^2/Vs under intense electric fields (Table 2).

Further, the photophysical characteristics were investigated by analysing the UV-vis absorption spectra in tetrahydrofuran and toluene solutions. These spectra revealed a faint *charge transfer* (CT) tail in the 400–500 nm range (Fig. 8).

**Fig. 8.** UV-Vis absorption profiles of a) **AcDbp** and b) **CzDbp** in toluene and THF solutions

Fluorescence spectra (Fig. 9) and PLQYs of toluene and THF solutions were recorded, and both compounds exhibited a Gaussian-shaped emission profile, further indicating the CT nature of the emissive states. Solutions of **CzDbp** showed higher values of PLQY than the solutions of **AcDbp** (Table 3). The values of PLQY of the solutions in TOL and THF of **AcDbp** were 2% and 0.5%, while those of **CzDbp** were 37% and 28%, respectively. Higher PLQY values of **CzDbp** may be attributed to a stronger TTA.

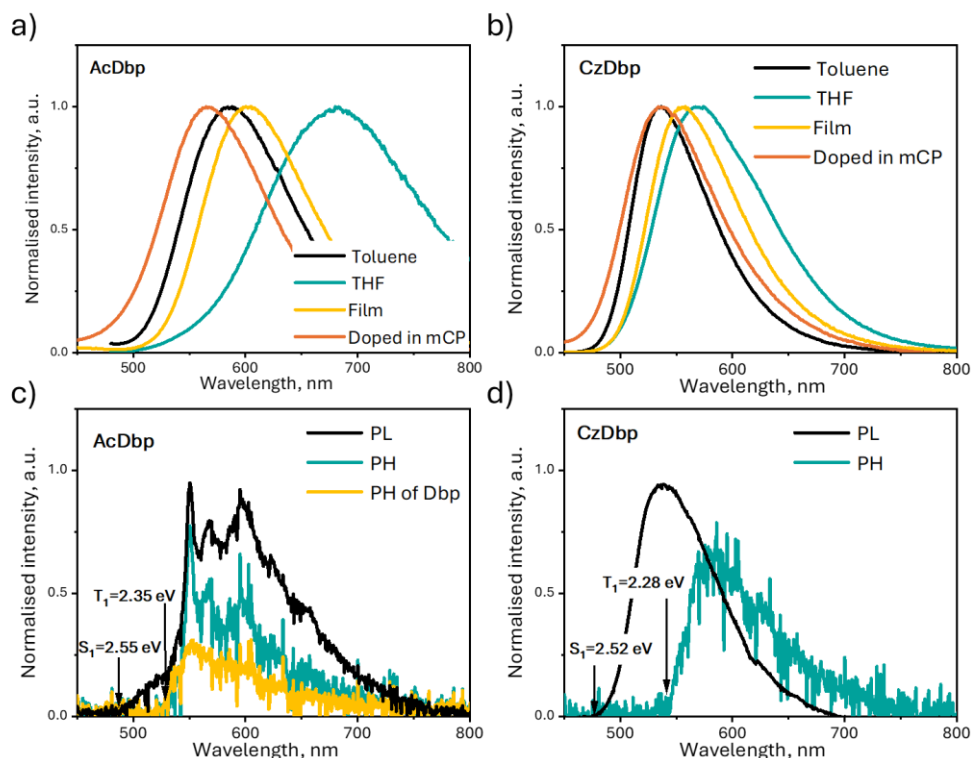


Fig. 9. Room-temperature a) fluorescence and b) PL spectra as well as c), d) PH spectra recorded at 77 K of THF solutions of **AcDbp** and **CzDbp** (PH spectrum of the solution of **Dbp** in THF recorded at 77 K is presented as the yellow line)

PL and PH spectra were used to estimate singlet-triplet energy differences for **AcDbp** and **CzDbp** solutions in THF at 77 K. **AcDbp**'s PL spectrum showed a structureless shoulder, indicating the CT nature of the emissive state. On the other hand, **CzDbp**'s PH spectrum showed a characteristic vibrational structure, indicating that the lowest emissive T_1 state corresponds to the local excitation (3LE) of the **Dbp**-core.

Table 3. Photophysical properties of **AcDbp** and **CzDbp**

	PLQY _{air} , %*	PLQY _{no oxygen} , %	S_1 , eV	T_1 , eV	ΔE_{ST} , eV
	THF/TOL/neat film/mCP/mCBP	THF/TOL	77 K THF		
AcDbp	0.5/2/3/4/8	0.6/3	2.55	2.35	0.20
CzDbp	28/37/15/11/21	44/53	2.52	2.28	0.24

* measured at air condition

Seeking to determine triplet harvesting properties of the investigated compounds, air-equilibrated and deoxygenated toluene solutions were measured by steady-state and time-resolved spectroscopy (Fig. 10). The PL spectra of standard and deoxygenated solutions of the compounds exhibited a striking resemblance, thus indicating that delayed fluorescence originated from the CT state identical to that of prompt fluorescence. Furthermore, the PL decay of **AcDbp** followed a double exponential pattern with a significant increase in the long-lived component lifetime after deoxygenation. This indicates that PL originates from the harvesting of triplets, most likely through TADF.

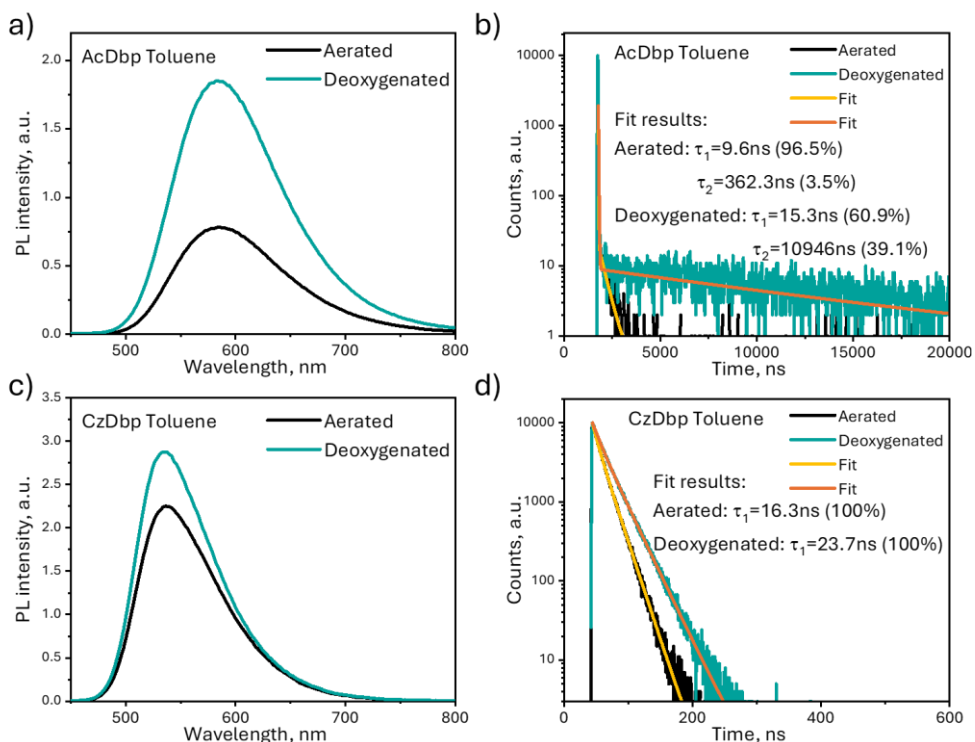


Fig. 10. a), c) PL spectra and b), d) the corresponding PL decay curves for air-equilibrated and deoxygenated toluene solutions of a), b) **AcDbp** and c), d) **CzDbp**

Interestingly, the toluene solutions of **CzDbp** displayed single-exponential PL decays, indicating only prompt fluorescence. On the other hand, after deoxygenation, the **CzDbp** solutions showed a 16% increase in PLQY, suggesting that the triplet states undoubtedly contribute to the PL mechanism of **CzDbp**. This contribution is likely through a mechanism different from that of TADF and is as fast as the immediate fluorescence.

Since delayed fluorescence can be activated by temperature, PL spectra and PL decay curves of neat and doped (10 wt. %) in mCP layers of **AcDbp** and **CzDbp** were recorded at different temperatures ranging from 77 to 300 K (Fig. 11). The PL intensities, and therefore the absolute PLQYs, of both the neat **AcDbp** film and the

doped in mCP film increased as the temperature was raised from approximately 220 K to 300 K. The observed rise in the PL intensity as the temperature increases can be attributed to the contribution of TADF.

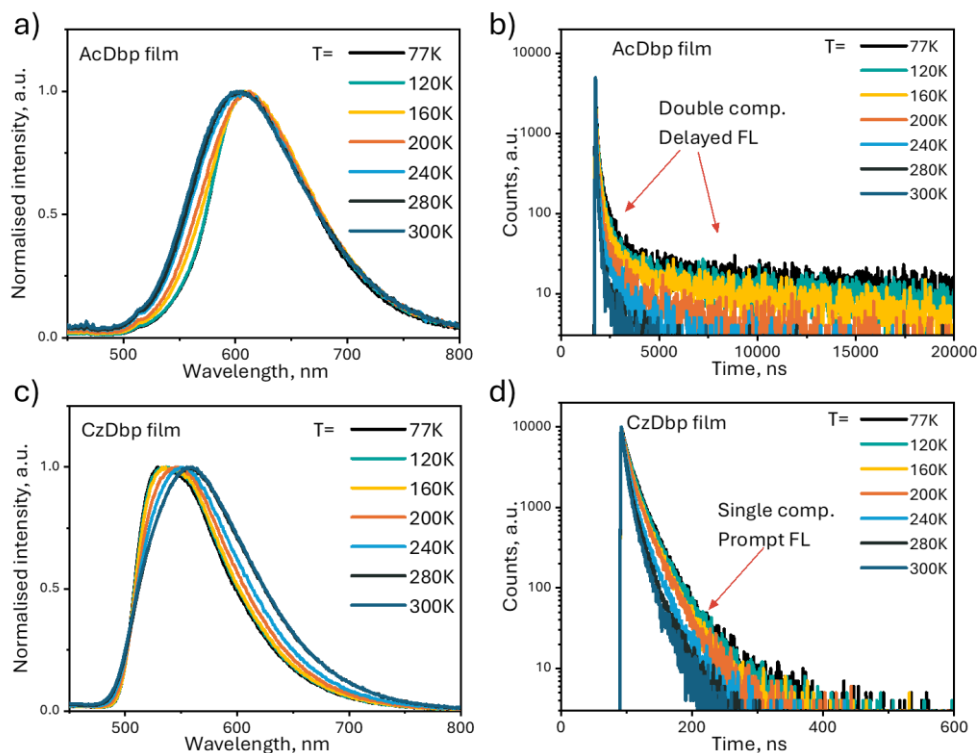


Fig. 11. a), c) PL spectra and b), d) corresponding PL decay curves acquired at various temperatures for neat layers of a), b) **AcDdbp** and c), d) **CzDdbp**

No phosphorescent or delayed fluorescent components were observed in the temperatures ranging from 77 to 300 K for the neat **CzDdbp** film (Fig. 11 c, d). The intensity of the photoluminescence decay profile decreased as the temperature increased due to the process of TTA.

The compound **AcDdbp** has shown potential as a TADF host for red OLEDs due to its charge-transporting properties and energy of the first triplet level. However, **CzDdbp** showed ambipolar charge-transporting properties and higher PLQY than **AcDdbp**. Thus, both **AcDdbp** and **CzDdbp** were used in phosphorescent-based OLEDs (PHOLEDs) to demonstrate their suitability as host materials for a commercial red phosphorescent emitter (piq)₂Ir(acac).

For the initial test, the following device structure was used:

- ITO/ MoO₃ (0.6 nm)/NPB (30 nm)/5 wt.% (piq)₂Ir(acac):**Host** (20 nm)/TPBi (70 nm)/LiF (0.8nm):Al

where **AcDbp** and **CzDbp** were employed as a host, together with a well-known host mCP used as a reference, thus producing PHOLED devices **A**, **B**, and **C**, respectively (Table 4).

PHOLEDs **A**, **B**, and **C** showed the classical (piq)₂Ir(acac) EL with a peak wavelength of 623 nm. Devices **A** and **B** exhibited a lower turn-on voltage compared to device **C**, thereby indicating excellent electron and hole injection. Device **B** with **CzDbp** demonstrated the best maximum current efficiency (CE_{max}), maximum power efficiency (PE_{max}), and external quantum efficiency (EQE_{max}). A higher EQE_{max} of 9% was obtained for **CzDbp**-based PHOLED **B** compared to 8% for one of the best conventional host mCP-based device **C**.

With the aim of further optimisation of the device structure, five devices with the following configuration were designed:

- ITO/HAT-CN [5 nm]/NPB [40 nm]/TCTA [10 nm]/mCBP [10 nm]/ 5 wt. % (piq)₂Ir(acac):Host [50 nm]/nBPhen [30 nm]/Liq [2 nm]/Al

where **AcDbp**, **CzDbp** and three more conventional hosts, namely, **mCBP**, **NPB**, and **nBPhen** were used, producing devices named **D**, **E**, **F**, **G** and **H**, respectively (Table 4).

Table 4. EL parameters of devices A–J

Device	Emissive layer	^a V _{ON} / ^b V _{Driving} , V	CE _{max} , cd/A	PE _{max} , lm/W	EQE _{max} , %
Structure: ITO/MoO3/NPB/ Emissive layer /TPBi/LiF:Al					
A	(piq) ₂ Ir(acac): AcDbp	3.0/3.85	6.3	4.6	6.0
B	(piq) ₂ Ir(acac): CzDbp	3.4/4.5	9.0	6.4	9.0
C	(piq) ₂ Ir(acac):mCP	4.0/5.2	8.6	5.6	8.0
Structure: ITO/HAT-CN/NPB/TCTA/mCBP/ Emissive layer /nBPhen/Liq/Al					
D	(piq) ₂ Ir(acac): AcDbp	3.2/5.2	9.8	9.1	13.2
E	(piq) ₂ Ir(acac): CzDbp	3.0/4.75	10.3	11.6	15.9
F	(piq) ₂ Ir(acac):mCBP	2.9/4.0	11.5	12.9	13.1
G	(piq) ₂ Ir(acac):NPB	3.2/4.5	6.6	6.7	9.0
H	(piq) ₂ Ir(acac):nBPhen	4.8/8.7	12.5	8.5	14.6
Structure: ITO/HAT-CN/NPB/TCTA/mCBP/ Emissive layer /nBPhen/Liq/Al					
I	AcDbp :mCBP	3.6/6.7	41.6	35.3	19.4
J	CzDbp :mCBP	3.7/7.0	54.4	46.2	22.1

^aV_{ON} was taken at 10 cd/m²; ^bV_{Driving} was taken at 10 mA/cm²

Due to improved charge-injecting properties, **D–H** devices based on (piq)₂Ir(acac) exhibited improved output EL characteristics. Device **E**, fabricated by using the developed host **CzDbp**, demonstrated the highest maximum EQE (15.9%) and the lowest roll-off compared to the reference devices **F–H** containing **mCBP**,

NPB, or **nBPhen** as the more traditional hosts (Table 4, Fig. 12). The high efficiency of device **E** is partly due to the utilisation of triplet excitons not only within the phosphorescent emitter (piq)₂Ir(acac), but also within the host **CzDbp** due to its strong ability of triplet harvesting.

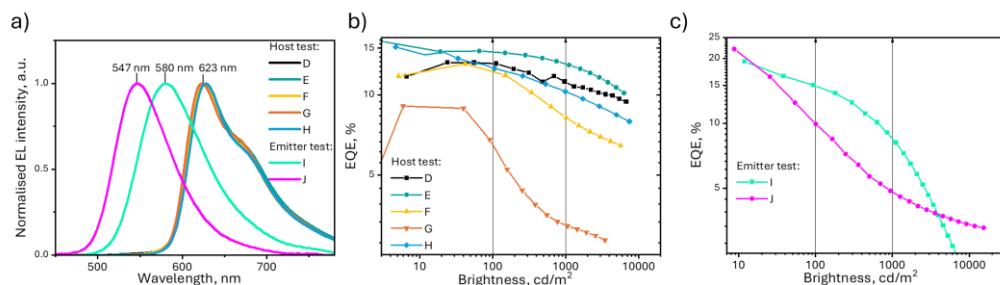


Fig. 12. a) EL spectra; b) and c) EQE as a function of brightness, for devices **D–J** employing **AcDbp** and **CzDbp** as either host or emitter materials

After acquiring promising results as a host, it was decided to test **AcDbp** and **CzDbp** compounds as emitters in the same structure dispersed in the mCBP host. Despite the low PLQYs of the investigated organic semiconductors, both of them delivered unexpectedly high EQEs of 19.4 and 22.1% for **AcDbp**:mCBP and **CzDbp**:mCBP, respectively. This disagreement can be linked to the potential loss mechanisms when the TADF molecules are optically excited as it was discussed in⁵⁷.

Two new D-A-D type molecules, **CzDbp** and **AcDbp** with bipolar charge transport and triplet exciton harvesting via TTA or TADF were studied. The optical absorption spectra of **AcDbp** and **CzDbp** show very low intensity CT-tails. **AcDbp** photoluminescence spectra and decay curves show TADF-induced delayed fluorescence, while **CzDbp** showed triplet exciton harvesting via the TTA mechanism but no delayed fluorescence. Triplet harvesting in the donor-acceptor molecules with small singlet-triplet splitting can occur through a faster and competitive TTA mechanism, and not only through TADF. Red PHOLEDs with the **CzDbp** as hosts had 15.9% external quantum efficiency and a lower efficiency roll-off than those with mCP, mCBP, NPB, and nBPhen hosts. External quantum efficiencies of 19.4% and 22.1% were achieved with **AcDbp** and **CzDbp** TADF/TTA emitters.

3.3. Dual versus Normal TADF of Pyridines Ornamented with Multiple Donor Moieties and their Performance in OLEDs (scientific publication No. 3, Q1, 10 quotations)

This sub-chapter is based on the paper published in *Journal of Materials Chemistry C*, 2021, 9, 3928 by P. Arsenyan, B. Vigante, K. Leitonas, D. Volyniuk, V. Andrulevičienė, L. Skhirtladze, S. Belyakov, J. V. Gražulevičius.⁵⁸

The utilisation of the multiple-donor approach has been extensively employed in the development of highly effective TADF emitters for OLEDs.⁵⁹ The high EQE of TADF-based OLEDs is directly related to the efficient capture of emissive triplet states through RISC in purely organic compounds.⁶⁰ This process is most effective

when the singlet-triplet energy splitting is small and the PLQYs are high in the solid state.⁶¹ Previously, researchers developed multiple-donor-acceptor TADF emitters which would have small ΔE_{ST} and high PLQY values when in the solid state. These emitters demonstrated efficient and relatively stable EL characteristics. For example, a TADF molecule containing three donor and three acceptor units was used in the production of solution-processed sky-blue TADF OLEDs, achieving a maximum EQE of 21.0%.⁶² TADF molecules containing four donor moieties exhibited an exceptionally high rate of RISC at $4.44 \times 10^6 \text{ s}^{-1}$, leading to OLEDs with maximum EQEs of up to 24.6%.⁶³ Moreover, TADF emitters containing a greater quantity of donor moieties exhibited reduced lifetimes of delayed fluorescence and increased lifetimes of the device compared to the reference compounds with a lower quantity of donor moieties.^{64,65}

The impact of various donor types on the efficiency of multiple donor-acceptor interactions in TADF compounds has not been investigated thus far. This study presents various donors incorporated into the molecular structure of multiple donor-acceptor TADF emitters, resulting in highly efficient TADF compounds containing two 3,6-di-tert-butyl-carbazole units. Two dicyanopyridines, which have multiple donors, were fully characterised by multiple spectroscopic techniques. One of the dicyanopyridines has three donors of the same type, specifically, 3,6-di-tert-butyl-carbazole (**5a**), while the other dicyanopyridine has two different types of donors, namely, 3,6-di-tert-butyl-carbazole and 3,7-dibromophenothiazine (**5b**), in its molecular structure (Fig. 13). The OLEDs that used the synthesised compound **5a** as the TADF emitter achieved a maximum EQE of 25%.

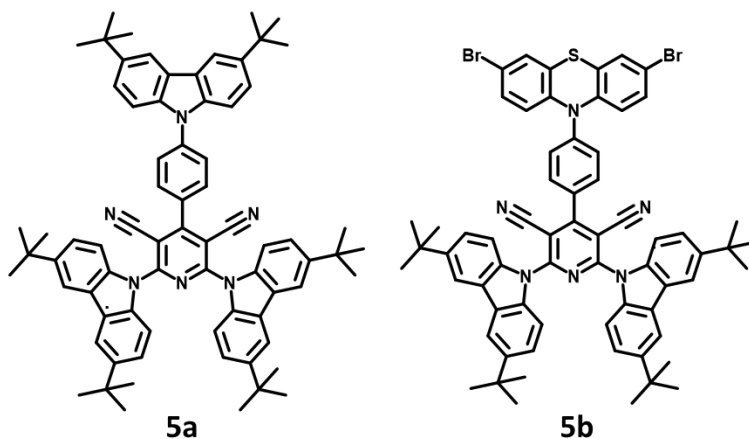


Fig. 13. Chemical structures of investigated compounds **5a** and **5b**

In this study, the electrochemical and photophysical properties of compounds **5a** and **5b** were investigated by using CV and PE spectroscopy (Fig. 14 a). The energy levels of the compounds were determined, with CV observed ionisation potentials (IP^{CV}) of 5.62 and 5.31 eV for compounds **5a** and **5b**. A lower IP^{CV} value was obtained

for **5b** compared to that of compound **5a** due to the presence of a strong electron-donating 3,7-dibromophenothiazine moiety.

The electronic structures in the ground and excited states of **5a** and **5b** were experimentally investigated by the UV-Vis, steady-state, and time-resolved luminescence spectroscopy. Close peak wavelengths (390 and 396 nm) of low-energy absorption bands were observed for the toluene solutions of **5a** and **5b**, which were in very good agreement with the band of the previously investigated dicyanopyridine-based corresponding compound **I** (Fig. 14 b, Table 5).⁶⁶

Table 5. Photophysical data for **5a** and **5b**^a

Compound	5a	5b
λ of absorption peak (toluene), nm	395	390
λ of PL max (neat/doped film ^a), nm	502/512	598/584
PLQY (neat/doped in mCP/ and mCBP film), %	18/20/22	12/17/20
S ₁ (THF/doped film ^a), eV	2.71/2.81	2.79/2.83
T ₁ (THF/doped film ^a), eV	2.61/2.7	2.75/—
ΔE_{ST} (THF/doped film ^a), eV	0.1/0.11	0.04/—

^a Doped films are **5a** (10 wt.%) in mCP and **5b** (10 wt.%) in mCP as well as **5a** (20 wt.%) in mCBP and **5b** (20 wt.%) in mCBP. First singlet (S₁) and triplet (T₁) levels were taken at set-on of PL and phosphorescence spectra recorded at 77 K, respectively. PLQYs of solid films were measured under air atmosphere

The neat films exhibited non-structured PL spectra, peaking at 502 and 598 nm, respectively, for **5a** and **5b**. The PL spectra of **5a** and **5b** exhibited a shift when compared to the PL spectrum of the compound **I** film.⁶⁶ This shift could be attributed to either their distinct dielectric constants or the formation of aggregates. A low-intensity shoulder was detected in the PL spectrum of the **5b**-doped mCP film, specifically within the wavelength range of 400 nm to 500 nm. Thus, the PL spectrum of compound **5b** is a result of the overlapping of at least two emission bands.

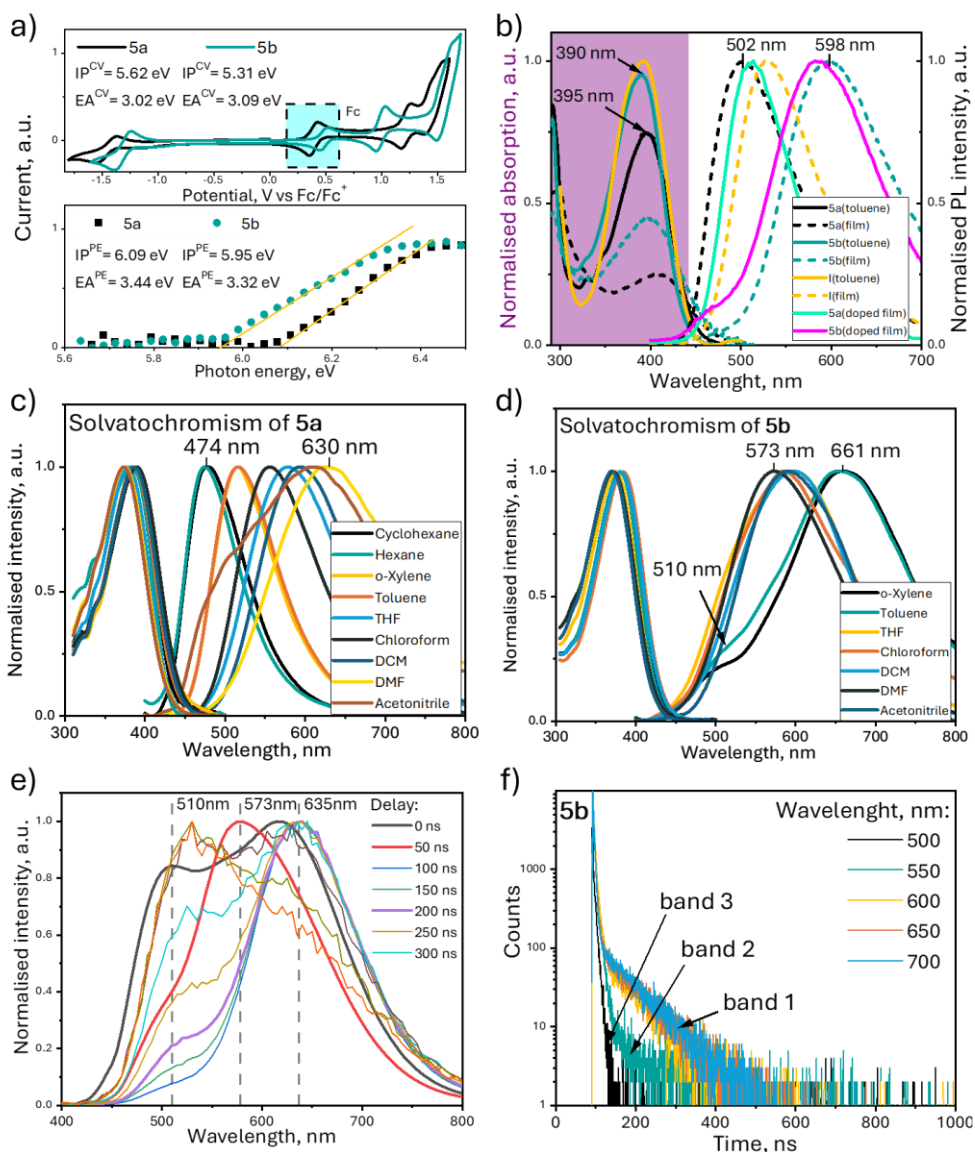


Fig. 14. a) CV and PE spectra of compounds **5a** and **5b**. b) UV-Vis and PL spectra (ex. 350 nm) of **5a**, **5b**, and **I** in toluene solution, as well as neat and doped films (mCP host). c) and d) Solvent effects on the UV-Vis and PL spectra of **5a** and **5b**, respectively, in dilute solutions (ca. 10^{-4} mg/mL). e) Time-resolved PL spectra of **5b** in toluene solution at different time delays after excitation. f) PL decay curves of **5b** in toluene solution recorded at various emission wavelengths

Furthermore, solvatochromic measurements allow more information to be obtained on the emission nature of organic compounds. In the case of normal TADF, organic compounds exhibit CT emission that is strongly sensitive to solvent polarity.

Therefore, non-structured emission spectra with a single broad band of the conventional TADF emitters must be broadened and red-shifted with an increasing solvent polarity due to the CT character of the first singlet excited state. Compound **5a** was characterised by broadened emission spectra from 78 nm of its *full width at half-maxima* (FWHM) for the solution in hexane to FWHM of 180 nm for the solution in DMF (Fig. 14 c).

In the case of dual TADF emitters, non-structured emission spectra with two broad bands have to be observed. Both bands have to be broadened and red-shifted with an increasing solvent polarity due to the CT character of the first and second singlet excited states being in disagreement with the Kasha rules at the same time. The PL spectra of the solutions of compound **5b** in solvents with a higher polarity were also recorded (Fig. 14 d). The emission of compound **5b** was observed by solvatochromic measurements, which revealed the overlap of three bands (at approximately 510, 573, and 635 nm) of different natures. These bands were separated by time-resolved PL measurements, allowing for the separation of prompt and delayed fluorescence spectra (Fig. 14 e, f). The high energy band, which was observed in the PL spectrum of the toluene solution of compound **5b**, reached its maximum at 510 nm. It is associated with fluorescence that occurs when the LE states recombine. This fluorescence is characterised by a single-exponential PL decay that occurs within the nanosecond range (Fig. 14 f). By varying the time delays for cutting the prompt fluorescence at 500 nm, it was found that the highest intensities were observed for the other bands (573 and 635 nm) which exhibit double exponential photoluminescence decays, thus suggesting a mixture of prompt and delayed fluorescence resulting from the recombination of various excited charge transfer states (Fig. 14 e, f).

In order to gain a deeper understanding of the emission nature of compounds **5a** and **5b**, PL spectra and PL decays of the films of **5a** and **5b** dispersed in mCP host were recorded at different temperatures (Fig. 15 a, b). A small ΔE_{ST} was obtained for THF solutions of **5a** and **5b** (0.1 eV and 0.04 eV, respectively) and for the film of **5a** doped in mCP (0.11 eV). Long-lived fluorescence of compounds **5a** and **5b** was identified as TADF since its intensity grew up with an increasing temperature.

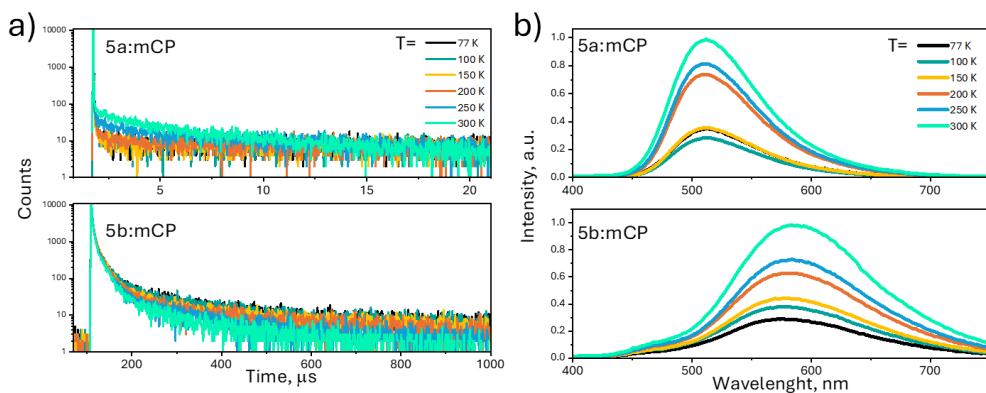


Fig. 15. a) PL decay curves and b) corresponding PL spectra recorded at various temperatures for films of compounds **5a** and **5b** doped in mCP

Based on theoretical computations (TD-DFT) (performed by a co-author of the article under discussion, Dr. Viktorija Andrulevičienė), it can be concluded that TADF of **5a** is related to CT transitions from 3,6-di-tert-butyl-9-phenylcarbazole moieties to phenylpyridine-3,5-dicarbonitrile units ($S_1 - S_0$), while the dual TADF of **5b** corresponds to CT transitions from 3,7-dibromophenothiazine moieties to phenylpyridine-3,5-dicarbonitrile units ($S_1 - S_0$) and pyridine-3,5-dicarbonitrile units ($S_2 - S_0$).

Further, the study was continued, and the investigated emitters were tested as emitters in neat and host-guest system configuration OLEDs. A device with the following structure was used to investigate the impact of the emitters **5a** and **5b** on the device efficiency:

- ITO/MoO₃ [0.6 nm]/NPB [35 nm]/mCP [6 nm]/**5a** (or **5b**) (30 or 100 wt.):mCP [25 nm]/TSPO1 [6 nm]/TPBi [35 nm]/LiF [0.6 nm]/Al

Neat and doped devices n-5a, d-5a, n-5b, and d-5b with light-emitting layers of **5a**, **5a** (30 wt.):mCP, **5b**, or **5b** (30 wt.):mCP were fabricated. In the device name, ‘n’ stands for ‘neat’, and ‘d’ stands for ‘doped’ in a host-guest system-based device. A stable green and orange EL was observed under different applied voltages for the devices based on **5a** and **5b**, respectively (Fig. 16 a).

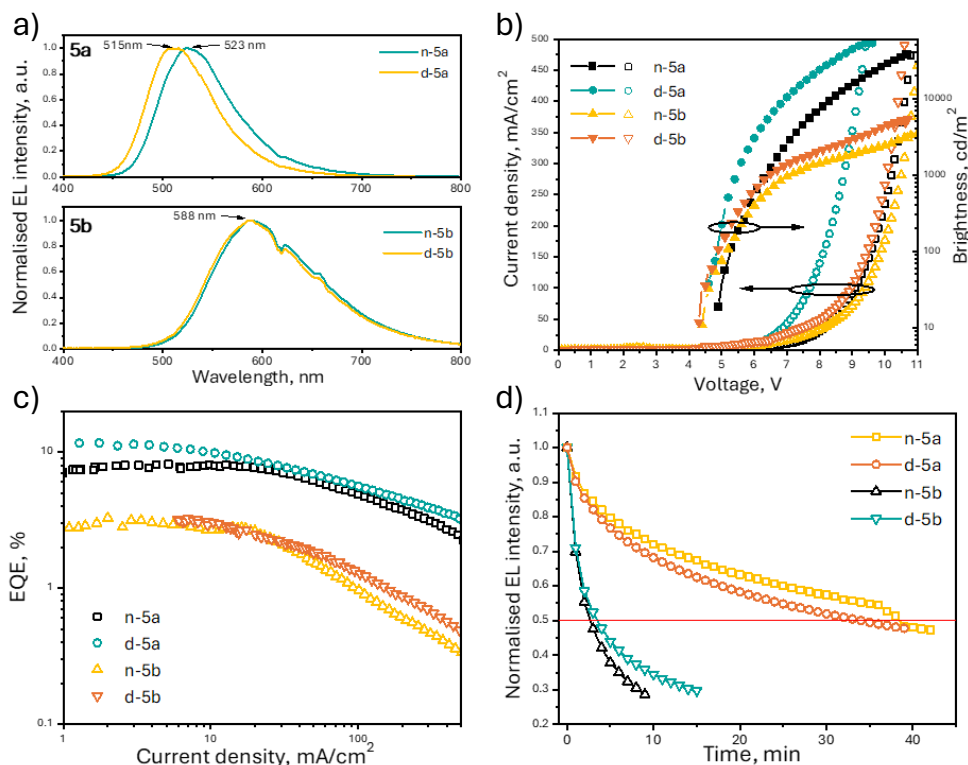


Fig. 16. a) EL spectra at 8 V; b) Current density and brightness as a function of voltage; c) EQE versus current density; and d) Operational lifetimes of non-passivated devices under ambient air conditions at a constant voltage of 5 V

The devices n-5a and d-5a had a higher turn-on voltage than those of the devices n-5b and d-5b. Such turn-on voltages are in good agreement with compound **5a** having a higher IP^{PE} value (6.09 eV) compared to **5b** (5.95 eV). Devices n-5a and d-5a exhibited a maximum brightness that exceeded 30,000 cd/m², while devices n-5b and d-5b had a maximum brightness approximately one magnitude lower, at >3,000 cd/m². This observation may be related to different efficiencies of the devices and/or to the different sensitivity of human eyes to green and orange light. Despite the comparable values of PLQY, a similar trend was observed for EQEs as well as brightness. Devices n-5a and d-5a demonstrated respectable values of 8.1 and 11.7% of EQE, while n-5b and d-5b exhibited approximately 3 times lower values at 3.1 and 3.2% of EQE, respectively (Fig. 16 c, Table 6). The different device efficiencies can also be explained by the different nature of the TADF of compounds **5a** and **5b**. In the event of a dual TADF emission of compound **5b**, energy transfer occurs through internal conversion (IC) from S_2 to S_1 with quantum yields lower than 100%. This additional energy transfer leads to a decrease in the emission efficiency and an extended emission decay of compound **5b**. This statement is supported by a long PL

decay of **5b**, reaching one millisecond (Fig. 15 a). The long emission lifetime of compound **5b** can enhance the probability of exciton–exciton and exciton–polaron annihilations under electrical excitation, which can lead not only to a low EQE, but also to low device lifetimes.⁶⁷ Indeed, the lifetimes of devices n-5b and d-5b were considerably shorter than those of devices n-5a and d-5a (Fig. 16 d).

Table 6. Electroluminescence parameters of the OLEDs

Devices	V _{on} ^a , V	λ _{EL} ^b , nm	EQE _{max} , EQE ₁₀₀ , EQE ₁₀₀₀ ^c (%)
n-5a	4.9	515	8.1, 8.0, 7.8
d-5a	4.6	523	11.7, 11.1, 10.7
o-5a	3.9	512	25.0, 15.2, 11.8
n-5b	4.4	588	3.1, 2.8, 2.6
d-5b	4.3	588	3.2, 3.1, 2.7
o-5b	5.1	582	5, 3.5, 0.6

^a V_{on} value taken at 10 cd/m². ^b λ_{EL} value taken at 5V. ^c EQE_{max}, EQE₁₀₀, and EQE₁₀₀₀ were taken at sets 10, 100, and 1000 cd/m², respectively

In order to optimise the OLEDs, the EL properties of TADF emitters **5a** and **5b** were also studied by exploring the device structure:

- ITO/HAT-CN [5 nm]/NPB [40 nm]/TCTA [10 nm]/ mCBP [10 nm]/**5a** (or **5b**) (20 wt.%):mCBP [50 nm]/NBPhen [30 nm]/Liq [2 nm]/Al

naming devices as o-5a and o-5b, respectively, where ‘o’ stands for ‘optimised’. By using this structure, efficient hole and electron injection/transport was achieved. This statement is further supported by the same EL spectra observed at the different applied voltages which are completely related to the emission of compounds **5a** and **5b** (Fig. 17 a, b). The trends in the dependencies of the current density – voltage and voltage brightness of devices o-5a and o-5b are in very good agreement with those of devices n-5a, d-5a, and n-5a, d-5a, respectively (Fig. 16 b, c).

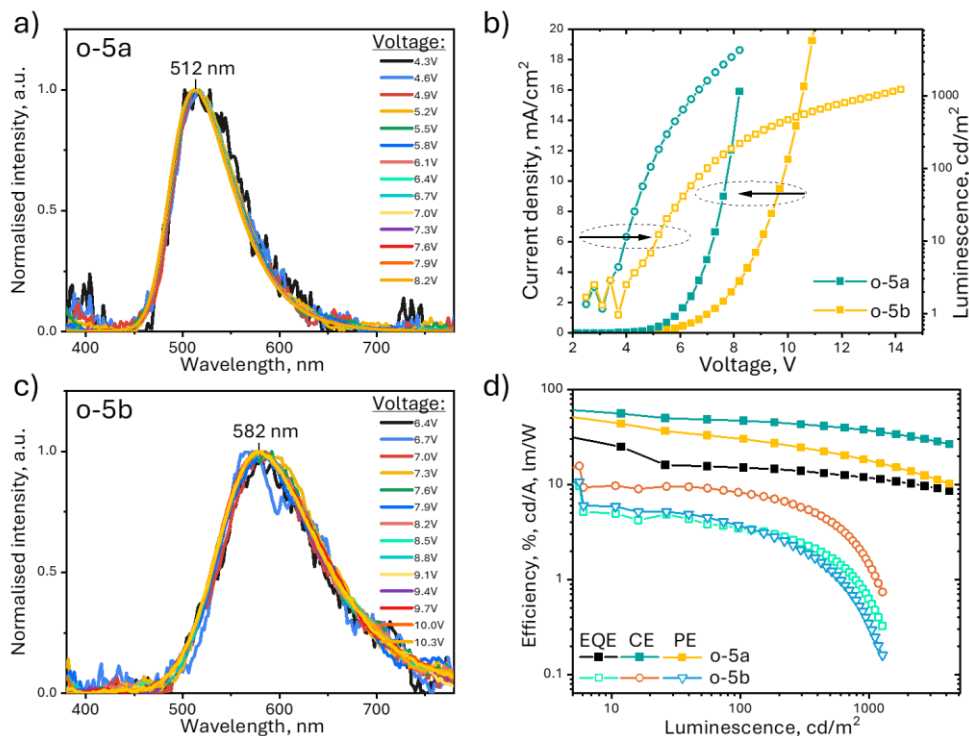


Fig. 17. a) and c) EL spectra recorded at various voltages; b) Current density and luminescence as a function of applied voltage; and d) EQE plotted against luminescence, all for the optimised devices o-5a and o-5b

Nevertheless, the optimisation of device structures allowed the improvement of maximum EQEs up to impressive 25% and 5% for devices o-5a and o-5b mainly due to the improvement of hole–electron recombination (Fig. 17 d).

This study investigated two dicyanopyridines that were substituted by multiple donors. One dicyanopyridine had three donors of the same type, specifically, 3,6-di-*tert*-butyl-carbazole, while the other dicyanopyridine had two types of donors, namely 3,6-di-*tert*-butyl-carbazole and 3,7-dibromophenothiazine, in its molecular structure. These compounds demonstrate effective green, and orange thermally activated delayed fluorescence as a result of the recombination of two intramolecular charge transfer states. OLEDs with 3,7-dibromophenothiazine and 3,6-di-*tert*-butyl-carbazole-containing emitter (**5b**) exhibiting dual TADF showed low device lifetimes and a low maximum EQE of 3.1 (for the neat emissive layer-based device) and 5% (for the doped device), while OLEDs based on 3,6-di-*tert*-butyl-carbazolyl multiple substituted dicyanopyridines (**5a**) exhibiting normal TADF showed relatively high device lifetimes and a high maximum EQE of 8.1 (for the neat emissive layer-based device) and 25% (for the doped one). It can be concluded that the ultra-long emission decay of **5b** prevents direct and efficient recombination of charges, thus letting us

know that shorter PL decays may be more favourable when looking for the overall stability and efficiency of OLEDs.

3.4. 3,5-Dicyanopyridine Motifs for Electron-Transporting Semiconductors: from Design and Synthesis to Efficient Organic Light-Emitting Diodes (scientific publication No. 4, Q1, 5 quotations)

This sub-chapter is based on the paper published in *Journal of Materials Chemistry C*, 2023, 11, 28 by K. Leitonas, B. Vigante, D. Volyniuk, R. Keruckienė, P. Dimitrijevs, T. L. Chiu, J. V. Gražulevičius, and P. Arsenyan.⁶⁸

Inorganic light-emitting diodes (LEDs) became popular in the late 1990s because of their superior efficiency, extended lifespan, and cost-effectiveness.⁶⁹ OLEDs emerged as competitors to LEDs because of their distinctive characteristics, such as optical transparency and flexibility.⁷⁰ In 1999, the development of phosphorescent emitters resulted in an increase in the theoretical IQE to 100%.⁷¹ Commercial OLED products currently utilise phosphorescent OLED emitters in green and red colours.⁷² Nevertheless, the duration of functionality and the financial burden associated with blue phosphorescent noble metal complexes continue to impede the development of blue-emitting OLEDs. In 2012, researchers demonstrated that thermally activated delayed fluorescence (TADF) materials can achieve a theoretical IQE of 100% while using singlet and triplet excitons.⁷³ TADF materials exhibit reduced toxicity, offer cost advantages, and have already achieved an EQE exceeding 40%.⁷⁴ Such state-of-the-art OLED efficiency was achieved with the help of a suitable host for an active emissive layer system. The hosts facilitate the enhancement of hole-electron recombination by ensuring charge equilibrium within the light-emitting layers. Furthermore, they enable the reduction of emission quenching phenomena, such as concentration quenching, singlet-triplet interactions, or triplet-triplet annihilations, among others.⁷⁵ Typically, most OLED hosts exhibit hole-transporting or bipolar properties, where the mobility of holes is higher than the mobility of electrons under the same electric field.^{76,77} However, there is a limited range of OLED hosts that are capable of transporting electrons.⁷⁸

In order to mitigate this constraint, the compound 3,5-dicyanopyridine was chosen as a fundamental component for the development of organic semiconductors that facilitate the transport of electrons. Pharmaceutical agents for medical applications have used derivatives of 3,5-dicyanopyridine,^{79,80,81,82,83,84} although their usage in optoelectronic devices remains limited. This study evaluated the suitability of 3,5-dicyanopyridine motifs for creating compounds specifically for optoelectronic purposes. Three derivatives of 3,5-dicyanopyridine (Fig. 18) were investigated by electrochemical, photophysical, electrooptical, and electroluminescent methods. OLEDs based on the TADF emitter 4,6-di(9,9-dimethylacridan-10-yl)isophthalonitrile (DAcIPN) and 3,5-dicyanopyridine host (**FPDD**) were created, achieving a maximum EQE of 21.9%. This is notably higher than the EQE observed for a reference OLED based on the commercially available mCBP host.

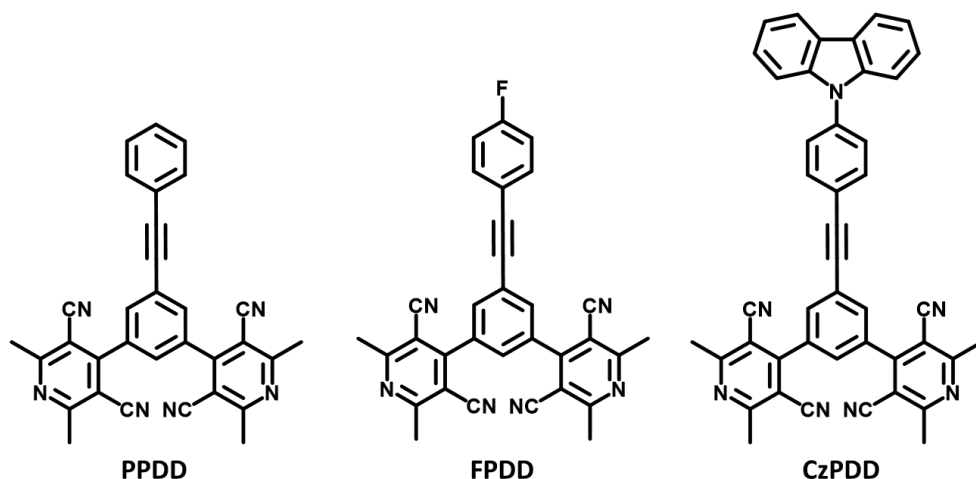


Fig. 18. Chemical structures of compounds **PPDD**, **FPDD** and **CzPDD**

In the first place, the study investigated the electrochemical properties of **PPDD**, **FPDD**, and **CzPDD** using CV. All three derivatives showed irreversible oxidation and quasi-reversible reduction processes in the potential range. The stronger electron-donating ability of the carbazole moiety resulted in a lower IP^{CV} value for compound **CzPDD** (5.7 eV) compared to **PPDD** (5.92 eV) and **FPDD** (6.06 eV). Electron affinity (EA^{CV}) values were comparable for all three compounds (2.95–2.98 eV). The **CzPDD** compound film had a slightly higher IP^{PE} value (5.94 eV) due to the interaction between the molecules in the film. Unfortunately, due to technical limitations of photoelectron emission spectroscopy in air, for the other two compounds, we were unable to obtain experimental IP^{PE} values. All IP values are given in Table 7.

Table 7. Electrochemical and photoelectrical parameters of compounds

	^a IP^{CV} , eV	^b EA^{CV} , eV	^c E_g^{opt} , eV	^d IP^{PE} , eV	^e EA^{PE} , eV
PPDD	5.92	2.96	3.74	n/a	n/a
FPDD	6.06	2.95	3.83	n/a	n/a
CzPDD	5.7	2.98	3.25	5.94	2.69

^a $IP^{CV}(\text{eV}) = E_{\text{onset, ox}}(\text{V}) + 4.8$, ^b $EA^{CV}(\text{eV}) = E_{\text{onset, red}}(\text{V}) + 4.8$, ^c Optical bandgap taken from onset of the low-energy absorption band, ^d Ionisation potentials (IP^{PE}) of the solid samples estimated by photoelectron emission in air, ^e electron affinity (EA^{PE}) was calculated by $IP^{PE} - E_g^{opt} = EA^{PE}$

The UV-Vis absorption and PL spectroscopies were employed to characterise the photophysical properties of **PPDD**, **FPDD**, and **CzPDD**. The absorption spectra of the compounds **PPDD** and **FPDD** were nearly identical, exhibiting a strong peak at approximately 280–290 nm, and a distinct shoulder at around 296 nm (Fig. 19 a). The compound **CzPDD**, which contains a phenyl carbazole group, displayed distinct

absorption spectra. It showed a high-energy band that reached its peak at approximately 290 nm, as well as a less intense band with a visible maximum at around 333 nm. An intramolecular charge-transfer (ICT) phenomenon was detected between the carbazole, which donates electrons, and the 3,5-dicyanopyridine, which accepts electrons, at wavelengths greater than 340 nm.

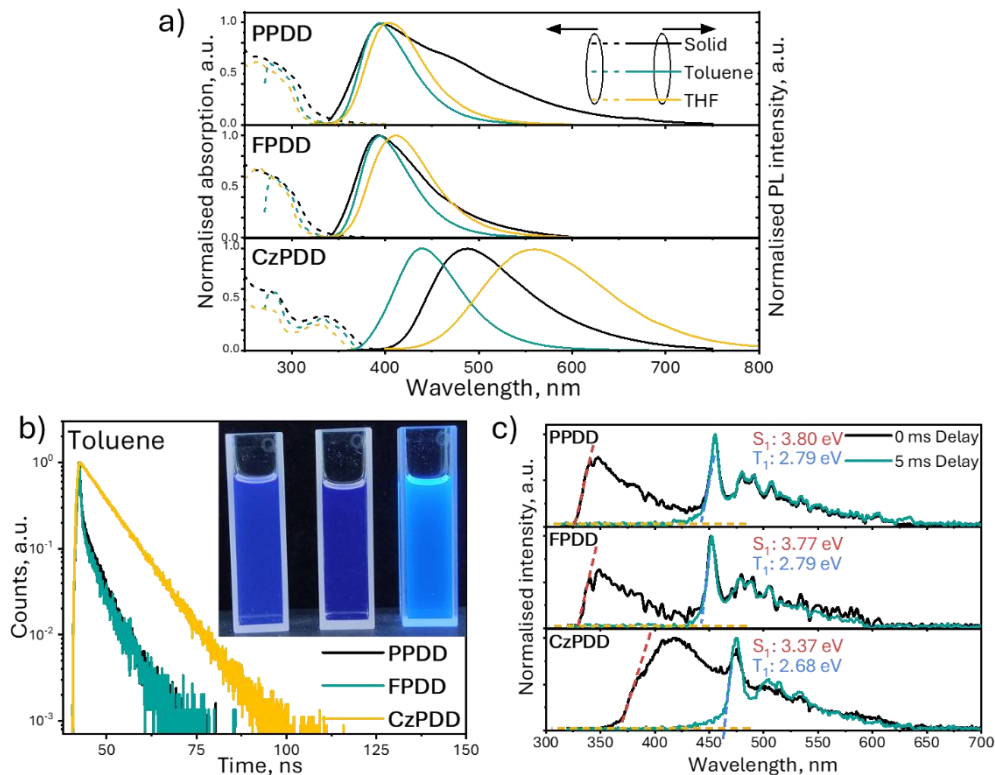


Fig. 19. a) Normalized UV-Vis and PL spectra comparing solid-state, toluene, and THF solutions (1×10^{-5} M) of **PPDD**, **FPDD**, and **CzPDD**. b) PL decay kinetics in toluene solutions. Inset: Sample images under UV illumination. c) Low-temperature (77 K) PL and PH spectra in THF (ex. 300 nm for **PPDD**, **FPDD**; 340 nm for **CzPDD**)

The absorption spectra of various solutions and films of **PPDD**, **FPDD**, and **CzPDD** did not exhibit significant variations. However, the compounds displayed an intensified absorption tail beyond wavelengths exceeding 350 nm. The lack of significant changes in the absorption maxima with a varying solvent polarity suggests that compound **CzPDD** has a relatively nonpolar ground state. The impact of the media polarity is clearly demonstrated in the excited states, as indicated by the red shifts observed in the photoluminescence spectra of compound **CzPDD** solutions when using solvents with a higher polarity (Fig. 19 a).

The triplet energy of organic electroactive compounds is a crucial factor in determining suitable hosts for phosphorescent or TADF OLEDs. Compounds **PPDD**

and **FPDD** exhibited an identical triplet energy of 2.79 eV, which aligns with the results obtained from steady-state PL spectrometry measurements. Compound **CzPDD** also showed a relatively high triplet energy of 2.68 eV, while its singlet (3.37 eV) was lower than those of compounds **PPDD** and **FPDD** (Fig. 19 c, Table 8). When the high triplet energies of **PPDD**, **FPDD**, and **CzPDD** are considered, it can be assumed that these compounds could be used as hosts for different OLED emitters.

The PL spectra of the diluted solutions of compound **CzPDD** exhibit a significant red shift, with the emission peak wavelength changing from 439 nm in a toluene solution with a low polarity to 560 nm in a THF solution (Fig. 20 a). The solid sample of compound **CzPDD** exhibited its highest emission intensity at 487 nm, which is between the emission intensities of toluene and THF solutions. The absorption spectra of the compounds under discussion showed a minor correlation with the solvent polarity, whereas the wavelengths and profiles of emissions were significantly influenced by the polarity of the surrounding medium.

However, compounds **PPDD** and **FPDD**, which contain phenyl and fluorophenyl groups, showed minimal disparities in the emission energy when dissolved in low polarity solvents (Fig. 20 a, b, c). Nevertheless, when the solutions were placed in highly polar solvents like dimethylformamide (DMF) and acetonitrile, significant shifts towards longer wavelengths and broadening of the spectra were observed. The highest emission wavelengths of the **PPDD** and **FPDD** solutions in toluene were observed at 394 nm, whereas for the solutions in DMF, they appeared at 431 nm and 440 nm, respectively. The FWHM for the solutions of compounds **PPDD** and **FPDD** in toluene was determined to be 60 nm and 62 nm, respectively. In contrast, the FWHM values for the solutions in DMF were measured to be 91 nm and 93 nm, respectively. This broadening of emission signifies the potential for CT emission. FWHM of **CzPDD** also increased dramatically from 83 nm for the solution in low-polarity toluene to 225 nm for the solution in polar DMF. This observation confirms intensive CT that occurs due to well-balanced donor and acceptor interactions.

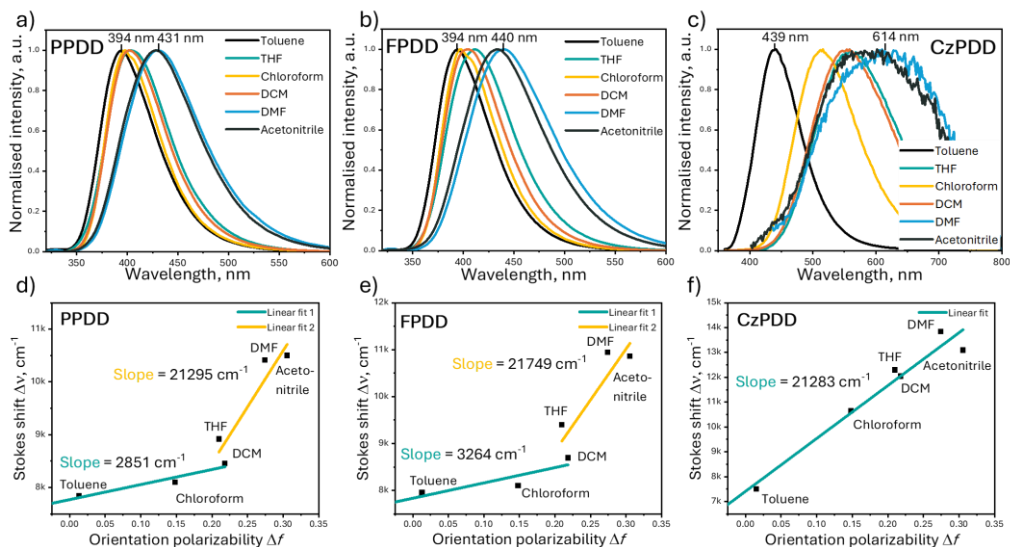


Fig. 20. Normalised PL spectra of the solutions (1×10^{-5} M) of a) **PPDD**, b) **FPDD**, and c) **CzPDD** in the solvents of the different polarity and the corresponding Lippert–Mataga plots d), e) and f) of dependencies of the Stokes shifts $\Delta\nu$ on solvent orientation polarizability function Δf

PPDD and **FPDD** display non-linear relationships of Lippert–Mataga equation plots (Fig. 20 d, e, f). The obtained non-linear data can be fitted by two linear functions for solvents with a low and high polarity. The presence of a dual tendency suggests the characteristics of hybridised local and charge transfer (HLCT) states.⁸⁵ The emission is primarily influenced by the relaxation of locally excited states of **PPDD** and **FPDD** molecules that are uniformly distributed in low-polarity media. However, the emission of **PPDD** and **FPDD** solutions in solvents of a higher polarity, such as THF and dichloromethane (DCM), can be attributed to CT states. Such a dual character of locally excited and CT emission further indicates HLCT-type emission for **PPDD** and **FPDD**.

The emission efficiency of the TADF emitters is influenced by the characteristics of the hosts employed.^{86,87} In order to evaluate the hosting capabilities of **PPDD**, **FPDD** and **CzPDD**, the highly effective TADF emitter DACIPN was chosen based on the overlap of the absorption spectrum of DACIPN and the emission spectra of the hosts investigated in the solid state. The high triplet energies of **PPDD**, **FPDD**, and **CzPDD** are anticipated to limit the dissipation of the triplet energy from DACIPN through the triplet levels of the host materials.

A comparison was made between the hosting properties of **PPDD**, **FPDD**, and **CzPDD** and the reference host mCBP. The PL spectra and PL decay curves of DACIPN (10 wt.%) that was dispersed at the molecular level were measured in various hosts (Fig. 21). Minor variations in the PL spectra of films containing DACIPN were detected, suggesting that the emission properties of the TADF emitter DACIPN are influenced by the conformational and static dielectric disorders of the host materials.⁸⁸

Different intensities of delayed fluorescence of DAClPN molecularly dispersed in hosts **PPDD**, **FPDD** and **CzPDD** and mCBP were observed, indicating the different TADF efficiency. The lowest intensity of the delayed fluorescence of DAClPN was detected when it was dispersed in the host **PPDD** (Fig. 21 b). The variation in the TADF efficiency of DAClPN can be attributed to the difference in ΔE_{ST} of DAClPN when it is dispersed in various hosts.

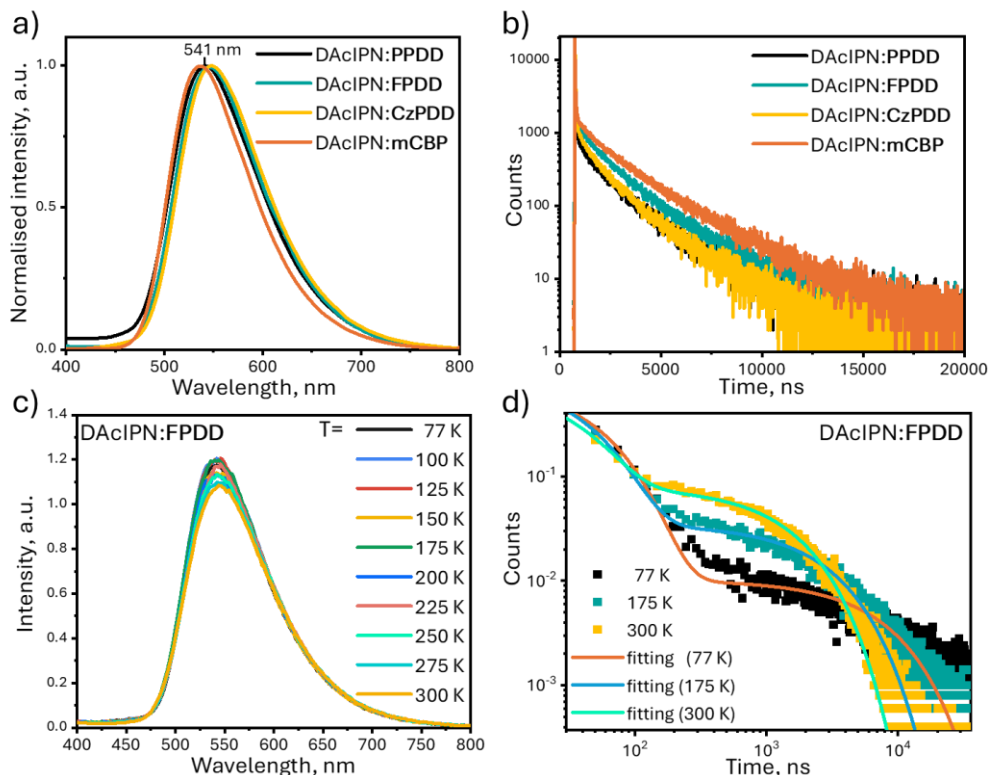


Fig. 21. a) PL spectra and b) corresponding PL decay curves recorded in vacuum for solid solutions of DAClPN (10 wt.%) in various hosts (**PPDD**, **FPDD**, **CzPDD**, and **mCBP**). c) PL spectra and d) PL decay curves of the DAClPN (10 wt.%) solid solution in **FPDD** host, measured at different temperatures

For further estimation of the host effects of the compounds, samples were investigated within a temperature range of 77 to 300 K (Fig. 21 c, d), which provided enough details to calculate the emission kinetics, such as reverse intersystem crossing (k_{RISC}). The DAClPN TADF emitter exhibited different k_{RISC} values when distributed uniformly at a molecular level in various host materials: $1 \times 10^5 \text{ s}^{-1}$ for **PPDD**, $1.3 \times 10^6 \text{ s}^{-1}$ for **FPDD**, $6 \times 10^5 \text{ s}^{-1}$ for **CzPDD**, and $1.7 \times 10^6 \text{ s}^{-1}$ for mCBP. Such results highlight that compounds **FPDD** and **CzPDD** are more promising as OLED hosts than compound **PPDD**.

The fabrication of OLEDs was conducted as the final phase of the experimental study. The study examined the performance of **FPDD** and **CzPDD** as hosts in OLEDs with the following structure:

- ITO/HAT-CN [5 nm]/NPB [40 nm]/TCTA [10 nm]/mCBP [10 nm]/DAcIPN:Host [50 nm]/NBPhen [30 nm]/Liq:Al

Figure 22 a shows the energetic configuration of OLEDs. The composition of the emissive layer was 90 wt.% of the host (compound **FPDD** in device **A**, **CzPDD** in device **B**, and **mCBP** in device **C**) (Fig. 22 a, Table 8). In all cases, the emissive layer also contained 10 wt.% of the emitter DAcIPN.

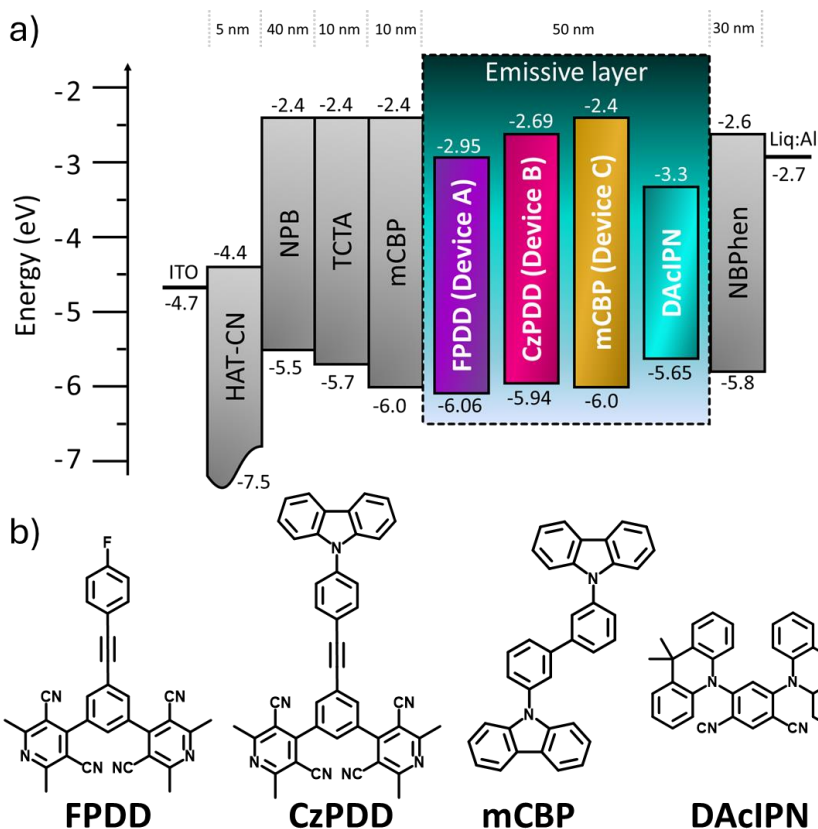


Fig. 22. a) Energy level diagram of devices **A–C** and b) molecular structures of the compounds used for the preparation of light-emitting layers of the devices

The EL spectra of devices **A–B** are very similar with a peak at 540 nm. Although, the PL spectrum of the reference OLED with the **mCBP** host was slightly blue-shifted and peaked at 526 nm. Since the emitter DAcIPN exhibits strong solvatochromic properties,⁸⁹ this minor EL shift is mainly related to a different polarity of the **mCBP** matrix compared to the polarities of the dicyanopyridine

derivatives **FPDD** and **CzPDD**. The EL spectra of devices **A–C** agree well with the PL spectra of the corresponding light emitting films (Fig. 21 a).

Table 8. EL characteristics of OLEDs **A–C**

Device	A	B	C
Emissive layer	DACIPN (10 wt.%): FPDD	DACIPN (10 wt.%): CzPDD	DACIPN (10 wt.%): mCBP
V_{ON} , V @ 10 cd/m ² ^a	3.76	3.2	4.3
CE_{max} , CE_{100} , CE_{1000} , cd/A ^b	43.2, 39.7, 31.7	14.6, 13.1, 12.4	23.9, 22.4, 18.8
PE_{max} , PE_{100} , PE_{1000} , lm/W ^c	36.7, 27.8, 17.0	14.8, 10.4, 7.1	17.5, 14.4, 9.6
EQE_{max} , EQE_{100} , EQE_{1000} , % ^d	21.9, 12.1, 9.5	8.6, 4.0, 3.7	12.2, 6.7, 5.6
Peak, nm @ 1000 cd/m ² ^e	540	542	526

^a Turn-on voltage measured at initial brightness of 10 cd/m². ^b Current efficiency. ^c Power efficiency and ^d External quantum efficiency taken at maximum brightness, at 100 and at 1000 cd/m². ^e Wavelengths of the peaks of EL spectra

Devices **A–C** demonstrated rather high maximum EQE values of 21.9, 8.6 and 12.2%, respectively (Fig. 23, Table 8). Furthermore, devices **A** and **B** with the investigated compounds **FPDD** and **CzPDD** as hosts exhibited low turn-on voltages (V_{ON}) of less than 4 V. Whereas, device **C**, with a commercial host **mCBP**, showed a V_{ON} value slightly higher than 4 V. The low V_{ON} indicates that the OLED energy structure was selected appropriately, and that there were no noticeable barriers for charges to overcome.

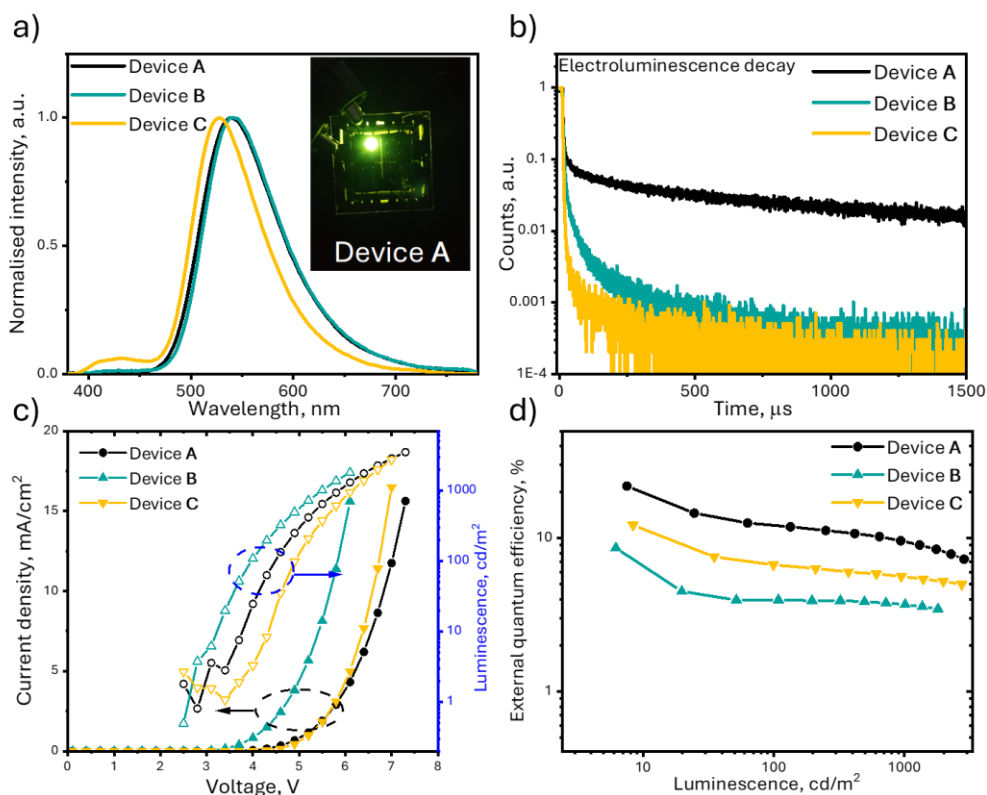


Fig. 23. a) Normalised EL spectra and b) corresponding decay curves for devices A–C. c) Current density and luminescence as a function of applied voltage, and d) EQE plotted against luminescence for devices A–C

Interestingly, device **A** with **FPDD** as a host showed nearly twice the efficiency of the reference device **C** with mCBP (21.9% vs 12.2%). The disparity in the EQE values of devices A–C can be explained by the better hosting properties of **FPDD** compared to those of **CzPDD** or mCBP. Apparently, triplets can be harvested more efficiently by the DAcIPN emitter when it is dispersed in the host **FPDD** than in the hosts **CzPDD** or mCBP. Furthermore, significantly longer EL decays were observed for device **A** compared to the other two devices (Fig. 23 b), thereby further supporting the statement of more efficient triplet harvesting.

The findings indicate that the dicyanopyridine derivative with a fluorophenyl group (**FPDD**) has a great potential to enhance the efficiency of green TADF OLEDs. Furthermore, the use of host **FPDD** extends beyond the green emitters. Considering its high triplet level of 2.79 eV, the host **FPDD** can be used for blue emitters that emit light at wavelengths greater than 450 nm. Based on its HOMO/LUMO values (6.06/2.95 eV), the host **FPDD** is suitable for emitters with bandgaps less than 3.11 eV.

4. CONCLUSIONS

4.1. In the course of this study, three types of vertical organic permeable-base light-emitting transistors (OPB-LETs) – namely orange, blue, and white – were investigated. It has been demonstrated that the application of the exciplex emitters in OPB-LETs, utilising a vertical device structure, successfully achieved high-quality white electroluminescence:

4.1.1. **Orange Exciplex Development:** It has been found that an orange exciplex could be created by combining a novel blue emitter with donor material TAPC in equal proportions. This exciplex displayed a minimal singlet-triplet energy splitting (ΔE_{ST}) of 0.02 eV and exhibited strong TADF properties. By using this combination in the emissive layer, previous challenges related to electron injection in OPB-LETs were overcome, thus marking a significant advancement in material utilisation.

4.1.2. **Performance of White OPB-LETs:** The newly developed white OPB-LETs were shown to achieve a maximum external quantum efficiency of 2.4%, coupled with a low turn-on voltage of 3.3V and a high maximum brightness of 300 cd/m². Additionally, these devices had the capability to modulate the current density (J_{EC}) and brightness by adjusting the base voltage (V_{EB}), underscoring the potential of these synthesised materials to enhance the efficiency and performance of electroluminescent devices.

4.1.3. **Colour Quality:** It was observed that the white OPB-LETs reached colour rendering indexes ranging from 77 to 93, along with stable CIE colour coordinates. These results suggest a high colour quality, making these devices potentially suitable for a variety of lighting applications.

The findings from this study not only further the understanding of TADF mechanisms in organic emitters but also underscore the practical viability of exciplex-based white OPB-LETs, paving the way for future innovations in the electroluminescent technology.

4.2. Further investigations were conducted on a series of newly synthesised donor-acceptor-donor (D-A-D) type molecules, specifically, carbazole or acridan-substituted dibenzo[a,c]phenazines (**CzDbp** and **AcDbp**). These molecules were examined through steady-state and time-resolved spectroscopy, which highlighted their efficacy in triplet exciton harvesting via both TTA and TADF mechanisms, along with their excellent emissive and hosting properties:

4.2.1. **Photophysical Properties:** The photophysical investigation indicated that **CzDbp** and **AcDbp** possess distinct properties that are beneficial for high-performance electroluminescent applications. These properties include efficient triplet harvesting through a combination of competitive TADF and TTA mechanisms, providing a deeper understanding of the mechanistic pathways that influence the device performance.

4.2.2. **Application in OLEDs:** Initially, these compounds were tested as triplet harvesting hosts for the red phosphorescent emitter (piq)₂Ir(acac) in OLEDs. It has been found that both compounds deliver performance which is comparable to or better than that of conventional hosts, with the **CzDbp** host achieving up to 15.9% of the external quantum efficiency. Furthermore, when tested as emitters, substantial external quantum efficiencies of 19.4% and 22.1% were achieved for orange (**AcDbp**) and yellow (**CzDbp**) OLEDs, respectively.

These investigations not only demonstrate the potential of **CzDbp** and **AcDbp** in advanced electroluminescent applications, but also contribute significantly to the field by showcasing the versatility and efficiency of these materials in high-performance OLEDs.

4.3. Further investigations were carried out on two types of multiple donor-substituted dicyanopyridines, where one type included three donors of one kind (3,6-di-tert-butyl-carbazole) (**5a**), and the other combined two types of donors (3,6-di-tert-butyl-carbazole and 3,7-dibromophenothiazine) (**5b**) within their molecular structures. These compounds were evaluated as TADF emitters for use in efficient OLEDs:

4.3.1. **TADF Emission:** It was observed that the compounds exhibited green and orange TADF from two distinct intramolecular charge transfer states. These findings demonstrate the potential of these materials for use in high-efficiency electroluminescent applications.

4.3.2. **Performance Evaluation of Emitters:** The emitter designated as **5b**, which features dual TADF, has been found to suffer from non-efficient excited state relaxation, resulting in low device lifetimes and the overall low OLED efficiency, achieving only 3.1% of external quantum efficiency for neat emissive layer-based devices and 5% for doped and optimised devices. Conversely, emitter **5a**, containing only one type of donor, proved to be significantly more efficient. This emitter not only delivered relatively long device lifetimes but also achieved a high maximum external quantum efficiency of 8.1% for neat emissive layer-based devices and an impressive 25% value for doped and optimised OLEDs, thereby further signifying that the simpler and more efficient charge transfer mechanism of normal TADF in **5a** leads to its superior performance compared to **5b**, which suffers from the complexity introduced by dual donor moieties.

These results underscore the critical influence of the donor type and configuration on the efficiency and stability of TADF OLEDs, contributing valuable insights into the design of materials for future high-performance electroluminescent devices.

4.4. Research was also conducted on three derivatives of (1,3-phenylene)bis(2,6-dimethylpyridine-3,5-dicarbonitrile) with different substituents attached to the phenylene moiety (**PPDD**, **FPDD**, and **CzPDD**) to evaluate their potential as triplet harvesting hosts for OLED applications:

- 4.4.1. **Triplet Energy and Charge Transport Properties:** It was observed that all the synthesised compounds exhibited practically identical high triplet energies ranging from 2.68 to 2.79 eV. These high triplet energies are essential for effective triplet exciton harvesting and minimising energy losses through non-radiative decay pathways. Furthermore, high ionisation potentials (5.7–6.06 eV) along with comparable electron affinities around 3.0 eV were detected. These properties suggest effective charge transport mechanisms within the OLEDs, which are crucial for achieving a high electroluminescent efficiency.
- 4.4.2. **Triplet Harvesting Mechanisms:** The investigation revealed that compounds **PPDD** and **FPDD**, which contain phenyl and fluorophenyl groups, respectively, exhibit HLCT. Conversely, **CzPDD**, which incorporates a phenylcarbazole moiety, demonstrated a TADF mechanism for triplet harvesting.
- 4.4.3. **Performance as OLED Hosts:** Further testing involved compounds **FPDD** and **CzPDD** as hosts for a green TADF emitter, DAcIPN, in OLEDs. **CzPDD**, in particular, showed outstanding hosting performance, delivering a significant maximum external quantum efficiency of 21.9%. This performance marks a substantial improvement over the 12.9% efficiency observed with the conventional host mCBP, demonstrating the superior triplet harvesting properties of the novel host.

These findings highlight the importance of molecular substituents in influencing the photophysical properties and efficiencies of OLED host materials, thereby offering insights into the design of more efficient electroluminescent devices.

5. SANTRAUKA

5.1. Įvadas

Aiškiai prisimenu, kaip pradėjome organinės chemijos kursą mokykloje. Tai buvo reikšmingas poslinkis nuo paprasto cheminių lygčių balansavimo iki sudėtingų, anglies pagrindu sukurtų grandinių ir šešiakampių žiedų analizės. Dar nežinojau, kad šios pirmosios organinės chemijos pamokos taps pagrindu suprasti sritį, kuri dabar yra modernių technologijų priešakyje.

Organinių puslaidininkių tyrinėjimą skatina jų potencialas ir iššūkiai. Šios medžiagos, daugiausia sudarytos iš anglies pagrindu sukurtų mažų molekulių arba polimerų, turi pranašumų prieš tradicinius neorganinius puslaidininkius. Jos yra iš prigimties lanksčios, potencialiai pigesnės gaminti ir gali būti apdorojamos tirpalais.¹ Dėl tokių savybių organiniai puslaidininkiai labai tinka lankstiems ekranams, dėvimai elektronikai ir biologiškai skaidiems jutikliams gaminti. Tai pažymi juos kaip svarbias dalis elektroninių prietaisų evoliucijoje link tvaresnių ir universalesnių technologijų^{2,3,4}.

Tačiau organiniai puslaidininkiai taip pat turi trūkumų. Istoriskai jų elektroninės ir optinės savybės atsiliko nuo neorganinių puslaidininkių, dažnai pasižyminčių mažesniu krūvininkų mobilumu ir operaciniu stabilumu.^{3,8,10,11,12} Šie trūkumai kelia reikšmingų iššūkių, bet taip pat skatina sritį vystytis, nes mokslininkai stengiasi išnaudoti ir pagerinti šių organinių medžiagų esmines savybes. Viena iš daugiausiai žadančių tyrimų krypčių yra efektyvus eksitonų – elektronų ir skylių būvių puslaidininkyje valdymas, todėl jos yra puikios kandidatės optoelektroninėms taikymo sritims.^{13,14} Vis dėlto efektyviai išnaudoti šiuos eksitonus šviesos emisijai išlieka iššūkiu. Norint tai pasiekti, tyrinėjami reiškiniai, tokie kaip termiškai aktyvuotoji uždelsta fluorescencijos (TADF), tripleto-tripleto anihiliacija (TTA) ir hibridizuotas ir vietinis krūvio pernešimas (HLCT).^{15,16,17,18,19} Šie mechanizmai leidžia konvertuoti tripletinius eksitonus, kurie paprastai neprisideda prie šviesos emisijos, į singletinius eksitonus, kurie skleidžia fotonus, taip pagerinant tokių prietaisų, kaip organiniai šviesą skleidžiantys diodai (OLED) ir organiniai šviesą skleidžiantys tranzistoriai (OLET), efektyvumą ir veikimą.²⁰

Šiuo metu vienas populiariausių aukšto efektyvumo organinių elektroluminescencinių prietaisų kūrimo būdų yra tripletų surinkimas (angl. *triplet harvesting*).^{15,17,18} Pagal sukinių statistiką (angl. *spin-statistics*), singletiniai eksitonai sudaro tik 25% visos populiacijos, o likusius 75% sudaro tripletiniai eksitonai.²¹ Šis pasiskirstymas daro tripletų surinkimą būtiną siekiant efektyvių OLED prietaisų, nes įprastiniuose visiškai organiniuose fluorescenciniuose prietaisuose tik singletiniai eksitonai gali būti naudojami fotonams generuoti.¹⁵ Tripletų surinkimas yra pagrįstas tripletinių eksitonų, kurie paprastai neskleidžia šviesos, konvertavimu į singletinius eksitonus, kurie skleidžia fotonus, taip padidinant teorinį vidinį kvantinį efektyvumą (IQE) nuo tik 25% iki beveik 100%.^{22,23,24}

Vienas iš efektyviausių šios konversijos metodų yra vadinamas termiškai aktyvuota uždelsta fluorescencija (TADF) kartu su atgaline interkombinacine konversija (RISC). TADF medžiagos naudoja šiluminę energiją ir labai mažą

energijos skirtumą tarp singletinių ir tripletinių lygių (ΔE_{ST}), kad konvertuotų tripletinius eksitonus atgal į singletinę būseną per RISC, leidžiant efektyvią šviesos emisiją.^{22,26,28} Tai ypač svarbu kuriant aukšto efektyvumo elektroluminescencinius prietaisus, nes tada jų gamybai nebereikia naudoti toksiškų fosforescuojančių medžiagų su sunkiaisiais metalais. TADF efekto pavyzdys yra mėlynųjų OLED prietaisų kūrimas, kurie dabar beveik prilygsta fosforescuojančioms alternatyvoms, žymintis reikšmingą pasiekimą OLED technologijoje.^{8,18} Kitas metodas, tripleto-tripletinio anihilacija (TTA), atsiranda, kai du tripletiniai eksitonai sąveikauja ir vienas perduoda energiją kitam, sudarydamas aukštesnės energijos singletinę būseną, kuri skleidžia šviesą.^{29,30,31,32} Hibridizuotas ir vietinis krūvio pernešimas (HLCT) apima naujovišką išdėstymą, kur molekulinė struktūra skatina sąveiką tarp lokalizuotų sužadintų būsenų (LE) ir krūvio pernešimo būsenų (CT).²² Ši sąveika didina tiek krūvio, tiek energijos pernešimą molekulėje, didindama šviesą skleidžiančių prietaisų stabilumą ir efektyvumą.^{34,35,36}

Nepaisant šios pažangos, iššūkių tripletų surinkimo srityje išlieka. Tripletinių eksitonų dinamikos valdymas, siekiant išvengti jų energijos praradimo ir maksimaliai padidinti šviesos emisijos efektyvumą, yra nuolatiniai šios srities mokslininkų rūpesčiai.²² Medžiagų, galinčių išnaudoti šiuos mechanizmus neprarandant spalvos kokybės ar stabilumo veikiant, kūrimas išlieka pagrindine tyrimų sritimi. Tripletų surinkimo technikų pažanga ne tik skatina vystyti organinės elektronikos sritį, bet ir remia platesnius tikslus kurti tvarius ir universalius elektroninius prietaisus. Sumažinant priklausomybę nuo retųjų ar toksiškų metalų ir didinant ekranų bei apšvietimo energijos efektyvumą, šios technologijos padeda skatinti aplinkos tvarumą ir ekonominį efektyvumą, atitinkantį ateities organinės elektronikos poreikius.

Atsižvelgiant į šiuos iššūkius, **šio darbo tikslas** yra tripletų į singletus energijos perėjimo procesų organiniuose spinduoliuose mechanizmų tyrimas ir optimizavimas, ypatingą dėmesį skiriant naujoms medžiagoms ir procesams, siekiant sukurti patobulintus didesnio efektyvumo elektroluminescencinius prietaisus.

Siekiant įgyvendinti disertacijos tikslą, buvo suformuluoti šie uždaviniai:

- Tirti eksiplekso spinduolių, demonstruojančių TADF, taikymo baltuose, organiniuose, pralaidžiosios bazės, šviesą skleidžiančiuose tranzistoriuose (OPB-LET) galimybę.
- Ištirti naujas dibenzo[a,c]fenazino pagrindu sukurtas TADF ir TTA švytinčias medžiagas ir įvertinti jų veikimą geltonai oranžiniuose-raudonuose OLED prietaisuose.
- Įvertinti skirtingų donoro tipų įtaką dicianopiridino pagrindu sukurtų TADF junginių efektyvumui OLED prietaisuose, ypatingą dėmesį skiriant prietaiso optimizavimui ir tarnavimo laikui.
- Ištirti naujų matricų tipo medžiagų veiksmingumą gerinant TADF OLED išorinio kvantinio efektyvumą (EQE), palyginti su komercine matricos medžiaga.

Darbo naujumas

- Buvo pagaminti naujos, vertikalios konfigūracijos baltą šviesą skleidžiantys organiniai tranzistoriai (OPB-LET). Pirmi bandymai su žinomais eksipleksiniais spinduoliais susidūrė su elektronų injekcijos problemomis, kurios buvo išspręstos naudojant naują oranžinį eksipleksus formuojantį spinduolį, 4,6-bis(4-(9H-karbazol-9-il)fenil)pirimidino-5-karbonitrilą (**CzPm**). Šis mėlynų eksitonų ir oranžinių eksipleksų emisijų derinys leido pasiekti didesnio ryškumo ir efektyvumo baltos šviesos emisiją, padidinant spalvų atkūrimo indeksą iki 93 ir pagerinant išorinį kvantinį efektyvumą (EQE).

- Buvo pasiekta OLED prietaisų pažanga tyrinėjant karbazolu arba akridanu modifikuotus dibenzo[a,c]fenazinus (**CzDbp** ir **AcDbp**) su donoro-akceptoriaus-donoro architektūra, siekiant išgauti TADF. Naudojant **CzDbp** kaip raudonojo fosforescuojančio spinduolio (piq)₂Ir(acac) matricą, pasiektas 15,9% EQE ir sumažintas efektyvumo sumažėjimas esant didesniai ryškumui. Kaip TADF/TTA spinduoliai, **CzDbp** ir **AcDbp** leido išgauti geltonos ir oranžinės spalvų OLED bei atitinkamai pasiekti 19,4% ir 22,1% EQE.

- Buvo ištirti nauji, keletu donorų pakeisti dicianopiridino pagrindo junginiai OLED prietaisams. Junginys **5b** pasižymėjo ribotu efektyvumu ir prietaiso tarnavimo laiku, o junginys **5a** – ilgesniu tarnavimo laiku ir išpūdingu maksimaliu 8,1% EQE ne legiruotoms sistemoms ir 25% legiruotoms sistemoms. Tai reiškia reikšmingą pažangą TADF OLED dizaino srityje.

- Buvo pristatyti trys elektronus transportuojantys puslaidininkiai, pagrįsti 3,5-dicianopiridino pagrindu. Šios medžiagos pasižymi aukštomis tripletinėmis energijomis ir jonizacijos potencialais. Du junginiai pasižymėjo HLCT tipo emisija, o trečiasis rodė gryną CT emisiją. Išsiskyrė OLED, naudojantis **FPDD** kaip matricą, kuris pasiekė maksimalų 21,9% EQE, reikšmingai pranokdamas įprastas matricas.

5.2. Paskelbtų publikacijų apžvalga

5.2.1. Baltieji vertikalūs organiniai pralaidžiosios bazės šviesą skleidžiantys tranzistoriai, gauti maišant mėlynojo eksitono ir oranžinio eksiplekso emisijas

Šis skyrius yra parašytas remiantis publikuotu straipsniu: *Journal of Materials Chemistry C*, **2022**, 10, 9786 // K. Leitonas, M. Gužauskas, U. Tsiko, J. Simokaitienė, D. Volyniuk, J. V. Gražulevičius.³⁷

Šiame tyrime buvo naudojami termiškai aktyvuotos uždelstos fluorescencijos (TADF) eksipleksiniai emiteriai baltos spalvos organinių pralaidžiosios bazės šviečiantiems tranzistoriams (OPB-LET). TADF medžiagos, nepaisant jų didelio potencialo kaip spinduolių OLED-ams, retai buvo naudojamos vienos spalvos OLET prietaisuose. Šiame darbe buvo panaudotas naujas bipolinis junginys 4,6-bis(4-(9H-karbazol-9-il)fenil)pirimidino-5-karbonitrilas⁴¹ (**CzPm**) OPB-LET gamybai, pasiekiant maksimalų išorinį kvantinį efektyvumą (EQE) 2,4% ir baltą elektroluminescenciją su CIE spalvų koordinatėmis (0,34; 0,36) ir spalvų atkūrimo indeksu (CRI) 93.

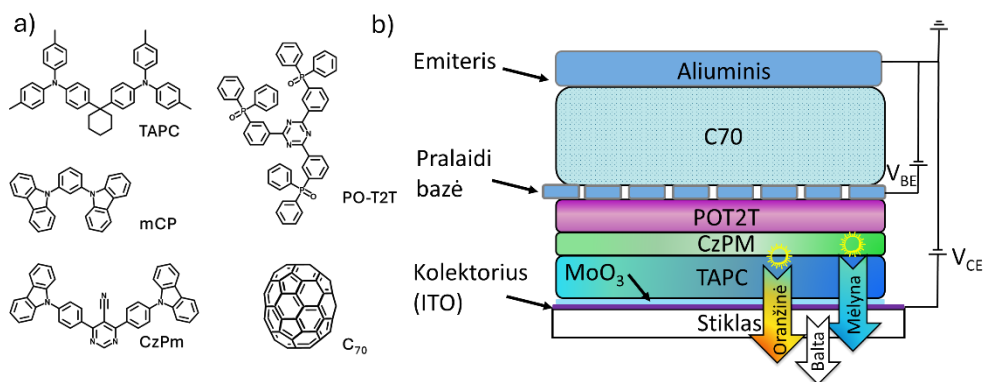
OPB-LET turėjo trijų elektrodų struktūrą, sudarytą iš dviejų organinių daugiasluoksnių dalių (24 pav., b). Pirmoji dalis, tarp viršutinio elektrodo (emiterio) ir vidurinio elektrodo (bazės), buvo sudaryta iš C70 elektronų transportavimo ir LiF elektronų injekcijos sluoksnių^{42,43}. Antroji dalis, tarp vidurinio elektrodo (bazės) ir apatinio elektrodo (kolektoriaus), veikė kaip OLED struktūra, siekiant efektyviai generuoti elektroliuminescenciją. Prietaisų struktūros buvo:

- **Oranžinis OPB-LET:** ITO/MoO₃ [3 nm]/TAPC [80 nm]/PO-T2T [40 nm]/Al [10 nm]/C70 [120 nm]/LiF [2 nm]/Al;

- **Mėlynas OPB-LET:** ITO/MoO₃ [1 nm]/TAPC [60 nm]/mCP [20 nm]/PO-T2T [40 nm]/Al [15 nm]/C70 [120 nm]/LiF [1 nm]/Al;

- **Baltas OPB-LET:** ITO/MoO₃ [1 nm]/TAPC [60 nm]/CzPm [20 nm]/PO-T2T [40 nm]/Al [15 nm]/C70 [120 nm]/LiF [1 nm]/Al.

MoO₃ ir TAPC sluoksnių buvimas palengvino efektyvią skylių injekciją ir transportavimą iš ITO elektrodo į šviesą skleidžiančią TAPC/PO-T2T sluoksnių sąsają⁴⁴, todėl oranžinė elektroliuminescencija turėjo 558 nm smailę. Elektroliuminescencijos spektras parodė efektyvų elektronų perėjimą per pralaidžiąją bazę, o minimalus srovės nutekėjimas buvo parodytas lyginant kolektoriaus srovės tankius (J_{EC}) ir bazės srovės tankius (J_{EB}), kurie buvo gerokai mažesni.



24 pav. Naudojamų junginių molekulinės struktūros a), balto OPB-LET prietaiso principinė struktūros schema b)

Tyrime buvo matuojamos srovės tankio (J_{EC}) ir emisijos ryškumo variacijos priklausomai nuo kolektoriaus įtampos (V_{EC}). Bazės įtampa (V_{EB}) buvo keičiama tarp „įjungta“ ($V_{EB}=4$ V) ir „išjungta“ ($V_{EB}=0$ V) būsenų, atskleidžiant ryškius J_{EC} ir ryškumo verčių skirtumus. Elektronų injekcijos efektyvumas didėjo su kartu su aukštesne V_{EB} , kas leido reguliuoti elektronų perėjimą per pralaidžiąją bazę. Tačiau oranžinio OPB-LET mažas maksimalus EQE (0,17%) rodė, kad reikalinga efektyvesnė emisinė sistema.

Siekiant padidinti efektyvumą, tarp TAPC ir PO-T2T sluoksnių buvo įdėtas mCP tarp sluoksnis, todėl buvo matoma mėlyna elektroliuminescencija su 478 nm intensyvumo viršūne.⁴⁵ Rekombinacijos zona buvo mCP/PO-T2T sluoksnių sąsajoje,

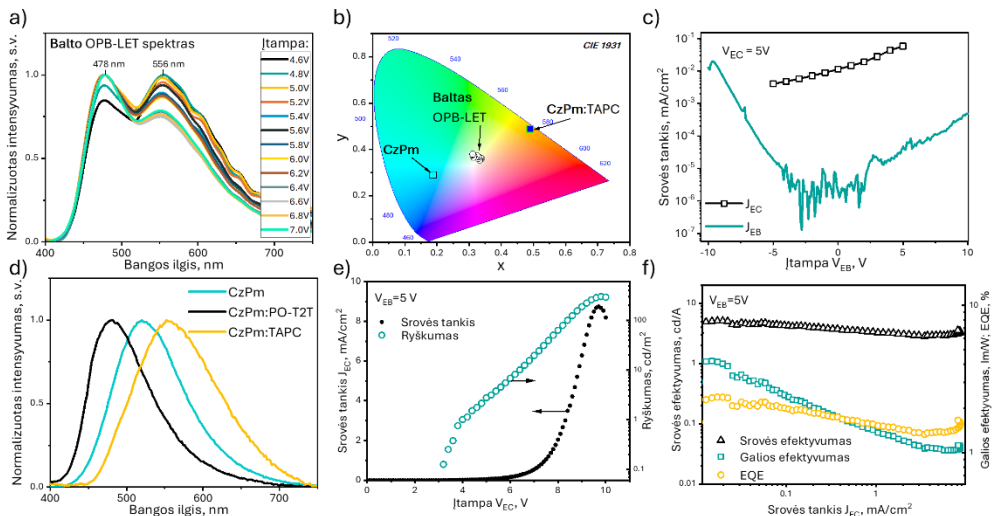
su reikšmingu energijos barjeru, neleidžiančiu elektronų injekcijos iš PO-T2T į mCP. Nuo įtampos priklausomi srovės tankio grafikai rodė minimalų srovės nutekėjimą per bazę. Nepaisant nedidelio skaiščio dėl žmogaus akies jautrumo mėlynai šviesai, mėlynasis OPB-LET pasiekė maksimalų EQE 1,2% (9 lentelė).

9 lentelė. Tirtų OPB-LET prietaisų elektroliuminescencijos parametrai

OPB-LET	V_{on} , V esant 0,1 cd/m ²	Maksimalus ryškumas, cd/m ²	EQE, %	EL smailė, nm	CIE 1931 koordinatės, (x; y)*	CRI*
Oranžinis	6,7	30	0,17	558		-
Mėlynas	3,6	7	1,2	478	(0,22, 0,31)	-
Baltas	3,3	300	2,4	478, 556	(0,34; 0,36)	93

* prieš įjungimo įtampos V_{on} .

Norint optimizuoti prietaisus siekiant geresnių EL savybių, naujas **CzPm** emiteris pakeistas mCP, sukuriant baltą elektroliuminescenciją su aukštos energijos emisijos juosta ties 478 nm ir žemos energijos juosta ties 556 nm. Mėlyna eksitonų emisija iš **CzPm** ir oranžinė eksipleksinė emisija iš **CzPm:TAPC** sąsajos sukūrė baltą elektroliuminescenciją su spalvų koordinatėmis (0,34; 0,36), artimomis natūraliai baltai spalvai ir CRI, nuo 77 iki 93. Baltas OPB-LET turėjo mažiausią įjungimo įtampą (3,3 V), didžiausią maksimalų šviesumą (300 cd/m²) ir aukščiausią EQE (2,4%).



25 pav. a) Baltos spalvos eksiplekso pagrindu veikiančio OPB-LET EL spektras ir b) CIE spalvinės koordinatės esant skirtingoms įtampoms; c) perdavimo srovės tankio ir įtampos charakteristikos; d) normalizuotas CzPm:PO-T2T, CzPm ir

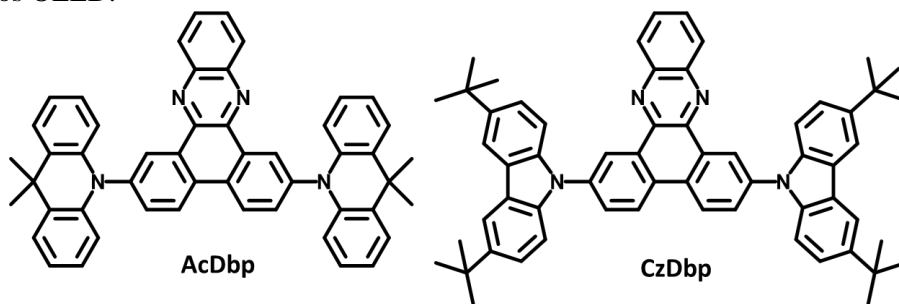
CzPm:TAPC plėvelių PL spektras; e) srovės tankio ir įtampos santykio bei ryškumo ir įtampos santykio grafikai, kai bazinė įtampa V_{EB} yra 5 V; f) srovės, galios ir išorinis kvantinis efektyvumas, palyginti su srovės tankiu kolektoriuje J_{EC} . **CzPm** eksitonų emisijos ir eksiplekso **CzPm**:TAPC emisijos spalvų koordinatės pridamos prie CIE spalvų diagramos b)

CzPm:TAPC eksiplekso TADF savybės buvo patvirtintos fotoluminescencijos spektrų ir PL skilimo kreivių tyrimais temperatūrose nuo 77 K iki 300 K. Laikinės skyros EL kreivės patvirtino TADF indėlį į oranžinę emisijos komponentę. Baltasis OPB-LET pademonstravo efektyvią elektroluminescenciją ir aktyvią srovės moduliaciją, teikiančią perspektyvių galimybių ateityje įvairiose srityse.

5.2.2. TADF ir TTA emisijos mechanizmai akridano ir karbazolo pakaitų dibenzo[a,c]fenazino pagrindo molekulėse: tripletus išnaudojantys spinduliai ir matricos

Šis skyrius yra parašytas remiantis publikuotu straipsniu: *Chemical engineering journal*, **2021**, 417, 127902 // V. Andrulėvičienė, K. Leitonas, D. Volyniuk, G. Sini, J. V. Grazulevičius, V. Getautis⁴⁶.

Šis tyrimas sutelktas į efektyvių TADF ir TTA mechanizmu pasižyminčių junginių, kurie yra žinomi dėl savo stipriai suktų molekulinę struktūrą, paprastai turinčių nepakankamas krūvinio transportavimo savybes, charakterizavimą ir analizę. Pristatytos naujos medžiagos su dibenzo[a,c]fenazino akceptoriumi, pakeistu C-2 arba C-7 pozicijose elektronus donuojančiomis karbazolo (**CzDbp**) arba akridano (**AcDbp**) grupėmis (26 pav.). Stebėtina, bet šios išvestinės medžiagos parodė TTA ir įprastą TADF, kas yra pranašumas kuriant labai efektyvius oranžinės-raudonos spalvos OLED.

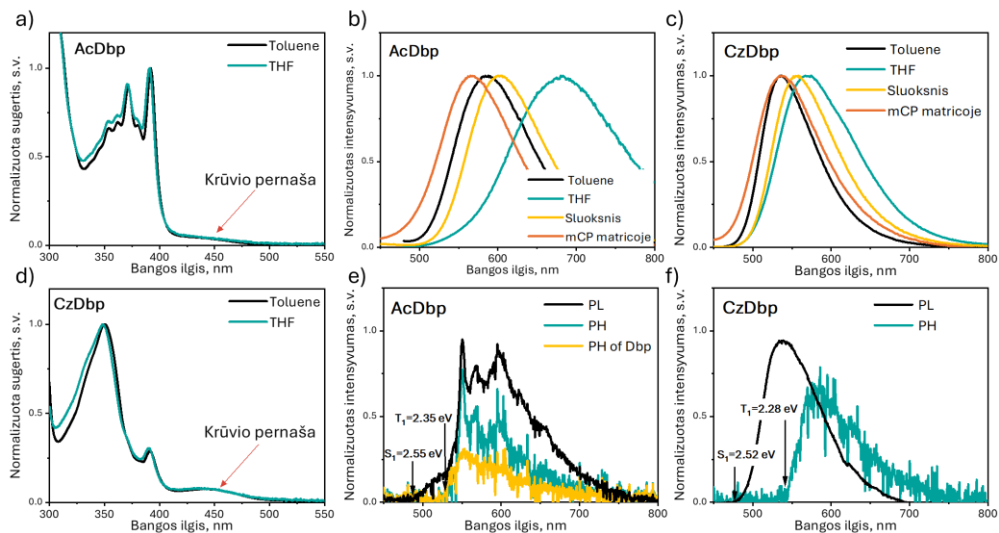


26 pav. Junginių **AcDbp** ir **CzDbp** cheminės struktūros

AcDbp ir **CzDbp** jonizacijos potencialai (IP) buvo tiriami naudojant fotoelektronų emisiją (PE) ir ciklinę voltamperometriją (CV). PE nustatyti jonizacijos potencialai abiem medžiagoms buvo 5,5 eV, o CV matavimų vertės buvo šiek tiek mažesnės dėl sustiprintų poliarizacijos efektų kietoje būsenoje. Vakuuminio garinimo metodu paruoštų **AcDbp** ir **CzDbp** sluoksnių krūvininkų transportavimo savybės buvo analizuojamos naudojant lėkio trukmės (ToF) techniką, parodydamos gebėjimą

transportuoti tiek skyles, tiek elektronus su krūvinio dreifo mobilumais daugiau nei $10^{-3} \text{ cm}^2/\text{Vs}$ esant intensyviems elektriniams laukams.

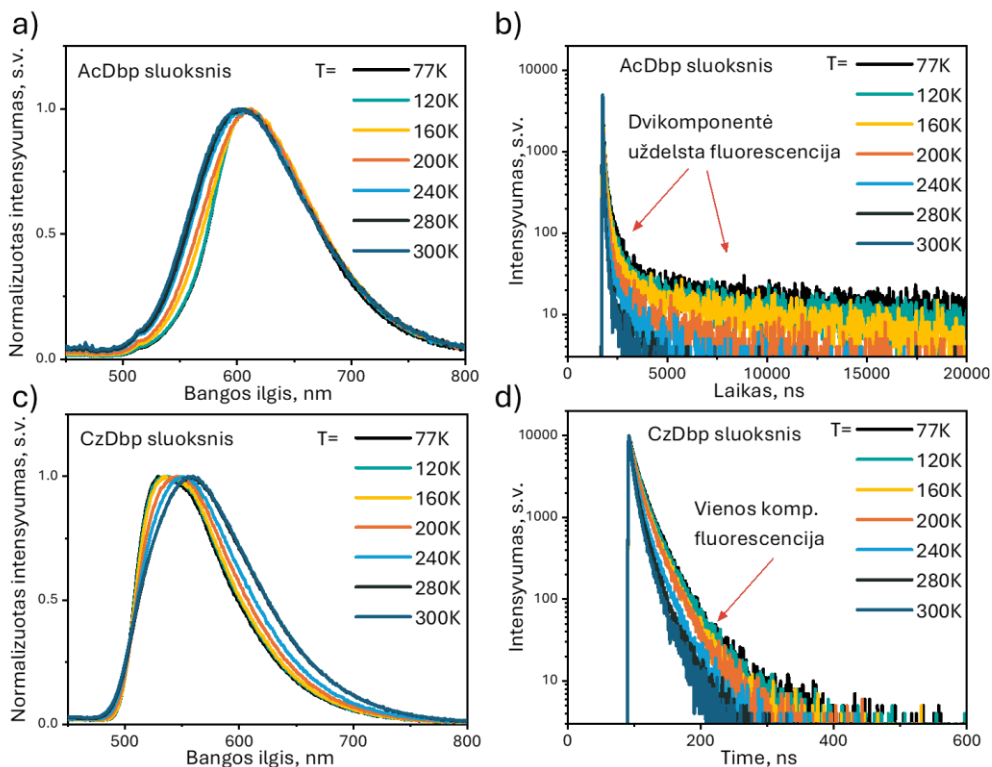
Fotofizikinės savybės buvo tiriamos analizuojant UV-vis absorbcijos spektrus tetrahidrodurano (THF) ir tolueno tirpaluose. Šie spektrai atskleidė silpną krūvio pernašos (CT) uodegą 400–500 nm diapazone (27 pav.). Fluorescencijos spektrai ir fotoluminescencijos kvantiniai našumai (PLQY) parodė Gauso formos emisijos profilį, rodantį CT būsenos prigimtį. **CzDbp** tirpalų PLQY vertės buvo didesnės nei **AcDbp**, tikėtina dėl stipresnio TTA.



27 pav. **AcDbp** ir **CzDbp** UV-Vis sugertis a), d), tirpalų ir plėvelių fluorescencijos spektrai kambario temperatūroje b), c), THF tirpalų fosforescencijos spektrai 77 K temperatūroje e), f)

Singletinės-tripletinės energijų skirtumai (ΔE_{ST}) buvo įvertinti **AcDbp** ir **CzDbp** tirpalams THF esant 77 K (27 pav.). **AcDbp** PL spektras rodė CT būsenos prigimtį, o **CzDbp** fosforescencijos (PH) spektras rodė, kad žemiausia emisijos T_1 būseną atitiko vietinę Dbp branduolio sužadavimo (3LE) būseną. Oro aplinkos ir bedeguonių tolueno tirpalų pastoviosios būsenos ir laikinės skyros spektroskopija parodė, kad uždelsta fluorescencija kilo iš CT būsenos, rodant tripletinių eksitonų perėmimą per TADF.

CzDbp tolueno tirpalai turėjo vieno eksponentinio PL gesimo kreivę, rodant tik greitą fluorescenciją, bet po deguonies pašalinimo **CzDbp** tirpalai pasižymėjo 16% PLQY padidėjimu, rodančiu kitokių tripletinių būsenų indėlio mechanizmą. Nuo temperatūros priklausomi PL spektrai ir PL gesimo kreivės nelegiruotiems ir legiruotiems **AcDbp** ir **CzDbp** sluoksniams rodė padidėjusius PL intensyvumus ir PLQY kylant temperatūrai, kas buvo priskirta TADF (28 pav.).



28 pav. PL spektrai a), c) ir PL gesimo kreivės b), d) nelegiruotų AcDbp ir CzDbp sluoksnių, kurie buvo išmatuoti skirtingose temperatūrose nuo 77 iki 300 K

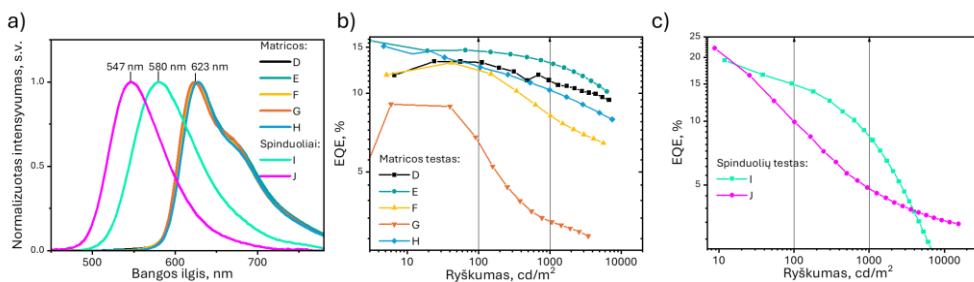
AcDbp parodė potencialą kaip TADF matricos raudoniems OLED dėl savo krūvininkų transportavimo savybių ir pirmosios tripletinės būsenos energijos. **CzDbp** turėjo ambipolines krūvinio transportavimo savybes ir didesnę PLQY. Abu junginiai buvo naudojami fosforescencinėse OLED (PHOLED), kad parodytų jų tinkamumą kaip matricos tipo medžiagų komerciniam raudonam fosforescenciniam emiteriui $(\text{piq})_2\text{Ir}(\text{acac})$. PHOLED prietaisas **B** su **CzDbp** kaip pagrindu pasižymėjo geriausiais rezultatais, ir pasiekė maksimalų EQE 9%, palyginti su prietaisu **C** 8%, kuriam naudota tradicinė mCP matrica (10 lentelė).

10 lentelė. Prietaisų A-J EL charakteristikos

Prietaisas	Emisinis sluoksnis	${}^aV_{ON}/$ ${}^bV_{Driving},$ V	$CE_{max},$ cd/A	$PE_{max},$ lm/W	$EQE_{max},$ %
Struktūra: ITO/MoO3/NPB/ Emissive layer /TPBi/LiF:Al					
A	$(piq)_2Ir(acac):AcDbp$	3,0/3,85	6,3	4,6	6,0
B	$(piq)_2Ir(acac):CzDbp$	3,4/4,5	9,0	6,4	9,0
C	$(piq)_2Ir(acac):mCP$	4,0/5,2	8,6	5,6	8,0
Struktūra: ITO/HAT-CN/NPB/TCTA/mCBP/ Emissive layer /nBPhen/Liq/Al					
D	$(piq)_2Ir(acac):AcDbp$	3,2/5,2	9,8	9,1	13,2
E	$(piq)_2Ir(acac):CzDbp$	3,0/4,75	10,3	11,6	15,9
F	$(piq)_2Ir(acac):mCBP$	2,9/4,0	11,5	12,9	13,1
G	$(piq)_2Ir(acac):NPB$	3,2/4,5	6,6	6,7	9,0
H	$(piq)_2Ir(acac):nBPhen$	4,8/8,7	12,5	8,5	14,6
Struktūra: ITO/HAT-CN/NPB/TCTA/mCBP/ Emissive layer /nBPhen/Liq/Al					
I	AcDbp:mCBP	3,6/6,7	41,6	35,3	19,4
J	CzDbp:mCBP	3,7/7,0	54,4	46,2	22,1

${}^aV_{ON}$ prie 10 cd/m²; ${}^bV_{Driving}$ prie 10 mA/cm².

Optimizuotos įrenginių struktūros su pagerintomis krūvinio injekcijos savybėmis turėjo geresnes elektroluminescencijos charakteristikas. Įrenginiai su **CzDbp** kaip matrica parodė didžiausią maksimalų EQE (15,9%) ir mažiausią efektyvumo kritimą kylant ryškumui, palyginti su referenciniais OLED su tradiciniais pagrindais (10 lentelė, 29 pav.). **AcDbp** ir **CzDbp** junginiai taip pat buvo ištestuoti kaip spinduoliai mCBP matricoje ir pasiekė netikėtai aukštus EQE – atitinkamai 19,4% ir 22,1%.



29 pav. Prietaisų D-J EL spektrai a); EQE priklausomybė nuo ryškumo, kai AcDbp ir CzDbp naudojami kaip matricos b) ir kai naudojami kaip spinduoliai c)

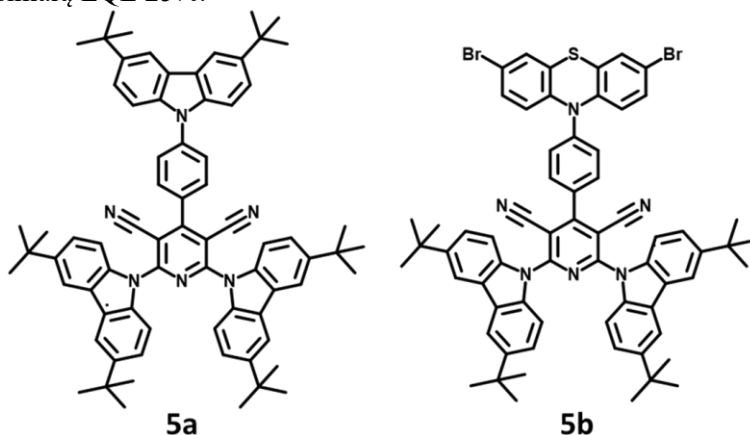
Apibendrinant reikia patebėti, kad naujos D-A-D tipo molekulės **CzDbp** ir **AcDbp**, pasižyminčios bipoliniu krūvinio transportavimu ir tripletinių eksitonų perėmimu per TTA arba TADF, taip pat daug žadančiais rezultatais. **AcDbp** ir **CzDbp**

demonstravo efektyvų tripletinių eksitonų panaudojimą, kas leidžia juos naudoti aukštos kokybės OLED prietaisuose.

5.2.3. Dvigubo ir įprastinio TADF mechanizmų priklausomybė nuo donoro pakaitų pirimidino junginiuose

Šis skyrius yra parašytas remiantis publikuotu straipsniu: *Journal of Materials Chemistry C*, **2021**, 9, 3928 // P. Arsenyan, B. Vigante, K. Leitonas, D. Volyniuk, V. Andrulevičienė, L. Skhirtladze, S. Belyakov, J. V. Gražulevičius⁵⁸.

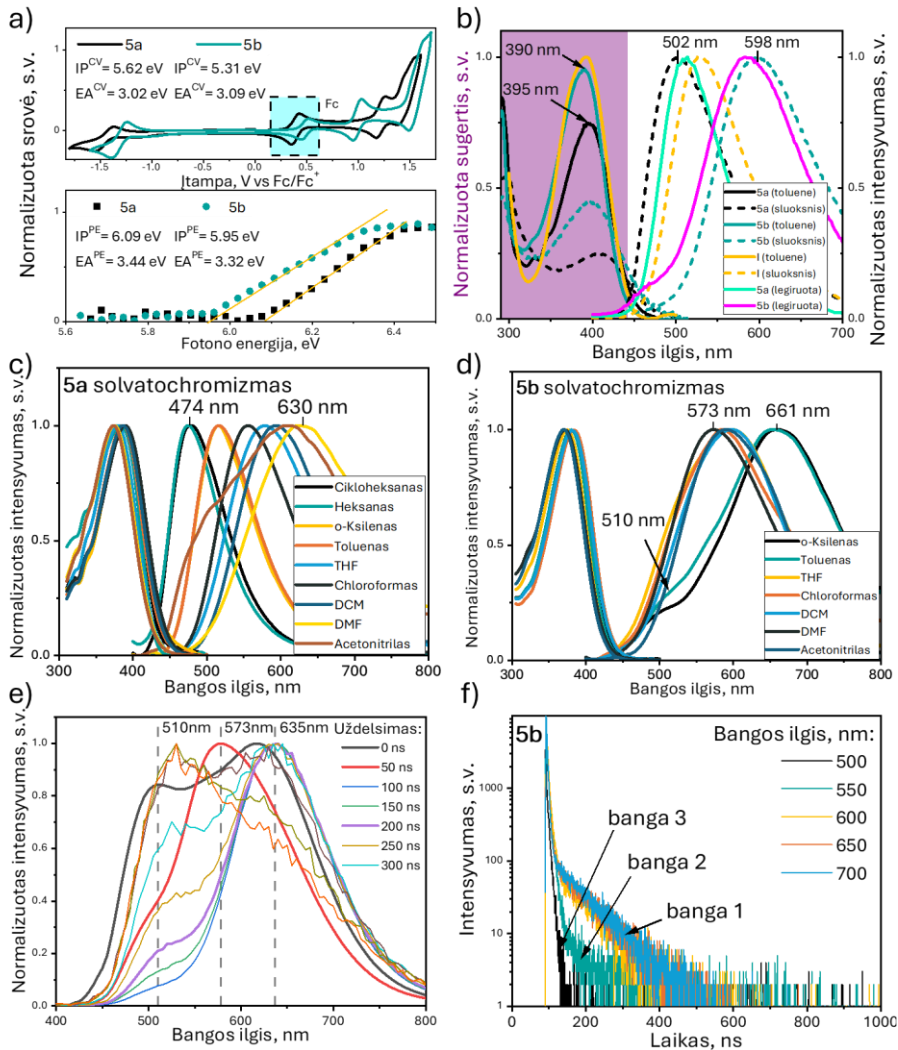
Skirtingų donorų tipų poveikis daugialypių donorinių-akceptorinių (D-A) sąveikų efektyvumui TADF junginiuose iki šiol nebuvo nuodugnai ištirtas. Siekiant aiškumo, šiame tekste vartojamas „daugialypių D-A sąveikų“ terminas yra vertinys iš anglų kalbos „multiple donor-acceptor interaction“, kuris reiškia, kad šiuo atveju molekulė turi 3 donorinius ir vieną akceptorinį fragmentus. Šiame tyrime pristatomi įvairūs donoriai, įtraukti į kelių D-A TADF emiterių molekulinę struktūrą, sukuriantys labai efektyvius TADF junginius, turinčius dvi arba tris 3,6-di-tert-butil-karbazolo dalis. Buvo išsamiai apibūdinti du dicianopiridiniai su keliais donoriais, naudojant įvairias spektroskopijos technikas. Vienas dicianopiridino pagrindo junginys, **5a**, turi tris tos pačios rūšies donorų grupes, konkrečiai 3,6-di-tert-butil-karbazolą, o kitas, **5b**, turi dviejų tipų donorų grupes: 3,6-di-tert-butil-karbazolą ir 3,7-dibromofenotiaziną (30 pav.). OLED, kuriuose buvo naudojamas junginys **5a** kaip TADF emiteris, pasiekė maksimalų EQE 25%.



30 pav. Cheminės junginių **5a** ir **5b** struktūros

Elektrocheminės ir fotofizikinės junginių **5a** ir **5b** savybės buvo tirtos naudojant ciklinę voltamperometriją (CV) ir fotoelektronų emisijos (PE) spektroskopiją. **5a** ir **5b** junginių jonizacijos potencialai (IP^{CV}) buvo atitinkamai 5,62 ir 5,31 eV. Žemesnis junginio **5b** IP^{CV} dėl stiprios elektronų donorinės 3,7-dibromofenotiazino grupės (31 pav., a). UV-Vis, pastovios būsenos ir laikinės skyros fotoluminescencijos (PL) spektroskopija atskleidė artimas absorbcijos bangų ilgio smailes (390 ir 396 nm) **5a** ir **5b** tolueno tirpaluose (31 pav., b).

Nelegiruotose **5a** ir **5b** plėvelėse buvo pastebimi nestruktūruoti PL spektrai su smailių vertėmis atitinkamai 502 ir 598 nm (31 pav., b). **5b** legiruotoje mCP matricos plėvelėje buvo aptiktas žemo intensyvumo petys PL spektre, rodantis persidengiančias emisijos juostas (31 pav., d).



31 pav. **5a** ir **5b** CV ir fotoelektronų emisijos spektrai a); **5a**, **5b** junginių tolueno tirpalų ir grynų bei legiruotų plėvelių absorbcijos ir emisijos spektrai (sužadinant bangos ilgiu 350 nm b); tirpiklio poliškumo poveikis **5a** c) ir **5b** d) junginių optinei sugerčiai ir PL spektrui tirpaluose, kurių koncentracija yra apie 10–4 mg/ml; **5b** tolueno tirpalo spektrai laike skirtinguose laiko intervaluose po sužadinimo, užregistruoti su skirtingais laiko uždelsimais e); **5b** tolueno tirpalo PL gesimo kreivė, užregistruota esant skirtingiems emisijos bangos ilgiams f)

Solvatochrominiai matavimai suteikė įžvalgų apie organinių junginių emisijos pobūdį. **5a** junginys turėjo platų emisijos spektrą, demonstruojantį smailės plotį pusės maksimumo aukštyje nuo 78 nm (heksane) iki 180 nm (DMF), būdingą normaliai TADF elgsenai. **5b** junginys turėjo nestruktūruotus emisijos spektrus su dviem plačiomis juostomis, besislenkančiomis raudonos spalvos bangos ilgių kryptimi didėjant tirpiklio poliškumui, rodant dvigubos prigimties TADF emisiją. Laiko išskaidytos PL matavimai atskyrė tiesioginės ir uždelstos fluorescencijos spektrus, atskleidžiant tris persidengiančias juostas (500, 573 ir 635 nm) **5b** junginiui.

5a ir **5b** plėvelių PL spektrai ir gesimo kreivės mCP matricijoje buvo užrašyti esant skirtingoms temperatūroms. Maži ΔE_{ST} buvo gauti THF tirpaluose **5a** ir **5b** (0,1 eV ir 0,04 eV) ir **5a** legiruotoje mCP plėvelėje (0,11 eV). Ilgainiui **5a** ir **5b** fluorescencija buvo identifikuota kaip TADF, nes intensyvumas didėjo kylant temperatūrai.

Teoriniai skaičiavimai (TD-DFT), atlikti bendraautorės Dr. Viktorijos Andrulevičienės, parodė, kad **5a** TADF yra susijęs su CT perėjimais iš 3,6-di-tert-butil-9-fenilkarbazolo grupių į fenilpiridino-3,5-dikarbonitrilo grupes (S1 – S0), o dvigubos prigimties **5b** TADF mechanizmas atitinka CT perėjimus iš 3,7-dibromofenotiazino grupių į fenilpiridino-3,5-dikarbonitrilo vienetus (S1 – S0) ir piridino-3,5-dikarbonitrilo vienetus (S2 – S0).

OLED buvo testuoti su emiteriais **5a** ir **5b** legiruotomis ir nelegiruotomis konfigūracijomis:

- ITO/MoO₃ [0.6 nm]/NPB [35 nm]/mCP [6 nm]/**5a** (arba **5b**) (30 arba 100 masės %):mCP [25 nm]/TSPO1 [6 nm]/TPBi [35 nm]/LiF [0.6 nm]/Al.

Nelegiruoti ir legiruoti prietaisai n-5a, d-5a, n-5b ir d-5b rodė stabilią žalią ir oranžinę elektroluminescenciją esant skirtingoms įtampoms. n-5a ir d-5a prietaisai turėjo aukštesnę įjungimo įtampą nei n-5b ir d-5b, atitinkančią **5a** aukštesnę IP^{PE} vertę (6,09 eV), palyginti su **5b** (5,95 eV). n-5a ir d-5a prietaisai pasiekė maksimalų šviesumą daugiau nei 30 000 cd/m², o n-5b ir d-5b pasiekė daugiau nei 3 000 cd/m². EQE n-5a ir d-5a buvo 8,1% ir 11,7%, o n-5b ir d-5b buvo mažesni – 3,1% ir 3,2%.

11 lentelė. OLED prietaisų EL parametrai

Prietaisas	V_{on}^a , V	λ_{EL}^b , nm	EQE_{max} , EQE_{100} , EQE_{1000}^c , %
n-5a	4,9	515	8,1; 8,0; 7,8
d-5a	4,6	523	11,7; 11,1; 10,7
o-5a	3,9	512	25,0; 15,2; 11,8
n-5b	4,4	588	3,1; 2,8; 2,6
d-5b	4,3	588	3,2; 3,1; 2,7
o-5b	5,1	582	5; 3,5; 0,6

^a V_{on} esant 10 cd/m². ^b λ_{EL} esant 5 V. ^c EQE_{max} , EQE_{100} ir EQE_{1000} esant atitinkamai 10, 100 ir 1000 cd/m².

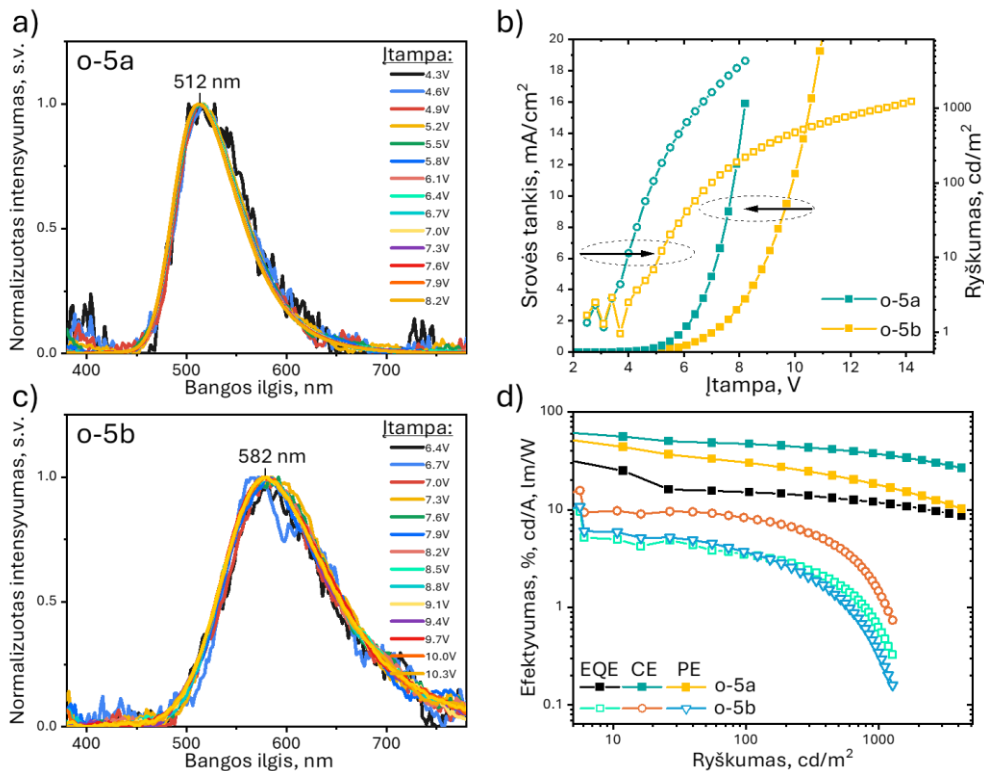
Mažesnis **5b** prietaisų efektyvumas gali būti priskirtas dvigubos prigimties TADF emisijai ir mažesniems kvantiniams našumams dėl energijos perdavimo per

vidinę konversiją (IC) iš S_2 į S_1 . Šis papildomas energijos perdavimas mažina emisijos efektyvumą ir prailgina emisijos gesimą, su **5b** rodant PL gyvavimo trukmes, siekiančias vieną milisekundę. Ilga emisijos trukmė padidina eksitonų-eksitonų ir eksitonų-polaronų anihiliacijos tikimybę, mažinant EQE ir prietaisų ilgaamžiškumą.

Optimizuota OLED su struktūra:

• ITO/HAT-CN [5 nm]/NPB [40 nm]/TCTA [10 nm]/mCBP [10 nm]/**5a** (arba **5b**) (20 masės %):mCBP [50 nm]/NBPhen [30 nm]/Liq [2 nm]/Al.

Pasiekė maksimalų EQE – 25% (**5a**) ir 5% (**5b**) dėl pagerėjusios skylių-elektronų rekombinacijos (11 lentelė, 32 pav.).



32 pav. EL spektrai esant skirtingoms įtampoms a) ir b); srovės tankio ir ryškumo priklausomybė nuo įtampos c); efektyvumo priklausomybė nuo srovės tankio d) optimizuotuose OLED

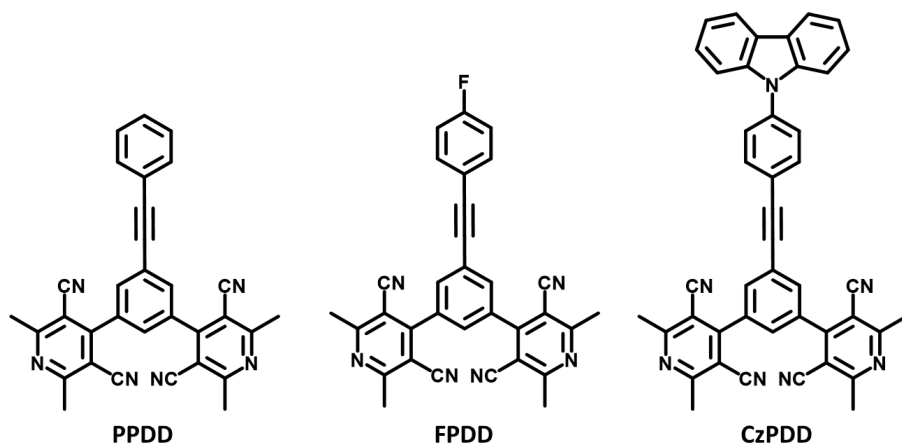
Taigi šiame tyrime buvo ištirti du dicianopiridino pagrindo junginiai su skirtingomis donorų konfigūracijomis. Junginys **5a**, pasižymintis įprastinėmis TADF savybėmis, pasiekė didelį prietaisų ilgaamžiškumą ir maksimalų EQE 25% legiruotuose ir optimizuotuose prietaisuose. Junginys **5b** su dvigubos prigimties TADF savybėmis rodė mažesnę prietaisų ilgaamžiškumą ir maksimalų EQE 5%. Tyrimas parodė, kad trumpesnės PL gyvavimo trukmės gali būti puikus indikatorius, siekiant bendro OLED stabilumo ir efektyvumo.

5.2.4. 3,5-Dicianopiridino pagrindo elektronus transportuojantys puslaidininkiams: nuo dizaino ir sintezės iki efektyvių organinių šviesos diodų

Šis skyrius yra parašytas remiantis publikuotu straipsniu: *Journal of Materials Chemistry C*, **2023**, 11, 28 // K. Leitonas, B. Vigante, D. Volyniuk, R. Keruckienė, P. Dimitrijevs, T. L. Chiu, J. V. Gražulevičius, P. Arsenyan⁶⁸.

Šiuolaikinis OLED efektyvumas buvo pasiektas dėl tinkamų aktyvios emisijos sluoksnio sistemų matricių. Šios matricios pagerina skylių ir elektronų rekombinaciją, užtikrindamos krūvių pusiausvyrą šviesą emituojančiuose sluoksniuose ir sumažindamos emisijos slopinimo reiškinius.⁷⁵ Dauguma OLED matricių turi skylių transportavimo arba bipolines savybes, kur skylių judrumas yra didesnis nei elektronų.^{76,77} Tačiau OLED matricių, galinčių transportuoti elektronus, pasirinkimas kol kas yra ribotas.⁷⁸

Siekiant išspręsti šią problemą, 3,5-dicianopiridinas buvo pasirinktas kaip pagrindinis komponentas organiniams puslaidininkiams, kurie palengvina elektronų transportavimą, kurti. Nors 3,5-dicianopiridino dariniai jau seniai naudojami farmacijoje^{79,80,81,82,83,84}, jų naudojimas optoelektroniniuose įrenginiuose išlieka ribotas. Šiame tyrime buvo įvertinta 3,5-dicianopiridino darinių tinkamumas junginių, skirtų specialiai optoelektronikai, kūrimui. Buvo ištirti trys 3,5-dicianopiridino dariniai (**PPDD**, **FPDD** ir **CzPDD**) (33 pav.) elektrocheminiais, fotofizikiniais, elektrooptiniais ir elektroluminescenciniais metodais. OLED, pagrįsti TADF spinduliu 4,6-di(9,9-dimetilakridan-10-il)isofalonitrilu (DAcIPN) ir 3,5-dicianopiridino matrica (**FPDD**), pasiekė maksimalų EQE 21,9%, kas yra daug daugiau nei užfiksuotas efektyvumas su komerciškai prieinamu mCBP pagrindu tomis pačiomis sąlygomis.



33 pav. Cheminės junginių **PPDD**, **FPDD** ir **CzPDD** struktūros

Tyrimas prasidėjo nuo elektrocheminių **PPDD**, **FPDD** ir **CzPDD** savybių tyrimo, naudojant ciklinę voltamperometriją (CV). Visi trys dariniai rodė negrįžtamus oksidacijos ir kvazigrįžtamos redukcijos procesus. Stipresnis karbazolo fragmento

elektronų donorinis gebėjimas lėmė mažesnę IP^{CV} vertę **CzPDD** (5,7 eV), palyginti su **PPDD** (5,92 eV) ir **FPDD** (6,06 eV). Elektronų giminingumo (EA^{CV}) vertės buvo panašios visų trijų junginių (2,95–2,98 eV). **CzPDD** junginio plėvelė turėjo šiek tiek didesnę IP^{PE} vertę (5,94 eV) dėl molekulių sąveikos plėvelėje (12 lentelė).

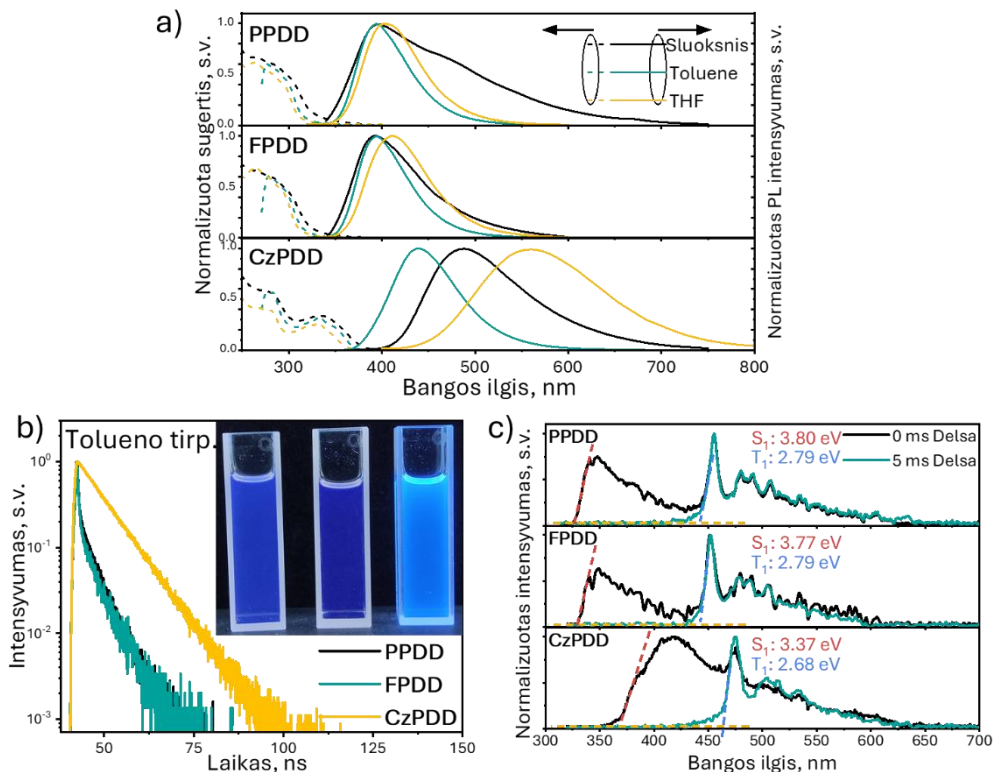
12 lentelė. Elektrocheminiai ir fotoelektriniai junginių **PPDD**, **FPDD** ir **CzPDD** parametrai

Junginys	^a IP^{CV} , eV	^b EA^{CV} , eV	^c E_g^{opt} , eV	^d IP^{PE} , eV	^e EA^{PE} , eV
PPDD	5,92	2,96	3,74	n/a	n/a
FPDD	6,06	2,95	3,83	n/a	n/a
CzPDD	5,7	2,98	3,25	5,94	2,69

^a $IP^{CV}(eV) = E_{onset, ox}(V) + 4,8$; ^b $EA^{CV}(eV) = E_{onset, red}(V) + 4,8$; ^c optinės draustinės juostos pločio reikšmė, gauta iš sugerties spektro tiesinės; ^d IP^{PE} , nustatyta iš plėvelių fotoelektronų emisijos ore metodu; ^e EA^{PE} apskaičiuotas pagal formulę: $IP^{PE} - E_g^{opt} = EA^{PE}$.

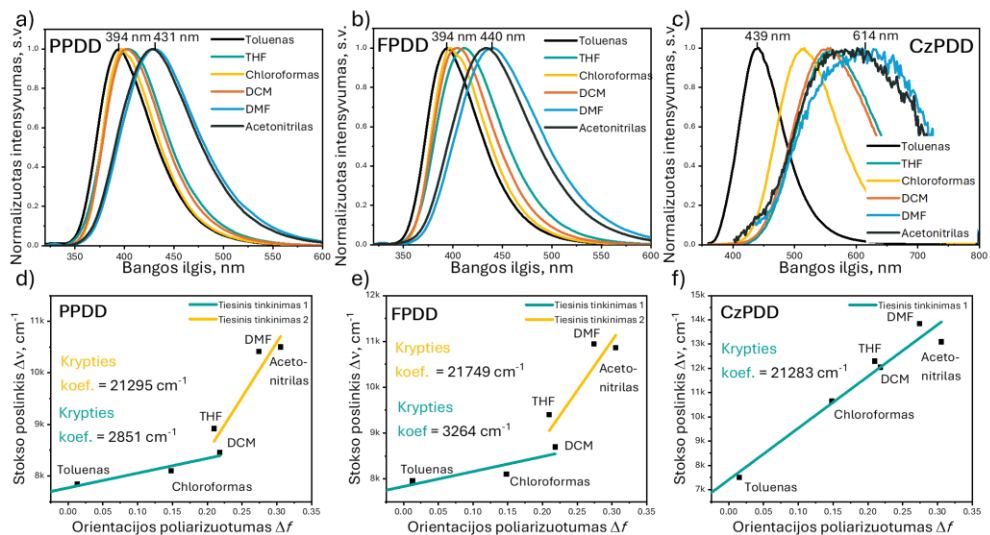
UV-Vis absorbcijos ir fotoluminescencijos (PL) spektroskopijos buvo naudojamos **PPDD**, **FPDD** ir **CzPDD** fotofizikinėms savybėms apibūdinti. **PPDD** ir **FPDD** absorbcijos spektrai buvo beveik identiški, su stipria smaile, maždaug 280–290 nm, ir aiškiai matoma 296 nm peties juosta. **CzPDD**, turintis fenilkarbazolo grupę, rodė skirtingus absorbcijos spektrus su aukštos energijos juosta, piko vertėje ties maždaug 290 nm ir mažiau intensyvia juosta ties 333 nm. Intramolekulinis krūvio pernešimas (ICT) buvo aptiktas tarp karbazolo ir 3,5-dicianopiridino ties bangos ilgiais virš 340 nm (34 pav., a).

Junginyje **CzPDD** buvo užfiksuoti minimalūs absorbcijos smailių pokyčiai, keičiant tirpiklio poliškumą, kas rodo, kad **CzPDD** turi santykinai nepolišką pagrindinę energijos būseną. Tačiau sužadintose būsenose buvo pastebėti poslinkiai raudonų bangų ilgių link **CzPDD** PL spektruose tirpaluose, esant didesniam tirpiklio poliškumui (34 pav., a). Organinių elektroaktyvių junginių tripletinės energijos yra svarbios parenkant tinkamas matricas fosforescenciniams arba TADF OLED. **PPDD** ir **FPDD** rodė identiškas tripletines energijas – 2,79 eV, o **CzPDD** tripletinė energija buvo 2,68 eV (34 pav., c).



34 pav. Normalizuoti UV-VIS ir PL a) spektrai plėvelių, tolueno ir THF tirpalų **PPDD**, **FPDD** ir **CzPDD** su 1×10^{-5} M koncentracija; tolueno tirpalų PL gesimo kreivės b); intarpas rodo mėginius UV šviesoje. THF tirpalų **PPDD**, **FPDD** ir **CzPDD** esant 77 K PL ir PH PH spektrai c); **PPDD** ir **FPDD** sužadavimo bangos ilgis (λ_{ex}) buvo 300 nm, o **CzPDD** – 340 nm

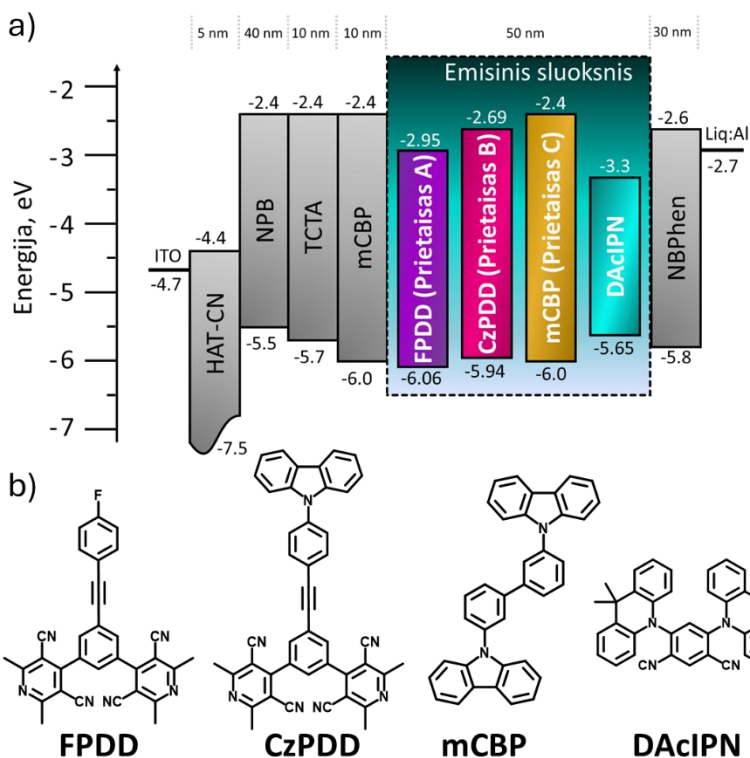
Praskiestų **CzPDD** tirpalų PL spektrai turėjo reikšmingą raudoną poslinkį su emisijos piko bangos ilgiu, besikeičiančiu nuo 439 nm tolueno tirpale iki 560 nm THF tirpale (34 pav., a). **CzPDD** plėvelės bandinys rodė didžiausią emisijos intensyvumą ties 487 nm, per vidurį tarp tolueno ir THF tirpalų emisijos intensyvumų. **PPDD** ir **FPDD** PL spektrai rodė minimalius emisijos energijos skirtumus ištirpinti mažo poliškumo tirpikliuose (35 pav., a, b). Tačiau didelio poliškumo tirpikliuose, tokiuose kaip DMF ir acetonitrilas, buvo pastebėti reikšmingi poslinkiai link ilgesnių bangų ilgių ir spektrų išsiplėtimas, rodantis galimą krūvio pernešimo (CT) emisiją. **PPDD** ir **FPDD** rodė netiesinius Lippert-Mataga grafikų ryšius, parodančius hibridizuotų lokalių ir krūvio pernešimo (HLCT) būsenų savybes.



35 pav. Normalizuoti praskiestų **PPDD**, **FPDD** ir **CzPDD** skirtingų poliškumų tirpalų spektrai a), b), c) ir atitinkami Lippert-Mataga grafikai d), e), f), kuriuose pavaizduota Stokso poslinkio $\Delta\nu$ priklausomybė nuo tirpiklio orientacijos polarizuotumo funkcijos Δf

TADF spinduolių emisijos efektyvumas smarkiai priklauso nuo matricų savybių. **PPDD**, **FPDD** ir **CzPDD** buvo įvertinti kaip galimos matricos labai efektyviam TADF emiteriui DAcIPN. Aukštos tyrinėtų medžiagų tripletų energijos gali padėti sukoncentruoti tripletinių būsenų energiją iš DAcIPN ir ją panaudoti emisinei rekombinacijai. OLED prietaisų gamyba buvo atlikta kaip galutinis eksperimentinio tyrimo etapas. Tyrime buvo nagrinėjamas **FPDD** ir **CzPDD** kaip matricų veikimas OLED prietaisams su šia struktūra (36 pav.):

- ITO/HAT-CN [5 nm]/NPB [40 nm]/TCTA [10 nm]/mCBP [10 nm]/DAcIPN:matrica [50 nm]/NBPhen [30 nm]/Liq [2 nm]/Al.



36 pav. OLED prietaisų sluoksnių ir energetinių lygmenų diagrama a) bei emisiniame sluoksnyje naudotų medžiagų cheminės struktūros b)

13 lentelė. OLED prietaisų A-C EL charakteristikos

Prietaisas	A	B	C
Emisinis sluoksnis	DAcIPN (10 masės %): FPDD	DAcIPN (10 masės %): CzPDD	DAcIPN (10 masės %): mCBP
V_{ON} , V @ 10 cd/m ²	3,76	3,2	4,3
EQE_{max} , EQE_{100} , EQE_{1000} , % ^a	21,9; 12,1; 9,5	8,6; 4,0; 3,7	12,2; 6,7; 5,6
EL smailė, nm prie 1000 cd/m ²	540	542	526

^a maksimali EQE vertė esant 100 ir prie 1000 cd/m² skaisčiui.

Įdomu tai, kad OLED su **FPDD** kaip matrica turėjo beveik dvigubai didesnę efektyvumą nei referencinis OLED su mCBP (21,9% ir 12,2%) (13 lentelė). EQE verčių skirtumai tarp OLED prietaisų A-C gali būti paaiškinami geresnėmis **FPDD** matricos savybėmis, palyginti su **CzPDD** arba mCBP. Akivaizdu, kad tripletai gali būti efektyviau surenkami DAcIPN emiteriu, kai jis yra išsklaidytas **FPDD** matricoje, nei kai jis yra **CzPDD** arba mCBP.

Rezultatai rodo, kad dicianopiridino darinys su fluorofenilų grupe (**FPDD**) turi didelį potencialą pagerinti žalių TADF OLED efektyvumą. Dėl aukštos tripletinės energijos (2,79 eV), **FPDD** taip pat gali būti naudojamas kaip matrica mėlyniems spinduoliams, kurie skleidžia šviesą ties bangos ilgiais, didesniais nei 450 nm.

5.3. Išvados

1. Tyrimo metu buvo ištirti trys vertikalių organinių pralaidžios bazės šviesą skleidžiančių tranzistorių (OPB-LET) tipai: oranžiniai, mėlyni ir balti. Buvo parodyta, kad TADF eksipleksiniai emiteriai OPB-LET prietaisuose su vertikalia struktūra sėkmingai pasiekė aukštos kokybės baltą elektroliuminescenciją:

1.1. **Oranžinio eksiplekso panaudojimas:** Nustatyta, kad oranžinis eksipleksas gali būti sukurtas derinant naują mėlyną emiterį su donorine medžiaga TAPC lygiomis dalimis. Šis eksipleksas rodė minimalų singletinio-tripletinio energijos skirtumą (ΔE_{ST}) – 0,02 eV ir stiprias TADF savybes. Naudojant šią kombinaciją emisiniame sluoksnyje, buvo įveikti ankstesni iššūkiai, susiję su elektronų injekcija OPB-LET prietaisuose, kas žymi reikšmingą medžiagų panaudojimo pažangą.

1.2. **Baltų OPB-LET veikimas:** Nauji balti OPB-LET pasiekė maksimalų išorinį kvantinį efektyvumą – 2,4 %, mažą įjungimo įtampą – 3,3 V ir aukštą maksimalų šviesumą – 300 cd/m². Be to, šie prietaisai galėjo moduluoti srovės tankį (J_{EC}) ir šviesumą, reguliuojant bazės įtampą (V_{EB}), kas pabrėžia panaudotų medžiagų potencialą didinti elektroliuminescencinių prietaisų efektyvumą ir veikimą.

1.3. **Spalvos kokybė:** Buvo pastebėta, kad balti OPB-LET pasiekė spalvų perteikimo indeksus nuo 77 iki 93 bei stabilias CIE spalvų koordinates. Šie rezultatai rodo aukštą spalvų kokybę, todėl tokia konfigūracija galėtų būti tinkama įvairiais apšvietimo taikymo atvejais.

Šio tyrimo rezultatai ne tik padidina TADF mechanizmų organiniuose emiteriuose supratimą, bet ir pabrėžia eksipleksais pagrįstų baltų OPB-LET praktiškumą, atveriant kelią būsimoms inovacijoms elektroliuminescencinių technologijų srityje.

2. Buvo atlikti tolesni naujai sukurtų donoro-akceptoriaus-donoro (D-A-D) tipo molekulių, konkrečiai karbazolu arba akridanu pakeistų dibenzo[a,c]fenazinų (**CzDbp** ir **AcDbp**), tyrimai. Šios molekulės buvo tiriamos pastovios būsenos ir laikinės skyros spektroskopijos metodais, kurie pabrėžė jų efektyvumą perimant tripletinius eksitonus per TTA ir TADF mechanizmus bei puikias emisines ir matricų savybes:

2.1. **Fotofizikinės savybės:** Fotofizikinė analizė parodė, kad **CzDbp** ir **AcDbp** turi savybių, kurios yra naudingos aukšto našumo elektroliuminescenciniams taikymams. Šios savybės apima efektyvų tripletinių eksitonų surinkimą, naudojant konkurencingus TADF ir TTA mechanizmus, suteikiant gilesnį supratimą apie mechanizmus, kurie daro įtaką prietaisų veikimui.

2.2. **Taikymas OLED:** Pradžioje šie junginiai buvo išbandyti kaip tripletinių eksitonų surenkančios matricos raudonajam fosforescenciniam emiteriui $(\text{piq})_2\text{Ir}(\text{acac})$ OLED prietaise. Buvo nustatyta, kad abiejų junginių veikimas buvo

palyginamas su arba geresnis už tradicinių matricos tipo junginių, o **CzDbp** matrica pasiekė iki 15,9 % išorinį kvantinį efektyvumą. Be to, išbandant juos kaip spinduolius, buvo pasiekti reikšmingi išoriniai kvantiniai efektyvumai – 19,4 % ir 22,1 % atitinkamai oranžiniams (**AcDbp**) ir geltoniems (**CzDbp**) OLED.

Šie tyrimai ne tik demonstruoja **CzDbp** ir **AcDbp** potencialą pažangiuose elektroluinescenciniuose taikymuose, bet ir reikšmingai prisideda prie šios srities, parodydami šių medžiagų universalumą ir efektyvumą aukšto našumo OLED.

3. Tolesni tyrimai buvo atlikti su dviem keletu donorų pakeistais dicianopiridiniais, kur vienas junginys turėjo tris tos pačios rūšies donorus (3,6-di-tert-butil-karbazolas) (**5a**), o kitas – dviejų tipų donorus (3,6-di-tert-butil-karbazolus ir 3,7-dibromofenotiaziną) (**5b**) jų molekulinėse struktūrose. Šie junginiai buvo vertinami kaip TADF emiteriai, skirti efektyviems OLED:

3.1. **TADF emisija:** Buvo pastebėta, kad junginiai rodė žalią ir oranžinę TADF tipo emisiją iš dviejų skirtingų intramolekulinių krūvio pernešimo būsenų. Šie rezultatai pažymi šių medžiagų potencialą būti panaudotoms aukšto efektyvumo elektroluinescenciniuose prietaisuose.

3.2. **Spinduolių savybių vertinimas:** Spinduolis, pažymėtas kaip **5b**, demonstruojantis dvigubos prigimties TADF, buvo pripažintas kaip neefektyvus dėl neefektyvios sužadintos būsenos relaksacijos, pasireiškiant trumpais prietaisų gyvavimo laikais ir bendrai mažu OLED efektyvumu, pasiekiančiu tik 3,1 % išorinio kvantinio efektyvumo nelegiruotuose ir 5 % legiruotuose bei optimizuotuose prietaisuose. Priešingai, emiteris **5a**, turintis tik vieno tipo donorus, pasirodė esąs daug efektyvesnis. Šis spinduolis ne tik suteikė santykinai ilgą prietaiso tarnavimo laiką, bet ir pasiekė aukštą maksimalų išorinį kvantinį efektyvumą – 8,1 % nelegiruotuose prietaisuose ir įspūdingus 25 % legiruotuose bei optimizuotuose OLED. Galima teigti, kad dviejų tipų donoriai (**5b**) šioje konfigūracijoje yra nenaudingi, nes sukūrė antrinius krūvio pernašos kanalus, todėl patyrė sunkumų tiesioginiame krūvininkų relaksacijos procese, didelę dalį energijos atpalaidavo nespinduliniu būdu. O spinduolis **5a** turi vieną krūvio pernašos kanalą tarp donoro ir akceptoriaus, dėl to eksitonai panaudojami daug efektyviau.

Šie rezultatai pabrėžia kritinę donoro tipo ir konfigūracijos įtaką TADF OLED efektyvumui ir stabilumui, suteikdami vertingų įžvalgų apie medžiagų dizainą būsimiesiems aukšto našumo elektroluinescenciniams prietaisams.

4. Tyrimai taip pat buvo atlikti su trimis (1,3-fenileno)bis(2,6-dimetilpiridino-3,5-dikarbonitrilo) dariniais, turinčiais skirtingus pakaitalus fenileno dalyje (**PPDD**, **FPDD** ir **CzPDD**), siekiant įvertinti jų potencialą kaip tripletinius eksitonus išnaudojančias matricas OLED prietaisams:

4.1. **Tripletinė energija ir krūvinio pernešimo savybės:** Buvo pastebėta, kad visi junginiai turėjo praktiškai identiškas aukštas tripletines energijas, svyruojančias nuo 2,68 iki 2,79 eV. Šios aukštos tripletinės energijos yra būtinos efektyviam tripletinių eksitonų surinkimui ir energijos nuostoliams per neradiacinius gesimo kelius mažinti. Be to, buvo nustatyti aukšti jonizacijos potencialai (5,7–6,06 eV) kartu su panašiais elektronų giminingumais apie 3,0 eV. Šios savybės rodo potencialą būti

efektyviems krūvinio pernešimo mechanizams OLED, kurie yra būtini aukštam elektroliuminescenciniam efektyvumui pasiekti.

4.2. **Tripletų surinkimo mechanizmai:** Tyrimas atskleidė, kad junginiai **PPDD** ir **FPDD**, turintys atitinkamai fenilų ir fluorofenilų grupes, , rodo hibridizuotos ir lokalsios krūvio pernašos (HLCT) savybes. O **CzPDD**, kuriame yra fenilkarbazolo grupė, demonstravo TADF mechanizmą tripletams perimti.

4.3. **OLED matricų efektyvumas:** Tolimesni bandymai apėmė **FPDD** ir **CzPDD** junginių kaip matricų naudojimą žaliame TADF emiteriui DAcIPN. Junginys **CzPDD** puikiai pasirodė kaip matrica, leisdamas pasiekti reikšmingą maksimalų išorinį kvantinį efektyvumą – 21,9 %. Šis rezultatas labai pagerina 12,9 % efektyvumą, nustatytą su tradicine matrica mCBP, tik dar labiau pabrėžia puikias naujosios matricos tripletų surinkimo savybes.

Šios išvados pabrėžia molekulinį pakaitų, įtakojančių fotofizikines savybes ir OLED matricų efektyvumą, svarbą bei suteikia įžvalgų, kaip kurti efektyvesnius elektroliuminescencinius prietaisus.

6. LITERATURE

1. SINGH, L. et al. *Organic light emitting diode (OLED) toward smart lighting and displays technologies : material design strategies, challenges and future perspectives*. . 2023. 256 p. ISBN 9781032197036.
2. STEPHEN, M. et al. Biodegradable Materials for Transient Organic Transistors. In *Advanced Functional Materials* . 2023. Vol. **33**, no. 6. [viewed on 2024-04-30]. .
3. LIGUORI, R. et al. Overcoming Challenges in OLED Technology for Lighting Solutions. In *Electronics 2024, Vol. 13, Page 1299* [interactive]. 2024. Vol. **13**, no. 7, p. 1299. [viewed on 2024-04-30]. Access via: <https://www.mdpi.com/2079-9292/13/7/1299/htm>.
4. MILLER, N.J. - LEON, F.A. OLED Lighting Products: Capabilities, Challenges, Potential. In [interactive]. 2016. [viewed on 2024-04-30]. Access via: <http://www.osti.gov/servlets/purl/1374109/>.
5. YI, J. et al. Advantages, challenges and molecular design of different material types used in organic solar cells. In *Nature Reviews Materials 2023 9:1* [interactive]. 2023. Vol. **9**, no. 1, p. 46–62. [viewed on 2024-10-08]. Access via: <https://www.nature.com/articles/s41578-023-00618-1>.
6. CHAUHAN, A.K. et al. Organic Devices: Fabrication, Applications, and Challenges. In *Journal of Electronic Materials 2021 51:2* [interactive]. 2021. Vol. **51**, no. 2, p. 447–485. [viewed on 2024-10-08]. Access via: <https://link.springer.com/article/10.1007/s11664-021-09338-0>.
7. LEE, H. et al. Quantitative Analysis of Degradation Factors in Blue-Fluorescent Organic-Light-Emitting Diodes. In *ACS Photonics* [interactive]. 2023. Vol. **10**, no. 6, p. 1944–1952. [viewed on 2024-10-08]. Access via: <https://pubs.acs.org/doi/full/10.1021/acsp Photonics.3c00374>.
8. TANKELEVIČIŪTĒ, E. et al. The Blue Problem: OLED Stability and Degradation Mechanisms. In *Journal of Physical Chemistry Letters* [interactive]. 2024. Vol. **15**, no. 4, p. 1034–1047. [viewed on 2024-05-02]. Access via: <https://pubs.acs.org/doi/full/10.1021/acspclett.3c03317>.
9. BAURI, J. et al. Recent advances in efficient emissive materials-based OLED applications: a review. In *Journal of Materials Science 2021 56:34* [interactive]. 2021. Vol. **56**, no. 34, p. 18837–18866. [viewed on 2024-10-08]. Access via: <https://link.springer.com/article/10.1007/s10853-021-06503-y>.
10. WANG, D. et al. Roll-to-roll fabrication of highly transparent Ca:Ag top-electrode towards flexible large-area OLED lighting application. In *Flexible and Printed Electronics* [interactive]. 2021. Vol. **6**, no. 3, p. 035001. [viewed on 2024-05-02]. Access via: <https://iopscience.iop.org/article/10.1088/2058-8585/abf159>.
11. MADHU SEETHARAMAN, S. et al. Challenges and Approaches Towards Defect Free Large Area Organic Light Emitting Diode Fabrication. In *2022 IEEE International Conference on Emerging Electronics, ICEE 2022* . 2022. [viewed on 2024-05-02]. .

12. LI, X. et al. Large-area OLED lightings and their applications. In *Semiconductor Science and Technology* [interactive]. 2011. Vol. **26**, no. 3, p. 034002. [viewed on 2024-05-02]. Access via: <https://iopscience.iop.org/article/10.1088/0268-1242/26/3/034002>.
13. SHIROTA, Y. - KAGEYAMA, H. Small molecular weight materials for (opto)electronic applications: overview. In *Handbook of Organic Materials for Optical and (Opto)Electronic Devices: Properties and Applications* . 2013. p. 3–82. [viewed on 2024-05-02]. .
14. MORAB, S. et al. Review on Charge Carrier Transport in Inorganic and Organic Semiconductors. In *Coatings 2023, Vol. 13, Page 1657* [interactive]. 2023. Vol. **13**, no. 9, p. 1657. [viewed on 2024-05-02]. Access via: <https://www.mdpi.com/2079-6412/13/9/1657/htm>.
15. CHEN, L. et al. Triplet harvesting aryl carbonyl-based luminescent materials: progress and prospective. In *Journal of Materials Chemistry C* [interactive]. 2021. Vol. **9**, no. 48, p. 17233–17264. [viewed on 2024-05-02]. Access via: <https://pubs.rsc.org/en/content/articlehtml/2021/tc/d1tc04184c>.
16. YERSIN, H. et al. The triplet state of organo-transition metal compounds. Triplet harvesting and singlet harvesting for efficient OLEDs. In *Coordination Chemistry Reviews* . 2011. Vol. **255**, no. 21–22, p. 2622–2652. [viewed on 2024-05-02]. .
17. ZENG, X.Y. et al. Management of Multi-Energy-Transfer Channels and Exciton Harvesting for Power-Efficient White Thermally Activated Delayed Fluorescence Diodes. In *Advanced Optical Materials* [interactive]. 2022. Vol. **10**, no. 11, p. 2200277. [viewed on 2024-05-02]. Access via: <https://onlinelibrary.wiley.com/doi/full/10.1002/adom.202200277>.
18. LIU, B. et al. Productive harvesting of triplet excitons in anthracene-based emitters toward high-performance deep-blue nondoped organic light-emitting diodes. In *Materials Today Chemistry* . 2022. Vol. **23**, p. 100630. [viewed on 2024-05-02]. .
19. KÖHLER, A. - BÄSSLER, H. Triplet states in organic semiconductors. In *Materials Science and Engineering: R: Reports* . 2009. Vol. **66**, no. 4–6, p. 71–109. [viewed on 2024-05-02]. .
20. ZHANG, Y. et al. Recent advances in n-type and ambipolar organic semiconductors and their multi-functional applications. In *Chemical Society Reviews* [interactive]. 2023. Vol. **52**, no. 4, p. 1331–1381. [viewed on 2024-05-02]. Access via: <https://pubs.rsc.org/en/content/articlehtml/2023/cs/d2cs00720g>.
21. MITSCHKE, U. - BÄUERLE, P. The electroluminescence of organic materials. In *Journal of Materials Chemistry* [interactive]. 2000. Vol. **10**, no. 7, p. 1471–1507. [viewed on 2024-05-02]. Access via: <https://pubs.rsc.org/en/content/articlehtml/2000/jm/a908713c>.
22. TAO, Y. et al. Thermally Activated Delayed Fluorescence Materials Towards the Breakthrough of Organoelectronics. In *Advanced Materials* [interactive]. 2014. Vol. **26**, no. 47, p. 7931–7958. [viewed on 2024-05-02]. Access via: <https://onlinelibrary.wiley.com/doi/full/10.1002/adma.201402532>.
23. ZHANG, D. et al. Sterically shielded blue thermally activated delayed fluorescence emitters with improved efficiency and stability. In *Materials Horizons* [interactive]. 2016.

Vol. 3, no. 2, p. 145–151. [viewed on 2024-05-02]. Access via: <https://pubs.rsc.org/en/content/articlehtml/2016/mh/c5mh00258c>.

24. FERNANDO DIAS, C.B. et al. Triplet Harvesting with 100% Efficiency by Way of Thermally Activated Delayed Fluorescence in Charge Transfer OLED Emitters. In *Advanced Materials* [interactive]. 2013. Vol. 25, no. 27, p. 3707–3714. [viewed on 2024-05-02]. Access via: <https://onlinelibrary.wiley.com/doi/full/10.1002/adma.201300753>.

25. PERRIN, F. La fluorescence des solutions - Induction moléculaire. – Polarisation et durée d'émission. – Photochimie. In *Annales de Physique* [interactive]. 1929. Vol. 10, no. 12, p. 169–275. [viewed on 2024-05-02]. Access via: <https://www.annphys.org/articles/anphys/abs/1929/12/anphys19291012p169/anphys19291012p169.html>.

26. UOYAMA, H. et al. Highly efficient organic light-emitting diodes from delayed fluorescence. In *Nature* 2012 492:7428 [interactive]. 2012. Vol. 492, no. 7428, p. 234–238. [viewed on 2024-05-02]. Access via: <https://www.nature.com/articles/nature11687>.

27. ENDO, A. et al. Efficient up-conversion of triplet excitons into a singlet state and its application for organic light emitting diodes. In *Applied Physics Letters* [interactive]. 2011. Vol. 98, no. 8. [viewed on 2024-05-02]. Access via: [/aip/apl/article/98/8/083302/340804/Efficient-up-conversion-of-triplet-excitons-into-a](http://aip/apl/article/98/8/083302/340804/Efficient-up-conversion-of-triplet-excitons-into-a).

28. MAIOLO, F. DI et al. Shedding light on thermally-activated delayed fluorescence. In *Chemical Science* [interactive]. 2024. Vol. 15, no. 15, p. 5434–5450. [viewed on 2024-05-02]. Access via: <https://pubs.rsc.org/en/content/articlehtml/2024/sc/d4sc00033a>.

29. ZHOU, J. et al. Charge-transfer-featured materials—promising hosts for fabrication of efficient OLEDs through triplet harvesting via triplet fusion. In *Chemical Communications* [interactive]. 2014. Vol. 50, no. 57, p. 7586–7589. [viewed on 2024-05-03]. Access via: <https://pubs.rsc.org/en/content/articlehtml/2014/cc/c4cc00576g>.

30. KONDAKOV, D.Y. Triplet–triplet annihilation in highly efficient fluorescent organic light-emitting diodes: current state and future outlook. In *Philosophical Transactions of the Royal Society A: Mathematical, Physical and Engineering Sciences* [interactive]. 2015. Vol. 373, no. 2044. [viewed on 2024-05-03]. Access via: <https://royalsocietypublishing.org/doi/10.1098/rsta.2014.0321>.

31. ZHAO, J. et al. Triplet–triplet annihilation based upconversion: from triplet sensitizers and triplet acceptors to upconversion quantum yields. In *RSC Advances* [interactive]. 2011. Vol. 1, no. 6, p. 937–950. [viewed on 2024-05-03]. Access via: <https://pubs.rsc.org/en/content/articlehtml/2011/ra/c1ra00469g>.

32. CHEN, C.-H. et al. Efficient Triplet–Triplet Annihilation Upconversion in an Electroluminescence Device with a Fluorescent Sensitizer and a Triplet–Diffusion Singlet-Blocking Layer. In *Advanced Materials* [interactive]. 2018. Vol. 30, no. 50, p. 1804850. [viewed on 2024-05-03]. Access via: <https://onlinelibrary.wiley.com/doi/full/10.1002/adma.201804850>.

33. LI, W. et al. Employing ~100% excitons in OLEDs by utilizing a fluorescent molecule with hybridized local and charge-transfer excited state. In *Advanced Functional Materials* . 2014. Vol. **24**, no. 11, p. 1609–1614. [viewed on 2024-05-03]. .
34. XIAO, S. et al. Highly efficient hybridized local and Charge-transfer (HLCT) Deep-blue electroluminescence with excellent molecular horizontal orientation. In *Chemical Engineering Journal* . 2022. Vol. **440**, p. 135911. [viewed on 2024-05-03]. .
35. LIU, T. et al. Hybridized local and charge-transfer excited state fluorophores enabling organic light-emitting diodes with record high efficiencies close to 20%. In *Chemical Science* [interactive]. 2021. Vol. **12**, no. 14, p. 5171–5176. [viewed on 2024-05-06]. Access via: <https://pubs.rsc.org/en/content/articlehtml/2021/sc/d1sc00272d>.
36. PAN, Y. et al. Theoretical investigation of high-efficiency organic electroluminescent material: HLCT state and hot exciton process. In *RSC Advances* [interactive]. 2017. Vol. **7**, no. 32, p. 19576–19583. [viewed on 2024-05-06]. Access via: <https://pubs.rsc.org/en/content/articlehtml/2017/ra/c7ra01270e>.
37. LEITONAS, K. et al. White vertical organic permeable-base light-emitting transistors obtained by mixing of blue exciton and orange interface exciplex emissions. In *Journal of Materials Chemistry C* [interactive]. 2022. Vol. **10**, no. 26, p. 9786–9793. [viewed on 2024-05-21]. Access via: <https://pubs.rsc.org/en/content/articlehtml/2022/tc/d2tc01326f>.
38. UOYAMA, H. et al. Highly efficient organic light-emitting diodes from delayed fluorescence. In *Nature* 2012 492:7428 [interactive]. 2012. Vol. **492**, no. 7428, p. 234–238. [viewed on 2024-04-08]. Access via: <https://www.nature.com/articles/nature11687>.
39. AHMAD, V. et al. High EQE and High Brightness Solution-Processed TADF Light-Emitting Transistors and OLEDs. In *Advanced Optical Materials* [interactive]. 2020. Vol. **8**, no. 18, p. 2000554. [viewed on 2024-04-08]. Access via: <https://onlinelibrary.wiley.com/doi/10.1002/adom.202000554>.
40. SOBUS, J. et al. High Performance p- and n-Type Light-Emitting Field-Effect Transistors Employing Thermally Activated Delayed Fluorescence. In *Advanced Functional Materials* [interactive]. 2018. Vol. **28**, no. 28, p. 1800340. [viewed on 2024-04-08]. Access via: <https://onlinelibrary.wiley.com/doi/10.1002/adfm.201800340>.
41. TSIKO, U. et al. Triphenylamino or 9-phenyl carbazolyl-substituted pyrimidine-5-carbonitriles as bipolar emitters and hosts with triplet harvesting abilities. In *Materials Today Chemistry* [interactive]. 2022. Vol. **25**, p. 100955. [viewed on 2024-04-08]. Access via: <https://linkinghub.elsevier.com/retrieve/pii/S2468519422001847>.
42. MCCARTHY, M.A. et al. Low-voltage, low-power, organic light-emitting transistors for active matrix displays. In *Science* [interactive]. 2011. Vol. **332**, no. 6029, p. 570–573. [viewed on 2024-04-08]. Access via: <https://www.science.org/doi/10.1126/science.1203052>.
43. DOLLINGER, F. et al. Vertical Organic Thin-Film Transistors with an Anodized Permeable Base for Very Low Leakage Current. In *Advanced Materials* [interactive]. 2019. Vol. **31**, no. 19, p. 1900917. [viewed on 2024-04-08]. Access via: <https://onlinelibrary.wiley.com/doi/full/10.1002/adma.201900917>.

44. TSENG, Z.L. et al. Thermally activated delayed fluorescence in commercially available materials for solution-process exciplex oleds. In *Polymers* [interactive]. 2021. Vol. **13**, no. 10, p. 1668. [viewed on 2024-04-08]. Access via: <https://www.mdpi.com/2073-4360/13/10/1668/htm>.
45. GUZAUSKAS, M. et al. Dual nature of exciplexes: exciplex-forming properties of carbazole and fluorene hybrid trimers. In *Journal of Materials Chemistry C* [interactive]. 2019. Vol. **7**, no. 1, p. 25–32. [viewed on 2024-04-09]. Access via: <http://xlink.rsc.org/?DOI=C8TC04708A>.
46. ANDRULEVICIENE, V. et al. TADF versus TTA emission mechanisms in acridan and carbazole-substituted dibenzo[a,c]phenazines: Towards triplet harvesting emitters and hosts. In *Chemical Engineering Journal*. 2021. Vol. **417**, p. 127902. [viewed on 2024-05-21].
47. BAN, X. et al. Design of efficient thermally activated delayed fluorescence blue host for high performance solution-processed hybrid white organic light emitting diodes. In *Chemical Science* [interactive]. 2019. Vol. **10**, no. 10, p. 3054–3064. [viewed on 2024-04-10]. Access via: <http://xlink.rsc.org/?DOI=C8SC05456H>.
48. ZHANG, L. - CHEAH, K.W. Thermally Activated Delayed Fluorescence Host for High Performance Organic Light-Emitting Diodes. In *Scientific Reports* [interactive]. 2018. Vol. **8**, no. 1, p. 8832. [viewed on 2024-04-10]. Access via: <https://www.nature.com/articles/s41598-018-27238-y>.
49. LIU, Y. et al. All-organic thermally activated delayed fluorescence materials for organic light-emitting diodes. In *Nature Reviews Materials* [interactive]. 2018. Vol. **3**, no. 4, p. 18020. [viewed on 2024-04-10]. Access via: <https://www.nature.com/articles/natrevmats201820>.
50. YANG, Z. et al. Recent advances in organic thermally activated delayed fluorescence materials. In *Chemical Society Reviews* [interactive]. 2017. Vol. **46**, no. 3, p. 915–1016. [viewed on 2024-04-10]. Access via: <http://xlink.rsc.org/?DOI=C6CS00368K>.
51. QIAO, X. - MA, D. Nonlinear optoelectronic processes in organic optoelectronic devices: Triplet-triplet annihilation and singlet fission. In *Materials Science and Engineering: R: Reports* [interactive]. 2020. Vol. **139**, p. 100519. [viewed on 2024-04-10]. Access via: <https://linkinghub.elsevier.com/retrieve/pii/S0927796X19301123>.
52. ZHOU, J. et al. Upconversion Luminescent Materials: Advances and Applications. In *Chemical Reviews* [interactive]. 2015. Vol. **115**, no. 1, p. 395–465. [viewed on 2024-04-10]. Access via: <https://pubs.acs.org/doi/10.1021/cr400478f>.
53. WEX, B. - KAAFARANI, B.R. Perspective on carbazole-based organic compounds as emitters and hosts in TADF applications. In *Journal of Materials Chemistry C* [interactive]. 2017. Vol. **5**, no. 34, p. 8622–8653. [viewed on 2024-04-10]. Access via: <http://xlink.rsc.org/?DOI=C7TC02156A>.
54. BEZVIKONNYI, O. et al. Diphenylsulfone-based hosts for electroluminescent devices: Effect of donor substituents. In *Dyes and Pigments* [interactive]. 2020. Vol. **175**, p. 108104. [viewed on 2024-04-10]. Access via: <https://linkinghub.elsevier.com/retrieve/pii/S014372081932443X>.

55. HSIN, M.-H. et al. P-161: 89.3% Lifetime Elongation of Blue TTA-OLED with Assistant Host. In *SID Symposium Digest of Technical Papers* [interactive]. 2016. Vol. **47**, no. 1, p. 1727–1729. [viewed on 2024-04-10]. Access via: <https://onlinelibrary.wiley.com/doi/10.1002/sdtp.11043>.
56. SONG, X. et al. Understanding and Manipulating the Interplay of Wide-Energy-Gap Host and TADF Sensitizer in High-Performance Fluorescence OLEDs. In *Advanced Materials* [interactive]. 2019. Vol. **31**, no. 35, p. 1901923. [viewed on 2024-04-10]. Access via: <https://onlinelibrary.wiley.com/doi/10.1002/adma.201901923>.
57. DIAS, F.B. et al. The Role of Local Triplet Excited States and D-A Relative Orientation in Thermally Activated Delayed Fluorescence: Photophysics and Devices. In *Advanced Science* [interactive]. 2016. Vol. **3**, no. 12, p. 1600080. [viewed on 2024-04-12]. Access via: <https://onlinelibrary.wiley.com/doi/10.1002/advs.201600080>.
58. ARSENYAN, P. et al. Dual versus normal TADF of pyridines ornamented with multiple donor moieties and their performance in OLEDs. In *Journal of Materials Chemistry C* [interactive]. 2021. Vol. **9**, no. 11, p. 3928–3938. [viewed on 2024-05-21]. Access via: <https://pubs.rsc.org/en/content/articlehtml/2021/tc/d0tc05745b>.
59. UOYAMA, H. et al. Highly efficient organic light-emitting diodes from delayed fluorescence. In *Nature* [interactive]. 2012. Vol. **492**, no. 7428, p. 234–238. [viewed on 2024-04-16]. Access via: <https://www.nature.com/articles/nature11687>.
60. SATO, K. et al. Organic Luminescent Molecule with Energetically Equivalent Singlet and Triplet Excited States for Organic Light-Emitting Diodes. In *Physical Review Letters* [interactive]. 2013. Vol. **110**, no. 24, p. 247401. [viewed on 2024-04-16]. Access via: <https://link.aps.org/doi/10.1103/PhysRevLett.110.247401>.
61. JEON, S.K. et al. Recent Progress of the Lifetime of Organic Light-Emitting Diodes Based on Thermally Activated Delayed Fluorescent Material. In *Advanced Materials* [interactive]. 2019. Vol. **31**, no. 34, p. 1803524. [viewed on 2024-04-16]. Access via: <https://onlinelibrary.wiley.com/doi/10.1002/adma.201803524>.
62. ZHENG, X. et al. Achieving 21% External Quantum Efficiency for Nondoped Solution-Processed Sky-Blue Thermally Activated Delayed Fluorescence OLEDs by Means of Multi-(Donor/Acceptor) Emitter with Through-Space/-Bond Charge Transfer. In *Advanced Science* [interactive]. 2020. Vol. **7**, no. 7, p. 1902087. [viewed on 2024-04-16]. Access via: <https://onlinelibrary.wiley.com/doi/10.1002/advs.201902087>.
63. KREIZA, G. et al. Suppression of benzophenone-induced triplet quenching for enhanced TADF performance. In *Journal of Materials Chemistry C* [interactive]. 2019. Vol. **7**, no. 37, p. 11522–11531. [viewed on 2024-04-16]. Access via: <http://xlink.rsc.org/?DOI=C9TC02408E>.
64. CHAN, C.-Y. et al. Efficient and stable sky-blue delayed fluorescence organic light-emitting diodes with CIEy below 0.4. In *Nature Communications* [interactive]. 2018. Vol. **9**, no. 1, p. 5036. [viewed on 2024-04-16]. Access via: <https://www.nature.com/articles/s41467-018-07482-6>.
65. ZOU, S. et al. High-Performance Nondoped Blue Delayed Fluorescence Organic Light-Emitting Diodes Featuring Low Driving Voltage and High Brightness. In *Advanced Science*

[interactive]. 2020. Vol. 7, no. 3, p. 1902508. [viewed on 2024-04-16]. Access via: <https://onlinelibrary.wiley.com/doi/10.1002/adv.201902508>.

66. VIGANTE, B. et al. Synthesis of Linear and V-Shaped Carbazolyl-Substituted Pyridine-3,5-dicarbonitriles Exhibiting Efficient Bipolar Charge Transport and E-Type Fluorescence. In *Chemistry (Weinheim an der Bergstrasse, Germany)* [interactive]. 2019. Vol. 25, no. 13, p. 3325–3336. [viewed on 2024-04-16]. Access via: <http://www.ncbi.nlm.nih.gov/pubmed/30536688>.

67. GIEBINK, N.C. et al. Intrinsic luminance loss in phosphorescent small-molecule organic light emitting devices due to bimolecular annihilation reactions. In *Journal of Applied Physics* [interactive]. 2008. Vol. 103, no. 4, p. 44509. [viewed on 2024-04-17]. Access via: [/aip/jap/article/103/4/044509/373538/Intrinsic-luminance-loss-in-phosphorescent-small](http://aip/jap/article/103/4/044509/373538/Intrinsic-luminance-loss-in-phosphorescent-small).

68. LEITONAS, K. et al. 3,5-Dicyanopyridine motifs for electron-transporting semiconductors: from design and synthesis to efficient organic light-emitting diodes. In *Journal of Materials Chemistry C* [interactive]. 2023. Vol. 11, no. 28, p. 9514–9526. [viewed on 2024-05-21]. Access via: <https://pubs.rsc.org/en/content/articlehtml/2023/tc/d3tc00841j>.

69. PIMPUTKAR, S. et al. Prospects for LED lighting. In *Nature Photonics* [interactive]. 2009. Vol. 3, no. 4, p. 180–182. [viewed on 2024-04-19]. Access via: <https://www.nature.com/articles/nphoton.2009.32>.

70. PHELAN, G.M. OLED Lighting Hits the Market. In *Information Display* [interactive]. 2018. Vol. 34, no. 1, p. 10–15. [viewed on 2024-04-19]. Access via: <https://sid.onlinelibrary.wiley.com/doi/10.1002/j.2637-496X.2018.tb01054.x>.

71. O'BRIEN, D.F. et al. Improved energy transfer in electrophosphorescent devices. In *Applied Physics Letters* [interactive]. 1999. Vol. 74, no. 3, p. 442–444. [viewed on 2024-04-19]. Access via: <https://pubs.aip.org/apl/article/74/3/442/107683/Improved-energy-transfer-in-electrophosphorescent>.

72. FLEETHAM, T. et al. Phosphorescent Pt(II) and Pd(II) Complexes for Efficient, High-Color-Quality, and Stable OLEDs. In *Advanced Materials* [interactive]. 2017. Vol. 29, no. 5, p. 1601861. [viewed on 2024-04-19]. Access via: <https://onlinelibrary.wiley.com/doi/10.1002/adma.201601861>.

73. UOYAMA, H. et al. Highly efficient organic light-emitting diodes from delayed fluorescence. In *Nature* [interactive]. 2012. Vol. 492, no. 7428, p. 234–238. [viewed on 2024-04-19]. Access via: <https://www.nature.com/articles/nature11687>.

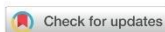
74. HU, Y.X. et al. Efficient selenium-integrated TADF OLEDs with reduced roll-off. In *Nature Photonics* [interactive]. 2022. Vol. 16, no. 11, p. 803–810. [viewed on 2024-04-19]. Access via: <https://www.nature.com/articles/s41566-022-01083-y>.

75. LI, N. et al. Host-Dopant Interaction between Organic Thermally Activated Delayed Fluorescence Emitter and Host Material: Insight into the Excited State. In *Advanced Optical Materials* [interactive]. 2022. Vol. 10, no. 1, p. 2101343. [viewed on 2024-04-19]. Access via: <https://onlinelibrary.wiley.com/doi/10.1002/adom.202101343>.

76. TAO, Y. et al. Organic host materials for phosphorescent organic light-emitting diodes. In *Chemical Society Reviews* [interactive]. 2011. Vol. **40**, no. 5, p. 2943. [viewed on 2024-04-23]. Access via: <https://xlink.rsc.org/?DOI=c0cs00160k>.
77. CHATTERJEE, T. - WONG, K. Perspective on Host Materials for Thermally Activated Delayed Fluorescence Organic Light Emitting Diodes. In *Advanced Optical Materials* [interactive]. 2019. Vol. **7**, no. 1, p. 1800565. [viewed on 2024-04-23]. Access via: <https://onlinelibrary.wiley.com/doi/10.1002/adom.201800565>.
78. LEE, J.-H. et al. Bistriazoles with a Biphenyl Core Derivative as an Electron-Favorable Bipolar Host of Efficient Blue Phosphorescent Organic Light-Emitting Diodes. In *ACS Applied Materials & Interfaces* [interactive]. 2020. Vol. **12**, no. 44, p. 49895–49904. [viewed on 2024-04-23]. Access via: <https://pubs.acs.org/doi/10.1021/acsami.0c13705>.
79. MACÍAS-RUVALCABA, N.A. - EVANS, D.H. Reversible dimerization of anion radicals: Studies of two cyanopyridines. In *Journal of Electroanalytical Chemistry* [interactive]. 2011. Vol. **660**, no. 2, p. 243–246. [viewed on 2024-04-23]. Access via: <https://linkinghub.elsevier.com/retrieve/pii/S1572665710004492>.
80. LUO, M. et al. Structural investigation, Hirshfeld surface analysis and quantum mechanical study of two dicyanopyridine derivatives. In *Journal of Molecular Structure* [interactive]. 2021. Vol. **1228**, p. 129748. [viewed on 2024-04-23]. Access via: <https://linkinghub.elsevier.com/retrieve/pii/S0022286020320615>.
81. CATARZI, D. et al. 4-Heteroaryl Substituted Amino-3,5-Dicyanopyridines as New Adenosine Receptor Ligands: Novel Insights on Structure-Activity Relationships and Perspectives. In *Pharmaceuticals* [interactive]. 2022. Vol. **15**, no. 4, p. 478. [viewed on 2024-04-23]. Access via: <https://www.mdpi.com/1424-8247/15/4/478/htm>.
82. HORTON, J.R. et al. Structural characterization of dicyanopyridine containing DNMT1-selective, non-nucleoside inhibitors. In *Structure* [interactive]. 2022. Vol. **30**, no. 6, p. 793–802.e5. [viewed on 2024-04-23]. Access via: <https://linkinghub.elsevier.com/retrieve/pii/S0969212622000909>.
83. COCCO, M.T. et al. Synthesis and in vitro antitumoral activity of new 3,5-dicyanopyridine derivatives. In *Bioorganic & Medicinal Chemistry* [interactive]. 2007. Vol. **15**, no. 4, p. 1859–1867. [viewed on 2024-04-23]. Access via: <https://linkinghub.elsevier.com/retrieve/pii/S096808960600959X>.
84. COCCO, M.T. et al. Synthesis and antiproliferative activity of 2,6-Dibenzylamino-3,5-dicyanopyridines on human cancer cell lines. In *European Journal of Medicinal Chemistry* [interactive]. 2005. Vol. **40**, no. 12, p. 1365–1372. [viewed on 2024-04-23]. Access via: <https://linkinghub.elsevier.com/retrieve/pii/S0223523405001868>.
85. LI, W. et al. A Twisting Donor-Acceptor Molecule with an Intercrossed Excited State for Highly Efficient, Deep-Blue Electroluminescence. In *Advanced Functional Materials* [interactive]. 2012. Vol. **22**, no. 13, p. 2797–2803. [viewed on 2024-04-23]. Access via: <https://onlinelibrary.wiley.com/doi/10.1002/adfm.201200116>.


86. SEREVIČIUS, T. et al. Temporal Dynamics of Solid-State Thermally Activated Delayed Fluorescence: Disorder or Ultraslow Solvation? In *Journal of Physical Chemistry Letters* [interactive]. 2022. Vol. **13**, no. 7, p. 1839–1844. [viewed on 2024-04-24]. Access via: <https://pubs.acs.org/doi/full/10.1021/acs.jpcclett.1c03810>.
87. ETHERINGTON, M.K. et al. Revealing the spin–vibronic coupling mechanism of thermally activated delayed fluorescence. In *Nature Communications* [interactive]. 2016. Vol. **7**, no. 1, p. 13680. [viewed on 2024-04-24]. Access via: <https://www.nature.com/articles/ncomms13680>.
88. PHAN HUU, D.K.A. et al. Thermally Activated Delayed Fluorescence: Polarity, Rigidity, and Disorder in Condensed Phases. In *Journal of the American Chemical Society* [interactive]. 2022. Vol. **144**, no. 33, p. 15211–15222. [viewed on 2024-04-24]. Access via: <https://pubs.acs.org/doi/full/10.1021/jacs.2c05537>.
89. SKUODIS, E. et al. Aggregation, thermal annealing, and hosting effects on performances of an acridan-based TADF emitter. In *Organic Electronics* [interactive]. 2018. Vol. **63**, p. 29–40. [viewed on 2024-04-25]. Access via: <https://linkinghub.elsevier.com/retrieve/pii/S1566119918304610>.

7. COPIES OF AUTHOR'S PUBLICATIONS



Cite this: *J. Mater. Chem. C*, 2022,
10, 9786

White vertical organic permeable-base light-emitting transistors obtained by mixing of blue exciton and orange interface exciplex emissions†

Karolis Leitonas,  Matas Guzauskas, Uliana Tsiko, Jurate Simokaitiene, Dmytro Volyniuk * and Juozas Vidas Grazulevicius *

In contrast to passive organic devices, such as organic light-emitting diodes and organic solar cells, which require a transistor in electrical circuits to modulate in/out-put signals and/or to reduce parasitic resistivity, organic light-emitting transistors expectedly have the highest market potential of all organic electronic devices, including for high-density logic applications and novel multifunctional photonic circuits. In this work, we aimed to develop white organic light-emitting transistors exploiting a vertical device structure on a permeable base. Before the fabrication of white vertical organic permeable-base light-emitting transistors (OPB-LETs), orange and blue exciplex-based OPB-LETs were studied using known exciplex emitters. Due to electron injection problems, these emitters did not show white electroluminescence in OPB-LETs. When a newly synthesised blue emitter 4,6-bis(4-(9H-carbazol-9-yl)phenyl)pyrimidine-5-carbonitrile (**CzPm**) with orange exciplex forming ability was used, white electroluminescence from OPB-LETs was achieved by mixing of the blue exciton and orange exciplex emissions. Orange exciplex **CzPm**:TAPC with the photoluminescence spectrum peaking at 558 nm was characterized by thermally activated delayed fluorescence. The white OPB-LETs demonstrated a maximum external quantum efficiency of 2.4%, CIE colour coordinates in the range of (0.31, 0.38)–(0.34, 0.36), and colour rendering index in the range from 77 to 93.

Received 1st April 2022,
Accepted 1st June 2022

DOI: 10.1039/d2tc01326f

rsc.li/materials-c

Introduction

Light-emitting devices are among the most required and used devices in human society.¹ Recently, organic light-emitting diodes (OLEDs) have entered the global display and lighting markets due to their competitiveness and environmental reasons.² In most of the applications, OLEDs are utilized in combination with transistors.³ Dual OLED and transistor functionality is characteristic of organic light-emitting transistors (OLETs) which have the potential to find applications in fields such as high-density logic applications, novel multifunctional photonic circuits, indication systems, advertising lighting, etc.^{4,5} OLET technology can potentially even outperform its OLED counterpart in terms of device efficiency when the same set of materials is used.^{6,7} Since OLETs may control light-emission, they can find applications in different fields including active-matrix displays, variable organic lasers or

indication systems.⁸ Several single-colour OLETs have been developed.^{4,5,7–9} To our surprise, information on white OLETs is very limited.¹⁰ There is one example of a white OLET based on a planar device configuration.^{9,10} In fact, this OLET configuration has many disadvantages including the main one related to the emitting area.⁷ In such transistors, only a small part of the active area is light-emitting. White-emitting single-component materials with bipolar charge transport properties reaching very high hole and electron mobilities are required for getting white planar OLETs with competitive output parameters. This task is still quite challenging for the scientific community. This has resulted in limited information on white OLETs. There is also one example of a white OLET with an electrolyte base electrode, which also is not the best candidate for display and lighting applications.¹¹ In contrast, vertical OLETs have the potential to be used as flexible and transparent OLEDs having a wide viewing angle, fast response, high brightness, low turn-on voltage, and emission in the optical range with friendly spectra to human eyes. The single-colour (blue, green and red) organic permeable-base light-emitting transistors (OPB-LETs) based on conventional phosphorescence OLED emitters show output characteristics comparable with those of OLEDs.⁸ The potential of OPB-LETs for white

Department of Polymer Chemistry and Technology, Kaunas University of Technology, Barsausko 59, LT-51423, Kaunas, Lithuania.

E-mail: dmytro.volyniuk@ktu.lt, juozas.grazulevicius@ktu.lt

† Electronic supplementary information (ESI) available. See DOI: <https://doi.org/10.1039/d2tc01326f>

electroluminescence has not been disclosed yet and this is the main aim of this work.

In this study, we aimed to develop white OPB-LETs using exciplex emitters exhibiting thermally activated delayed fluorescence (TADF). Since the first report on TADF materials as promising heavy-metal-free emitters for OLEDs,¹² they have been very rarely used in single-colour OLETs.^{13,14} To our knowledge, TADF emitters have not yet been used in white OLETs. OPB-LETs were developed in this work using the newly synthesized bipolar compound 4,6-bis(4-(9*H*-carbazol-9-yl)phenyl)pyrimidine-5-carbonitrile.¹⁵ They showed white electroluminescence (with CIE colour coordinates of (0.34, 0.36) and colour rendering index of 93) and maximum external quantum efficiency of 2.4%. The entire active area (crossing area between three electrodes) of such OPB-LETs is light-emitting.

Experimental

Materials

The following commercially available functional materials were used for the fabrication of OPB-LETs. Molybdenum trioxide

(MoO₃) was used for the deposition of the hole injection layer, 1,1-bis[(di-4-tolylamino)phenyl]cyclohexane (TAPC) was used as a hole-transporting material, 1,3-bis(9-carbazolyl)benzene (mCP) was used as an exciplex-forming donor, 2,4,6-tris[3-(diphenylphosphinyl)phenyl]-1,3,5-triazine (PO-T2T) was used as an exciplex-forming acceptor, [5,6]-fullerene-C70 (carbon 70 fullerenes, or C70) were used as electron-transporting materials, and lithium fluoride (LiF) was used for the deposition of the electron injection layer (Fig. 1(a)). These materials were purchased either from Lumtec, Ossila or Sigma-Aldrich. 4,6-Bis(4-(9*H*-carbazol-9-yl)phenyl)pyrimidine-5-carbonitrile (CzPm) was synthesised according to the procedure described elsewhere.¹⁵ Compound CzPm was selected as a blue emitter taking into account its blue emission with high photoluminescence quantum yield (PLQY) exceeding 90% and bipolar charge-transporting properties with a relatively high hole mobility value of $2.1 \times 10^{-3} \text{ cm}^2 \text{ V}^{-1} \times \text{s}$ and *ca.* two orders of magnitude lower electron mobility value of $4 \times 10^{-5} \text{ cm}^2 \text{ V}^{-1} \times \text{s}$ at an electric field of $3.6 \times 10^5 \text{ V cm}^{-1}$.¹⁵ Photoelectron spectroscopy was used for the investigation of the charge injecting properties of the film of CzPm. The values of

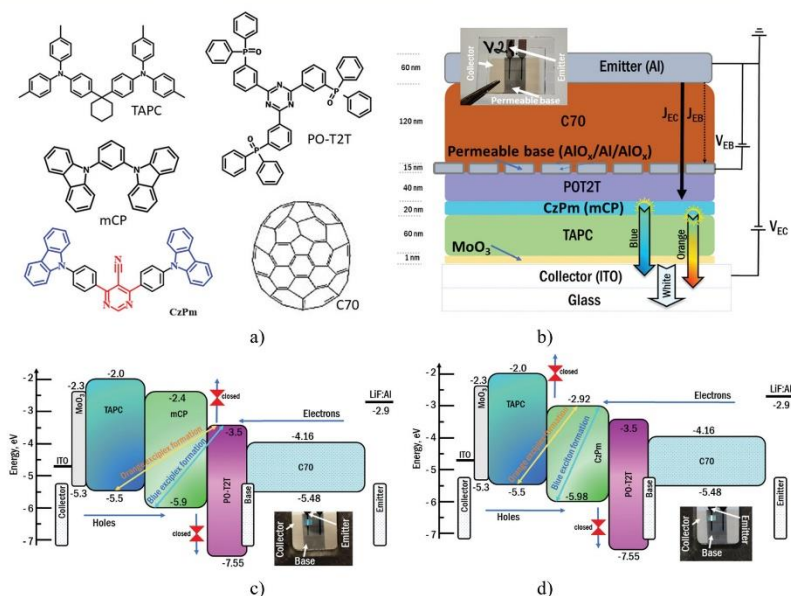


Fig. 1 Molecular structures of the compounds used (a), scheme of the device structure of white (blue) OPB-LETs (b), and equilibrium energy diagrams for the blue (orange) (c) and white (d) OPB-LETs. The values of the highest occupied molecular orbital (HOMO) and lowest unoccupied molecular orbital (LUMO) energy levels are given in [eV]. Insets show photos of the blue (c) and white (d) OPB-LETs under absent (b) or applied (c, d) voltages between the emitter and the collector.

5.98 and 2.92 eV were obtained for the ionization potential and electron affinity of the film of **CzPm**, respectively.¹⁵ Such charge injecting and charge-transporting properties of the film of **CzPm** allowed the application of this compound not only as an emitter but also as a host in organic light-emitting diodes.¹⁵ In addition, compound **CzPm** was characterized by emissive triplet harvesting by upper-level triplet-singlet intersystem crossing. It is concluded in ref. 15 that this mechanism of emissive triplet harvesting may be partly in combination with the contribution of TADF and/or TTA, although their evidence is very limited/non-observed. Indium tin oxide (ITO) covered and pre-patterned glass substrates with ITO resistance of 20 Ω square⁻¹ were purchased from Ossila.

Device fabrication and characterization

The vertical organic permeable base light-emitting transistors were fabricated by a thermo-vacuum deposition. The structures of the devices were the following: ITO/MoO₃[3 nm]/TAPC[80 nm]/PO-T2T[40 nm]/Al[10 nm]/C70[120 nm]/LiF[2 nm]/Al (orange OPB-LET), ITO/MoO₃[1 nm]/TAPC[60 nm]/mCP[20 nm]/PO-T2T[40 nm]/Al[15 nm]/C70[120 nm]/LiF[1 nm]/Al (blue OPB-LET) and ITO/MoO₃[1 nm]/TAPC[60 nm]/CzPm[20 nm]/PO-T2T[40 nm]/Al[15 nm]/C70[120 nm]/LiF[1 nm]/Al (white OPB-LET) (Fig. 1(b)). In OPB-LETs, the top electrode LiF/Al functioned as the emitter (E), the bottom indium tin oxide (ITO) electrode acted as the collector (C) and the middle Al electrode served as the permeable base (B).

The permeable base was a pinhole-containing Al electrode. This middle Al electrode was covered by a self-passivating AlO_x layer by the procedure described elsewhere.^{8,16} To ensure the flow of emitter-collector current (J_{EC}) through the permeable base, the area of the base was much wider than the area of the emitter (Fig. 1(b), inset). The active area of the OPB-LETs, which is the crossing area between the emitter and collector electrodes, was 0.45 mm² (Fig. 1(b)–(d), insets). Sixteen samples were fabricated of one type of orange, blue or white OPB-LET. During vacuum deposition, the arrangement of the different shadow masks for the organic, middle and top electrodes has to be controlled. If there are no problems with the control of the arrangement, there are no problems with the device reproduction.

Output and transfer characteristics of the fabricated OPB-LETs were recorded using Keithley 2400C and Keithley 6517B source electrometers in combination with the certificated photodiode PH100-Si-HA-D0 together with the PC-Based Power and Energy Monitor 11S-LINK (from STANDA). Electroluminescence (EL) spectra were recorded using the Avantes AvaSpec-2048XL spectrometer.

Emission spectra of the exciplexes were recorded using an Edinburgh Instruments FLS980. Photoluminescence (PL) decay curves were taken by the same spectrometer using a PicoQuant LDH-D-C-375 laser (wavelength 374 nm) as the excitation source. PL quantum yields (PLQY) were measured using an integrating sphere (inner diameter of 120 mm) on an Edinburgh Instruments FLS980 spectrometer. To perform PL measurements at different temperatures and under vacuum or an

inert atmosphere (N₂), an Optistat DN2 liquid nitrogen cryostat was used.

Results and discussion

The three-electrode-containing structure of the designed OPB-LETs was based on two parts of organic multilayers. The first one (placed between the top-electrode E and middle electrode B) contained just C70 electron-transporting and LiF electron-injecting layers. The arguments for the selection of the C70 electron-transporting layer were the same as described in the previously published studies.^{8,16} The second part (placed between the middle electrode and bottom electrode) played the role of an OLED structure. Thus, the functions of the second part were charge injection/transport/recombination and exciton formation/radiative recombination, which were expected to result in efficient electroluminescence. The layers of MoO₃ and TAPC ensure efficient injection and transport of holes from the ITO electrode to the light-emitting interface TAPC/PO-T2T (Fig. 1(c) and (d)). The relatively low energy barrier between the LUMO–LUMO levels of C70 and PO-T2T ensures reaching of the interface TAPC/PO-T2T by electrons from the top electrode (emitter). Because of the very big energy barriers between the HOMO–HOMO (2.05 eV) and LUMO–LUMO (1.5 eV) levels of TAPC and PO-T2T, the hole–electron interaction can lead to the formation of interface exciplexes between these two molecules. Indeed, yellowish orange EL was observed from the orange OPB-LETs with the EL spectrum peaking at 558 nm (Fig. 2(a)). The obtained EL spectrum was very similar to the PL spectrum of exciplex TAPC:PO-T2T.¹⁷

The observed EL proved that electrons can pass through the permeable base. Fig. 2(b) shows the transfer curves of orange OPB-LETs which are the current density *versus* voltage plots recorded on the collector and base using the electrical connections schematically shown in Fig. 1(b). Comparison of collector current densities (J_{EC}) and base current densities (J_{EB}) (J_{EC} is much higher than J_{EB}) shows that the leakage current to the permeable base was relatively low. The base leakage current density J_{EB} is lower by more than three orders of magnitude than J_{EC} at the same external voltages. This observation indicates the high insulating efficiency of the self-passivating AlO_x layer (Fig. 1(a)). Collector J_{EC} current density *versus* collector V_{EC} voltage plots recorded at the different base voltages V_{EB} for the orange OPB-LET are shown in Fig. 2(c). The trend of these output curves was the same as those earlier reported for single-color OPB-LETs.^{8,16} At V_{EB} of 4 V, the turn-on voltage of 6.7 V and the maximum brightness of 30 cd m⁻² were observed (Fig. 2(d) and Table 1).

To demonstrate the current (EL) modulation effect, the dependences of the current density J_{EC} and brightness on collector voltage V_{EC} were recorded changing V_{EB} in a very narrow range from 7 to 7.08 V with a small step (Fig. 2(e)). The brightness in a.u. was collected as the response of the photodiode. Selection of such parameters of the experiment (using ultra low voltage step) allowed the recording of these

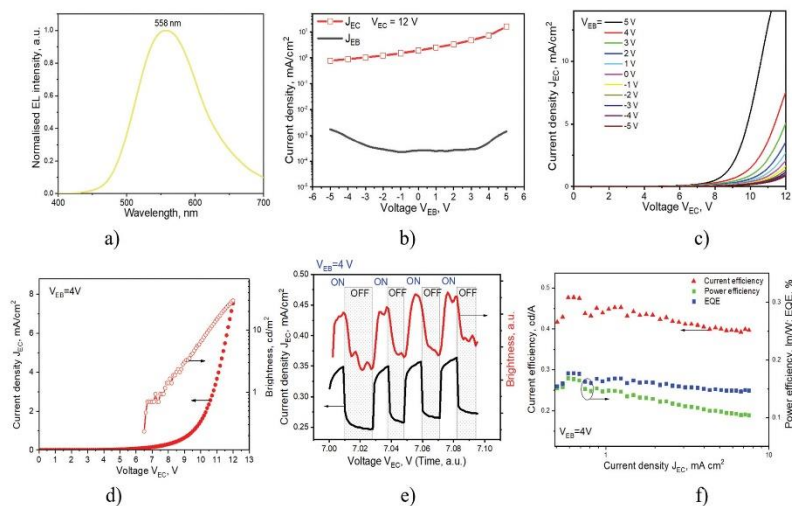


Fig. 2 EL spectrum recorded at 12 V (a), transfer (b) and output (c) current density–voltage characteristics, current density versus voltage and brightness versus voltage dependences at the base voltage V_{EB} of 4 V (d) and at two states “on” ($V_{EB} = 4$ V) and “off” ($V_{EB} = 0$ V) (e), current, power and external quantum efficiencies versus current density on the collector J_{EC} . (f) for the orange exciplex-based OPB-LET.

Table 1 EL parameters of orange, blue and white OPB-LETs

OPB-LETs	V_{on} [V] at set 0.1 [cd m ⁻²]	Max brightness [cd m ⁻²]	Current efficiency	Power efficiency	External quantum efficiency [%]	EL maximum* [nm]	CIE 1931 UCS coordinates (x, y)*	CRI*
			[cd A ⁻¹]	[lm W ⁻¹]				Max
Orange	6.7	30	0.46	0.16	0.17	558		—
Blue	3.6	7	1.75	1.2	1.2	478	(0.22, 0.31)	—
White	3.3	300	5.2	4.16	2.4	478, 556	(0.34, 0.36)	93

*At turn-on voltages.

characteristics during *ca.* 10 s. In the course of the measurements, the base voltage V_{EB} was switched between two states “on” ($V_{EB} = 4$ V) and “off” ($V_{EB} = 0$ V). As a result, clear differences between the corresponding collector current density J_{EC} and output brightness were observed at the different V_{EB} states. In the case of the “on” state, electrons injected from the emitter electrode can pass through the base electrode followed by radiative hole–electron recombination (EL) at the interface of TAPC and PO-T2T (Fig. 1(c)). The efficiency of emitter electrode electron injection increased with the increase of the voltage V_{EB} (Fig. 2(c)). This observation means that electrons passed through the pinhole-containing permeable base can be controlled by the base voltage V_{EB} . The transport of electrons is forced by collector voltage V_{EC} . It is affected by the electron

concentration gradient at pinhole places of the permeable base. Collector current density J_{EC} observed at V_{EB} of 4 V was higher than that observed at $V_{EB} = 0$ V. As a result, different EL brightness was observed at the different voltages V_{EB} (Fig. 2(c)). Small amounts of electrons can pass through the base electrode at the “off” state. No injection of electrons from the base was observed. As a result, the values of collector current density J_{EC} and brightness simultaneously decreased (Fig. 2(e)). These values are well reversible when “on” and “off” states are switched. In the case of the “on” state, higher values of J_{EC} and brightness are observed at longer times due to the higher voltage V_{EC} (7–7.08 V) applied at the collector in comparison to the initial values of J_{EC} and brightness at zero time, and thus at V_{EC} of 7 V. To record current density versus voltage and brightness versus voltage dependences at the base voltage V_{EB} of 4 V (Fig. 2(d)) and at

two states “on” ($V_{EB} = 4$ V) and “off” ($V_{EB} = 0$ V) (Fig. 2(e)), we selected the collector voltage V_{EC} close to the turn-on voltage. The relatively low on/off ratio was observed due to low collector voltage V_{EC} selected. Low maximum external efficiency of 0.17% of orange OPB-LETs suggested replacement of exciplex TAPC:PO-T2T by a more efficient one. With this purpose, the layer of mCP was deposited between the layers of TAPC and PO-T2T (Fig. 1(b) and (c)). Such modification of the structure of the OPB-LET resulted in blue EL with the intensity peak at 478 nm (Fig. 3(a)). This observation is in very good agreement with the PL spectrum of exciplex mCP:PO-T2T and with the EL spectrum of the OLED based on emission of the same exciplex.¹⁸ The hole–electron recombination zone was at the interface of the layers of mCP and PO-T2T (Fig. 1(c)). No electron injection from PO-T2T to mCP occurred due to the high LUMO–LUMO energy barrier of 1.1 eV at the interface mCP/PO-T2T. To visualize those barriers, an energy band diagram with the data for all the studied exciplex-forming compounds is added to the ESI† (Fig. S1). This energy band diagram is also useful for understanding the emission colour origin of the exciplexes. This visualization is also given in Fig. 1(c) and (d). As a result, the EL spectra of the blue OPB-LET did not contain any additional band which may, for instance, originate from the TAPC:exciplex.¹⁹

The transfer current density versus voltage plots (Fig. 3(b)) show that the blue OPB-LET is not characterized by high current leakages through the base ($J_{EC} \gg J_{EB}$). Application of higher voltages to the base leads to higher collector current J_{EC} .

of the blue OPB-LET (Fig. 3(c)). A similar effect was observed for orange OPB-LET at $V_{EC} = 7$ V and $V_{EB} = 4$ V, and maximum brightness of only 7 cd m⁻² was obtained (Fig. 3(d) and Table 1). Fig. 3(e) illustrates the current and brightness modulation effect, which is obtained by switching V_{EB} between “on” and “off” states. Despite low brightness of the blue OPB-LET observed partly because of low sensitivity of the human eye to blue light, the maximum EQE of 1.2% was estimated for the device. For the enhancement of the efficiency of OPB-LETs, the search for more efficient emitters was performed. When the newly synthesised blue emitter **CzPm** was used, white electroluminescence was observed for the modified OPB-LET (Fig. 1(d) and 4(a)).

The high-energy emission band peaking at 478 nm and the low-energy band with the intensity maximum at 556 nm bands can be recognised in the EL spectra of the white OPB-LET (Fig. 4(a)). The band peaking at 478 nm is related to blue exciton emission of **CzPm**. The lower-energy band is apparently related to orange exciplex emission at the interfaces **CzPm**/PO-T2T or **CzPm**/TAPC. To disclose the nature of the emission at 556 nm, PL spectra of solid mixtures **CzPm**:PO-T2T(50:50 wt%) and **CzPm**:TAPC(50:50 wt%) were recorded (Fig. 5(a)). The blue shift of the PL spectrum of the mixture **CzPm**:PO-T2T relative to the PL spectrum of the film of **CzPm** is attributed to the solid-state solvatochromism-like process. The red shift of the PL spectrum of the mixture of **CzPm** and TAPC

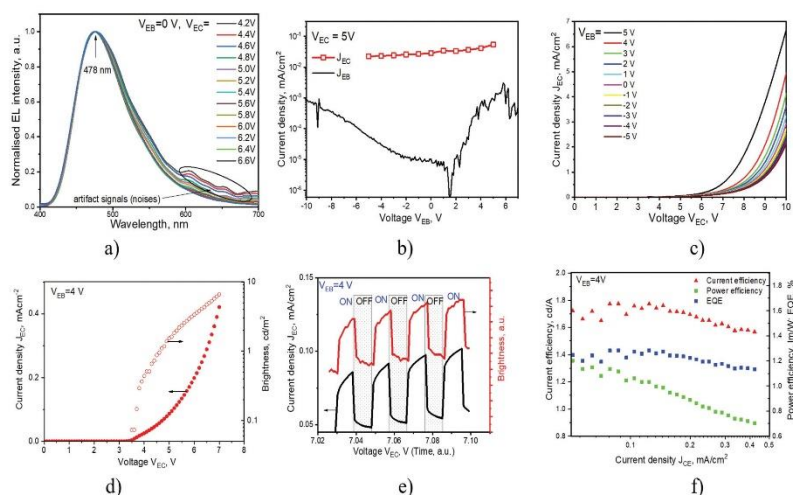


Fig. 3 EL spectra recorded at different voltages (a); transfer (b) and output (c) current density–voltage characteristics; current density versus voltage and brightness versus voltage plots at the base voltage V_{EB} of 4 V (d) and at two states “on” ($V_{EB} = 4$ V) and “off” ($V_{EB} = 0$ V) (e); current, power and external quantum efficiencies versus current density on the collector J_{EC} . (f) for the blue exciplex-based OPB-LET.

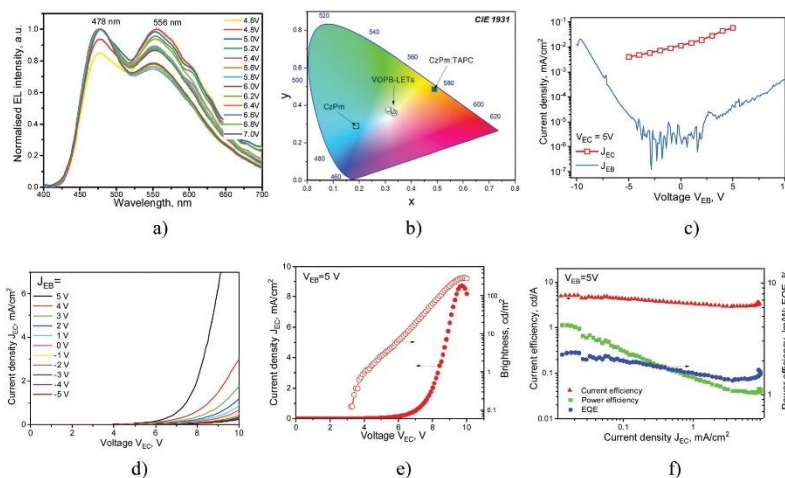


Fig. 4 EL spectra (a) and CIE 1931 colour coordinates (b) observed at the different voltages; transfer (c) and output (d) current density–voltage characteristics; current density versus voltage and brightness versus voltage plots at the base voltage V_{EB} of 5 V (e); current, power and external quantum efficiencies versus current density on the collector J_{EC} (f) for the white exciplex-based OPB-LET. The colour coordinates of exciton emission of **CzPm** and of the emission of exciplex **CzPm:TAPC** are added to the CIE colour diagram (b).

with respect to the PL spectrum of the film of **CzPm** can be attributed to exciplex formation. Typically, exciplex emission is characterized by TADF.²⁰ If it is so, more intensive emission should be observed of exciplex **CzPm:TAPC** when triplets are not quenched by oxygen. Indeed, a clear increase of intensity of exciplex emission of **CzPm:TAPC** was observed after evacuation (Fig. 5(b) and Fig. S2, ESI†). Long-lived TADF was observed for exciplex **CzPm:TAPC** due to its small ΔE_{ST} of 0.02 eV and activation energy (E_a) of 11 meV (Fig. 5(c) and (d)). To obtain the activation energy E_a , the temperature dependences of the rate of reverse intersystem crossing (k_{RISC}) were fitted using the Arrhenius dependence $k_{RISC} = A \times \exp(-E_a/k_B T)$, where k_B is the Boltzmann constant and A is the frequency factor involving the spin–orbit coupling constant (Fig. 5(d)). The fitting was provided in the range of temperatures from 140 to 300 K where phosphorescence was not observed. In contrast, PL spectra and PL decays of the film of the mixture of **CzPm** and PO-T2T were not sensitive to oxygen (Fig. S3, ESI†).

To provide more details on the TADF properties of exciplex-forming molecular mixture **CzPm:TAPC**, its PL spectra and PL decay curves were recorded at the different temperatures (Fig. 5(e) and (f)). At 77 K, the curve of decay of exciplex emission of **CzPm:TAPC** (marked by red colour) is shorter than that observed at the temperature of 140 K indicating the thermal activation process. However, at 300 K, the curve of the decay of exciplex emission of **CzPm:TAPC** (marked by

brown colour) is also shorter than that observed at the temperature of 140 K indicating non-emissive energy loss. This claim is in agreement with the intensity of the exciplex emission of **CzPm:TAPC**, which decreased with the increase of the temperature from 140 to 300 K (Fig. 5(e)). A similar observation for exciplex emission was recently reported and explained by the undermining of thermal activation by decreasing population of triplet states of exciplex-forming moieties/molecules.²¹ At 300 K, exciplex emission of **CzPm:TAPC** was characterized by PLQY of 11%. Relatively low PLQY of exciplex emission of the molecular mixture of TAPC and **CzPm** is caused by the increase of non-radiative rates of the triplet (k_{nr}^3) and singlet (k_{nr}^1) states with increasing temperature (Table S1, ESI†). It is difficult to answer on how to prevent the increase in non-radiative rates with increasing temperature. Apparently, new exciplex-forming molecular mixtures have to be used to reach better device performance. The development of such systems will hopefully be initiated by this study.

To confirm the TADF contribution to the exciplex emission of the molecular mixture TAPC:**CzPm** exciplex, we additionally recorded transient EL curves of blue and orange components of EL of the TAPC:**CzPm** based device (Fig. 6). The TADF contribution of the orange component of the TAPC:**CzPm** exciplex can be additionally supported by the long-lived decay curves. At 440 nm, a shortened EL decay curve was observed. Nevertheless, the triplet harvesting of the blue component of **CzPm**

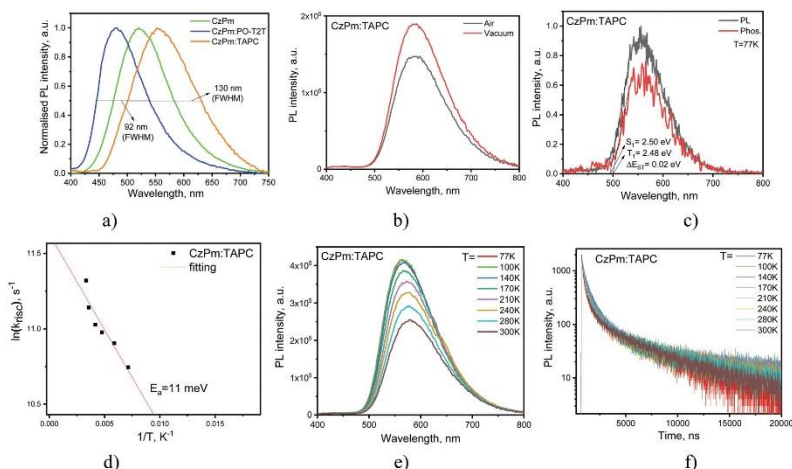


Fig. 5 Normalized PL spectra (a) of the films of **CzMm:PO-T2T**, **CzMm**, and **CzMm:TAPC**; PL spectra (b) of the film of **CzMm:TAPC** recorded in air and under vacuum; PL spectrum and phosphorescent spectrum (recorded with delay of 0.1 ms after excitation) of the film of **CzMm:TAPC** recorded at 77 K (c); the rate of reverse intersystem crossing (d) of **TAPC:CzMm** as a function of temperature. PL spectra (e) and PL decays (f) of the film of **CzMm:TAPC** recorded at different temperatures.

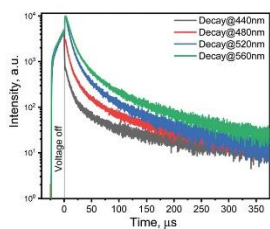


Fig. 6 Transient EL curves of the **TAPC:CzMm** based device.

emission was also evident. This observation is related to the upper triplet singlet intersystem crossing as it is discussed elsewhere.¹³

Due to the mixing of blue exciton emission of **CzMm** and orange exciplex emission of **CzMm:TAPC**, the **CzMm**-based OPB-LET was characterized by white EL with colour coordinates close to colour coordinates (0.33, 0.33) of nature white colour (Fig. 4(b) and Table 1). The recorded EL spectra were characterized by colour rendering index (CRI) falling in the range of 77 to 93 (Fig. S4, ESI†). Such high CRI values can be explained by broad orange exciplex emission with full width at half maximum (FWHM) of the spectrum of 130 nm (Fig. 5(a)). With

increasing intensity of the blue band with FWHM of 92 nm under higher voltages, CRI values slightly decreased (Fig. S4, ESI†). For comparison, we collected the representative parameters of the known white light-emitting OLETs in Table S2 (ESI†). In addition, characteristics of single-colour light-emitting OLETs with a permeable-base are given in Table S2 (ESI†).

The observation of exciplex emission of **CzMm:TAPC** shows that injected electrons reached the interface of the layers of **CzMm** and **TAPC** due to the relatively low LUMO value of **CzMm** (Fig. 1(d)). The transfer and output current density-voltage characteristics of white OPB-LET were similar to those of the above described orange and blue OPB-LETs (Fig. 4(c) and (d)). This observation indicates the similar working mechanism of the white OPB-LET of single-colour OPB-LETs.⁸ Compared to the orange and blue OPB-LETs, the white OPB-LET was characterized by a low turn-on voltage of 3.3 V, high maximum brightness of 300 cd m^{-2} , and high EQE of 2.4%. These results can be explained by the TADF properties of the newly observed exciplex **CzMm:TAPC**, and good charge injecting and charge transporting properties of the film of **CzMm**. The developed first example of a white OPB-LET is a good starting point for the significant improvement of its characteristics when more efficient emitters are available.

Conclusions

Three types of vertical organic permeable-base light-emitting transistors (orange, blue and white) were investigated

exploiting emissions of interface exciplexes. The exploitation of the complex of useful properties, such as the formation of an exciplex exhibiting orange TADF, relatively deep LUMO of -2.92 eV, and hole and electron transport, blue emission of the newly synthesized compound 4,6-bis(4-(9H-carbazol-9-yl)phenyl)pyrimidine-5-carbonitrile allowed white electro-luminescence to be obtained from the vertical organic permeable-base light-emitting transistor. It showed a low turn-on voltage of 3.3 V, high maximum brightness of 300 cd m $^{-2}$, and high external quantum efficiency of 2.4%.

Data availability

The raw/processed data required to reproduce these findings cannot be shared at this time as the data also forms part of an ongoing study initially titled as "Triphenylamino or 9-phenyl carbazolyl substituted pyrimidine-5-carbonitriles as bipolar emitters and hosts with upper triplet harvesting abilities".¹³

Conflicts of interest

There are no conflicts to declare.

Acknowledgements

This project has received funding from the European Regional Development Fund (project no. 01.2.2-LMT-K-718-01-0015) under grant agreement with the Research Council of Lithuania (LMTLT).

References

- R. F. Service, *Science*, 2005, **310**, 1762–1763.
- S. Reineke, F. Lindner, G. Schwartz, N. Seidler, K. Walzer, B. Lüssem and K. Leo, *Nature*, 2009, **459**, 234–238.
- H.-S. Kim and D.-K. Kim, *IEEE J. Solid-State Circuits*, 2018, **53**, 484–500.
- Z. Wu, Y. Liu, E. Guo, G. Darbandy, S.-J. Wang, R. Hübner, A. Kloes, H. Kleemann and K. Leo, *Nat. Mater.*, 2021, **20**, 1007–1014.
- Z. Qin, H. Gao, H. Dong and W. Hu, *Adv. Mater.*, 2021, **33**, 2007149.
- R. Capelli, S. Toffanin, G. Generali, H. Usta, A. Facchetti and M. Muccini, *Nat. Mater.*, 2010, **9**, 496–503.
- L. Hou, X. Zhang, G. F. Cotella, G. Carnicella, M. Herder, B. M. Schmidt, M. Pätzelt, S. Hecht, F. Cacialli and P. Samori, *Nat. Nanotechnol.*, 2019, **14**, 347–353.
- M. A. McCarthy, B. Liu, E. P. Donoghue, I. Kravchenko, D. Y. Kim, F. So and A. G. Rinzler, *Science*, 2011, **332**, 570–573.
- T.-H. Ke, R. Gehlhaar, C.-H. Chen, J.-T. Lin, C.-C. Wu and C. Adachi, *Appl. Phys. Lett.*, 2009, **95**, 063303.
- C. Liu, X. Liu, W. Lai and W. Huang, *Adv. Mater.*, 2018, **30**, 1802466.
- J. Liu, S.-Y. Chou, K. Tong, X. Luan, F. Zhao, Q. Pei and H. Li, *J. Phys. Chem. C*, 2017, **121**, 10112–10118.
- H. Uoyama, K. Goushi, K. Shizu, H. Nomura and C. Adachi, *Nature*, 2012, **492**, 234–238.
- V. Ahmad, J. Sobus, F. Bencheikh, M. Mamada, C. Adachi, S. Lo and E. B. Namdas, *Adv. Opt. Mater.*, 2020, **8**, 2000554.
- J. Sobus, F. Bencheikh, M. Mamada, R. Wawrzinek, J. Ribierre, C. Adachi, S. Lo and E. B. Namdas, *Adv. Funct. Mater.*, 2018, **28**, 1800340.
- U. Tsiko, D. Volyniuk, V. Andruleviciene, K. Leitonas, G. Sych, O. Bezikonny, V. Jasinskas, V. Gulbinas, P. Stakhira and J. V. Grazulevicius, *Mater. Today Chem.*, 2022, **22**, 100955.
- F. Dollinger, K. G. Lim, Y. Li, E. Guo, P. Formánek, R. Hübner, A. Fischer, H. Kleemann and K. Leo, *Adv. Mater.*, 2019, **31**, 1900917.
- Z.-L. Tseng, W.-L. Huang, T.-H. Yeh, Y.-X. Xu and C.-H. Chiang, *Polymers*, 2021, **13**, 1668.
- M. Guzauskas, D. Volyniuk, A. Tomkeviciene, A. Pidluzhna, A. Lazauskas and J. V. Grazulevicius, *J. Mater. Chem. C*, 2019, **7**, 25–32.
- C. K. Vipin, A. Shukla, K. Rajeev, M. Hasan, S.-C. Lo, E. B. Namdas, A. Ajayaghosh and K. N. N. Unni, *J. Phys. Chem. C*, 2021, **125**, 22809–22816.
- K. Goushi, K. Yoshida, K. Sato and C. Adachi, *Nat. Photonics*, 2012, **6**, 253–258.
- K. Traskovskis, A. Sebris, I. Novosjolova, M. Turks, M. Guzauskas, D. Volyniuk, O. Bezikonny, J. V. Grazulevicius, A. Mishnev, R. Grzibowski and A. Vembris, *J. Mater. Chem. C*, 2021, **9**, 4532–4543.



TADF versus TTA emission mechanisms in acridan and carbazole-substituted dibenzo[a,c]phenazines: Towards triplet harvesting emitters and hosts

Viktorija Andrulevičienė^a, Karolis Leitonas^b, Dmytro Volyniuk^b, Gjergji Sini^{c,*}, Juozas Vidas Grazulevičius^{b,*,†}, Vytautas Getautis^a

^a Department of Organic Chemistry, Kaunas University of Technology, Radvilainų pl. 19, LT-50254 Kaunas, Lithuania

^b Department of Polymer Chemistry and Technology, Kaunas University of Technology, K. Barausko g. 59, LT-51423 Kaunas, Lithuania

^c Laboratoire de Physicochimie des Polymères et des Interfaces, CY Cergy Paris Université, TA 2528, 5 mail Gay-Lussac, Cergy-Pontoise Cedex 95031, France

ARTICLE INFO

Keywords:

Thermally activated delayed fluorescence
Triplet-triplet annihilation
Organic light emitting diode
Bipolar charge transport
"Dynamical" state energy diagram

ABSTRACT

Carbazole or acridan-substituted dibenzo[a,c]phenazines (**CzDbp** and **AcDbp**, respectively) were synthesized and investigated exploiting the donor-acceptor-donor (D-A-D) architecture expecting thermally activated delayed fluorescence (TADF) in both cases. Unexpectedly, while experimental microsecond-lived TADF behaviour was observed for **AcDbp** efficiency of which was found to be dependent on environment, **CzDbp** exhibited nanosecond-lived fluorescence complemented by triplet-triplet annihilation (TTA). Theoretical calculations by means of the ω B97XD functional with optimally tuned range separation parameter α , were performed for both molecules, supporting their experimentally established electrochemical, optical and photophysical properties. Using the same emitter and device structure, **CzDbp** as the bipolar host allowed to achieve by 12.5% better external quantum efficiency and better roll-off efficiency of organic light-emitting diodes (OLEDs) in comparison to that of OLEDs based on the commercial host 1,3-bis(N-carbazolyl)benzene (mCP). In optimized OLED structure, device based on **CzDbp** host showed higher external quantum efficiency reaching 15.9% and lower roll-off efficiency in comparison to that of reference devices containing commercial hosts. This achievement can be explained by both the fast TTA triplet harvesting enhancing the substantial fluorescence efficiency of **CzDbp**, and by relatively high charge mobilities exceeding 10^{-3} cm²/V·s for holes and 10^{-4} cm²/V·s for electrons. **CzDbp** and **AcDbp** as TADF/TTA emitters were used, respectively, external quantum efficiencies of 19.4% and 22.1% for doped yellow and orange devices were achieved. The detailed discussion on TADF mechanism is presented, and the new "dynamical" state-energy diagram is proposed as the means allowing to better understand the TADF mechanism and the experimental results.

1. Introduction

Materials exhibiting thermally activated delayed fluorescence (TADF) have attracted significant interest in the field of organic optoelectronics [1]. TADF based organic light emitting diodes (OLEDs) can achieve 100% internal quantum efficiency (IQE), which can be attained due to harvesting of triplet excitons through the reverse intersystem crossing (RISC). Concerning TADF hosts based devices, the energy can be transmitted to the guest through the Förster energy transfer (FET) to reach 100% of its utilization [2,3]. It is well known that very small singlet-triplet energy gap (ΔE_{ST}) is essential parameter to achieve

efficient TADF effect via RISC [4]. Low ΔE_{ST} can be obtained using compounds with spatially separated donor (D) and acceptor (A) units with dihedral angle between D and A fragments approaching the orthogonality [5,6]. However, the TADF efficiency is determined not only by ΔE_{ST} but also by the spin-orbit coupling (SOC). The drawback of this architecture is consequently the smallness of SOC, which decreases in parallel with the decreasing ΔE_{ST} : due to the unification of the S₁ and T₁ character when $\Delta E_{ST} = 0$ (both become of CT nature), their coupling tends zero as stipulated by El Sayed's empirical rule [7].

Organic materials emit prompt fluorescence even when ΔE_{ST} is too large for getting RISC. However OLEDs based on prompt fluorescence

* Corresponding authors.

E-mail addresses: gjergji.sini@u-cergy.fr (G. Sini), juozas.grazulevicius@ktu.lt (J.V. Grazulevičius).

<https://doi.org/10.1016/j.cej.2020.127902>

Received 9 September 2020; Received in revised form 24 November 2020; Accepted 26 November 2020

Available online 1 December 2020

1385-8947/© 2020 Elsevier B.V. All rights reserved.

with a theoretical external quantum efficiency (EQE) of 5% cannot meet the industrial requirements. TADF was observed even for compounds with relatively large ΔE_{ST} , witnessing the complexity of TADF mechanisms [8]. Organic materials with large ΔE_{ST} have big potential to be used in OLED technology when they exhibit triplet-triplet annihilation (TTA) (also co-called triplet-triplet fusion) [9,10], "hot excitons" [11], or upper level triplet-singlet intersystem crossing [12]. In this case, two low-energy triplet excitons can be fused to one high-energy singlet exciton. In case of TTA emitters, the theoretical IQE is 62.5%, corresponding to an EQE of 12.5% of OLEDs [9]. EQE values of over 10% were reported for TTA OLEDs [13,14].

Both TADF and TTA materials can be used in OLEDs as hosts when they meet the requirements raised for host including high and balanced charge mobilities, wide transporting band gap with appropriate HOMO and LUMO energy levels for charge injection, high optical, thermal and electrochemical stability [15–17]. Such hosts are used not only for overcoming of aggregation induced quenching of OLED emitters in solid state and for ensuring hole-electron recombination within the light-emitting layer but also for additional triplet harvesting within host [18]. If appropriate combination of TADF host and conventional fluorescent emitter are used, OLEDs (co-called hyperfluorescent OLEDs) with 100% theoretical EQE can be fabricated [19–21]. While the favourable impact of TADF hosts is currently evident, knowledge on TTA OLED hosts is very limited. In this work, we partly aimed to focus on this issue. The development of efficient TADF and TTA hosts is not a routine task since TADF and TTA materials are characterized by highly twisted molecular structures usually inducing poor charge transporting properties.

The use of theoretical predictions before synthesis of potential TADF and TTA materials is essential for saving the developing time and for getting the required properties. Time-dependent density functional theory (TDDFT) is a well-established tool to study S and T excited states of organic molecules. However, TDDFT calculations based on standard functionals can underestimate the excitation energies of the D-A molecules with the CT characteristics hence strongly impact the pertinence of theoretical diagrams of state energies. Range-separated exchange (RS) density functionals with optimally tuned range separation parameter ω were found to perform better in overcoming this problem [22].

Here, we report on new D-A-D compounds with dibenzo[a,c]phenazine acceptor [23,24] substituted at its C-2 and/or C-7 positions by electron donating carbazole or acridan moieties [25,26]. In contrast to low-molar-mass acceptor groups such as $-\text{CF}_3$, $-\text{CN}$, [27], dibenzo[a,c]phenazine as the acceptor was selected expecting appropriate arrangements between planar dibenzo[a,c]phenazine units in solid films required for high electron mobility required for efficient OLED hosts [28]. The compounds were designed as TADF materials, however, contrary to the expectations, TTA was observed for the developed dibenzo[a,c]phenazine derivatives. We should note that Tang et al [29] recently reported on dibenzo[a,c]phenazine derivatives with the different number of acridan moieties at C-3 and/or C-6 positions of dibenzo[a,c]phenazine moiety. These compounds as TADF emitters demonstrated conventional TADF favourable for the fabrication of efficient orange-red OLEDs. Neither evidence of TTA nor application as hosts in OLEDs were previously reported for dibenzo[a,c]phenazine derivatives to the best of our knowledge. Since the developed here compounds demonstrated relatively high mobilities of holes and electrons, they were used not only as triplet harvesting emitters but also as triplet harvesting hosts. Theoretical calculations were performed using ωB97XD functional with optimally tuned range separation parameter ω in order to get insight on the optical, electrochemical and photophysical properties of the compounds.

2. Experimental section

2.1. Materials

In case of OLED fabrications, commercially available molybdenum oxide (MoO_3), hexaazatriphenylenehexacarbonitrile (HAT-CN), di(1-naphthyl)-N,N'-diphenyl (NPB), tris(4-carbazoyl-9-ylphenyl)amine (TCTA), 1,3-bis(N-carbazoyl)benzene (mCP), 3,3-di(9H-carbazol-9-yl)biphenyl (mCBP), bis(1-phenyl-isoquinoline-C2,N)(acetylacetonato)iridium(III) ($\text{Ir}(\text{piq})_2(\text{acac})$), 2,2',2''-(1,3,5-benzinetriyl)-tris(1-phenyl-1-H-benzimidazole) (TPBi), 2,9-bis(naphthalen-2-yl)-4,7-diphenyl-1,10-phenanthroline (nBPhen), fluorolithium (LiF), 8-quinolinolato lithium (Liq) were purchased from Sigma-Aldrich or Ossila and used as received.

In case of synthesis, 9,10-Phenanthrenequinone (Aldrich), N-bromosuccinimide (Aldrich), o-phenylenediamine (Aldrich), zinc chloride (Aldrich), 2-chloro-2-methylpropane (Aldrich), bis(tri-tert-butylphosphine)palladium(0) (Aldrich), sodium tert-butoxide, (Aldrich), 9H-carbazole (Reakhim), 9,9-dimethyl-9,10-dihydroacridine (Center for Physical Sciences and Technology) were purchased as reagent grade chemicals and used as received. 2,7-Dibromo-9,10-phenanthrenequinone, 2,7-dibromodibenzo[a,c]phenazine (BDbp) and 3,6-di-tert-butyl-9H-carbazole were synthesized as reported earlier.[30–32] Thin layer chromatography was performed by using TLC plates covered with a silica gel matrix on aluminum backing (Aldrich).

2.1.1. 2,7-bis(3,6-di-tert-butyl-9H-carbazol-9-yl)dibenzo[a,c]phenazine (CzDbp)

BDpb (0.35 g, 0.8 mmol) and 3,6-di-tert-butyl-9H-carbazole (0.56 g, 2.0 mmol) was dissolved in dry toluene under argon. Then, bis(tri-tert-butylphosphine)palladium(0) (0.008 g, 0.016 mmol) and sodium tert-butoxide (0.38 g, 4.0 mmol) was added. The reaction mixture was heated at 90 °C for 24 h. After cooling to room temperature, the reaction mixture was added into water and was extracted with chloroform. The combined organic layers were washed with water and dried over anhydrous sodium sulfate. After filtration and evaporation, the crude product was purified by column chromatography using hexane/ethylacetate (8/1) as eluent. Compound was obtained as yellow solids in 54% yield. IR (ν in cm^{-1}): 3042 (C-H ar.), 2960 (C-H alk.), 2863 (C-H alk.), 1491 (C-H alk.), 1477 (C-H alk.), 1295 (C-N), 1263 (C-N). ^1H NMR (400 MHz, CDCl_3 - d_6 , δ): 1.43 (s, 36H, CH_3), 7.44–7.51 (m, 8H, ar.), 7.75 (dd, $J = 6.6$ Hz, $J = 3.4$ Hz, 2H, ar.), 7.96 (dd, $J = 8.5$ Hz, $J = 2.2$ Hz, 2H, ar.), 8.15 (s, 4H, ar.), 8.20 (dd, $J = 6.5$ Hz, $J = 3.4$ Hz, 2H, ar.), 8.72 (d, $J = 8.7$ Hz, 2H, ar.), 9.61 (d, $J = 2.2$ Hz, 2H, ar.). ^{13}C NMR (101 MHz, CDCl_3 - d_6 , δ): 32.1, 34.8, 109.4, 116.4, 123.7, 123.8, 124.0, 124.8, 128.6, 130.2, 130.2, 132.1, 138.1, 139.3, 142.5, 143.2. MS (APCI $^+$), $m/z = 835$ [M] $^+$. Anal calcd for $\text{C}_{60}\text{H}_{58}\text{N}_4$: C 86.29; H 6.98; N 6.71; found: C 86.29; H 6.96; N 6.98.

2.1.2. 2,7-bis(9,9-dimethylacridin-10(9H)-yl)dibenzo[a,c]phenazine (AcDbp)

Compound was synthesized according to the same procedure as described above for the synthesis of CzDbp, except that 9,9-dimethyl-9,10-dihydroacridine (0.24 g, 1.1 mmol) was used instead of 3,6-di-tert-butyl-9H-carbazole. The crude product was purified by column chromatography using hexane/ethylacetate (8/1) as eluent. It was recrystallized from eluent. Compound was obtained as orange crystals in 43% yield. IR (ν in cm^{-1}): 3059 (C-H ar.), 3033 (C-H ar.), 2954 (C-H alk.), 2924 (C-H alk.), 2853 (C-H alk.), 1475 (C-H alk.), 1449 (C-H alk.), 1325 (C-N), 1262 (C-N). ^1H NMR (400 MHz, CDCl_3 - d_6 , δ): 1.74 (s, 12H, CH_3), 6.35–6.37 (m, 4H, ar.), 6.88–6.93 (m, 8H, ar.), 7.46–7.48 (m, 4H, ar.), 7.76 (dd, $J = 6.3$ Hz, $J = 2.9$ Hz, 4H, ar.), 8.18 (dd, $J = 6.5$ Hz, $J = 3.4$ Hz, 2H, ar.), 8.84 (d, $J = 8.6$ Hz, 2H, ar.), 9.42 (d, $J = 2.1$ Hz, 2H, ar.). ^{13}C NMR (101 MHz, CDCl_3 - d_6 , δ): 31.5, 36.1, 114.2, 120.8, 125.5, 126.5, 129.5, 130.2, 140.9. MS (APCI $^+$), $m/z = 695$ [M] $^+$. Anal calcd for $\text{C}_{50}\text{H}_{38}\text{N}_4$: C 86.42; H 5.51; N 8.06; found: C 86.56; H

5.24; N 8.19

2.2. Computational methodology

The density functional theory (DFT) [33] and time dependent density functional theory (TD-DFT) [34–36] calculations for molecules were obtained employing the ω B97XD/6-31G(d,p) in gas phase and CPCM/ ω B97XD/6-31G(d,p) in solvents where the value of the ω parameter was tuned by considering the effect of the media. Test calculations with the default ω B97XD and B3LYP functionals were also performed for the comparison of results. Up to 40 excited states were calculated by considering a band half-width at half-maximum of 0.3 eV obtaining the theoretical absorption spectra. The calculations of natural transition orbitals (NTOs) were carried out to visualize molecular orbitals of selected excited-states. The vertical ionization potentials (IP) were calculated as energy difference between neutral and cation radical species at the neutral state geometry. All calculations were performed with the Gaussian16 software.

2.3. Instrumentation

^1H NMR and ^{13}C NMR spectra were obtained of the solutions in deuterated chloroform (CDCl_3-d_6) with a Bruker Avance III spectrometer. The data are given as chemical shifts in δ (ppm) and tetramethylsilane was used as Elemental analysis was performed with an Exeter Analytical CE-440 elemental analyser, Model 440C/H/N/, an internal standard. Mass spectra were obtained on a Waters ZQ 2000 mass spectrometer. IR spectra were recorded with a Vertex 70 Bruker spectrometer. Elemental analysis was performed with an Exeter Analytical CE-440 elemental analyser, Model 440C/H/N. Thermogravimetric analysis (TGA) was performed on a TA Instruments Q50 apparatus at a heating rate of 20 °C/min under nitrogen atmosphere. Differential scanning calorimetry (DSC) measurements were performed on a 100 TA Instruments Q2000 thermal analyser at a heating/cooling rate of 10 °C/min under nitrogen atmosphere. Optical and photophysical properties of solutions in THF, TOL and layers of the synthesized compounds were recorded using a Perkin Elmer Lambda 35 and an Edinburgh Instruments FLS980 spectrometers. Cyclic voltammetry (CV) measurements were carried out using Autolab potentiostat PGSTAT20 in a three electrode cell using platinum rod as a counter electrode, glassy carbon as working electrode and Ag/AgNO₃ as the reference electrode. The experiments were carried out in dry dichloromethane solution containing 0.1 M tetrabutylammonium perchlorate as electrolyte at room temperature under nitrogen atmosphere at a scan rate 50 mV/s. The measurements were calibrated using the internal standard ferrocene/ferrocenium (Fc/Fc⁺). The ionization potentials (IP_{PE}) of the layers of the synthesized compounds were measured by the electron photoemission in air method. [37] Hole drift mobility of the materials was estimated by a time-of-flight (TOF) method. The samples were fabricated with structures of ITO/compound/Al. Commercial indium tin oxide (ITO) coated glass was used as a substrate, which was first cleaned chemically using a bath of distilled water and acetone. Organic and Al films were sequentially vacuum-deposited onto precleaned ITO-coated glass substrates under the vacuum of 2.5-10⁻⁵ mBar using vacuum equipment from Kurt J. Lesker in-built in an MB EcoVap4G glove box. In the TOF experiments, charges were generated by a pulsed third-harmonic Nd:YAG laser EKS-PLA NL300 working at a pulse duration of 3–6 ns and the wavelength of 355 nm. Electric fields were applied by a Keithley 6517B electrometer. A digital storage oscilloscope Tektronix TDS 3032C was used to record TOF transients. The drift mobility was calculated by using the formula $\mu = d^2/U t_b$, where d is the layer thickness, and U the surface potential at the moment of illumination, and t_b is the transit time which was taken from the TOF transients. A Keithley source meter 2400-C was utilized for recording of the current density–voltage characteristics. The current density–luminance characteristics were estimated using a calibrated silicon photodiode with the 6517B Keithley electrometer.

Electroluminescence (EL) spectra were recorded by an Avantes AvaSpec-2048XL spectrometer. The current, power and external quantum efficiencies were estimated utilizing the current density, luminance, and EL spectra as reported earlier. [38]

3. Results and discussion

3.1. Synthesis

As shown in Scheme 1, we designed and synthesized compounds with donor–acceptor–donor (D–A–D) architecture composed of dibenzo [a,c]phenazine (Dbp) acceptor core and peripheral aromatic donor moieties such as 9,9-dimethylacridine (Ac) and 3,6-di-*tert*-butyl-carbazole (Cz). The intermediate compound **BDbp** was prepared through a condensation reaction between 2,7-dibromo-9,10-phenanthrenequinone and *o*-phenylenediamine. The Buchwald–Hartwig amination of **BDbp** with 3,6-di-*tert*-butyl-9H-carbazole or 9,9-dimethyl-9,10-dihydroacridine in the presence of bis(tri-*tert*-butylphosphine)palladium(0) as a catalyst afforded **CzDbp** and **AcDbp**, respectively. The target products were purified by column chromatography. Their chemical structures were confirmed by ^1H and ^{13}C nuclear magnetic resonance (NMR), infrared (IR) spectroscopies, mass spectrometry and elemental analysis.

3.2. Computational details

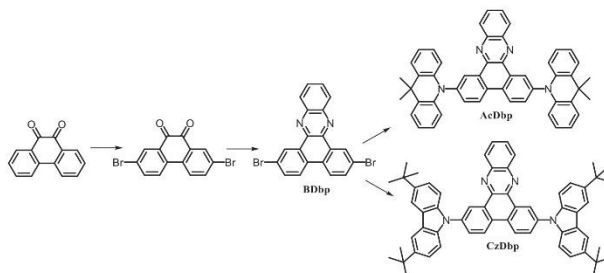
Theoretical calculations were performed using ω B97XD functional with optimally tuned range separation parameter in toluene (TOL) and tetrahydrofuran (THF). Solvents effect was taken into account within the conductor-like polarizable continuum model (CPCM). The ω values were optimally tuned by minimizing a function $J(\omega)$, where ϵ_{HOMO} and ϵ_{LUMO} denote the energies of the HOMO and LUMO, IP and EA are the vertical ionization potential and electron affinity of the molecule, respectively: [39]

$$J(\omega) = [\epsilon_{\text{HOMO}}(\omega) + IP(\omega)]^2 + [\epsilon_{\text{LUMO}}(\omega) + EA(\omega)]^2$$

Calculations using ω B97XD (ω^{default}), ω B97XD with ω tuned in gas (ω^{gas}) and B3LYP functionals were performed for the comparison of the obtained results, and the corresponding results are shown in the Annex I (Supporting information).

3.3. Geometry and molecular orbitals

Theoretical calculations performed with ω tuned in solvents revealed that dihedral angles between Dbp and Ac fragments is 90° in **AcDbp** (Table 1). While analogous dihedral angle between Dbp and Cz moieties in **CzDbp** is affected by the ω meaning of ω B97XD functional. Table 1 indicates that the dihedral angle D-A obtained with the lower $\omega = 0.0011 \text{ \AA}^{-1}$ is $\sim 76^\circ$ and that calculated with the higher $\omega = 0.0337 \text{ \AA}^{-1}$ is $\sim 61^\circ$. The larger dihedral angles in the case of **AcDbp** are due to the shorter (C)–H...Dbp distances as compared to **CzDbp**, in turn stemming from the larger C–C–C angle in the six-atom central ring in Ac as compared to five-atom central ring in Cz ($\sim 122^\circ$ and $\sim 108^\circ$ respectively). The HOMO of **AcDbp** is distributed on the both peripheral Ac units, whereas the LUMO is localized exceptionally over the molecule **Dbp** core (Fig. 1). The spatial separation of the HOMO and LUMO appears because of the perpendicular dihedral angles D-A. In the case of **CzDbp**, HOMO of **CzDbp** at ω^{TOL} B97XD is localized on the Cz moieties extending to the Dbp core, while calculations at ω^{THF} B97XD show HOMO localization on the donor fragments, with less contribution from the Dbp (Fig. 1). As for LUMO of **CzDbp**, in both cases it is localized on the acceptor core.



Scheme 1. Synthetic route for AcDbp and CzDbp.

Table 1

Inter-fragment dihedral angles (degrees), energies of frontier orbitals and vertical ionization potential values for compounds AcDbp and CzDbp calculated at the DFT/6-31G⁺⁺.

	ω B97XD			
	$\omega^{\text{THF}} = 0.0011 \text{ \AA}^{-1}$	$\omega^{\text{TOL}} = 0.0337 \text{ \AA}^{-1}$	$\omega^{\text{THF}} = 0.0011 \text{ \AA}^{-1}$	$\omega^{\text{TOL}} = 0.0322 \text{ \AA}^{-1}$
dihedral angle	AcDbp 90.1	90.3	CzDbp 75.6	60.7
HOMO, eV	-5.01	-5.34	-5.31	-5.56
LUMO, eV	-2.30	-1.91	-2.31	-1.91
IP^{opt} , eV	4.98	5.28	5.28	5.49

3.4. Ionization potentials and charge mobilities

The ionization potentials (IP) of investigated materials were estimated using photoelectron emission (PE) method in air (Fig. S1) and cyclic voltammetry (CV) (Fig. S2). The same IP^{PE} value of 5.5 eV for AcDbp and CzDbp was found which is larger as compared to the IP^{CV} values of 5.25 eV and 5.44 eV, respectively (Table 2). The difference stems from the stronger polarization effects in the solid state (PE measurements). Additionally, CV measurements reveal reduction peaks of the compounds which were used to estimate electron affinity (EA^{CV}) values of 3.12 eV for AcDbp and 3.11 eV for CzDbp (Table 2). The values of EA^{PE} were obtained from the IP^{PE} values and the optical band

gaps (E_g^{opt}), which were deduced from the edges of the absorption spectra of the vacuum deposited layers (Fig. S3). The calculated EA^{PE} value of AcDbp was by 0.24 eV higher than that of CzDbp (2.77 eV and 2.53 eV, respectively). The difference between CV and PE values stem from not only the environmental polarization effects, but also from the fact that the optical gap values used in the calculation of EA^{PE} are larger than the $IP^{\text{CV}} \cdot EA^{\text{CV}}$ gap by 0.6 eV and 0.64 eV of AcDbp and CzDbp, respectively, corresponding to the electron-hole binding energy in the first excited state. In order to extend theoretical investigation of the compounds, IP^{theor} values were calculated. The analysis revealed, that experimental IP^{CV} values of 5.25 eV and 5.44 eV well coincide with the values of IP^{theor} obtained by ω^{TOL} B97XD of 5.28 eV and 5.49, respectively (Table 1, 2).

Charge transporting properties of the vacuum deposited layers of AcDbp and CzDbp were characterized by time-of-flight (ToF) technique. ToF current transients with well recognized transit times were

Table 2
Ionization potential, electron affinity and charge mobility data for AcDbp and CzDbp.

	IP^{PE} , eV	E_g^{opt} , eV	EA^{PE} , eV	IP^{CV} , eV	EA^{CV} , eV	μ_h^a , cm ² /Vs	μ_e^a , cm ² /Vs
AcDbp	5.50	2.73	2.77	5.25	3.12	$2.4 \cdot 10^{13}$	$1.2 \cdot 10^3$
CzDbp	5.50	2.97	2.53	5.44	3.11	$3.8 \cdot 10^{13}$	$1.0 \cdot 10^4$

^a Charge mobility at $2.02 \cdot 10^5$ V/cm.

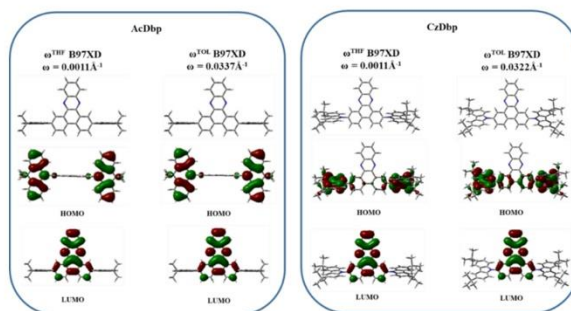


Fig. 1. Geometry and plots of frontier orbitals of AcDbp and CzDbp at B97XD calculated with ω tuned in THF and TOL.

recorded applying positive and negative electric fields (Fig. S4). These results show that solid layers of AcDbp and CzDbp are able to transport both holes and electrons (Fig. 2a). The layers of compounds showed charge-drift mobilities exceeding 10^{-3} cm²/Vs at high electric fields except the electron-drift mobility in the layer of CzDbp which was by one order of magnitude lower. The lower electron mobility of CzDbp may stem from the smaller D-A dihedral angle which might result in larger disorder in packing between LUMO-containing moieties. Compound CzDbp exhibits flexible D-A dihedral angle of ca. 76° in THF and of ca. 61° in toluene, which allows for non-negligible pi-orbital overlaps between donor and acceptor. Meanwhile, AcDbp exhibits constrained angle (of ca. 90° in THF and toluene) because of the rigidity of acridan moiety which is translated in practically zero overlaps between donor and acceptor moieties. On the other hand, the impact of dihedral oscillations is minimal around zero (dihedrals of 90°) as compared to smaller dihedral angles (faster evolution of overlaps). As a result, the D-A dihedral angle in the solid-layer of CzDbp can change in a wider range causing variations in molecular geometry, an increase of the geometrical randomness component of the energetic disorder [40], resulting in reduced electron-drift mobility.

In addition, the smaller electron mobility of CzDbp may result from the *tert*-butyl substituents of carbazole moieties. *Tert*-butyl substituents apparently increase the distance between neighboring CzDbp molecules in the solid films. The increased intermolecular distance may also reduce LUMO-LUMO overlapping between neighboring molecules causing difficulties for electron hopping, thus causing the lower electron mobility of CzDbp relative to that of AcDbp containing the same electron-accepting unit dibenzo[a,c]phenazine but unsubstituted donor moieties.

3.5. Thermal characteristics

AcDbp and CzDbp showed high thermal stability with 5% weight loss at 480 °C and 453 °C, respectively, as confirmed by thermogravimetric analysis (TGA) (Fig. 2b). The morphological transitions of the compounds were investigated by differential scanning calorimetry (DSC). Fig. 2c shows DSC heating and cooling curves for AcDbp. This compound was obtained after the synthesis and purification as the crystalline substance. It showed two endothermic melting signals at 387 °C and 427 °C during the first DSC heating scan. The cooling and the second heating scans revealed only a glass transition at 164 °C. In the heating and cooling scans of CzDbp no signals of melting, crystallization or glass transition were observed (Fig. S5).

3.6. Photophysical properties

Absorption. The experimental absorbance spectra of AcDbp and CzDbp were compared with the computed ones at the TD-DFT level with $\omega^{\text{THF,TOL}}$ B97XD (Fig. 3). The position of theoretical absorption bands of AcDbp and CzDbp were in good agreement with the experimental ones. This observation can be related to the improved description of origin of excitations provided by the optimization of the ω . Analysis of the most

intense transitions (Table S1) revealed that absorption band at 370 nm of AcDbp described transition $S_0 \rightarrow S_9$. In order to identify the nature of transition, natural transition orbitals (NTO) were calculated which showed that this absorption band of AcDbp is associated with the local electronic excitations in Dbp core (Fig. S6). Meanwhile, absorption band at 350 nm of CzDbp obtained at ω^{THF} B97XD and ω^{TOL} B97XD corresponds to the combination of electronic transitions towards two excited states of S_8 , S_9 and S_7 , S_9 , respectively (Table S1). According to the NTO, $S_0 \rightarrow S_8$ and $S_0 \rightarrow S_7$ are dominated by the charge transfer from Cz units to Dbp core, with small contribution from the local Dbp excitations, and $S_0 \rightarrow S_9$ is associated only with the local electronic transitions in Dbp core (Fig. S6).

The theoretical results indicate that the six lowest energy transitions (S_1 - S_6) of AcDbp demonstrate charge transfer (CT) from donors to acceptor, exhibiting practically zero oscillator strengths due to the orthogonal geometry of the molecule (Table S1). However, experimental spectra of the solutions in tetrahydrofuran (THF) and toluene (TOL) exhibit a weak CT tail in the region of 400–500 nm (Fig. 3). This suggests an increased oscillator strength for the CT states stemming due to shifted dihedral angle from 90° between Ac and Dbp. While the lowest energy transitions S_1 - S_4 for CzDbp correspond to the CT between donors and acceptor giving a small intensity band in the range 450–600 nm (Table S1).

The larger absorption intensity of CT bands in experimental absorption spectra as compared to theoretical ones can be observed. This observation can be explained by the smaller dihedral angle D-A of molecules than the theoretical calculated ones (Fig. 3). The intramolecular differences may appear due to some degree of aggregation in the ground state in solutions. To check such assumption, the absorption spectra of the different concentrations of AcDbp and CzDbp in TOL and THF solutions revealed increase of intensity of CT bands when concentrations of the compounds in solutions increases (Fig. S7). Such differences revealed presence of aggregates in the solutions. The theoretical calculations confirmed that oscillator strength of the CT states depends on the size of dihedral angle D-A. The smaller dihedral angle resulted in the larger value of oscillator strengths at S_1 state for AcDbp and CzDbp (Table S2).

Emission. Fluorescence spectra and photoluminescence quantum yield (PLQY) of the solutions of AcDbp and CzDbp in the solvents of different polarity ($\epsilon^{\text{TOL}} = 2.38$ and $\epsilon^{\text{THF}} = 7.50$) were recorded (Table 3, Fig. 4a). Both the compounds exhibited structureless PL profiles, indicating CT nature of the emissive states. This observation is in line with the nature of the lowest absorption bands in solutions of AcDbp and CzDbp. The stronger solvatochromic effect was detected in the fluorescence spectra of the solutions of AcDbp compared to those of CzDbp because of the dominant CT nature in AcDbp, which is coherent with the corresponding D-A dihedral angle, hence the purer CT states in the case of AcDbp as compared to CzDbp. Solutions of CzDbp showed higher values of PLQY than solutions of AcDbp (Table 3). The values of PLQY of the solutions in TOL and THF of AcDbp were 2% and 0.5% while those of the solutions of CzDbp were 37% and 28%, respectively. Again, these

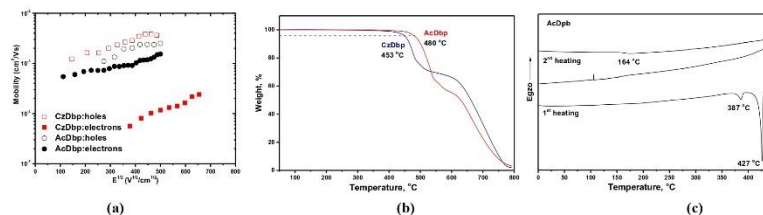


Fig. 2. Electric field dependences of charge mobilities for the layers (a) of AcDbp and CzDbp, TGA curves of AcDbp and CzDbp (b) and DSC curves of AcDbp (c).

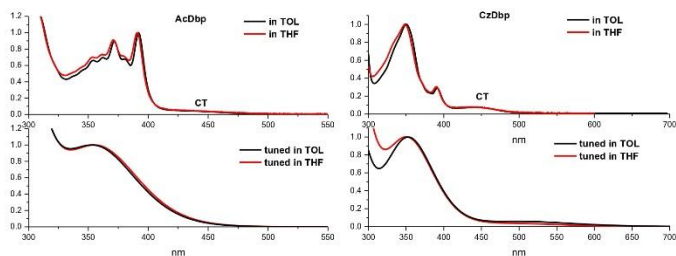


Fig. 3. Experimental and theoretical absorption spectra of AcDbp and CzDbp.

Table 3
Photophysical properties of AcDbp and CzDbp.

	PLQY ^{meas} at 96%	PLQY ^{theor} , %	S ₁ , eV	T ₁ , eV	ΔE _{ST} , eV
	THF/TOL/non-doped/ mCP/mCP	THF/TOL	THF		
AcDbp	0.5/2/3/4/8	0.6/3	2.55	2.35	0.20
CzDbp	28/37/15/11/21	44/53	2.52	2.28	0.24

*Measured at air condition.

results are in line with the corresponding geometries, the orthogonal D-A geometry in AcDbp preventing from any efficient S₁ → S₀ fluorescence in spite of the efficiency of the triplet → singlet conversion efficiency. Indeed, the theoretical results indicate a dark S₁ state in the case of AcDbp (zero oscillator strength), as compared to 0.023 for CzDbp (Table S1).

The measurements of the degassed solutions showed interesting differences: while solutions of AcDbp showed insignificant increase of PLQY, CzDbp demonstrated increase of PLQY by 16% for both the solutions, which, as we show below, could stem from TTA. To support this assumption, the plots of PL intensity versus excitation intensity (λ_{excitation} = 400 nm) (Fig. S8) were recorded for powders and THF solutions (0.5 mg/ml) of AcDbp and CzDbp using neutral filters according

to the method described in ref. [41]. Integrated PL intensities versus excitation intensities for powders and THF solutions of AcDbp and CzDbp are plotted in Fig. 4b. The linear fits of these dependences in the different excitation intensity ranges (9–100% (Fig. 4b) and 24–100% (Fig. 4b inset)), revealed the slopes higher than unity displaying contribution of TTA emission [9,10,13,14,41].

The onsets of photoluminescence (PL) and phosphorescence (PH) spectra of the solutions of AcDbp and CzDbp in THF recorded at 77 K were used to estimate singlet-triplet energy differences (ΔE_{ST}) (Fig. 4a, Table 3). The PL spectrum of AcDbp exhibited a structureless shoulder with the onset estimated at 2.55 eV (Fig. 4a), indicative of CT nature of the emissive state. This observation is in line with the lowest energy band of the corresponding absorption spectra. PH spectrum of AcDbp showed characteristic vibrational structure, indicating that the lowest emissive T₁ state at 77 K corresponds to the local excitation (³LE) of Dbp-core. As for, Both PL and PH spectra of THF solution of CzDbp exhibited broad and structureless emission indicating CT nature of S₁ and T₁ excited states. Analysis of molecular orbitals of AcDbp and CzDbp indicates that for both the compounds, ¹CT and ³CT occur due to transition from donor to acceptor, while ¹LE transition takes place between orbitals delocalized over the Dbp core (Fig. S9, S10).

The experimental estimation of the singlet-triplet energy splitting (ΔE_{ST}) revealed values of 0.24 eV and 0.20 eV for CzDbp and AcDbp, respectively. The experimental ΔE_{ST} value for CzDbp is in good

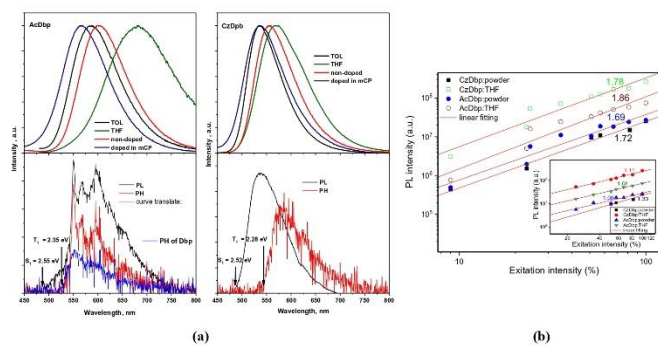


Fig. 4. Room-temperature fluorescence spectra and photoluminescence as well as phosphorescence spectra recorded at 77 K of THF solutions of AcDbp and CzDbp (phosphorescence spectrum of the solution of Dbp in THF recorded at 77 K is presented as blue line) (a) and plots of integrated PL intensities versus excitation intensities for powders and THF solutions of AcDbp and CzDbp (b). (For interpretation of the references to colour in this figure legend, the reader is referred to the web version of this article.)

agreement with the theoretical vertical ΔE_{ST} values of 0.20 eV (THF) and 0.21 (TOL) (Table S2, and Fig. S11). However, for acridan-containing compound (AcDbp) the theoretical vertical ΔE_{ST} value is zero (Table S2, Fig. S11). The dichotomy between theory and experiment is also witnessed by the different nature of the corresponding lowest triplet state. While the experimental emissive triplet state is a local one of 2.35 eV (PH spectrum in Fig. 4a), the theoretical LE corresponds to T_3 at 2.33 eV, T_1 and T_2 being of CT nature (Fig. S10, S11). Interestingly, the lowest energy absorption band in the experimental absorption spectrum of AcDbp is a CT one (Fig. 3). A recent report [42] indicated that THF becomes solid at 77 K and geometric relaxation of the solvent is no longer possible. This effect was shown to blue-shift the PL maximum at 77 K by roughly 0.4 eV as compared to room temperature, which was traced back to the inefficient stabilization of the emissive CT state. Following these results, it is possible that CT in AcDbp is not entirely stabilized by solvent, thus resulting in emission from LE state. In the case of CzDbp, CT state could be stabilized by the electronic polarization of the adjacent CzDbp molecules [42], given that this compound was found to form aggregates (Fig. S7).

PL spectra and PL decay curves of the solutions of AcDbp and CzDbp in TOL and THF were recorded before and after degassing. As shown in Fig. 5 and Fig. S12, the solution of AcDbp exhibited double exponential decay. The air equilibrated TOL and THF solutions showed lifetimes of long-lived component (τ_2) of 362 ns and 420 ns, respectively. Meanwhile, under oxygen free conditions τ_2 increased to 10946 ns for TOL solution and 2437 ns for THF solution suggesting a radiative PL stemming from triplet harvesting assumedly through TADF. The shapes of emission spectra of non-degassed and degassed solutions of the compounds were very similar showing that delayed fluorescence originated from the same CT state as prompt fluorescence (Fig. 5, S11). Intriguingly, the solutions of CzDbp in TOL and THF exhibited single exponential PL decays showing only prompt fluorescence (Fig. 5, S11). The solutions of CzDbp exhibited increase of PLQY by 16% after

deoxygenation. This observation shows that the triplet states do play a role in the PL of CzDbp, which should consequently be realized through a channel different from TADF, being as fast as the prompt fluorescence.

Since the delayed fluorescence can be activated by temperature, PL spectra and PL decay curves of non-doped and doped (10 wt%) in mCP layers of AcDbp and CzDbp were recorded at the different temperatures ranging from 77 K to 300 K (Fig. 6, S13, S14). The PL intensities, thus absolute PLQYs of the layers of both non-doped AcDbp and doped in mCP increased when the temperature was increased from ca. 220 K to 300 K (Fig. S14). Such increase of PL intensity with increasing temperature can be explained by TADF contribution [1]. However, the intensity of the decay profile of delayed fluorescence, thus contribution of delayed fluorescence (τ_{TADF}), decreases with an increase of temperature for the layer of non-doped AcDbp (Fig. 6b). Such PL decay behaviour under different temperatures for TADF compounds are not typical and it is rarely described/discussed in the literature [41,43]. For example, J. Grüne et al. demonstrated that negative temperature dependence of the transient electroluminescent decays at increasing temperature of exciplex-based TADF emitters are mainly related to contribution of TTA [41]. We found similarities between PL decay behavior under different temperatures of the layer of AcDbp and temperature-dependent transient electroluminescence (EL) decays of OLED with emission layer of mTDATA:3TPYMB described in ref. 41. Precise fitting of the temperature-dependent transient EL decays in ref. 41 proved that unusual temperature-dependent transient EL decays are mainly related to TTA. Since experimental evidence of TTA was also obtained for compounds AcDbp(CzDbp), the obtained unusual temperature-dependent PL decays of AcDbp(CzDbp) are also related to TTA emission mechanism.

To demonstrate more evidences of TADF for AcDbp, from the plots of RISC rate versus temperature at the temperatures exceeding 200 K (at which phosphorescence is absent) by Arrhenius equation [44] (Fig. S15), activation energies (E_a) of 72 and 55 meV were obtained for

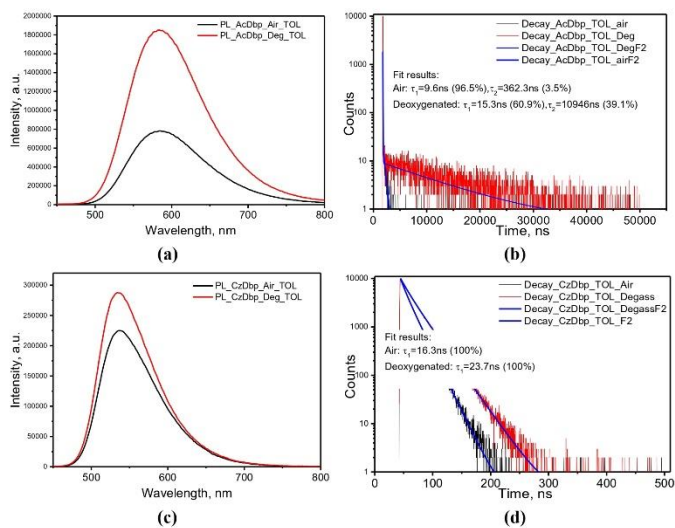


Fig. 5. PL spectra (left) and PL decay curves (right) of air equilibrated and deoxygenated solutions of AcDbp (a-b) and CzDbp (c-d) in TOL.

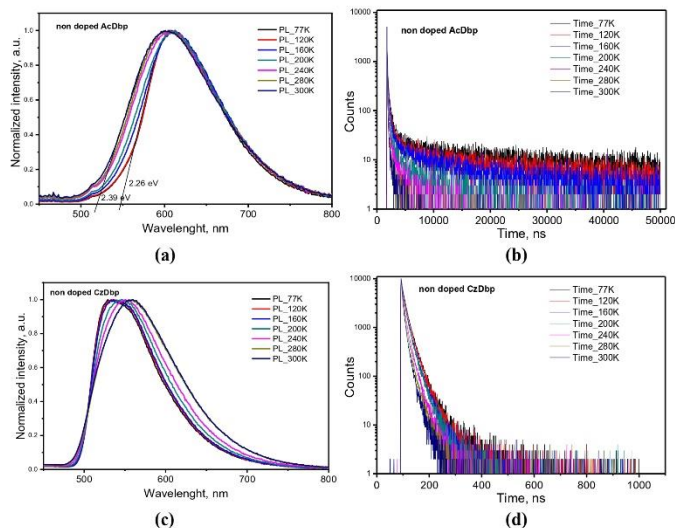


Fig. 6. PL spectra (left) and PL decay curves (right) of the layers of non-doped AcDBp (a-b) or CzDBp (c-d) recorded at different temperatures.

the layers of non-doped and doped in mCP of 10 wt% AcDBp. Relatively low E_s values and small difference between the values of the layers of non-doped and doped AcDBp. Such result is in agreement with low ΔE_{ST} value for AcDBp (Table 3). Thus, population of the emissive singlet state via RISC from the triplet state is allowed. Such E_s values are in good agreement with corresponding values of previously reported TADF compounds. [45,46]

PL decay curves of the layers of CzDBp, in the temperatures ranging from 77 K to 300 K revealed only prompt fluorescence. No long-lived components assigned to phosphorescence or delayed fluorescence were detected (Fig. 6d, S13d). No phosphorescence was experimentally observed neither for the layer of non-doped CzDBp nor for that of doped 10 wt% CzDBp in mCP. It should be noted that the intensity of the PL decay profile decreases with increasing of temperature for the non-doped CzDBp because of the TTA as it was mentioned above (Fig. 6d). For CzDBp, no delayed fluorescence was recorded. The reasons are additionally discussed in the section "Mechanistic considerations".

3.7. Electroluminescent properties

Compound AcDBp has potential as TADF host for red OLEDs taking into account its charge-transporting properties, energy of first triplet level, and ability to exhibit TADF. On the other hand, CzDBp showed ambipolar charge-transporting properties and higher PLQY than AcDBp. Consequently, both AcDBp and CzDBp were used in PHOLED, in order to demonstrate their suitability as host materials for a commercial red phosphorescent emitter (piq)₂Ir(acac). The analogous PHOLED based on well-known host mCP was also fabricated for comparison. All functional layers in the fabricated PHOLEDs were the same except light-emitting layers. Three devices with the configuration ITO/ MoO₃ (0.6 nm)/NPB (30 nm)/5 wt% (piq)₂Ir(acac): AcDBp or CzDBp or mCP (20 nm)/TPBi (70 nm)/LiF (0.8 nm):Al fabricated using hosts AcDBp, CzDBp or mCP were named as devices A, B, or C, respectively (Fig. 7, Table 4).

PHOLEDs A, B and C showed classical (piq)₂Ir(acac) emissions with the peak wavelength of 623 nm (Fig. S16). Only the emission of phosphorescent emitter was observed in electroluminescence spectra of devices A and B, manifesting complete energy transfer from host to (piq)₂Ir(acac). In the case of PHOLED C, additional weak emission in the range 350–500 nm is detected since the mCP host is not the best host for the selected red phosphorescent (piq)₂Ir(acac). As it will be discussed below, no additional bands were observed when a more appropriate host was selected for the reference device (Fig. 8a, S20–24).

Devices A and B exhibited lower turn-on voltage (V_{on}) compared to that of device C indicating excellent electron and hole injection (Fig. S17). The best maximum current efficiency (CE_{max}), maximum power efficiency (PE_{max}) and external quantum efficiency (EQE_{max}) was demonstrated by device B with CzDBp as a host (Fig. S18). Higher EQE_{max} of 9% was obtained for CzDBp-based PHOLED B in comparison to EQE_{max} of 8% observed for the reference mCP-based device C. Knowing that mCP is one of the best conventional host, the result is exciting and is apparently related to the additional triplet harvesting by host via TADF or TTA. To further study EL characteristics of devices A–C, brightness versus current density were plotted in log-log scales. Two different linear regions can be recognized and linearly fitted ($1 > R^2 > 0.98$) (Fig. 7 b–d, S19). At low current density, the slope of ca. 1 (1.013) was obtained for mCP-based device C, which is typically expected for conventional fluorescent and phosphorescent OLEDs where one photon is created by recombination of one exciton.[47] However, despite the same emitter used, the slopes higher than unity were obtained for devices A and B at low current density (Fig. 7b,c). This result points to some contribution from the TTA mechanism, given that harvesting of 100% of triplets by means of the TTA manifests with the slope reaching the value of 2.[13,48,49] This observation indicates that electroluminescence of devices A and B is related to both emission of the (piq)₂Ir(acac) and emission enhancement by TTA mechanism. It should be noted, that TTA efficiency of host CzDBp should be higher than that of

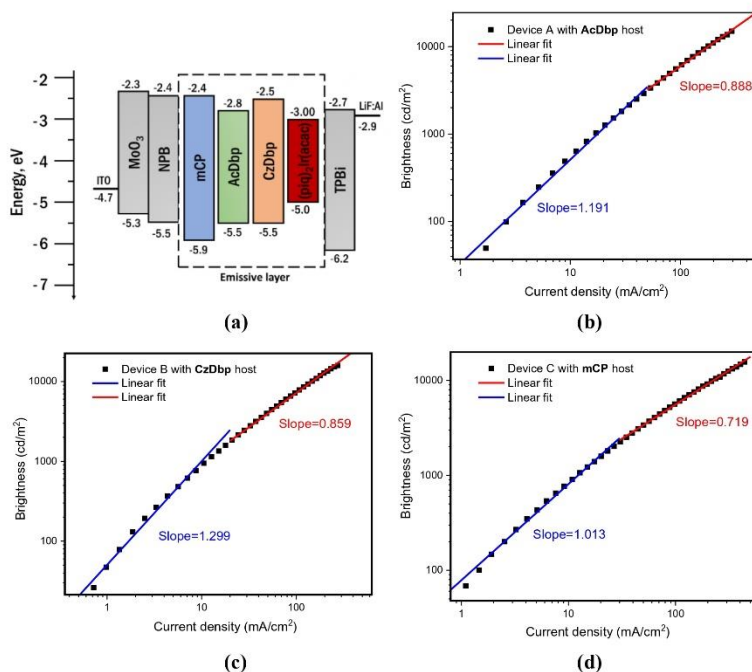


Fig. 7. Equilibrium energy diagram (a) of devices A-C. IP^{PE} and EA^{PE} values of solid samples of AcDbp and CzDbp were taken for the design of the device structures (Table 2). Linear fits to current density versus brightness plots for devices A-C (b-d).

Table 4
EL parameters of the devices A-J.

Device	Emissive layer	$^a V_{ON}/N_{D,DRIFT}$, V	CE_{max} , cd/A	PE_{max} , lm/W	EQE_{max} , %	CIE 1931(x, y)
Host tests using structure: ITO/MoO ₃ /NPB/ Emissive layer /TPBI/LiF/Al						
A	(piq) ₂ Ir(acac):AcDbp	3.0/3.85	6.3	4.6	6.0	(0.658, 0.340)
B	(piq) ₂ Ir(acac):CzDbp	3.4/4.5	9.0	6.4	9.0	(0.655, 0.313)
C	(piq) ₂ Ir(acac):mCP	4.0/5.2	8.6	5.6	8.0	(0.633, 0.329)
Host tests using structure: ITO/HAT-CN/NPB/TCTA/mCBP/ Emissive layer /nBPhen/Liq/Al						
D	(piq) ₂ Ir(acac):AcDbp	3.2/5.2	9.8	9.1	13.2	(0.671, 0.324)
E	(piq) ₂ Ir(acac):CzDbp	3.0/4.75	10.3	11.6	15.9	(0.677, 0.32)
F	(piq) ₂ Ir(acac):mCBP	2.9/4.0	11.5	12.9	13.1	(0.674, 0.322)
G	(piq) ₂ Ir(acac):NPB	3.2/4.5	6.6	6.7	9.0	(0.665, 0.32)
H	(piq) ₂ Ir(acac):nBPhen	4.8/8.7	12.5	8.5	14.6	(0.677, 0.318)
Emitter tests using structure: ITO/HAT-CN/NPB/TCTA/mCBP/ Emissive layer /nBPhen/Liq/Al						
I	AcDbp:mCBP	3.6/6.7	41.6	35.3	19.4	(0.513, 0.479)
J	CzDbp:mCBP	3.7/7.0	54.4	46.2	22.1	(0.395, 0.578)

^a V_{ON} was taken at 10 cd/m²; ^b $V_{D,DRIFT}$ was taken at 10 mA/cm²; ^c CIE (x,y) was taken 1000 cd/m².

host AcDbp. The corresponding slope (1.299) of device B is higher than that (1.191) of device A.

At high current density, the slopes of all devices A-C were lower than unity which is related to the efficiency roll-off (Fig. 7b-d, S19). Efficiency roll-off of devices A and B was lower (the slopes are closer to the unity) than that of device C. This observation additionally highlights

higher efficiency of the developed TADF/TTA hosts in comparison to the conventional mCP.

With the aim of additional optimization of device structure, five devices with the configuration ITO/HAT-CN(5 nm)/NPB(40 nm)/TCTA(10 nm)/mCBP(10 nm)/ 5 wt% (piq)₂Ir(acac): AcDbp or CzDbp or mCBP or NPB or nBPhen (50 nm)/nBPhen (30 nm)/Liq(2 nm)/Al were

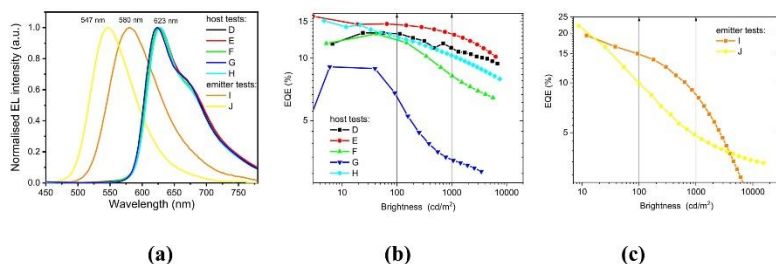


Fig. 8. EL spectra (a) and EQE efficiencies versus brightness (b, c) characteristics for the devices D-J with **AcDbp** and **CzDbp** as host or emitter.

fabricated using hosts **AcDbp**, **CzDbp**, **mCBP**, **NPB**, or **nBPhen** and named as devices **D**, **E**, **F**, **G** or **H**, respectively (Fig. 8, Table 4). EL spectra recorded at the different voltages of PHOLEDs **D-H** were completely related to $(\text{piq})_2\text{Ir}(\text{acac})$ emissions (Fig. 8a, S20–S24). Due to improved charge-injecting properties, $(\text{piq})_2\text{Ir}(\text{acac})$ -based devices **D-H** exhibited improved out-put electroluminescent characteristics. Device **E** fabricated using the developed host **CzDbp**, demonstrated the higher maximum EQE (15.9%) in comparison to the reference devices **F-H** containing **mCBP**, **NPB** or **nBPhen** as hosts (Fig. 8b, S20–S24, Table 4). The differences between EQE values of device **E** and **F-H** are related to either their different charge-balance factors (γ), efficiency of exciton production (χ), PLQY or the outcoupling efficiency (η_{out}) according to the formula [48]

$$\text{EQE} = \gamma \times \text{PLQY} \times \chi \times \eta_{\text{out}} \quad (1)$$

Since the thicknesses of all functional layers and device structure of OLEDs **D-H** was the same, their outcoupling efficiency should be similar. It should be noted that the layers 5 wt% solid solutions of $(\text{piq})_2\text{Ir}(\text{acac})$ in **mCP**, **NPB** or **nBPhen** (9, 15, or 7%, respectively) showed slightly higher PLQY values than 5 wt% solid solutions of $(\text{piq})_2\text{Ir}(\text{acac})$ in **AcDbp** and **CzDbp** (7 and 8%, respectively) (Fig. S25). The different PLQYs of $(\text{piq})_2\text{Ir}(\text{acac})$ can be related to higher polarity of donor–acceptor–donor type hosts **AcDbp** and **CzDbp** hosts than that of electron donating hosts **mCP**, **NPB** and electron-accepting host **nBPhen**. Thus, the higher maximum EQE of device **E** is not related to the higher PLQY of the light-emitting layer of 5 wt% solid solution of $(\text{piq})_2\text{Ir}(\text{acac})$ in **CzDbp**. It should be noted that the values of PLQYs recorded for $(\text{piq})_2\text{Ir}(\text{acac})$ dispersed in the different hosts are lower than the previously reported PLQY (20%) of the same emitter [50]. Such differences were apparently obtained since the above PLQYs were taken under air conditions. In any case, the obtained PLQYs should not be used for the calculation of the theoretical maximum EQE for $(\text{piq})_2\text{Ir}(\text{acac})$ -based devices by formula (1). It is known that, in case of phosphorescent emitters, low PLQYs (thus, disagreement between the theoretical and experimental maximum EQEs) can be obtained if quantum yields of singlet – triplet conversion (STC) efficiency of phosphorescent complexes are below 100%, which is a typical case [51]. Apparently, because of that, experimental EQE of 22.6% was reached for $(\text{piq})_2\text{Ir}(\text{acac})$ -based devices despite experiment PLQY of 20% recorded for the emitter $(\text{piq})_2\text{Ir}(\text{acac})$ [50,52]. Therefore, one of the highest experimental EQE values reported for $(\text{piq})_2\text{Ir}(\text{acac})$ based devices which reached 22.6% was selected for the comparison with EQE values of our devices [52]. For example, device **E** demonstrated EQE of 15.9% which is not far below of that observed for the previously published $(\text{piq})_2\text{Ir}(\text{acac})$ based devices. To provide comparison of characteristics of **AcDbp** and **CzDbp** based devices with the reference devices, the concentration of $(\text{piq})_2\text{Ir}(\text{acac})$ dopant of 5 wt% in light-emitting layer was selected. It is predictively possible to improve the efficiency of **AcDbp** and **CzDbp**

based devices when the concentration of the $(\text{piq})_2\text{Ir}(\text{acac})$ dopant or/ and thicknesses of additional layers are optimised.

Both charge-balance factors and efficiency of exciton production can be responsible for high EQE of device **E**. The TOF experiment showed, that the balance of hole and electron transport in the host **AcDbp** should be even better than that in **CzDbp**. However, device **D** did not show higher maximum EQE value than device **E** (Fig. 8b). The balance hole and electron transport of devices **F-H** should be also good. Taking into account the similarities/differences of hole-electron balance, the high efficiency of device **E** is partly attributed to harvesting of triplet excitons not only within phosphorescent emitter $(\text{piq})_2\text{Ir}(\text{acac})$ but also within the host **CzDbp** due to its TTA/TADF properties. Thus, the higher efficiency of device **E** is partly attributed to the higher efficiency of exciton production in comparison to that of the similar/reference devices **D**, **F-H**.

Not only compound **AcDbp** but also compound **CzDbp** are characterized by TADF. Thus, both the compounds are characterized by media dependent combination of TADF and TTA. TADF of compounds **AcDbp** and **CzDbp** is evident from very high maximum EQEs of 19.4 and 22.1% observed for devices **I** and **J** based on the light-emitting layers **AcDbp** (20 wt%:mCBP and **CzDbp**(20 wt%):mCBP in which **AcDbp** or **CzDbp** were used as emitters in the same device structures as those of devices **D-H** (Fig. 8c, Table 4). Experimental maximum EQEs of 19.4 and 22.1% observed for devices **I** and **J** respectively are not in agreement with the theoretical maximum EQEs (2.4 and 6.3%, assuming η_{out} of 0.3) estimated by formula (1) using PLQYs of 8 and 21% of the light-emitting layers **AcDbp**(20 wt%):mCBP and **CzDbp**(20 wt%):mCBP, respectively (Table 3). This disagreement can be related to the possible loss mechanisms when the TADF molecules are optically excited as those discussed in [53]. Devices **I** and **J** showed orange and yellow electroluminescence with CIE1931 colour coordinates of (0.513, 0.479) and (0.395, 0.578), respectively (Fig. S26, S27, Table 4). EL spectra were completely related to emissions of **AcDbp** or **CzDbp** indicating that hole-electron recombination took place within the light-emitting layers.

3.8. Mechanistic considerations

The triplet harvesting in **AcDbp** and **CzDbp** systems occurs by means of different either TADF or TTA mechanisms.

Static diagrams. In order to understand these differences, we focus first on the TADF mechanism. Following Adachi[54] and Gibson[55], energy diagrams representing only a selected set of excited states of **AcDbp** and **CzDbp** are shown in Fig. 9a,b. The energy of ^3LE for **AcDbp** (2.35 eV) was taken from the PH spectrum of the solution in THF at 77 K. Below, we consider that this energy value remains roughly similar in the case of the films of pure and doped in **mCP AcDbp**. Note that ^1LE energy level of **AcDbp** (in THF at 77 K) is below ^3CT and ^3CT energy levels of **AcDbp** doped in **mCP** (2.56 eV and 2.53 eV, respectively), but is

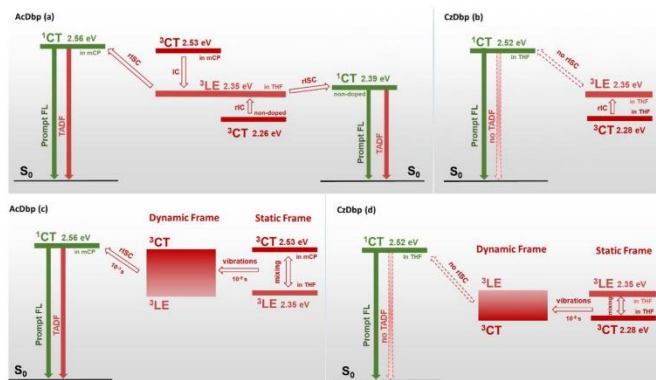


Fig. 9. Diagrams of excited states energies of AcDdbp (a) and CzDdbp (b); diagrams illustrating the “dynamic” mechanism of mixing between LE and CT states through dihedral vibrations [56,57,58] in AcDdbp (c) and CzDdbp (d).

between ^1CT and ^3CT of non-doped AcDdbp (2.39 eV and 2.26 eV, respectively). Based on these diagrams (Fig. 9a), interpretation of the delayed fluorescence in AcDdbp seems to be straightforward: while mixing of ^3CT with ^3LE by means of IC makes the symmetry allowed $^3\text{LE} \rightarrow ^1\text{CT}$ rISC more efficient, the $\Delta E_{\text{ST}}(^1\text{LE} \rightarrow ^1\text{CT})$ values seem to be very different depending on the conditions, adopting a relatively large upper limit value of 0.21 eV for AcDdbp doped in mCP, but much smaller (0.04 eV) for the pure compound (Fig. 9a). Consequently, TADF should be of different efficiencies for the layers of molecular dispersion of AcDdbp in mCP and for the layer of pure compound, which seems to be incoherent with the close values of PLQY of 3 and 4% respectively. A possible and partial explanation could stem from the practically orthogonal geometry of this compound: the prompt fluorescence is very inefficient, differences in TADF efficiency should be of secondary importance with respect of the total emission (prompt FL + TADF).

In the case of CzDdbp, ^1CT and ^3CT energy levels (2.52 eV and 2.28 eV, respectively) were taken from the PL and PH spectra of the solutions in THF at 77 K. The experimental value of ^3LE for CzDdbp is not accessible experimentally, given that T_1 is of CT nature. One could consider, however, the value of 2.35 eV measured for the ^3LE of AcDdbp as a first approximation for the ^3LE state of CzDdbp in THF at 77 K, which seems coherent with the similar space localization of this state for both the compounds only on the Ddbp core (Fig. S10). In this case, $\Delta E_{\text{ST}}(^1\text{LE} \rightarrow ^1\text{CT}) = 0.17$ eV deduced from Fig. 9b for CzDdbp is smaller than 0.21 eV estimated for AcDdbp in mCP, for which the TADF seems efficient, thus making difficult to explain the absence of delayed fluorescence in the emission of CzDdbp.

Dynamic diagrams. The diagrams and comparisons presented above lack of the impact of mixing in the energy levels. In order to better understand this effect, we remember some of the milestone ideas and insights: (i) El Sayed’s rule indicates that rISC between electronic states of the similar nature such as $\pi\text{-}\pi^*$ CT states is forbidden, thus preventing the interconversion between pure ^3CT and singlet ^1CT excited states in TADF compounds. (ii) The direct $^3\text{LE} \rightarrow ^1\text{CT}$ spin-orbit coupling was shown to be very small (merely several cm^{-1}) [56], failing consequently to explain the experimental rISC rate constants. (iii) The important information on the TADF mechanism was obtained by finding that the vibronic coupling between S_1 (T_1) and S_2 (T_2) is mandatory to promote $T_1 \rightarrow S_1$ rISC. [55,56] (iv) Calculations taking into account the contribution of IC or rIC between several low-lying excited states provide the

crucial insight that ISC or rISC processes cannot be explained in a static frame; dynamical processes through the dihedral-angle oscillations, which are by several orders of magnitude faster than ISC or rISC, were shown to be a key factor determining the TADF efficiency. [56,57,58] Indeed, the dihedral-angle oscillations and deformations around the D-A bond at excited states allow exploration of ensemble of conformations reachable at room temperature.

In addition to these findings, we suggest that the impact of these oscillations and deformations is the mixing between states: the nature of T_1 can change from pure CT to a mixed LE-CT state or vice-versa. This creates “new” excited states at intermediate energies between “static” ^3CT and ^3LE states, which are absent in the static-frame energy diagrams (deduced from the onset excitation energies). Fig. 10a,b show the dependence of the nature of “new” triplet state (T_1) from dihedral angle D-A size. These “dynamical” states allow molecules to profit from the LE contribution in T_1 to make the $T_1 \rightarrow S_1$ transition “allowed” (satisfy to El Sayed’s rule) (Fig. 10a), hence increase the intensity of the $T_1 \rightarrow S_1$ transition (spin-orbit coupling, SOC), but also increase the intensity of $S_1 \rightarrow S_0$ transition, hence the PLQY of fluorescence. On the other hand, these oscillations and deformations could result in the increased ΔE_{ST} (Fig. 10b), which is detrimental for rISC. Nevertheless, at some point (a given geometry), the combination of SOC and ΔE_{ST} becomes convenient for effective rISC. [59] It is worth remembering the results from [59] showing the drastic decrease of rISC rates when ΔE_{ST} approaches 0.2 eV and beyond.

The ensemble of the above results and ideas, [56,57,58,59] are illustrated by means of a new diagram for AcDdbp doped in mCP shown in Fig. 9c. In this figure, from right to left, the static frame with well-defined energies of ^3LE and ^3CT states (similarly to Fig. 9a) is followed by a “dynamic” frame, corresponding to dynamically created mixed $^3(\text{LE-CT})$ states of intermediate energies between $^3\text{LE} \rightarrow ^3\text{CT}$. Note, that dynamical energy levels below- or above the static LE (CT) and CT (LE) could also be expected; nevertheless, we show in the dynamical diagrams only the energy levels in between those of LE- and CT.

In this context, while different rISC pathways would be predicted in a static frame, depending on the relative energy order between ^3LE and ^3CT , in the dynamic frame a fundamentally identical pathway could be predicted: $^3(\text{CT} \leftrightarrow \text{LE}) \xrightarrow{\text{rISC}} ^1\text{CT}$. Considering now AcDdbp doped in mCP, mixing of CT and LE characters in the same state is also accompanied by increase in the energy level somewhere in the mid-gap

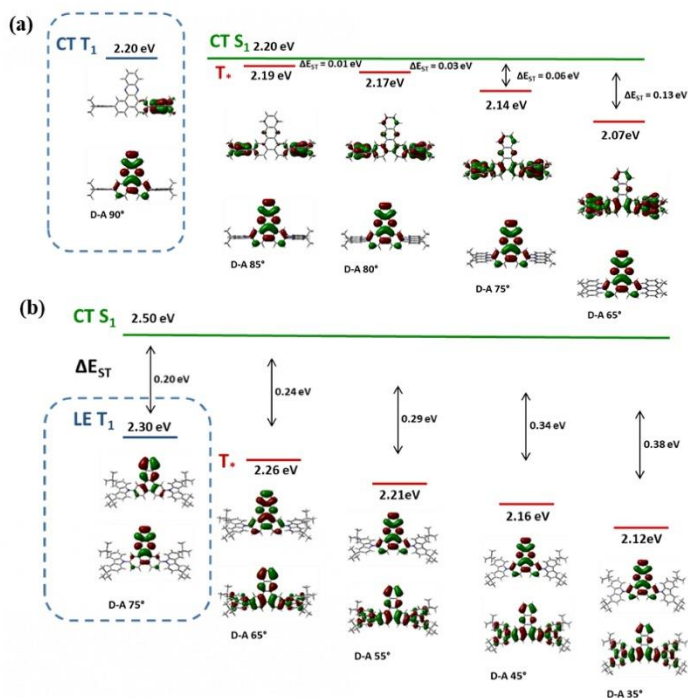


Fig. 10. Dependence of the nature of the first triplet state marked as T₁ of **AcDbp** (a) and **CzDbp** (b) on the D-A dihedral angle (obtained from TD-DFT calculations at ω^{THF}/B97XD).

between ³LE and ³CT, resulting in reduced ΔE_{ST} as compared to the value of 0.21 eV deduced from the diagram shown in Fig. 9a thus making the TADF more efficient.

In the case of **CzDbp** the same mechanism should hold true (Fig. 9d), but the energy of the mid-gap mixed states created “dynamically” (in-between ³LE-³CT) would correspond to increased ΔE_{ST} as compared to the value of 0.17 eV deduced from the diagram shown in Fig. 9b. This effect seems opposite to what occurs in case of **AcDbp**, and the increase of ΔE_{ST} from 0.17 eV to 0.24 eV could explain the inefficiency (absence) of delayed fluorescence.[59] Additionally, the theoretical (vertical) T₁ state for **CzDbp** is not a pure CT state, as shown in the experimental diagram of Fig. 9b,d, but a mixed ³(LE-CT) one (Fig. S28). This means that the contribution of this state to the rISC by means of the second-order nonadiabatic coupling between ³LE and ³(CT-LE) would be less efficient than that between ³LE and ³(CT), again providing a possible explanation on the absence of delayed FL through the TADF channel in the case of **CzDbp**. The support to theoretical result related to the mixed ³(LE-CT) nature of T₁ could rise from the shape of PL profiles of the films of pure **CzDbp** at very low temperatures (77–120–160 K, Fig. 6c. A weak vibrational character is visible in PL spectra, that we assume originating from phosphorescence contribution related to a mixed ³(LE-CT) emitting state.

The above discussion provides possible explanations of the absence of triplet harvesting by means of TADF mechanism for **CzDbp** in THF and TOL solutions as well as in non-doped and doped in mCP layers. While, device J with **CzDbp** as emitter in mCPB demonstrating EQE of 22.1% shows that triplet harvesting via TADF can occur, thus there are media in which **CzDbp** exhibit efficient TADF.

Triplet-triplet annihilation. Our findings indicate that degassing of THF and TOL solutions of **CzDbp** results in increase of PLQY by 16% of both solutions. This means that the triplet states do play a role in the PL of **CzDbp**, which should consequently be realized through a channel different from TADF being as fast as prompt fluorescence. One possible mechanism could be TTA, as shown in the section “Photophysical properties”. Indeed, integrated PL intensities versus different excitation intensities give slope values higher than unity for **CzDbp** and **AcDbp** (Fig. 4b). Thus evidencing that the TTA mechanism contributes to the triplet harvesting in both compounds [48,49], when **CzDbp** as well as **AcDbp** plays the roles of both the synthesiser and the annihilator. This is in agreement with the higher slope than unity for brightness versus current density plots for devices A (1.191) and B (1.299) containing **AcDbp** and **CzDbp**, respectively. In addition, this is coherent with the fact that the maximum wavelengths of the PL spectra of **CzDbp** recorded in degassed and in-air conditions are identical (Fig. 5c) and is consistent

with the assumption that S_n , the new singlet state created by the interaction of two triplet molecules, relax to S_1 before radiative transition towards the ground state. The increase of PLQY by 16% after deoxygenation of the solution is in good agreement with the reported maximum theoretical value of 20%. [9,60] Concerning to the fast TTA supposed in the case of **CzDdp**, the experimental support comes from the fast TTA (in ns range; $k_{TTA} > 10^9 \text{ M}^{-1}\cdot\text{s}^{-1}$) previously reported, for example, for perylene [61] and many other TTA materials [10].

4. Conclusions

We have synthesized two new D-A-D type molecules, **CzDdp** and **AcDdp**, and have characterized them by means of experimental and theoretical methods. The solid layers of both the semiconductors exhibit bipolar charge transport with drift mobilities exceeding $10^{-3} \text{ cm}^2/\text{Vs}$ at high electric fields. The compounds are able to harvest triplet excitons by either triplet-triplet annihilation (TTA) or thermally activated delayed fluorescence (TADF) mechanisms.

The experimental optical absorption spectra of **AcDdp** and **CzDdp** in different media indicate presence of very-low intensity CT-tails for both the compounds, the intensity of which increases with the increasing concentration of compounds. Photoluminescence spectra and decay curves of **AcDdp** revealed the presence of delayed fluorescence occurring through the TADF mechanism. In the case of **CzDdp**, no delayed fluorescence was observed, however, triplet exciton harvesting through the TTA mechanism was evidenced. The absence of delayed fluorescence is assumed to stem from a combination of two effects. Compared to TADF timescales observed for **AcDdp** (10^{-3} s), faster triplet harvesting in **CzDdp** through TTA channel was evidenced through electroluminescence. The timescale is supposed to be similar to emission timescales of the prompt fluorescence. This leads to an increase of PLQY of the solutions by 16% after degassing. Independently from the faster (hence competitive) TTA channel for triplet harvesting, the TADF mechanism was found to be inefficient in the case of **CzDdp**, due to a combination of large singlet-triplet splitting reaching 0.24 eV, and limited contribution from the mixing (second-order nonadiabatic coupling) between ^3LE and $^3(\text{CT-LE})$. This is due to the relatively small dihedral angles in **CzDdp** resulting in mixing of LE and CT characters in T_1 , thus reducing the contribution of CT character to the $T_1 \rightarrow S_1$ rISC.

From a fundamental standpoint, our results demonstrate that triplet harvesting in donor acceptor molecules with small singlet-triplet splitting is not necessary related to TADF as it is widely accepted, but can proceed through eventually faster and competitive TTA mechanism. "Dynamic" state-energy diagrams, which consider the dynamical CT-LE mixing through fast vibrational motions allow better understanding of the experimental results related to TADF mechanism, as compared to the static state-energy diagrams.

In view of the interesting properties of **AcDdp** and **CzDdp**, these compounds were used as hosts in red PHOLEDs. The device with **CzDdp** host exhibited superior parameters of electrophosphorescence allowing to achieve higher external quantum efficiency of 15.9% as well as lower efficiency roll-off in comparison to those of the device based on the widely utilised mCP, mCBP, NPB and nBPhen hosts. External quantum efficiencies of 19.4% and 22.1% for doped yellow and orange devices were achieved when the compounds **CzDdp** and **AcDdp** were used as TADF/TTA emitters, respectively.

Declaration of Competing Interest

The authors declare that they have no known competing financial interests or personal relationships that could have appeared to influence the work reported in this paper.

Acknowledgements

This project has received funding from European Social Fund

(project No 09.3.3-LMT-K-712-02-0106) under grant agreement with the Research Council of Lithuania (LMTLT)

Appendix A. Supplementary data

Supplementary data to this article can be found online at <https://doi.org/10.1016/j.cej.2020.127902>.

References

- Y. Liu, C. Li, Z. Ren, S. Yan, M.R. Bryce, All-organic thermally activated delayed fluorescence materials for organic light emitting diodes, *Nat. Rev. Mater.* 18020 (2018) 1–20, <https://doi.org/10.1038/natrevmats.2018.20>.
- L. Zhang, K.W. Cheah, Thermally activated delayed fluorescence host for high performance organic light emitting diodes, *Sci. Rep.* 8832 (2018) 1–6, <https://doi.org/10.1038/s41598-018-27238-y>.
- X. Ban, F. Chen, Y. Liu, J. Pan, A. Zhu, W. Jiang, Y. Sun, Design of efficient thermally activated delayed fluorescence blue host for high performance solution-processed hybrid white organic light emitting diodes, *Chem. Sci.* 10 (2019) 3054–3064, <https://doi.org/10.1039/C8SC035561>.
- Z. Yang, Z. Mao, Z. Xie, Y. Zhang, S. Liu, J. Zhao, I. Xu, Z. Chi, M.P. Aldred, Recent advances in organic thermally activated delayed fluorescence materials, *Chem. Soc. Rev.* 46 (2017) 915–1016, <https://doi.org/10.1039/C6CS00368K>.
- M.K. Etherington, J. Gibson, H.F. Higginbotham, T.J. Penfold, A.P. Monkman, Revealing the spin vibronic coupling mechanism of thermally activated delayed fluorescence, *Nat. Commun.* 7 (13680) (2016) 1–7, <https://doi.org/10.1038/ncom13680>.
- G. Myles, K. Goushia, W.J. Pottsavage Jr., C. Adachi, Influence of host matrix on thermally-activated delayed fluorescence: Effects on emission lifetime, photoluminescence quantum yield, and device performance, *Org. Electron.* 15 (2014) 2027–2037, <https://doi.org/10.1016/j.orgel.2014.05.027>.
- S.K. Lower, M.A. El Sayed, The triplet state and molecular electronic processes in organic molecules, *Chem. Rev.* 66 (1966) 199–241, <https://doi.org/10.1021/cr00240a004>.
- D.M. Mayder, C.M. Tonge, Z.M. Hudson, Thermally activated delayed fluorescence in 1,3,4-oxadiazoles with π -extended donors, *J. Org. Chem.* 85 (2020) 11094–11103, <https://doi.org/10.1021/acs.joc.0c00908>.
- X. Qiao, D. Ma, Nonlinear optoelectronic processes in organic optoelectronic devices: Triplet-triplet annihilation and singlet fission, *Mater. Sci. Eng. R* 139 (100519) (2020) 1–38, <https://doi.org/10.1016/j.mser.2019.100519>.
- J. Zhou, Q. Liu, W. Feng, Y. Sun, F. Li, Upconversion Luminescent Materials: Advances and Applications, *Chem. Rev.* 115 (2015) 395–465, <https://doi.org/10.1021/cr4004478c>.
- J. Liu, Z. Li, T. Hu, X. Wei, R. Wang, X. Hu, Y. Liu, Y. Yi, Y. Yamada-Takesuna, Y. Wang, P. Wang, Experimental evidence for "Hot Exciton" thermally activated delayed fluorescence emitters, *Adv. Optical Mater.* 7 (1801190) (2019) 1–9, <https://doi.org/10.1002/adom.201801190>.
- Y. Xu, X. Liang, X. Zhou, P. Yuan, J. Zhou, C. Wang, B. Li, D. Hu, X. Qiao, X. Jiang, L. Liu, S. J. Su, D. Ma, Y. Ma, Highly efficient blue light emitting diodes based on upper level triplet-singlet intersystem crossing, *Adv. Mater.* 31 (1807388) (2019) 1–8, <https://doi.org/10.1002/adma.201807388>.
- J. H. Lee, C. H. Chen, P. H. Lee, H. Y. Lin, M. K. Leung, T. L. Chiu, C. F. Lin, Blue organic light emitting diodes: current status, challenges, and future outlook, *J. Mater. Chem. C* 7 (2019) 5874–5888, <https://doi.org/10.1039/C9JC00204A>.
- N.A. Kalduta, T. Matulaitis, D. Volyniuk, K. Ivaniuk, P. Turyk, P. Staklairs, J. V. Grazulevičius, A.P. Monkman, Deep-blue high-efficiency TTA OLED using para- and meta-conjugated cyanotriphenylbenzene and carbazole derivatives as emitter and host, *J. Phys. Chem. Lett.* 8 (2017) 6199–6205, <https://doi.org/10.1021/acs.jpclett.7b02867>.
- B. Wex, B.R. Kharfaran, Perspective on carbazole-based organic compounds as emitters and hosts in TADF applications, *J. Mater. Chem. C* 5 (2017) 8622–8653, <https://doi.org/10.1039/C7TC02156A>.
- O. Bezvikomiy, D. Gudėika, D. Volyniuk, M. Rutkis, J.V. Grazulevičius, Diphenylsulfone-based hosts for electroluminescent devices: Effect of donor substituents, *Dyes Pigm.* 175 (108104) (2020) 1–10, <https://doi.org/10.1016/j.dyepig.2019.108104>.
- M. H. Hsin, C.-Y. Lee, Y.-C. Chen, P.-Y. Chen, Y.-H. Chen, H.-H. Lu, Y.-H. Lin, B.-Y. Lin, M. Z. Lee, T. L. Chiu, C. F. Lin, J. H. Lee, 89.3% lifetime elongation of blue TTA-OLED with assistant host, *SID 2016 DIGEST*, 1727-1729, <https://doi.org/10.1002/adip.11043>.
- X. Song, D. Zhang, Y. Liu, C. Yin, L. Understanding and Manipulating the Interplay of Wide Energy-Gap Host and TADF Sensitizer in High-Performance Fluorescence OLEDs, *Adv. Mater.* 31 (1901923) (2019) 1–9.
- X. Chen, C. Xu, T. Wang, C. Zhou, J. Du, Z. Wang, H. Xu, T. Xie, G. Bi, J. Jiang, X. Zhang, J.N. Demas, C.O. Trindle, Y. Luo, G. Zhang, Versatile Room-Temperature-Phosphorescent Materials Prepared from N-Substituted Naphthalimides: Emission Enhancement and Chemical Conjugation, *Angew. Chem. Int. Ed.* 55 (2016) 9872–9876, <https://doi.org/10.1002/ange.201601252>.
- T. Higuchi, H. Nakamoto, C. Adachi, High efficiency white organic light-emitting diodes based on a blue thermally activated delayed fluorescent emitter combined with green and red fluorescent emitters, *Adv. Mater.* 27 (2015) 2019–2023, <https://doi.org/10.1002/adma.201404967>.

- [21] F. Khana, E. Urbonus, D. Volyniuk, J.V. Grazulevicius, S.M. Mobin, R. Misra, White hyperelectrofluorescence from solution-processable OLEDs based on phenothiazine substituted tetraphenylethylene derivatives, *J. Mater. Chem. C*, 2020, Accepted Manuscript. <https://doi.org/10.1039/D0TC03136D>.
- [22] H. Sun, C. Zhang, J.-L. Breeds, Reliable prediction with tuned range-separated functionals of the singlet-triplet gap in organic emitters for thermally activated delayed fluorescence, *J. Chem. Theory Comput.* 11 (2015) 3851–3858, <https://doi.org/10.1021/acs.jctc.5b00431>.
- [23] S. Boixi, D. Jana, Parthas, P. Parui, B.K. Ghosh, Dibenzofuran, ciplhenazine based donor-acceptor (D-A) tetra branched molecules: fine tuning of optical properties, 3 (2018) 6953–6959, <https://doi.org/10.1002/solc.201801530>.
- [24] C. Zhou, S. Xiao, W. Man Wang, H. Jiang, S. Liu, B. Yang Zhang, Modulation of excited state property based on benzo-f, ciplhenazine acceptor: three typical excited states and electroluminescence performance, *Front. Chem.* 7 (141) (2019) 1–10, <https://doi.org/10.3389/fchem.2019.00141>.
- [25] F. M. Xie, Z. D. An, M. Xie, Q. Li, G. H. Zhang, S. J. Zou, L. Chen, J. D. Chen, T. Cheng, J.-X. Tang, tert Butyl substituted hetero-donor TADF compounds for efficient solution processed non doped blue OLEDs, *J. Mater. Chem. C* 8 (2020) 5769–5776, <https://doi.org/10.1039/C9TC02248D>.
- [26] Y. Liu, M. Kim, Y.-J. Cho, J.-A. Seo, K.S. Yook, J.-Y. Lee, Molecular design strategy of organic thermally activated delayed fluorescence emitters, *Chem. Mater.* 29 (2017) 1946–1963.
- [27] A. Fromanekaiter, R. Lygaitis, S. Raišys, K. Kozlauskas, G. Kreiza, D. Volyniuk, D. Gudkeša, S. Jusasas, J.V. Grazulevicius, Structure–property relationship of blue solid state emissive phenanthroimidazole derivatives, *Phys. Chem. Chem. Phys.* 19 (2017) 16737–16748, <https://doi.org/10.1039/C7CP02248D>.
- [28] K. Yamaguchi, Y. Esaki, T. Matsushima, C. Adachi, A 1,4,5,8,9,11 hexaazatriphenylenehexacarbonitrile (HAT CN) transport layer with high electron mobility for thick organic light-emitting diodes, *Appl. Adv.* 10 (055304) (2020) 1–5, <https://doi.org/10.1063/1.50097310>.
- [29] F.M. Xie, H.Z. Li, G.D. Lai, Y.Q. Li, T. Cheng, M. Xie, J.X. Tang, X. Zhang, Rational molecular design of dibenzofuran, ciplhenazine-based thermally activated delayed fluorescence emitters for orange-red OLEDs with EQE up to 22.0%, *ACS Appl. Mater. Interfaces* 12 (16) (2020) 18730–18738.
- [30] W. Liu, X. Luo, Y. Bao, Y.P. Liu, G. H. Ning, L. Abdelwalab, L. Li, C.T. Nai, Z.G. Hu, D. Zhao, B. Liu, S.Y. Quirk, K.P. Ish, A two-dimensional conjugated aromatic polymer via C–C coupling reaction, *Nat. Chem.* 9 (2017) 563–570, <https://doi.org/10.1038/nchem.2696>.
- [31] E.K. Unver, S. Tarkuc, Y.A. Udmun, C. Tanyeli, L. Toppare, Effect of conjugated core building block dibenzofuran, ciplhenazine unit on π -conjugated electrochromic polymers: Red-shifted absorption, *J. Polym. Sci. A Polym. Chem.* 48 (2010) 1714–1720, <https://doi.org/10.1002/pola.22925>.
- [32] P. Moonsoo, N. Prachumrak, R. Rattanasorn, T. Kowin, S. Jungsittiwong, T. Sudyodsuk, V. Promrak, Carbazole dendronised triphenylamines as solution processed high Tg amorphous hole-transporting materials for organic electroluminescent devices, *Chem. Commun.* 48 (2012) 3382–3384, <https://doi.org/10.1039/C2CC16878E>.
- [33] W. Kohn, L.J. Shem, Self-consistent equations including exchange and correlation effects, *Phys. Rev.* 140 (1965) A1133–A1138, <https://doi.org/10.1103/PhysRev.140.A1133>.
- [34] E.K.U. Gross, W. Kohn, Time-dependent density-functional theory, *Adv. Quantum Chem.* 21 (1990) 255–291, [https://doi.org/10.1016/S0065-3276\(08\)60600-0](https://doi.org/10.1016/S0065-3276(08)60600-0).
- [35] R. Baumechnitt, R. Alhrichs, Treatment of electronic excitations within the adiabatic approximation of time dependent density functional theory, *Chem. Phys. Lett.* 256 (1996) 454–464, [https://doi.org/10.1016/0009-2614\(96\)00440-X](https://doi.org/10.1016/0009-2614(96)00440-X).
- [36] M.E. Casida, C. Jamorski, K.C. Casida, D.R. Salahdin, Molecular excitation energies to high-lying bound states from time-dependent density-functional response theory: characterization and correction of the time-dependent local density approximation ionization threshold, *J. Chem. Phys.* 108 (1998) 4439–4449, <https://doi.org/10.1063/1.473855>.
- [37] E. Miyamoto, Y. Yamaguchi, M. Yokoyama, Ionization potential of organic pigment film by atmospheric photoelectron emission analysis, *Electrochromography* 28 (1989) 364–370, <https://doi.org/10.1137/0128.364>.
- [38] S. Okamoto, K. Tanaka, Y. Izumi, H. Adachi, T. Yamaji, T. Suzuki, Simple measurements of quantum efficiency in organic electroluminescent devices, *Jpn. J. Appl. Phys.* 40 (2001) 783–784, <https://doi.org/10.1143/JJAP.40.L783>.
- [39] Z. Zhang, D.A. Egger, J. L. Brédas, L. Kronik, Y. Coropceanu, Effect of solid state polarization on charge transfer excitations and transport levels at organic interfaces from a screened range-separated hybrid functional, *J. Phys. Chem. Lett.* 8 (2017) 3277–3283, <https://doi.org/10.1021/acs.jpclett.7b01276>.
- [40] V. Minaitis, J.V. Grazulevicius, R. Laurinaviciute, D. Volyniuk, V. Jankauskas, G. Sini, Can hydrogen bonds improve the hole-mobility in amorphous organic semiconductors? Experimental and theoretical insights, *J. Mater. Chem. C* 3 (2015) 11660–11674, <https://doi.org/10.1039/C5TC02594F>.
- [41] J. Grune, N. Bunzmann, M. Meinecke, V. Dyakonov, A. Sperlich, Kinetic modeling of transient electroluminescence reveals TTA as an efficiency-limiting process in exciplex based TADF OLEDs, *J. Phys. Chem. C* (2020), <https://doi.org/10.1021/acs.jpcc.0c06528>.
- [42] A.A. Rudnik, S. Bagnich, D. Wagner, S. Athanasopoulos, P. Strohrriegel, A. Köhler, The influence of torsion on excimer formation in bipolar host materials for blue phosphorescent OLEDs, *J. Chem. Phys.* 144 (214906) (2016) 1–6, <https://doi.org/10.1063/1.4953102>.
- [43] Y. Wang, Y. Wu, P. Wang, Y. Chen, X. Wei, R. Wang, Z. Li, Y. Liu, R. Duan, J. Liu, Y. Yamada Takamura, Triplet decay induced negative temperature dependence of the transient photoluminescence decay of thermally activated delayed fluorescence emitter, *J. Mater. Chem. C* (2017), <https://doi.org/10.1039/C7TC04025C>.
- [44] A.E. Nikolacenko, M. Cass, F. Bourcet, D. Mohammad, M. Roberts, Thermally activated delayed fluorescence in polymers: A new route toward highly efficient solution processable OLEDs, *Adv. Mater.* 27 (2015) 7236–7240, <https://doi.org/10.1002/adma.201501090>.
- [45] J.J. Kim, L.S. Park, C.-Y. Chan, M. Tanaka, Y. Tsuchiya, H. Nakanoami, C. Adachi, Nanosecond-time-scale delayed fluorescence molecule for deep-blue OLEDs with small efficiency rolloff, *Nat. Commun.* 11 (1765) (2020) 1–8, <https://doi.org/10.1038/s41467-020-15538-5>.
- [46] N. Bunzmann, S. Weissenel, L. Kodriashova, J. Grune, B. Krugmann, J. V. Grazulevicius, A. Sperlich, V. Dyakonov, Optically and electrically excited intermediate electronic states in donor-acceptor based OLEDs, *Mater. Horiz.* 7 (2020) 1126–1137, <https://doi.org/10.1039/C9MH01475F>.
- [47] C.-G. Zeng, Y.-F. Dai, W.-L. Zeng, Z. Ma, Z.-K. Chen, J. Kieffer, Achieving highly efficient fluorescent blue organic light-emitting diodes through optimizing molecular structures and device configuration, *Adv. Funct. Mater.* 21 (2011) 699–707, <https://doi.org/10.1002/adfm.201002195>.
- [48] P. Y. Chou, H. H. Chou, Y. H. Chen, T. H. Su, C. Y. Liao, H. W. Lin, W. C. Lin, H. Y. Yen, L.-C. Chena, C.-H. Cheng, Efficient delayed fluorescence via triplet-triplet annihilation for deep blue electroluminescence, *Chem. Commun.* 50 (2014) 6869–6871, <https://doi.org/10.1039/C4CC01851F>.
- [49] C. Guozorig, M. Fujilára, A possible mechanism for enhanced electrofluorescence emission through triplet-triplet annihilation in organic electroluminescent devices, *Appl. Phys. Lett.* 81 (2002) 3137–3139, <https://doi.org/10.1063/1.1515129>.
- [50] Y.-J. Su, H.-L. Huang, C.-L. Li, C.-H. Chien, Y.-T. Tao, R.-F. Chou, S. Datta, R.-S. Liu, Highly efficient red electrophosphorescent devices based on iridium isquinoline complexes: remarkable external quantum efficiency over a wide range of current, *Adv. Mater.* 15 (11) (2003) 884–888, <https://doi.org/10.1002/adma.200304630>.
- [51] S. Tofghi, P. Zhao, R.M. O'Donnell, J. Shi, P.Y. Zavalij, M.V. Bondar, D.J. Hagan, E.W. Van Stryland, Fast triplet population in iridium(III) complexes with less than unity singlet to triplet quantum yield, *J. Phys. Chem. C* 113 (2010) 13846–13855, <https://doi.org/10.1021/acs.jpcc.9b00539>.
- [52] C. H. Fan, P. Sun, T. H. Su, C. H. Cheng, Host and dopant materials for idealized deep-red organic electrophosphorescent devices, *Adv. Mater.* 23 (2011) 2981–2985, <https://doi.org/10.1002/adma.201100610>.
- [53] F.B. Dias, J. Santos, D.R. Graves, P. Data, R.S. Nohyabu, M.A. Fox, A.S. Batsanov, T. Palucira, M.N. Berberan Santos, M.R. Bryce, A.P. Monkman, The role of local triplet excited states and a δ relative ionization in thermally activated delayed fluorescence: photophysics and devices, *Adv. Sci.* 3 (1600080) (2016) 1–10, <https://doi.org/10.1002/advs.201600080>.
- [54] T. Kobayashi, A. Niwa, K. Takaki, S. Haseyama, T. Negase, K. Goushi, C. Adachi, H. Naito, Contributions of a higher triplet excited state to the emission properties of a thermally activated delayed fluorescence emitter, *Phys. Rev. Applied* 7 (034002) (2017) 1–10, <https://doi.org/10.1103/PhysRevApplied.7.034002>.
- [55] J. Gibson, A.P. Monkman, T.J. Penfold, The importance of vibronic coupling for efficient reverse intersystem crossing in thermally activated delayed fluorescence molecules, *Commun.* 17 (2016) 2956–2961, <https://doi.org/10.1002/cplc.201600562>.
- [56] X. K. Chen, S. F. Zhang, J. X. Fan, A. M. Ren, Nature of highly efficient thermally activated delayed fluorescence in organic light-emitting diode emitters: nonadiabatic effect between excited states, *J. Phys. Chem. C* 119 (2015) 9728–9733, <https://doi.org/10.1021/acs.jpcc.5b00276>.
- [57] B.R. Henry, W. Siebrand, Spin-orbit coupling in aromatic hydrocarbons. Analysis of nonradiative transitions between singlet and triplet states in benzene and naphthalene, *J. Chem. Phys.* 54 (1971) 1072–1085, <https://doi.org/10.1063/1.1674940>.
- [58] Y. Olivier, B. Yurash, L. Muccioli, G. D'Avino, O. Mikhnenko, J.C. Sancho Garcia, C. Adachi, T. Q. Nguyen, D. Beljonne, Nature of the singlet and triplet excitations mediating thermally activated delayed fluorescence, *Phys. Rev. Materials* 1 (075602) (2017) 1–6, <https://doi.org/10.1103/PhysRevMaterials.1.075602>.
- [59] P.K. Samanta, D. Klu, V. Coropceanu, J. L. Brédas, Up-conversion intersystem crossing rates in organic emitters for thermally activated delayed fluorescence: Impact of the nature of singlet vs triplet excited states, *J. Am. Chem. Soc.* 139 (2017) 4042–4051, <https://doi.org/10.1021/jacs.6b12124>.
- [60] R. Ieji, K. Goushi, C. Adachi, Triplet-triplet upconversion enhanced by spin-orbit coupling in organic light-emitting diodes, *Nat. Commun.* 10 (5283) (2019) 1–10, <https://doi.org/10.1038/s41467-019-13044-1>.
- [61] C. Ye, Y. Gny, J. Martensson, K. Borjesson, Annihilation versus excimer formation by the triplet pair in triplet-triplet annihilation process upon upconversion, *J. Am. Chem. Soc.* 141 (2019) 9578–9584, <https://doi.org/10.1021/jacs.9b02302>.

Cite this: *J. Mater. Chem. C*, 2021,
9, 3928

Dual versus normal TADF of pyridines ornamented with multiple donor moieties and their performance in OLEDs†

Pavel Arsenyan,^a *[‡] Brigita Vigante,^a Karolis Leitonas,^b Dmytro Volyniuk,^b Viktorija Andruleviciene,^b Levani Skhirtladze,^b Sergey Belyakov^b and Juozas Vidas Grazulevicius^b *[‡]

A procedure for post-functionalization by 3,6-di-*tert*-butyl-carbazole or 3,7-dibromophenothiazine of dicyanopyridines was developed. Pyridine rings in new pyridines exist in a twist-conformation in the solid state. Green and orange thermally activated delayed fluorescence (TADF) with close emission quantum yields in solid-state resulting from recombination of two different intramolecular charge transfer (ICT) states was observed for compounds post-functionalized by 3,6-di-*tert*-butyl-carbazole and 3,7-dibromophenothiazine moieties, respectively. Non-doped and doped organic light-emitting diodes exhibiting green and orange electroluminescence were developed using the synthesized compounds as normal/dual TADF emitters. The device based on 3,7-dibromophenothiazine-containing emitters exhibiting dual TADF showed low device life-times and a low maximum external efficiency of 3.1 (for the non-doped device) and 5% (for the doped device). Organic light-emitting diodes with 3,6-di-*tert*-butyl-carbazole-containing emitters exhibiting normal TADF showed relatively high device life-times and a high maximum external efficiency of 8.1 (for the non-doped device) and 25% (for the doped device). Because of the energy distribution between the two ICT states in dual-TADF emitters, ultra-long lifetime of fluorescence (up to milliseconds) was detected which results in exciton–exciton and exciton–polaron annihilations under electrical excitation and low stability and efficiency of the device.

Received 7th December 2020,
Accepted 8th February 2021

DOI: 10.1039/d0tc05745b

rsc.li/materials-c

Introduction

Starting from the first publication on application of materials with thermally activated delayed fluorescence (TADF) in organic light-emitting diodes (OLEDs), the multiple-donor approach has been widely used in the design of efficient TADF emitters.¹ High external quantum efficiency (EQE) of TADF based OLEDs is directly related to emissive triplet harvesting *via* reverse triplet → singlet intersystem crossing (RISC) in purely organic compounds with small singlet–triplet energy splitting (ΔE_{ST}) and high photoluminescence quantum yields (PLQYs) in the solid state.² Some multiple-donor–acceptor TADF emitters with small ΔE_{ST} and high

PLQYs in the solid-state were previously developed and showed efficient and relatively stable electroluminescence.³ For example, a TADF molecule with three donor and three acceptor units was used in the fabrication of non-doped solution-processed sky-blue TADF OLEDs with a maximum EQE up to 21.0%.⁴ TADF molecules with four donor moieties showed an ultra-high RISC rate of $4.44 \times 10^6 \text{ s}^{-1}$ resulting in maximum EQEs of OLEDs up to 24.6%.⁵ It was also demonstrated that TADF emitters with a higher number of donor moieties showed shorter lifetimes of delayed fluorescence and longer device lifetimes than the reference compounds with a lower number of donor moieties.^{6,7} Donating abilities of the donors can be tuned by attaching *tert*-butyl, methyl, phenyl and other groups to the same donor moiety. Examples of asymmetrical donor–acceptor–donor* TADF molecules with two donors of different types are limited.^{8,9} Multiple-donor–acceptor TADF emitters with a high number (3–4) of electron-donating units usually contain one-type of donor (*e.g.*, carbazole units). The effect of the presence of different types of donors on TADF efficiency of multiple-donor–acceptor compounds, to our knowledge, has not been studied yet.

Interestingly, utilization of two different donors in the same molecule can lead to realization of dual TADF, the first example

^a Latvian Institute of Organic Synthesis, Aizkraukles 21, LV-1006, Riga, Latvia.
E-mail: pavel@ios.lv

^b Department of Polymer Chemistry and Technology, Kaunas University of Technology, Radvilenu pl. 19, LT-50254, Kaunas, Lithuania.
E-mail: juozas.grazulevicius@ktu.lt

[‡] Electronic supplementary information (ESI) available: Details on instrumentation (sample fabrication and investigation) and materials used for OLED fabrication, computational details, and ¹H, ¹³C NMR and IR spectra are given. CCDC 1989801 and 1989803. For ESI and crystallographic data in CIF or other electronic format see DOI: 10.1039/d0tc05745b

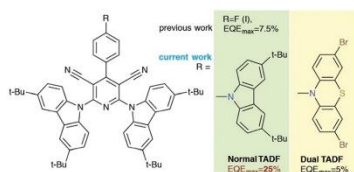


Fig. 1 Molecular design approach of the dual TADF emitters.

of which has been recently reported.¹⁰ Dual TADF was observed for unsymmetrical donor/acceptor alternate (D-A-D*) compounds having two different donors, *i.e.*, phenothiazine (D) and *N*-(1*h*-indole-5-yl) acetamide (D') and diphenylsulfone as the acceptor unit (A). The compound with dual TADF was applied for integrating time-resolved imaging. However, dual TADF emitters have not been tested yet in OLEDs, which we aimed to do in this study.

With the above aim, in this study we introduced different types of donors to the molecular structure of multiple donor-acceptor TADF emitters. Recently, we developed efficient TADF compounds with two 3,6-di-*tert*-butyl-carbazole moieties (Fig. 1).¹¹ Following the aim of this work, 2,6-bis-(3,6-di-*tert*-butylcarbazol-9-yl)-4-(4-fluorophenyl)-pyridine-3,5-carbonitrile (**1**) was further post-functionalized by attaching 3,6-di-*tert*-butylcarbazole or 3,7-dibromophenothiazine moieties. Two multiple donor-substituted dicyanopyridines with three donors of one-type (3,6-di-*tert*-butyl-carbazole) or two-types (3,6-di-*tert*-butylcarbazole and 3,7-dibromophenothiazine) in their molecular structures were synthesized and fully characterized (Fig. 1). The effect of such structures of multiple-donor-acceptor TADF emitters on their photophysical and electroluminescence properties including the OLED performance stability was investigated. A maximum EQE of 25% was obtained for OLEDs based on the developed compound **5a** as the TADF emitter. This is considerably a higher value than the maximum EQE of 7.5% observed for OLEDs based on the previously reported 2,6-bis-(3,6-di-*tert*-butylcarbazol-9-yl)-4-(4-fluorophenyl)-pyridine-3,5-carbonitrile.¹¹

Materials and methods

Unless otherwise stated, all reagents were purchased from commercial suppliers and used without further purification. Thin layer chromatography (TLC) was performed using MERCK Silica gel 60 F254 plates and visualized by UV (254 nm) fluorescence. ZEOCHEM silica gel (ZEOprep 60/35–70 microns – SI23501) was used for column chromatography. ¹H and ¹³C NMR spectra were recorded on a Bruker 400 spectrometer at 400 and 101 MHz correspondingly at 298 K in CDCl₃. The ¹H chemical shifts are given relative to the residual CHCl₃ signal (7.26 ppm), and ¹³C chemical shifts are given relative to CDCl₃ (77.16 ppm). The melting points were determined using a "Digital melting point analyser" (Fisher), and the results are given without correction. For **5a** diffraction data were collected

at *T* = 150 K using a Rigaku XtaLAB Synergy, Dualflex, HyPix diffractometer using CuK α -radiation (λ = 1.54184 Å). For **5b** diffraction data were collected at *T* = 193 K using a Bruker-Nonius KappaCCD diffractometer using MoK α -radiation (λ = 0.71073 Å). The crystal structures were solved by direct methods and refined by full-matrix least squares with the help of Olex2¹² and ShelXT¹³ software. CCDC 1989801 (for **5a**) and CCDC 1989803 (for **5b**) contain the supplementary crystallographic data for this paper.[†]

4-(3,6-Di-*tert*-butylcarbazol-9-yl)benzaldehyde (**1a**)

A mixture of 4-fluorobenzaldehyde (1.06 mL, 10 mmol), K₂CO₃ (4.15 g, 30 mmol) and 3,6-di-*tert*-butyl-9*H*-carbazole (2.79 g, 10 mmol) in DMF (15 mL) was refluxed for 12 h. After cooling the mixture was poured into ice water and extracted with DCM (3 × 50 mL). The organic phase was dried over anhydrous Na₂SO₄ and evaporated. The crude product was purified by flash chromatography on silica gel using the mixture of DCM : petroleum ether (1 : 1) as the eluent affording a pale-yellow powder (2.37 g, 63%). The ¹H NMR spectrum is in accordance with ref. 14.

4-Phenothiazin-10-yl-benzaldehyde (**1b**)

The mixture of phenothiazine (1.67 g, 8.4 mmol), 4-bromobenzaldehyde (1.0 g, 9.5 mmol), potassium carbonate (2.0 g, 14.49 mmol), Pd(OAc)₂ (0.1 g, 0.5 mmol) and tri-*tert*-butylphosphine (0.3 mL, 1 M solution in toluene, 0.6 mmol) in 10 mL of anhydrous toluene was refluxed under argon for 24 h. Then the solvent was removed under reduced pressure and the residue was purified by flash column chromatography on silica gel (eluent: petroleum ether/DCM 2 : 1 (by volume)) to afford aldehyde **1b** as a white solid (1.36 g, 53%). The ¹H-NMR data correspond to those available in the literature for **1b**.¹⁵

(*E,Z*)-2-Cyano-3-[4-(3,6-di-*tert*-butylcarbazol-9-yl)-phenyl]-acrylamide (**2a**)

The mixture of **1a** (3.90 g, 10.2 mmol), 2-cyanoacetamide (1.72 g, 20.4 mmol) and piperidine (2.01 mL, 20.4 mmol) in methanol (120 mL) was stirred at rt overnight. After cooling in refrigerator, the precipitates were filtered off and washed with methanol affording 3 g (66%) of **2a** as bright yellow powder which was used in the next step without additional purification. Mp > 200 °C. ¹H-NMR (400 MHz, DMSO-*d*₆): 8.34–8.27 (m, 3H), 8.22 (d, *J* = 8.6 Hz, 2H), 7.97 (s, 1H), 7.86 (d, *J* = 8.6 Hz, 2H), 7.82 (s, 1H), 7.54–7.38 (m, 4H), 1.42 (s, 18H). ESI-MS: *m/z*: 450 [M + H]⁺.

(*E,Z*)-2-Cyano-3-(4-phenothiazin-10-yl-phenyl)-acrylamide (**2b**)

The mixture of **1b** (1.08 g, 3.56 mmol), 2-cyanoacetamide (0.6 g, 7.13 mmol) and piperidine (0.7 mL, 7.13 mmol) in methanol (20 mL) was stirred under argon for 24 h. After cooling the bright yellow precipitates were filtered off and purified by flash column chromatography on silica gel (eluent: petroleum ether/ethyl acetate 1 : 2 (by volume)) to afford acrylamide **2b** as bright yellow powder (0.82 g, 62%). ¹H-NMR (400 MHz, DMSO-*d*₆): 8.11 (s, 1H), 7.99–7.91 (m, 2H), 7.82 (s, 1H), 7.68 (s, 1H), 7.45 (dd, *J* = 7.7, 1.5 Hz, 2H), 7.32 (ddd, *J* = 7.9, 7.4, 1.5 Hz, 2H), 7.26–7.11 (m, 6H). ¹³C NMR (DMSO-*d*₆): 163.44, 150.08, 147.54, 141.50,

132.79, 129.63, 128.73, 128.19, 126.86, 126.12, 124.37, 119.91, 117.37, 104.03. ESI-MS: *m/z*: 370 [M + H]⁺.

4-[4-(3,6-Di-*tert*-butylcarbazol-9-yl)-phenyl]-6-hydroxy-2-oxo-1,2-dihydropyridine-3,5-dicarbonitrile piperidine salt (3a)

The mixture of **2a** (1.34 g, 3 mmol), ethyl cyanoacetate (0.64 mL, 6 mmol) and piperidine (0.59 mL, 6 mmol) in dry chloroform (50 mL) was refluxed for 48 h. After cooling in refrigerator, the precipitates were filtered off and washed with cold chloroform. The obtained salt was triturated with methanol and filtered affording **3a** as grey powder (0.86 g, 48%) which was used in the next step without additional purification. Mp > 200 °C. ¹H-NMR (400 MHz, DMSO-*d*₆): 10.65 (s, 1H), 8.36–8.26 (m, 2H), 7.76–7.65 (m, 4H), 7.52 (dd, *J* = 8.7, 2.0 Hz, 2H), 7.40–7.35 (m, 2H), 3.04–2.97 (m, 4H), 1.68–1.59 (m, 4H), 1.58–1.51 (m, 2H), 1.43 (s, 18H). ¹³C NMR (DMSO-*d*₆): 164.45, 163.83, 161.54, 143.22, 138.67, 138.51, 130.20, 126.07, 124.24, 123.49, 119.28, 117.17, 116.69, 109.52, 82.09, 44.23, 34.95, 32.25, 25.75, 22.66, 22.04. ESI-MS: *m/z*: 513 [M – H][–].

4-(4-(10*H*-Phenothiazin-10-yl)phenyl)-6-hydroxy-2-oxo-1,2-dihydropyridine-3,5-dicarbonitrile piperidine salt (3b)

The mixture of **2b** (0.8 g, 2.17 mmol), ethyl cyanoacetate (0.35 mL, 3.25 mmol) and piperidine (0.32 mL, 3.25 mmol) in dry chloroform (60 mL) was refluxed for 48 h. After cooling, the precipitates were filtered off and carefully washed with chloroform and methanol yielding piperidine salt **3b** (0.53 g, 47%) as white powder, which was used in the next step without additional purification. ¹H-NMR (400 MHz, DMSO-*d*₆): 8.30 (s, 1H), 7.59 (d, *J* = 8.6 Hz, 2H), 7.40 (d, *J* = 8.7 Hz, 2H), 7.20 (dd, *J* = 7.5, 1.6 Hz, 2H), 7.07 (ddd, *J* = 8.2, 7.4, 1.6 Hz, 2H), 6.98 (td, *J* = 7.5, 1.3 Hz, 2H), 6.48 (dd, *J* = 8.1, 1.3 Hz, 2H), 3.04–2.93 (m, 4H), 1.69–1.48 (m, 6H). ESI-MS: *m/z*: 435 [M + H-piperidine]⁺.

2,6-Dibromo-4-(4-(di-*tert*-butylcarbazol-9-yl)-phenyl)-pyridine-3,5-carbonitrile (4a)

A mixture of **3a** (1.20 g, 2.0 mmol) and POBr₃ (1.55 g, 5.4 mmol) and quinoline (1 mL) in dry toluene (50 mL) was heated with stirring at 110 °C for 3 h. The hot toluene was decanted, and the residue was carefully washed with boiling toluene (3 × 40 mL). Combined toluene extracts were washed with water and saturated aqueous NaCl solution and dried over Na₂SO₄. After solvent evaporation, the crude product was purified by flash column chromatography on silica gel (eluent: DCM/petroleum ether 1:1) yielding **4a** (0.90 g, 70%) as white powder. Mp: > 200 °C. ¹H-NMR (400 MHz, CDCl₃): 8.14 (t, *J* = 1.3 Hz, 2H), 7.90–7.84 (m, 2H), 7.83–7.76 (m, 2H), 7.51 (d, *J* = 1.3 Hz, 4H), 1.48 (s, 18H). ESI-MS: *m/z*: 641 [M + H]⁺. Anal. calcd for C₃₃H₂₈Br₂N₄: C, 61.89; H, 4.41; N, 8.75; found: C, 61.72; H, 4.52, N, 8.26.

2,6-Dibromo-4-(4-(3,7-dibromo-10*H*-phenothiazin-10-yl)phenyl)-pyridine-3,5-dicarbonitrile (4b)

A mixture of pyridone **3b** (0.48 g, 0.92 mmol), POBr₃ (0.79 g, 2.77 mmol) and quinoline (1 mL) in dry toluene (30 mL) was heated with stirring at 110 °C for 1 h. The hot toluene was decanted, and the residue was carefully washed with boiling

toluene (3 × 40 mL). Combined toluene extracts were washed with water and saturated aqueous NaCl solution and dried over Na₂SO₄. After solvent evaporation, the crude product was purified by flash column chromatography on silica gel (eluent: DCM/petroleum ether 1:1 → 2:1) yielding **4b** (0.48 g, 73%) as grey powder. Mp: > 200 °C. ¹H-NMR (400 MHz, DMSO-*d*₆): 7.85–7.71 (m, 2H), 7.60 (d, *J* = 2.3 Hz, 1H), 7.55–7.44 (m, 3H), 7.39 (dd, *J* = 8.6, 2.3 Hz, 1H), 7.31 (dd, *J* = 8.7, 2.3 Hz, 1H), 6.71 (d, *J* = 8.7 Hz, 1H), 6.47 (d, *J* = 8.8 Hz, 1H). ESI-MS: *m/z*: 718 [M]⁺. Anal. calcd for C₂₅H₁₆Br₄N₄S: C, 41.82; H, 1.40; N, 7.80; found: C, 41.56; H, 1.35, N, 7.65.

2,6-Bis(3,6-di-*tert*-butylcarbazol-9-yl)-4-[4-(3,6-di-*tert*-butylcarbazol-9-yl)-phenyl]-pyridine-3,5-dicarbonitrile (5a)

3,6-Di-*tert*-butyl-9*H*-carbazole (275 mg, 0.984 mmol) was added to a suspension of NaH (60% oil dispersion, 35.3 mg, 1.05 mmol) in THF (3 mL) at 0 °C under an argon atmosphere. The reaction mixture was stirred for an additional 30 min at 0 °C and then a DMF (2 mL) solution of **4a** (210 mg, 0.328 mmol) was added. The mixture was stirred at rt for 3 h and then it was poured into ice-water. The mixture was extracted with DCM (4 × 50 mL), washed with water, saturated aqueous NaCl solution, and dried over Na₂SO₄. The solvent was removed under reduced pressure and the crude product was washed twice with acetonitrile and then purified by flash chromatography on silica gel (eluent chloroform/petroleum ether/acetone 10:12:0.4 by volume), yielding **5a** as light yellow powder (170 mg, 51%), Mp > 200 °C. IR *ν*_{max} (film): 2226, 1604, 1541, 1511. ¹H NMR (400 MHz, chloroform-*d*): 8.16–8.09 (m, 8H), 7.96 (d, *J* = 8.6 Hz, 2H), 7.77 (dd, *J* = 8.8, 0.6 Hz, 4H), 7.56 (dd, *J* = 8.7, 0.6 Hz, 2H), 7.54–7.46 (m, 6H), 1.47–1.48 (m, 54 H). ¹³C NMR (CDCl₃): 154.61, 146.47, 143.78, 141.94, 138.45, 136.98, 131.48, 130.54, 126.69, 125.73, 124.17, 123.96, 123.89, 116.58, 116.35, 114.31, 112.40, 109.99, 109.46, 99.10, 34.89, 34.76, 31.94, 31.79. Anal. calcd for C₇₃H₇₆N₆: C, 84.52; H, 7.38; N, 8.10; found: C, 84.36; H, 7.39, N, 8.05.

2,6-Bis(3,6-di-*tert*-butyl-9*H*-carbazol-9-yl)-4-(3,7-dibromo-10*H*-phenothiazin-10-yl)phenylpyridine-3,5-dicarbonitrile (5b)

3,6-Di-*tert*-butyl-9*H*-carbazole (0.62 g, 2.23 mmol) was added to a suspension of NaH (60% oil dispersion, 78.6 mg, 2.34 mmol, 4.2 eq.) at 0 °C under an argon atmosphere. The reaction mixture was stirred for an additional 30 min at 0 °C and then a DMF (3 mL) solution of **4b** (0.4 g, 0.56 mmol) was added. The mixture was stirred at rt for 3 h and then it was poured into ice-water. The mixture was extracted with DCM (4 × 50 mL), washed with water, saturated aqueous NaCl solution, and dried over Na₂SO₄. The solvent was removed under reduced pressure and the crude product was washed twice with acetonitrile and then purified by flash chromatography on silica gel (eluent: petroleum ether/DCM 1:1 → 1:2 by volume), yielding **5b** as bright yellow powder (0.47 g, 68%), Mp > 230 °C. IR *ν*_{max} (film): 2228, 1605, 1550, 1504. ¹H NMR (400 MHz, chloroform-*d*): 8.11 (dd, *J* = 2.0, 0.6 Hz, 4H), 7.96–7.88 (m, 2H), 7.74 (dd, *J* = 8.7, 0.6 Hz, 4H), 7.52–7.40 (m, 8H), 7.31 (dd, *J* = 8.6, 2.3 Hz, 2H), 6.86 (d, *J* = 8.6 Hz, 2H), 1.47 (s, 36H). ¹³C NMR (CDCl₃): 162.82,

154.56, 146.45, 146.34, 140.90, 136.95, 131.87, 130.51, 130.41, 130.26, 128.66, 125.72, 124.13, 123.79, 122.08, 117.87, 116.55, 114.42, 112.41, 98.74, 34.88, 31.86, 31.78. Anal. calcd for $C_{65}H_{58}Br_2N_6S$: C, 70.01; H, 5.24; N, 7.54; found: C, 70.15; H, 5.40, N, 7.30.

Results and discussion

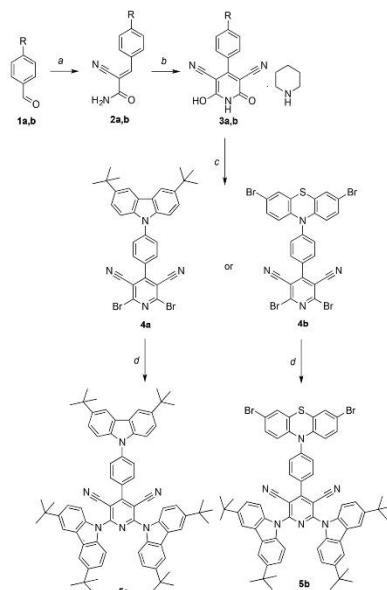
Synthesis and molecular structures

In continuation of our research in the field of carbazolyl substituted dicyanopyridines¹¹ we decided to add additional carbazole moieties. Unfortunately, our attempts to substitute fluoro atoms with carbazole in previously obtained 2,6-bis(3,6-di-*tert*-butyl-9*H*-carbazol-9-yl)-4-(4-fluorophenyl)pyridine-3,5-dicarbonitrile (**1**) failed as carbazolyl substituents in positions 2 and 6 were sensitive to basic conditions and elevated temperature. Alternatively, we realized the synthesis of desired products **5a** and **5b** starting with 4-(3,6-di-*tert*-butylcarbazol-9-yl)benzaldehyde **1a**¹¹ and 4-phenothiazin-10-yl-benzaldehyde **1b**.¹¹ Aldehydes **1a** and **1b** were treated with 2-cyanoacetamide in the presence of piperidine (Scheme 1).

As a result, (*E,Z*)-2-cyano-3-[4-(3,6-di-*tert*-butylcarbazol-9-yl)-phenyl]-acrylamide **2a** and (*E,Z*)-2-cyano-3-(4-phenothiazin-10-yl-phenyl)-acrylamide **2b** were isolated instead of the expected cyclization products. Further continuous heating of **2a** and **2b** with ethyl cyanoacetate and piperidine in chloroform led to the formation of **3a** and **3b** in acceptable yields. Then, these salts were converted to the corresponding dibromopyridines **4a** and **4b**. Notably, 2,6-dibromo-4-[4-(di-*tert*-butylcarbazol-9-yl)-phenyl]-pyridine-3,5-dicarbonitrile **4a** was isolated in good yield, however, the heating of **3b** with POBr₃ in quinolone led to the additional bromination of phenothiazine ring in positions 3 and 7 yielding 2,6-dibromo-4-[4-(3,6-di-*tert*-butyl-10*H*-phenothiazin-10-yl)phenyl]pyridine-3,5-dicarbonitrile **4b** in 73% yield as grey powder. Finally, desired **5a** and **5b** were obtained by a previously elaborated method^{11,16} by amination of dibromides **4a** and **4b** with 3,6-di-*tert*-butyl-9*H*-carbazole in DMF using sodium hydride as the base.

Fig. 2A shows a perspective view with atomic numbering scheme of the molecular structure of **5a** (ESI† contains the stereo view figure of **5a**). Crystals were grown from dilute solution of acetonitrile. It unambiguously confirms the formation of completely substituted pyridine. The dihedral angle between the pyridine and phenyl ring in position 4 is 65.8(7). Besides, 3,6-di-*tert*-butyl-carbazole moieties in positions 2 and 6 form dihedral angles between least squares planes equal to 45.5(8) (N7) and 39.9(8) (N43). In its turn the dihedral angle between the phenyl ring and the 3,6-di-*tert*-butyl-carbazole with N28 is 77.4(9).

The considerable values of these dihedral angles testify steric overload of the molecular structure by indication of the Cremer-Pople parameters for the pyridine cycle. Calculation of the Cremer-Pople parameters analogously to carbohydrate cycles¹⁷ led us to the following values for a pyridine cycle = 125.9 and 51.1 and $Q = 1.486 \text{ \AA}$. These parameters correspond to **2E** conformation in Cremer-Pople abbreviations, which



Scheme 1 Preparation of **5a** and **5b**. Reaction conditions: (a) 2-cyanoacetamide (2 equiv.), piperidine, MeOH, rt, overnight; (b) ethyl cyanoacetate (2 equiv.), piperidine (2 equiv.), CHCl₃, reflux, 48 h; (c) POBr₃ (2.8 equiv.), quinoline, dry toluene, reflux, 3 h; (d) NaH (2 equiv.), 3,6-di-*tert*-butyl-9*H*-carbazole (2 equiv.), THF/DMF, 0 °C.

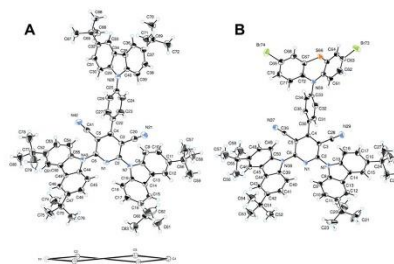


Fig. 2 (A) Molecular structure of **5a** with anisotropic displacement ellipsoids drawn at 50% probability and conformation of the pyridine cycle (below) in molecules of **5a** (atoms are shown as small spheres of arbitrary radii); (B) molecular structure of **5b** with anisotropic displacement ellipsoids drawn at 50% probability.

indicates that pyridine ring in **5a** exists in a twist-conformation in the solid state (Fig. 2A). Also, no shortened intermolecular contacts were found in the crystal structure; there are only weak hydrophobic interactions between *tert*-butyl groups.

Electrochemical and photophysical properties

The energy levels of the compounds were studied by cyclic voltammetry (CV) and photoelectron emission (PE) spectroscopy. Ionization potentials (I_p^{CV}) of 5.62 and 5.31 eV were observed by CV for compounds **5a** and **5b** (Fig. 3A). A smaller I_p^{CV} value was obtained for **5b** in comparison to that of compound **5a** due to the presence of strong electron-donating 3,7-dibromophenothiazine moieties. The onset potentials of the first reduction band against ferrocene were used for the estimation of electron affinities (E_A^{CV}) of the compounds. The E_A^{CV} values of **5a** and **5b** were practically the same since the same electron-accepting moiety is present in both the molecules (Scheme 1). Since higher energy is required

to release electrons from a molecule in the solid state than in solutions, higher ionization potentials (I_p^{PE}) of 6.09 and 5.95 eV were obtained for vacuum-deposited films of **5a** and **5b**, respectively, by PE measurements (Fig. 3B). Electron affinities (E_A^{PE}) of 3.44 and 3.32 eV were calculated for compounds **5a** and **5b** in the solid state using the formula $E_A = I_p^{PE} - E_g$ where E_g is the optical band-gap energy of the corresponding neat films. Both I_p^{PE} and E_A^{PE} values are necessary for the design of OLEDs.

Electronic structures in ground and excited states of **5a** and **5b** were experimentally investigated by UV spectroscopy as well as by steady-state and time-resolved luminescence spectroscopy. The close peak wavelengths (390 and 396 nm) of low-energy absorption bands were observed for the solutions of **5a** and **5b** in toluene (Fig. 3C and Table 1). The positions of these bands were in very good agreement with that of the corresponding band of compound **1**.¹¹ Based on the TD-DFT calculations, low-energy absorption bands are assigned to the several electronic transitions

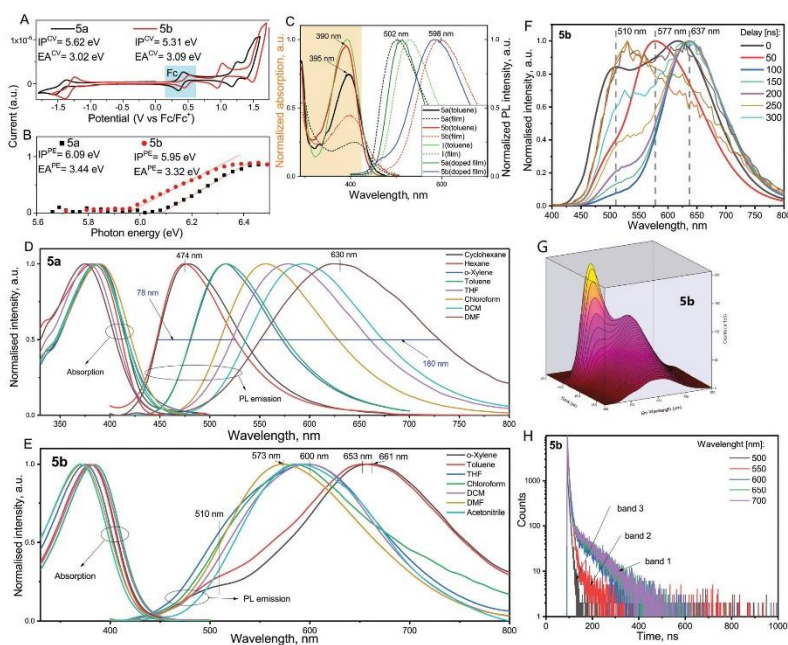


Fig. 3 Cyclic voltammograms (A) and photoelectron emission spectra (B) of **5a** and **5b**. Absorption and emission (C) spectra (under excitation at 350 nm) of the solutions of compounds **5a**, **5b** and **1** in toluene and of neat and doped films. 1,3-Bis(9-carbazolyl)benzene (mCP) was used as a low-polarity host. Solvent effects on optical absorption and PL spectra of compounds **5a** (D) and **5b** (E) in solutions with concentration ca. 10^{-4} mg mL⁻¹. Time-resolved spectra of toluene solution of **5b** at different time windows after excitation recorded with the different time delays (F and G). PL decays of toluene solution of **5b** recorded at the different emission wavelengths (H).

Table 1 Photophysical data for **5a** and **5b**^a

Compound	5a	5b
Wavelength of absorption maxima (toluene), nm	395	390
Wavelength of PL max (neat/doped film), nm	502/512	598/584
PLQY (neat/mCP and mCBP doped film), %	18/20/22	12/17/20
S ₁ (THF/doped film), eV	2.71/2.81	2.79/2.83
T ₁ (THF/doped film), eV	2.61/2.7	2.75/—
ΔE _{ST} (THF/doped film), eV	0.1/0.11	0.04/—

^a Doped films are **5a**(wt 10%) in mCP and **5b**(wt 10%) in mCP as well as **5a**(wt 20%) in mCBP and **5b**(wt 20%) in mCBP. First singlet (S₁) and triplet (T₁) levels were taken at set-on of PL and phosphorescence spectra recorded at 77 K, respectively (Fig. 6D). PLQYs of solid films were measured under air.

(S₀ → S₁ and S₀ → S₂ for **5a**; S₀ → S₂, S₀ → S₃ and S₀ → S₀ for **5b**) corresponding to charge transfer (CT) from 3,6-di-*tert*-butyl-9-phenylcarbazole to phenylpyridine-3,5-dicarbonitrile moieties with contribution from the local excitations (Fig. S1, ESI[†]). The calculated oscillator strengths of **5a** and **5b** at lowest energy transition (S₁) are 0.3233 and 0.0007, respectively, suggesting a reduced wavefunction overlap between the donor and acceptor in **5b** compared to **5a**. The transition S₀ → S₁ of **5b** exhibits CT from 3,7-dibromophenothiazine to the acceptor with practically zero oscillator strength due to the orthogonal geometry of the molecule (Fig. S1, ESI[†]).

Neat films of **5a** and **5b** showed non-structured photoluminescence (PL) spectra with peak wavelengths of 502 and 598 nm, respectively (Fig. 3C). The PL spectra of **5a** and **5b** were found to be shifted in comparison to the PL spectrum of the film of compound **1** apparently because of either their different dielectric constants or aggregate formation.¹¹ Affected by the different polarity of the mCP host or aggregate formation,¹⁸ slight PL shifts were observed for the doped films **5a**(10 wt%):mCP and **5b**(10 wt%):mCP (Fig. 3C). Additionally, a low-intensity shoulder was observed in the range of 400 nm to 500 nm in the PL spectrum of the film of **5b** doped in mCP. Thus, the PL spectrum of compound **5b** results from overlapping of at least two emission bands.

Solvatochromic measurements allow obtaining more information on the emission nature of organic compounds. In case of normal TADF, organic compounds exhibit CT emission which is strongly sensitive to solvent polarity. Thus, non-structured emission spectra with a single broad band of the conventional TADF emitters have to be broadened and have to be redshifted with the increasing solvent polarity due to the CT character of the first singlet excited state. Compound **5a** was characterized by broadened emission spectra from 78 nm of its full width at half maxima (FWHM) for the solution in hexane to FWHM of 180 nm for the solution in DMF. The PL intensity maximum was redshifted from 474 nm for the solution in hexane to 630 nm for the solution in DMF (Fig. 3D). As a result, a high slope of 17 072 cm⁻¹ was obtained by fitting in the whole range of the Stokes shift *versus* solvent polarity dependence for compound **5a** according to the Lippert–Mataga solvatochromic model (Fig. S2a, ESI[†]). Such a slope proved the strong CT character of emission of compound **5a**.

In the case of dual TADF emitters, non-structured emission spectra with two broad bands have to be observed. Both bands

have to be broadened and have to be red-shifted with increasing solvent polarity due to the CT character of the first and second singlet excited states being in disagreement with the Kasha rules at the same time. The PL spectra of the solutions of compound **5b** in low-polarity solvents (toluene and *o*-xylene) were recorded. A band observed at 653 nm for toluene solution was shifted to the wavelength of 661 nm for *o*-xylene solution allowing the consideration of the CT character of the emission (Fig. 3E). Additionally, a shoulder at *ca.* 510 nm was observed from which the CT character of emission was not clear from the first glance. The PL spectra of the solutions of compound **5b** in solvents with higher polarity were also recorded. The blue-shifted PL bands were observed at 573 nm for DMF solution and at 600 nm for DCM solution. This second band is different in nature from the band observed at 653 nm for toluene solution. Since the second band peaked at different wavelengths in the spectra of different solutions, its CT character is evident. As a result, the Stokes shift *versus* solvent polarity dependences can be obtained for two bands, the fitting of which gives two slopes demonstrating different CT characters of dual emission of compound **5b** (Fig. S2b, ESI[†]). It should be noted that the Lippert–Mataga fitting for compound **5b** gives certain error because of the overlapping of the three bands. The nature of the shoulder at *ca.* 510 nm (the third band) of the PL spectrum of THF solution of compound **5b** is not yet clear similarly to that of the toluene solution.

Taking into account the results of solvatochromic measurements, which showed that the emission of compound **5b** resulted from the overlapping of three bands being different in nature (thus, they should be characterised by the different PL decays), these bands can be separated by time-resolved PL measurements. The results of time-resolved PL measurements carried out for toluene solution of compound **5b** are presented in Fig. 3F–H and Fig. S3 (ESI[†]). The PL spectra and PL decays were recorded within different time windows and using different time delays which allowed the separation of the spectra of prompt and delayed fluorescence. As a result, additional evidence that the total emission (steady-state emission) of compound **5b** resulted from overlapping of three bands at *ca.* 500, 573 and 635 nm was obtained from Fig. 3F, G and Fig. S3 (ESI[†]). As seen from Fig. 3G, the most intensive band at *ca.* 500 nm (prompt fluorescence) was observed in the PL spectrum of toluene solution of compound **5b** recorded without delay after excitation. When different time delays were used for cutting the prompt fluorescence at *ca.* 500 nm, the highest intensities could be observed for the other bands (delayed fluorescence with the different PL decays) (Fig. 3G). The high-energy band peaked at 500 nm belonged to fluorescence resulting from the recombination of LE states. It is characterized by a single-exponential PL decay in the ns range (Fig. 3H). Since other bands peaking at 573 and 635 nm are characterized by double exponential PL decays, their emission can be regarded as a combination of prompt and delayed fluorescence resulting from emissive recombination of different excited CT states. The nature of delayed fluorescence and the different excited CT states of compound **5b** will be discussed below.

In order to prove the nature of the emissions of **5b**, the energy diagrams of the excited states were proposed on the

basis of TDDFT with implicit consideration of the environment (THF and toluene) via the conductor-like polarizable continuum model (CPCM) (Fig. 4A and B). It is noted that the theoretical values of the vertical excitation energies do not match with the experimental ones obtained from PL spectra of the solutions of **5b** in THF and toluene. However, these diagrams provide visualization of the possible characters of the recorded PL bands. Three experimental PL bands were assigned to the S_1 , S_2 and S_3 excited states. According to the CPCM for the solution in toluene, the $S_1 \rightarrow S_0$ and $S_2 \rightarrow S_0$ transitions involve CT, while the $S_3 \rightarrow S_0$ transition is associated with CT and LE (Fig. 4A). Because of incomplete internal conversion (IC), responsible for the transition from the higher to the lower electronic state $S_3 \rightarrow S_2 \rightarrow S_1$, the most intensive PL band at 653 nm along with low-intensity bands at 573 nm and 500 nm was observed (Fig. 3E and Fig. S3, ESI[†]). Calculations using CPCM for THF solution revealed that the nature of transitions at considered excited states differs from those obtained with CPCM for toluene solutions. In this case, $S_1 \rightarrow S_0$ and $S_3 \rightarrow S_0$ correspond to CT, while $S_2 \rightarrow S_0$ is related to CT and LE (Fig. 4B). It is assumed, that the most intensive PL band observed at 600 nm for THF solution is attributed to emission from S_2 . Despite the IC, the intensity of the PL band corresponding to S_1 is very weak since the polarity of THF inhibits CT emission.

To study the emission nature of **5a** and **5b** in more detail, PL spectra and PL decays of the films of **5a** and **5b** dispersed in mCP were recorded at different temperatures (Fig. 5A and B). The PL spectra recorded at 77 and 300 K were found to be similar showing similarity in fluorescence and phosphorescence spectra of **5a** and **5b**. As a result, small singlet-triplet energy splitting (ΔE_{ST}) was obtained for THF solutions of **5a** and **5b** (0.1 eV and 0.04 eV, respectively) and for the film of **5a** doped in mCP (0.11 eV) (Fig. 5D). The broad PL spectrum of **5b** doped in mCP (Fig. 5D) is similar to that recorded for toluene solution (Fig. 3E and F) confirming triple emission. Therefore,

the ΔE_{ST} of **5b** doped in mCP cannot be determined. Long lived fluorescence of compounds **5a** and **5b** was identified as TADF since its intensity grew up with the increasing temperature (Fig. 5A-C). Based on the time-resolved PL spectra (Fig. 3F and G) and PL decays (Fig. 3H) of the solution of **5b** in toluene, it can be concluded that the solid solution of **5b** in mCP shows dual TADF corresponding to emissions from S_1 and S_2 . Different shapes of PL decays were observed for the films of **5a** doped in mCP and of **5b** doped in mCP because of the different nature of emissions of **5a** and **5b**. Based on TDDFT it can be concluded that TADF of **5a** is related to CT from 3,6-di-*tert*-butyl-9-phenylcarbazole moieties to phenylpyridine-3,5-dicarbonitrile units ($S_1 \rightarrow S_0$), while dual TADF of **5b** corresponds to the CT transitions from 3,7-dibromophenothiazine moieties to phenylpyridine-3,5-dicarbonitrile ($S_1 \rightarrow S_0$) and pyridine-3,5-dicarbonitrile units ($S_2 \rightarrow S_0$) (Fig. 4A and C).

Electroluminescence

Taking into account the TADF properties of **5a** and **5b**, they were tested as emitters in non-doped and doped OLEDs. The effect of the concentration of emitters **5a** and **5b** in mCP on device efficiency was studied using the device structure of ITO/HAT-CN(4 nm)/TAPC(40 nm)/mCP(8 nm)/**5a** (5, 15, 30, or 100 wt%)mCP (24 nm)/TSPO1(4 nm)/TPBi(40 nm)/LiF:Al. Equilibrium energy diagrams and roles of functional layers of OLEDs are given in ESI[†] Fig. S4. The highest maximum EQE values and pure EL spectra from emission of **5a** (**5b**) were observed for non-doped devices (with 100 wt% of emitter concentration) and for devices with high concentration of emitters (30 wt%) (Fig. S5, ESI[†]). Because of the host and aggregation effects,¹⁹ the maxima of EL spectra were found in the range from 492 to 533 nm for devices with different concentrations (5–100 wt%) of emitter **5a** (Fig. S6, ESI[†]). Maxima of EL spectra of **5b**-based devices were not shifted with the increase of concentration of the emitter. This observation is apparently related to the dual TADF emission of compound **5b**

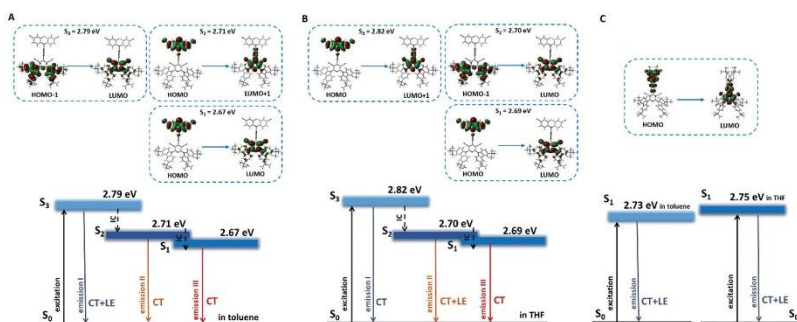


Fig. 4 Energy diagram of the vertical excited states and their nature calculated using TD-DFT B3LYP(d,p) with CPCM in toluene of **5b** (A) in THF of **5b** (B) and in both solvents of **5b** (C) (TD-DFT B3LYP(d,p) level).

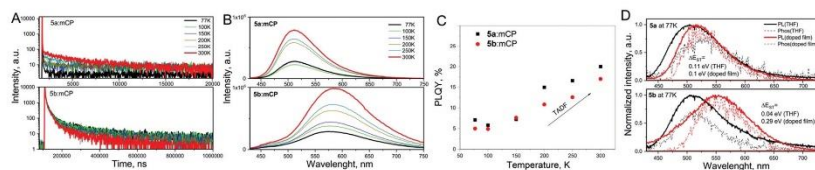


Fig. 5 PL decays (A) and PL spectra (B) recorded at the different temperatures of the films of the compounds **5a** and **5b** doped in mCP. PLOQY versus temperature plots (C) obtained taking PLOQYs measured at 300 K and the total PL intensity (Fig. 4B) of the doped films of **5a** and **5b** at different temperatures. PL and phosphorescence spectra (D) of the solutions of **5a** and **5b** in THF and of the solid solutions in mCP at 77 K.

(Fig. 3B). Because of inefficient hole \rightarrow guest energy transfers for **5a** doped in mCP and **5b** doped in mCP, low EQEs were obtained for OLEDs containing the layers with low concentration of emitters (5 and 15%) (Fig. S6, ESI[†]). Since high turn-on voltages of the devices were observed, further optimization of device structures and thicknesses of functional layers was required.

The modified devices had structure ITO/MoO₃(0.6 nm)/NPB(35 nm)/mCP(6 nm)/**5a** (or **5b**) (30 or 100 wt%):mCP (25 nm)/TSPO1(6 nm)/TPBi(35 nm)/LiF(0.6 nm):Al (Fig. S1, ESI[†]). Non-doped and doped devices n-**5a**, d-**5a**, n-**5b**, and d-**5b** with light-emitting layers of **5a**, **5a**(30 wt%):mCP, **5b**, or **5b**(30 wt%):mCP were fabricated. Stable green and orange electroluminescence was observed under different applied voltages for the devices based on **5a** and **5b**, respectively (Fig. 6A and Fig. S7, ESI[†]).

Slightly higher turn-on voltages were observed for devices n-**5a** and d-**5a** in comparison to those of devices n-**5b**, and d-**5b**. Such turn-on voltages are in good agreement with IP^{PE} values of compounds **5a** (6.09 eV) and **5b** (5.95 eV). Higher energy barriers in OLEDs based on **5a** resulted in higher turn-on voltages in

comparison to those of **5b**-based devices (Fig. 6B and Table 2). The maximum brightness exceeded 30 000 cd m⁻² for devices n-**5a** and d-**5a** (Fig. 6B and Table 2). In contrast, devices n-**5b** and d-**5b** showed *ca.* one magnitude lower maximum brightness (>3000 cd m⁻²). This observation may be related to different efficiencies of the devices and/or to the different sensitivity of human eyes to green and orange light. Non-doped device n-**5a** showed a high maximum EQE of 8.1% (Fig. 6C). Since compound **5a** showed poor charge-transporting properties (Fig. S8, ESI[†]), the probability of hole-electron recombination within the light-emitting layer **5a**:mCP is apparently lower than 100%. Indeed, the maximum EQE of the doped device d-**5a** was improved up to 11.7% most probably due to the improvement of hole-electron recombination probability in the emitting layer by usage of bipolar host mCP taking into account that PLOQYs of doped and non-doped **5a**-based films are similar (Table 1). Despite close values of PLOQYs of doped and non-doped **5b**-based films to those of **5a**-based films (Table 1), *ca.* three times lower maximum EQEs (3.1 and 3.2%) were obtained for devices n-**5b** and d-**5b** (Fig. 6C). This result can partly be attributed to the poor charge-transporting properties of compound **5b**, the charge

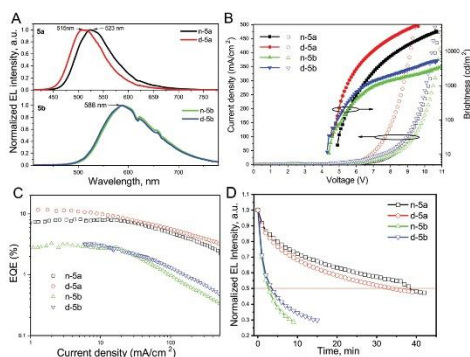


Fig. 6 EL spectra at 8 V (A); current density and brightness versus voltage (B); EQE versus current density (C) plots and life-times of the non-passivated devices under air at constant 5 V (D).

Table 2 Electroluminescence parameters of the optimized OLEDs

Devices	V_{on} [V] at set 10 cd m^{-2}	EL maximum at 5 V [nm]	$CE_{max}, CE_{100}, CE_{1000}^a$ (cd A^{-1})	$PE_{max}, PE_{100}, PE_{1000}^a$ (lm W^{-1})	$EQE_{max}, EQE_{100}, EQE_{1000}^a$ (%)
n-5a	4.9	515	28, 25, 17	12, 11, 8.4	8.1, 8.0, 7.8
d-5a	4.6	523	40, 38, 30	24, 21, 16	11.7, 11.1, 10.7
o-5a	3.9	512	55.9, 47.2, 37.1	43.9, 30.4, 18.0	25.0, 15.2, 11.8
n-5b	4.4	588	6.5, 6.0, 1.2	3.7, 2.8, 0.6	3.1, 2.8, 2.6
d-5b	4.3	588	6.9, 6.1, 1.4	3.8, 3.1, 0.7	3.2, 3.1, 2.7
o-5b	5.1	582	9.7, 8.3, 1.5	5.9, 3.7, 0.3	5, 3.5, 0.6

^a Current efficiency (CE_{max} , CE_{100} , and CE_{1000}), power efficiency (PE_{max} , PE_{100} , and PE_{1000}) and EQE_{max} , EQE_{100} , and EQE_{1000} were taken at sets 10, 100, and 1000 cd m^{-2} , respectively.

mobilities of which were out of the measurement range of the TOF method (Fig. S8, ESI[†]). The different device efficiencies can also be explained by the different nature of TADF of compounds **5a** and **5b** (Fig. 3–5). Energy transfer through IC from S_2 to S_1 with quantum yields lower than 100% takes place in case of dual TADF emission of compound **5b**. This additional energy transfer leads to both decrease of emission efficiency and extended emission decay of compound **5b**. This statement is supported by extremely long PL decay of **5b** reaching one millisecond (Fig. 5A). The long emission lifetime of compound **5b** can enhance the probability of exciton–exciton and exciton–polaron annihilations under electrical excitation,¹⁹ which can lead not only to low EQEs but also to low device life-times. Indeed, life-times of devices n-5b and d-5b were considerably shorter than those of devices n-5a and d-5a (Fig. 6D and Fig. S9, ESI[†]). The data presented in Fig. 6D were recorded for non-passivated samples under air conditions, thus it demonstrates the relative life-times of the optimized devices. Nevertheless, it can be concluded that devices based on dicyanopyridine bearing two kinds of donors (3,6-di-*tert*-butyl-carbazole and 3,7-dibromophenothiazine) suffer from lower device efficiencies and life-times in comparison to those of OLEDs based on dicyanopyridine bearing multiple

3,6-di-*tert*-butyl-carbazolyl substituents. This result can be explained by the formation of two kinds of CT states between phenylpyridine-3,5-dicarbonitrile and 3,7-dibromophenothiazine as well as between pyridine-3,5-dicarbonitrile and 3,7-dibromophenothiazine in compound **5b** leading to the prolonged emission lifetime. In contrast, one-type of CT state of **5a** can be formed between dicyanopyridine and 3,6-di-*tert*-butyl-carbazole units inducing its relatively short emission lifetime which is necessary for efficient and long-lived devices.

In addition, to achieve close to 100% probability of hole–electron recombination within the light-emitting layers of **5a** and **5b** based devices, the electroluminescence properties of TADF emitters **5a** and **5b** were additionally studied by exploring the device structure ITO/HAT-CN(5 nm)/NPB(40 nm)/TCTA(10 nm)/mCBP(10 nm)/**5a** (or **5b**) (20 wt%)/mCBP (50 nm)/NBPhen(30 nm)/LiQ(2 nm)/Al naming devices as o-5a and o-5b, respectively (Fig. S4, ESI[†]). 3,3'-Di(9*H*-carbazol-9-yl)-1,1'-biphenyl (mCBP), 2,9-dinaphthalen-2-yl-4,7-diphenyl-1,10-phenanthroline (NBPhen), and 8-hydroxyquinolinolato-lithium (LiQ) were used in the fabrication of OLEDs o-5a and o-5b. Using multilayer HAT-CN/NPB/TCTA/mCBP and NBPhen/LiQ, efficient hole and electron injection/transport respectively was achieved. This statement is supported by the same

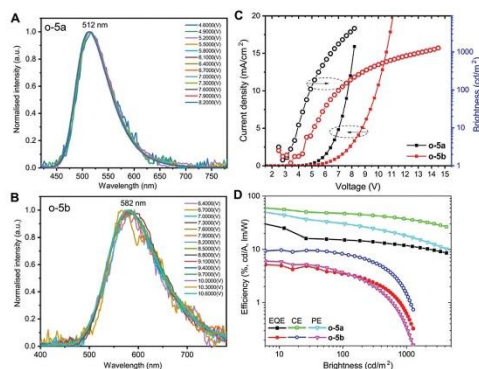


Fig. 7 EL spectra recorded at the different voltages (A and B); current density and brightness versus voltage (C); and EQE versus current density (D) plots of the optimized devices o-5a and o-5b.

EL spectra observed at the different applied voltages which are completely related to the emission of compounds **5a** and **5b** (Fig. 7A and B). The trends of current density-voltage and voltage-brightness dependencies of devices **o-5a** and **o-5b** are in very good agreement with those of devices **n-5a**, **d-5a** and **n-5a**, **d-5a**, respectively (Fig. 6B and 7C). Nevertheless, the optimization of device structures allowed the improvement of maximum EQEs up to 25% and 5% for devices **o-5a** and **o-5b** mainly due to the improvement of hole-electron recombination (Fig. 7D). Sixteen devices were fabricated in this work. The characteristics for the most efficient one are given above. The other devices were characterized by slightly lower EQEs of >24% as shown in Fig. S10 (ESI[†]), for example. Apparently, “perfect” film morphology, thus “perfect” interface properties for “perfect” charge injection and charge balance within light-emitting layers were achieved in the case of the best device with the untypical slope of the EQE dependence (Fig. 7D). As the result, a maximum EQE of 25% was achieved. For the pixel 1 (Fig. S10, ESI[†]), the untypical slope was not obtained but there is an artefact point at ca. 450 cd m⁻². Apparently, the artefact point at ca. 35 cd m⁻² can explain the untypical slope for the most efficient device (Fig. 7D).

It may be interesting to know how high EQEs can be obtained for the emitters with relatively low PLQYs (Table 1). The given PLQYs were measured under air without precise selection of excitation wavelengths. Thus, PLQYs were affected by oxygen quenching and by efficiency of formation of charge transfer states. Light-emitting layers of **5a**(20 wt%):mCBP and **5b**(20 wt%):mCBP were used for the fabrication of optimized OLEDs **o-5a** and **o-5b**, respectively. PLQYs of these layers were found to be of 22 and 20%, respectively. The measurements were performed using an integral sphere in air at an excitation wavelength of 340 nm. PLQYs of these two emitters and their doped films were found to be relatively low in air since their TADF emission was partly quenched by oxygen (Fig. S11, ESI[†]). In addition, much higher experimental PLQY values of 35 and 44% were obtained when an excitation wavelength of 390 nm was used. This observation is in agreement with the results previously published in studies on TADF emitters showing that low PLQYs (thus, disagreement between the theoretical and experimental maximum EQEs) can be obtained for TADF emitters if their charge transfer absorption band is not directly excited during PLQY measurements.²⁰ Taking into account the oxygen quenching and different excitation sources (optical and electrical ones), a high EQE of 25% can be obtained despite relatively low experimental PLQY values recorded. The maximum EQE values of OLEDs depend not only on the PLQY of light-emitting layers but also on the efficiency of exciton production (100% in case of TADF). They also depend on the charge-balance factor (it can be close to 100% for device **o-5a**) and the out-coupling efficiency (it can be higher than 30% if there is molecular orientation within the light-emitting layer of **5a**:mCBP).

Conclusions

Two multiple donor substituted dicyanopyridines with three donors of one-type (3,6-di-*tert*-butyl-carbazole) or of two types

(3,6-di-*tert*-butyl-carbazole and 3,7-dibromophenothiazine) in their molecular structures were synthesized. The calculations of the Cremer-Pople parameters led us to approve ²E conformation in Cremer-Pople abbreviations, which means that pyridine rings in **5a** exist in a twist-conformation in the solid state; besides, Cremer-Pople parameters for the pyridine cycle in **5b** also confirm a twist-conformation (S51 conformation on the Cremer-Pople sphere). These compounds are characterized by efficient green and orange thermally activated delayed fluorescence which results from the recombination of two intramolecular charge transfer states. OLEDs with 3,7-dibromophenothiazine and 3,6-di-*tert*-butyl-carbazole containing emitters exhibiting dual TADF showed low device life-times and a low maximum external efficiency of 3.1 (for the non-doped device) and 5% (for the doped device). OLEDs based on the 3,6-di-*tert*-butyl-carbazolyl multiple substituted dicyanopyridine exhibiting normal TADF showed relatively high device life-times and a high maximum external efficiency of 8.1 (for the non-doped device) and 25% (for the doped one). Such device stability and efficiency effects are partly related to ultra-long emission decay (up to milliseconds) which can enhance the probability of exciton-exciton and exciton-polaron annihilations under electrical excitation. Our further research will be connected with the development of more sophisticated compounds containing two or more dicyanopyridine moieties.

Conflicts of interest

There are no conflicts to declare.

Acknowledgements

This work was supported by the project of scientific co-operation program between Latvia, Lithuania and Taiwan “Synthesis and studies of high-triplet-energy materials for blue OLEDs” (grant LV-LT-TW/2018/11) and European Regional Development Fund (project no 01.2.2-LMT-K-718-01-0015) under grant agreement with the Research Council of Lithuania (LMTLT).

Notes and references

- H. Uoyama, K. Goushi, K. Shizu, H. Nomura and C. Adachi, *Nature*, 2012, **492**, 234–238.
- K. Sato, K. Shizu, K. Yoshimura, A. Kawada, H. Miyazaki and C. Adachi, *Phys. Rev. Lett.*, 2013, **110**, 247401.
- S. K. Jeon, H. L. Lee, K. S. Yook and J. Y. Lee, *Adv. Mater.*, 2019, **31**, 1803524.
- X. Zheng, R. Huang, C. Zhong, G. Xie, W. Ning, M. Huang, F. Ni, F. B. Dias and C. Yang, *Adv. Sci.*, 2020, 1902087.
- G. Kreiza, D. Banevičius, J. Jovaišaitė, K. Maleckaitė, D. Gudeika, D. Volyniuk, J. V. Gražulevičius, S. Juršėnas and K. Kazlauskas, *J. Mater. Chem. C*, 2019, **7**, 11522–11531.
- C.-Y. Chan, M. Tanaka, H. Nakanotani and C. Adachi, *Nat. Commun.*, 2018, **9**, 5036.
- S.-J. Zou, F.-M. Xie, M. Xie, Y.-Q. Li, T. Cheng, X.-H. Zhang, C.-S. Lee and J.-X. Tang, *Adv. Sci.*, 2020, **7**, 1902508.

- 8 H. Liu, J. Zeng, J. Guo, H. Nie, Z. Zhao and B. Z. Tang, *Angew. Chem.*, 2018, **130**, 9434.
- 9 D. Gudeika, O. Bezvikonnyi, D. Volyniuk and J. V. Grazulevicius, *Dyes Pigm.*, 2020, **172**, 107789.
- 10 M. Luo, X. Li, L. Ding, G. Baryshnikov, S. Shen, M. Zhu, L. Zhou, M. Zhang, J. Lu, H. Ågren, X. Wang and L. Zhu, *Angew. Chem., Int. Ed.*, 2020, **59**, 17018–17025.
- 11 B. Vigante, K. Leitonas, D. Volyniuk, V. Andruleviciene, J. Simokaitiene, A. Ivanova, A. Bucinskas, J. V. Grazulevicius and P. Arsenyan, *Chem. – Eur. J.*, 2019, **25**, 3325.
- 12 O. V. Dolomanov, L. J. Bourhis, R. J. Gildea, J. A. K. Howard and H. Puschmann, *J. Appl. Crystallogr.*, 2009, **42**, 339–341.
- 13 G. M. Sheldrick, *Acta Crystallogr.*, 2015, **A71**, 3–8.
- 14 O. Bagheri and H. Dchghani, *Electrochim. Acta*, 2015, **186**, 43–49.
- 15 R. Jiang, M. Liu, H. Huang, L. Huang, Q. Huang, Y. Wen, Q.-Y. Cao, J. Tian, X. Zhang and Y. Wei, *Appl. Surf. Sci.*, 2018, **434**, 1129–1136.
- 16 W. Liu, C.-J. Zheng, K. Wang, Z. Chen, D.-Y. Chen, F. Li, X.-M. Ou, Y.-P. Dong and X.-H. Zhang, *Appl. Mater. Interfaces*, 2015, **7**, 18930–18936.
- 17 D. Cremer and J. A. Pople, *J. Am. Chem. Soc.*, 1975, **97**, 1354–1358.
- 18 D. Peckus, T. Matulaitis, M. Franckevičius, V. Mimaite, T. Tamulevičius, J. Simokaitiene, D. Volyniuk, V. Gulbinas, S. Tamulevičius and J. V. Gražulevičius, *J. Phys. Chem. A*, 2018, **122**, 3218–3226.
- 19 N. C. Giebink, B. W. D'Andrade, M. S. Weaver, P. B. Mackenzie, J. J. Brown, M. E. Thompson and S. R. Forrest, *J. Appl. Phys.*, 2008, **103**, 044509.
- 20 F. B. Dias, J. Santos, D. R. Graves, P. Data, R. S. Nobuyasu, M. A. Fox, A. S. Batsanov, T. Palmeira, M. N. Berberan-Santos, M. R. Bryce and A. P. Monkman, *Adv. Sci.*, 2016, **3**, 1600080.

Cite this: *J. Mater. Chem. C*, 2023,
11, 9514

3,5-Dicyanopyridine motifs for electron-transporting semiconductors: from design and synthesis to efficient organic light-emitting diodes†

Karolis Leitonas,^a Brigita Vigante,^d Dmytro Volyniuk,^b Audrius Bucinskas,^a
Rasa Keruckiene,^b Pavels Dimitrijevs,^b Tien-Lung Chiu,^{b,c}
Juozas Vidas Grazulevicius^{b,*} and Pavel Arsenyan^{b,*}

Proposing 3,5-dicyanopyridine motifs for the design of electroactive materials for optoelectronic devices, three electron-transporting semiconductors are synthesised. The compounds are characterised by high triplet energies of 2.68–2.79 eV, high glass-transition temperatures reaching 185 °C, ionisation potentials of ca. 6 eV and electron affinities of ca. 2.7–2.9 eV. Two compounds show deep-blue emissions caused by the relaxation of hybridised local and charge-transfer states. In contrast, another compound with the additional carbazole donor unit demonstrates pure charge-transfer emission. The compounds are characterised by different hosting properties causing very different efficiencies of thermally activated delayed fluorescence (TADF) of the emitter 4,6-di(9,9-dimethylacridan-10-yl)-isophthalonitrile (DAcIPN). The different reverse intersystem crossing (RISC) rates and RISC activation energies of DAcIPN are in the ranges of 1×10^5 – 1.7×10^6 s⁻¹ and 26–34 meV, respectively. An organic light-emitting diode based on the same TADF emitter and the newly synthesised host demonstrates a maximum external quantum efficiency of 21.9% which is considerably higher than that (12.9%) of devices based on the conventional host 3,3'-di(9H-carbazol-9-yl)-1,1'-biphenyl. Time-resolved electro-luminescence study proves efficient emissive harvesting of triplets when a 3,5-dicyanopyridine-based host is used.

Received 8th March 2023,
Accepted 31st May 2023

DOI: 10.1039/d3tc00841j

rsc.li/materials-c

Introduction

Inorganic light-emitting diodes (LEDs) gained popularity due to their high efficiency, long lifetime, and acceptable price.¹ In the late 90s of the last century, organic light-emitting diodes (OLEDs) started to compete and share the display and lighting markets with LEDs partly due to their unique properties, including optical transparency and flexibility.² At that time, fluorescent emitters were used in OLED structures, limiting their theoretical internal quantum efficiency (IQE) to 25% due to the harvesting of only singlet excitons.³ In 1999, a significant

breakthrough was reached in OLED technology through the development of phosphorescent emitters, thus increasing their theoretical EQEs to 100%.⁴ It was achieved using phosphorescent noble metal complexes which convert singlet excitons to triplet ones through the intersystem crossing process.⁵ The maximum external quantum efficiencies (EQEs) of phosphorescent OLEDs exceed 30%.⁶ Green and red phosphorescent OLED emitters are currently used in commercial OLED products.⁷ However, the lifetime and cost of blue phosphorescent noble metal complexes are still the limiting factors for blue-emitting OLEDs. In 2012, it was demonstrated that the theoretical IQE of 100% can be reached by employing singlet and triplet excitons through thermally activated delayed fluorescence (TADF).⁸ TADF materials attracted the attention of the scientific OLED community and industry. They contain no heavy atoms and are less toxic. In addition, their synthesis is more cost-effective compared with that of metal complexes. The EQE of TADF OLEDs already exceeded 40%.⁹ Such state-of-the-art OLEDs were obtained using OLED hosts. The hosts allow improving the hole–electron recombination by ensuring charge balance within light-emitting layers. In addition, they allow

^a Department of Polymer Chemistry and Technology, Kaunas University of Technology, Baršausko Str. 59, LT-51423, Kaunas, Lithuania.
E-mail: juozas.grazulevicius@ktu.lt

^b Latvian Institute of Organic Synthesis, Aicraukles 21, LV-1006, Riga, Latvia.
E-mail: pavel@osi.lv

^c Department of Electrical Engineering, Yuan Ze University, Taiwan

^d Electronic supplementary information (ESI) available: Copies of NMR spectra, DSC, theoretical and recorded UV spectra, PL, PL decay curves and phosphorescence spectra, TADF parameters, and TOF signals. See DOI: <https://doi.org/10.1039/d3tc00841j>

minimising emission quenching effects, such as concentration quenching, singlet–triplet, or triplet–triplet annihilations, etc.¹⁰ Most OLED hosts are characterised by hole-transporting or bipolar properties with higher hole mobility than electron mobility at the same electric field.^{11,12} Meanwhile, the number of electron-transporting OLED hosts is limited.¹³ To reduce this limitation, we selected 3,5-dicyanopyridine as a molecular building block with strong electron-accepting abilities for the design of electron-transporting organic semiconductors.

The synthesis of 3,5-dicyanopyridine-based pharmaceutical agents for medical applications was previously reported.^{14–19} For example, 3,5-dicyanopyridine units were found in the structures of highly potent adenosine A₁ receptor agonists.^{14,15} Furthermore, 3,5-dicyanopyridine derivatives were developed as non-nucleoside inhibitors selective to DNMT1, which maintains critical processes in DNA.¹⁶ From perspectives of medical applications, the structural and electrochemical investigations were performed for some 3,5-dicyanopyridines.^{17–19} However, 3,5-dicyanopyridine derivatives are not yet widely used in optoelectronic devices. The only known examples are derivatives of 3,5-dicyanopyridine which exhibited TADF and allowed it to reach maximum EQEs of OLEDs up to 17.1%.²⁰ The charge-transporting properties of 3,5-dicyanopyridine-based TADF emitters were not studied.

In this work, we estimated the applicability of 3,5-dicyanopyridine motifs in the design of compounds intended for optoelectronic applications. Three derivatives of 3,5-dicyanopyridine were designed and synthesized. Their thermal, electrochemical, charge-injecting, charge-transporting, photophysical, electrooptical, and electroluminescent properties were investigated by exploiting various experimental and theoretical approaches. The hosting properties of the compounds were investigated using the TADF emitter 4,6-di(9,9-dimethylacridan-10-yl)isophthalonitrile (DAcIPN) and compared with those of the conventional host 3,3′-di(9H-carbazol-9-yl)-1,1′-biphenyl (mCBP). TADF-based OLEDs with a maximum EQE of 21.9% were fabricated. This EQE value is considerably higher than that observed for mCBP-based TADF OLEDs (12.2%).

Materials, instrumentation and methods

Unless otherwise stated, all reagents were purchased from commercial suppliers and used without further purification. Thin layer chromatography (TLC) was performed using MERCK Silica gel 60 F254 plates and visualized by UV (254 nm) fluorescence. ZEOCHEM silica gel (ZEOprep 60/35–70 microns – SI23501) was used for column chromatography. ¹H and ¹³C NMR spectra were recorded on a Bruker 400 spectrometer at 400 and 101 MHz, respectively, at 298 K in CDCl₃. The ¹H chemical shifts are given relative to the residual CHCl₃ signal (7.26 ppm), ¹³C – relative to CDCl₃ (77.16 ppm). The melting points were determined on a “Digital melting point analyser” (Fisher), and the results are given without correction. Mass spectra were recorded on a Waters Synapt GII Q-ToF

UPLC/MS system instrument; infrared spectra were recorded on a Shimadzu FT-IR spectrometer. Reagents and solvents were purchased from common vendors such as ACROS, Fluorochem, ABCR and others. Thermogravimetric analysis (TGA) was performed on a TA Instruments TGA Q50 apparatus at a heating rate of 20 °C min^{−1} under a nitrogen atmosphere. Differential scanning calorimetry (DSC) measurements were carried out on a TA Instruments DSC Q2000 series thermal analyser at a heating rate of 10 °C min^{−1} in a nitrogen atmosphere.

Cyclic voltammetry (CV) measurements were performed with an mAUTOLAB Type III galvanostat and a glassy carbon working electrode in a three-electrode cell. The measurements were carried out using 0.1 M *tert*butyl ammonium hexafluorophosphate as an electrolyte and anhydrous dichloromethane at room temperature in a nitrogen atmosphere. The potentials were measured against silver as a quasi-reference electrode. Platinum wire was used as a counter electrode. The potentials were calibrated with the standard ferrocene/ferrocenium (Fc/Fc⁺) redox system.

The ionisation potential (IPPE) was determined by electron photoemission spectrometry. The samples for recording the photoelectron emission spectra were prepared as a thin film by vacuum deposition under 2 × 10^{−6} mbar pressure onto cleaned fluorine-doped tin oxide (FTO)-coated glass substrates. A negative voltage of 300 V was applied to the sample substrate. A Spectral Products®30 W deep UV deuterium light source (180–400 nm) ASBN-D130-CM and a CM110 1/8 m monochromator were used to illuminate the sample with monochromatic light. A Keithley 6517B electrometer/high-resistance meter was connected to the counter electrode to measure the photocurrent flowing in the circuit under illumination. Energy scan of the incident photons was performed while increasing the incident photon energy. It was done by changing the wavelength of the monochromator from 280 to 180 nm in 1 nm steps. The photocurrent (contributed to dU/dt) depends on the incident light photon energy ($h\nu$). Therefore, the IP_{PE} was estimated as the intersection point of the extrapolated linear part of the dependence $(dU/dt)^{\frac{1}{2}} = f(h\nu)$ and the $h\nu$ axis.

Theoretical calculations

The ground-state geometries were optimized by using the B3LYP (Becke three parameters hybrid functional with the Lee–Yang–Perdew correlation)²¹ functional at the 6-31G (d, p) level in vacuum with the Gaussian program.

Firstly, the equilibrium conformer search at the ground state was performed by using the MMFF (molecular mechanics force fields) method, and then this geometry was used for further optimization. The time-dependent DFT (TD-DFT) calculations were carried out with the Gaussian 16 software package. Molecular orbitals were visualized by using GaussView.

The UV-Vis absorbance and emission spectra of the solutions or the films of the compounds were recorded using Avantes AvaSpec-2048XL and Edinburgh Instruments FL5980 spectrometers, respectively. The phosphorescence spectra of THF solutions were recorded at a temperature of 77 K, with a delay

time of 5 ms after excitation. The steady-state and time-resolved temperature-dependent (at 77–300 K) photoluminescence (PL) spectra of the thin films were recorded using an Oxford Instruments Optistat DN2 cryostat cooled with liquid nitrogen. PL decay curves were obtained using the PicoQuant LDH-D-C-375 laser (operating at a wavelength of 374 nm) as the excitation source. PL quantum yields (PLQYs) were measured using a dedicated integrated sphere (with an inner diameter of 120 mm) on an Edinburgh Instruments FLS980 spectrometer.

For the estimation of hole and electron mobilities of vacuum-deposited layers of the compounds, the time-of-flight (TOF) and charge extraction by linearly increasing voltage (CELIV) methods were used. TOF experiments were performed using the samples with the following structure: indium tin oxide (ITO)/several μm thick organic layer/aluminum. Deposition of the samples was done under a vacuum deeper than 2×10^{-6} mBar. A laser (EKSPALA NL300, 355 nm wavelength) was used as the excitation source in the TOF setup. Various positive and negative external voltages (U) were applied to the samples using a 6517B electrometer (Keithley) for the estimation of hole and electron mobilities in the layers at the different electric fields. A TDS 3032C oscilloscope (Tektronix) was used to record the photocurrent transients of holes or electrons.

OLEDs were deposited layer by layer by vacuum thermal evaporation in the structure ITO/HAT-CN [5 nm]/NPB [40 nm]/TCTA [10 nm]/mCBP [10 nm]/Emissive layer [50 nm]/mBPhen [30 nm]/Liq [2 nm]/Al [100 nm]. ITO substrates were prepared by 10 min treatment with a UV ozone cleaner and then immediately transferred to a glovebox, quickly followed by the Oerlikon-Leybold UNIVEX 350G evaporator system vacuum chamber. The deposition rate was controlled by the SQC 310 controller with two quartz crystal sensors. The deposition rate of the organic layers was $0.5\text{--}0.8 \text{ \AA s}^{-1}$, while the aluminium deposition rate was 1 \AA s^{-1} . After the deposition of the electrodes, the OLED samples were encapsulated by glass caps with a UV-curable epoxy resin. Electroluminescence and current density–voltage characteristics of OLEDs were estimated using a McScience M7000 Auto $I\text{--}V\text{--}L$ Test System. The measurements of the electrical characteristics of the encapsulated OLEDs were carried out at 25 °C under atmospheric conditions. The compounds used for the fabrication of OLEDs were purchased from Merck or Ossila and were used as received.

4,4'-(5-Bromo-1,3-phenylene)bis(2,6-dimethyl-1,4-dihydropyridine-3,5-dicarbonitrile) (2). A mixture of 5-bromoisophthalaldehyde **1** (1.0 g, 4.7 mmol, 1 equiv.) and 3-aminocrotononitrile (1.0 g, 12.2 mmol, 2.6 equiv) in glacial acetic acid (3 mL) was refluxed for 6 h. After cooling, the precipitates were filtered off and washed with acetic acid and methanol, giving **2** (0.67 g, 30%) as a white powder, which is used in the next reaction without purification. $^1\text{H-NMR}$ (400 MHz, DMSO- d_6): 9.60 (s, 2H), 7.39 (d, $J = 1.6$ Hz, 2H), 7.18 (t, $J = 1.6$ Hz, 1H), 4.52 (s, 2H), 2.04 (s, 12H). MS (ES^+) m/z : 472 ($[\text{M} + \text{H}]^+$, 100).

4,4'-(5-Bromo-1,3-phenylene)bis(2,6-dimethylpyridine-3,5-dicarbonitrile) (3). Compound **2** (0.67 g, 1.42 mmol) was dissolved in glacial acetic acid (6 mL) at 60 °C. Sodium nitrite (0.98 g, 14.20 mmol) was added portionwise at 60 °C, and the

mixture was stirred for additional 15 min at the same temperature. After cooling, the mixture was diluted with water. The precipitates were filtered off and purified by flash chromatography on silica gel (eluent: chloroform/petroleum ether/acetone/methanol, 9:7:2:1 by volume), yielding **3** (0.55 g, 83%) as a pale-yellow powder. M.p. > 200 °C. $^1\text{H NMR}$ (400 MHz, chloroform- d): 7.90 (d, $J = 1.6$ Hz, 2H), 7.61 (t, $J = 1.6$ Hz, 1H), 2.89 (s, 12H). MS (ES^+) m/z : 468 ($[\text{M} + \text{H}]^+$, 100).

General method for the synthesis of PPDD, FPDD, and CzPDD

The mixture of **3** (187 mg, 0.4 mmol, 1 equiv.), tetrakis(tri-phenylphosphine)palladium (0) (23.1 mg, 0.02 mmol, 0.05 equiv.), and CuI (2.29 mg, 0.012 mmol, 0.03 equiv.) in 2 mL of DMF was degassed with Ar. An appropriate ethynyl derivative (0.52 mmol, 1.3 equiv.) and 1 mL of triethyl amine were added, and the mixture was heated under Ar at 90 °C overnight. The mixture was poured on ice and extracted with dichloromethane (4×30 mL). Combined organic layers were filtered through a Celite pad and dried over Na_2SO_4 . The solvent was removed under reduced pressure, and the yellow powder was purified by flash chromatography on silica gel (eluent: chloroform/light petroleum/acetone/methanol 9:7:1:0 \rightarrow 9:7:1:1 (by volume)). The obtained light-grey powder was crystallized from the mixture of methanol/acetic acid.

4,4'-(5-Phenylethynyl)-1,3-phenylenebis(2,6-dimethylpyridine-3,5-dicarbonitrile) (PPDD). Yield: 88 mg (45%); off-white solid, mp > 200 °C. IR ν_{max} (film): 2228, 1600, 1559. $^1\text{H NMR}$ (400 MHz, chloroform- d): 7.89 (d, $J = 1.7$ Hz, 2H), 7.60 (t, $J = 1.7$ Hz, 1H), 7.57–7.52 (m, 2H), 7.41–7.33 (m, 3H), 2.90 (s, 12H). $^{13}\text{C NMR}$ (chloroform- d): 165.5, 154.0, 134.3, 133.8, 131.9, 129.1, 128.5, 127.8, 126.3, 122.2, 114.6, 107.3, 93.2, 86.7, 24.8. MS (ES^+) m/z : 489 ($[\text{M} + \text{H}]^+$, 100). Anal. calcd for $\text{C}_{32}\text{H}_{20}\text{N}_4$: C, 78.67; H, 4.13; N, 17.20; found: C, 78.30; H, 4.07; N, 17.03. HPLC: 96.7% ($\lambda = 254$ nm, RT = 10.89 min, Apollo C18-9 (4.6 mm \times 150 mm), mobile phase 40–95% acetonitrile + 0.1% H_3PO_4 , 1 mL min^{-1} , 40 °C).

4,4'-(5-((4-Fluorophenyl)ethynyl)-1,3-phenylene)bis(2,6-dimethylpyridine-3,5-dicarbonitrile) (FPDD). Yield: 154 mg (76%); off-white solid, m.p. > 200 °C. IR ν_{max} (film): 2228, 1593, 1559. $^1\text{H NMR}$ (400 MHz, chloroform- d): 7.87 (d, $J = 1.7$ Hz, 2H), 7.60 (dd, $J = 1.7$ Hz, $J = 1.7$ Hz, 1H), 7.56 – 7.51 (m, 2H), 7.10–7.05 (m, 2H), 2.90 (s, 12H). $^{13}\text{C NMR}$ (chloroform- d): 165.5, 164.2, 161.7, 154.0, 134.3, 133.9, (d, $J = 8.1$ Hz), 128.0, 126.1, 118.3 (d, $J = 4.1$ Hz), 115.9 (d, $J = 22.2$ Hz), 114.6, 107.3, 92.4, 86.4, 24.8. MS (ES^+) m/z : 507 ($[\text{M} + \text{H}]^+$, 100). Anal. calcd for $\text{C}_{32}\text{H}_{19}\text{FN}_4$: C, 75.88; H, 3.78; N, 16.59; found: C, 75.45; H, 3.70; N, 16.44. HPLC: 98.5% ($\lambda = 254$ nm, RT = 11.02 min, Apollo C18-9 (4.6 mm \times 150 mm), mobile phase 40–95% acetonitrile + 0.1% H_3PO_4 , 1 mL min^{-1} , 40 °C).

4,4'-(5-((4-9H-Carbazol-9-yl)phenyl)ethynyl)-1,3-phenylene-bis(2,6-dimethylpyridine-3,5-dicarbonitrile) (CzPDD). Yield: 123 mg (47%); off-white solid, mp > 200 °C. IR ν_{max} (film): 2228, 1595, 1559, 1514. $^1\text{H NMR}$ (400 MHz, chloroform- d): 8.15 (dt, $J = 7.7$, 1.0 Hz, 2H), 7.94 (d, $J = 1.7$ Hz, 2H), 7.83–7.75 (m, 2H), 7.64–7.60 (m, 3H), 7.31 (ddd, $J = 8.1$, 6.7, 1.4 Hz, 2H), 2.91 (s, 12H). $^{13}\text{C NMR}$ (chloroform- d): 165.6, 154.0, 140.4,

138.4, 134.4, 133.7, 133.5, 128.1, 126.9, 126.1, 126.1, 123.6, 121.0, 120.4, 114.6, 109.8, 107.3, 92.4, 87.6, 24.8. MS (ES⁺) *m/z*: 654 ([M + H]⁺, 100). Anal. calcd for C₁₄H₂N₂: C, 80.84; H, 4.16; N, 15.00; found: C, 79.13; H, 4.13; N, 14.67. HPLC: 97.7% (λ = 254 nm, RT = 8.63 min, Apollo C18-9 (4.6 mm × 150 mm), mobile phase 40–95% acetonitrile + 0.1% H₃PO₄, 1 mL min⁻¹, 40 °C).

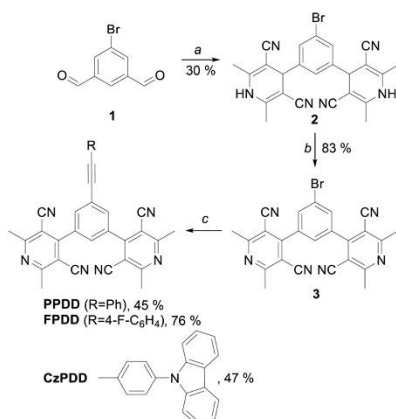
Results and discussion

Synthesis

Derivatives **PPDD**, **FPDD**, and **CzPDD** bearing two dicyanopyridine motifs were synthesized starting with 5-bromoisophthalaldehyde (**1**) (Scheme 1). Aldehyde **1** was treated with excess of aminocrotonitrile in refluxing acetic acid, yielding bis(dihydropyridine) **2**, which has been oxidized to the corresponding bispyridine **3** with 10 equivalents of sodium nitrite in 83% yield. Next, the desired ethynyl derivatives **PPDD**, **FPDD**, and **CzPDD** were prepared in good yields under Sonogashira coupling conditions in DMF/triethyl amine solution employing tetrakis(triphenylphosphino)palladium and copper iodide as catalysts.

Thermal properties

The thermal investigation of **PPDD**, **FPDD**, and **CzPDD** was carried out by differential scanning calorimetry (DSC) and thermogravimetric analysis (TGA). DSC thermograms are presented in Fig. 1(a) and Fig. S1 (ESI[†]). The thermal characteristics are listed in Table 1. **PPDD**, **FPDD**, and **CzPDD** were found to be capable of glass formation with high glass-transition temperatures falling between 123 and 185 °C. This observation can be attributed to molecular



Scheme 1 Preparation of **PPDD**, **FPDD**, and **CzPDD**. Reaction conditions: (a) aminocrotonitrile (2.6 equiv.), AcOH, reflux, 6 h; (b) NaNO₂ (10 equiv.), AcOH, 60 °C, 1 h; (c) ethynyl arene (1.3 equiv.), (PPh₃)₂Pd (0.05 equiv.), CuI (0.03 equiv.), DMF, Et₃N, 60 °C, overnight.

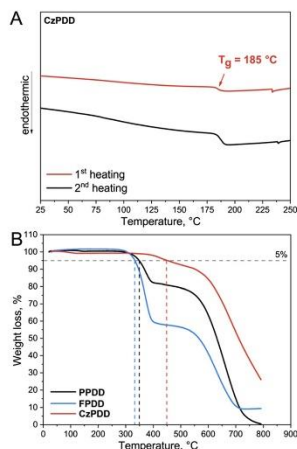


Fig. 1 DSC curves of **CzPDD** (A) and TGA curves of **PPDD**, **FPDD**, and **CzPDD** (B) (dashed lines represent 5% weight loss temperature).

Table 1 Thermal, electrochemical, and optical parameters of **PPDD**, **FPDD**, and **CzPDD** including theoretically predicted HOMO/LUMO values

Parameter	PPDD	FPDD	CzPDD
T_m^a [°C]	—/—	240/238	—/—
T_g^b [°C]	139	123	185
$T_d^{5\%}$ [°C]	349	332	449
E_{onset}^{ox} [V]	1.56	1.68	1.30
$E_{onset}^{ox}/re^{c,d}$ [V]	1.12	1.26	0.90
E_{onset}^{red} [V]	-1.40	-1.43	-1.42
$E_{onset}^{red}/re^{c,d}$ [V]	-1.84	-1.85	-1.82
IP_{cv}^e [eV]	5.92	6.06	5.70
EA_{cv}^f [eV]	2.96	2.95	2.98
E_g^g [eV]	2.96	3.11	2.73
HOMO/LUMO ^h [eV]	-6.10/-2.31	-6.10/-2.35	-5.43/-2.36

^a Melting temperature at the first/second heating scan at a rate of 10 °C min⁻¹, N₂ atmosphere. ^b Glass-transition temperature at the second heating scan. ^c 5% weight loss temperature at the scan rate of 20 °C min⁻¹, N₂ atmosphere. ^d Corrected values with the inner ferrocene standard. ^e IP_{cv} (eV) = E_{onset}^{ox} (V) + 4.8. ^f EA_{cv} (eV) = E_{onset}^{red} (V) + 4.8. ^g Calculated by the equation $E_g = IP_{cv} - EA_{cv}$. ^h Calculated using the B3LYP/6-31G(d,p) method.

rigidity of the compounds. During the first and second DSC scans, non-fluorinated derivatives **PPDD** and **CzPDD** showed no crystallization and melting transitions, proving their amorphous nature. DSC revealed the potential morphological instability of molecular glass of compound **FPDD**. The second DSC heating scan of this compound revealed after glass transition the exothermic signal of crystallization at 210.5 °C and the endothermic signal of melting at 238 °C. TGA curves of **PPDD** and **FPDD** are shown in Fig. 1(b). At least two stages of the thermal degradation were observed for all three compounds. Their 5% weight loss temperatures fall in the

range of 332–449 °C (Fig. 1(b)). The highest glass-transition temperature and 5% weight loss temperature were detected for compound CzPDD, which possesses a rigid carbazole moiety and the highest molecular weight (Table 1).

Theoretical calculations and electrochemical properties

The geometries and electronic structures of the target compounds PPDD, FPDD, and CzPDD were studied using density functional theory (DFT) with the B3LYP functional at 6-31G(d) basis set.²² The visualized HOMOs/LUMOs are shown in Fig. 2. In the optimized ground state geometries, the dihedral angles of the electron-accepting unit 3,5-dicyanopyridine and phenyl- (PPDD), 4-fluorophenyl- (FPDD), and phenylcarbazole (CzPDD) units slightly differ (13° for PPDD; 56° for FPDD; 40° for compound CzPDD).

The overall small dihedral angle values lead to a planar geometry that results in high molecular orbital overlap, as is observed in Fig. 2. The LUMOs of PPDD, FPDD, and CzPDD are located mainly on the electron-accepting 3,5-dicyanopyridine fragments and phenyl spacer. The HOMOs are dispersed throughout electron-donating moieties including the triple-bond linker with noticeable overlap over the phenyl ring in the cases of compounds PPDD and FPDD and a spatial separation in the case of phenylcarbazole-based compound CzPDD.

The calculated HOMO/LUMO values are presented in Table 1. The HOMO values of PPDD and FPDD are both -6.10 eV, indicating similar electronic structures and the lack of effect of fluorine atoms. However, the higher HOMO values of compound CzPDD indicate the stronger electron-donating nature of the phenylcarbazole moiety than the phenyl groups in PPDD and FPDD.

Electrochemical properties

Electrochemical properties of PPDD, FPDD, and CzPDD were investigated by cyclic voltammetry (CV). The CV curves of

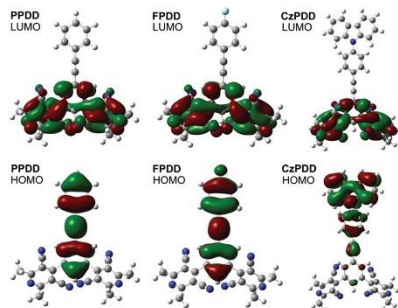


Fig. 2 Visualisation of theoretical HOMO and LUMO distribution of PPDD, FPDD, and CzPDD.

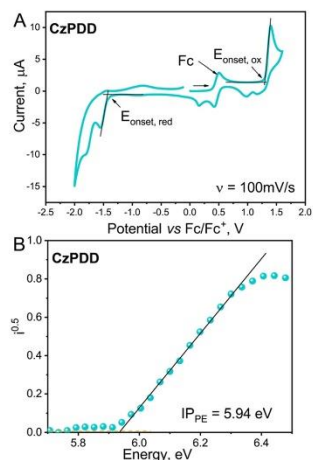


Fig. 3 Cyclic voltammogram (A) of the DCM solution of **6** (scan rate $\nu = 100$ mV s⁻¹) and PE spectrum of the film of **6** (B).

PPDD, FPDD, and CzPDD are shown in Fig. 3 and Fig. S2a, b (ESI[†]). The data are listed in Table 1.

All three derivatives showed irreversible oxidation and quasi-reversible reduction processes in the potential range from -2.0 to 1.8 V. The carbazole moiety is known to oxidize at 1.2 V and form a radical cation that tends to couple with either another radical cation or a parent molecule, forming an extended π -electron conjugated system.²³ The stronger electron-donating ability of the carbazole moiety resulted in a lower IP_{CV} value of compound CzPDD, correlating well with the theoretical assumptions. The electron affinity values observed for all three compounds were found to be comparable (2.95 – 2.98 eV).

For the film of compound CzPDD, the IP value was also estimated by electron photoemission (PE) spectroscopy. Due to the interaction between the molecules in the film of compound CzPDD, the IP_{PE} value (5.94 eV) was found to be slightly higher compared to that (IP_{CV}) obtained for the solution (5.70 eV) (Table 1). Ionization potentials and electron affinities obtained experimentally using CV and PE spectrometry are in good agreement with the calculated HOMO/LUMO values.

Photophysical properties

Photophysical characterization of PPDD, FPDD, and CzPDD was performed by UV-VIS absorption and photoluminescence (PL) spectroscopies. UV-VIS absorption spectra of the solid samples and dilute solutions (1×10^{-5} M) are shown in Fig. 4(a) and Fig. S4 (ESI[†]). The data are listed in Table 2. Almost identical absorption spectra were obtained for compounds PPDD and FPDD with the intensive peak at ca. 280 – 290 nm and a

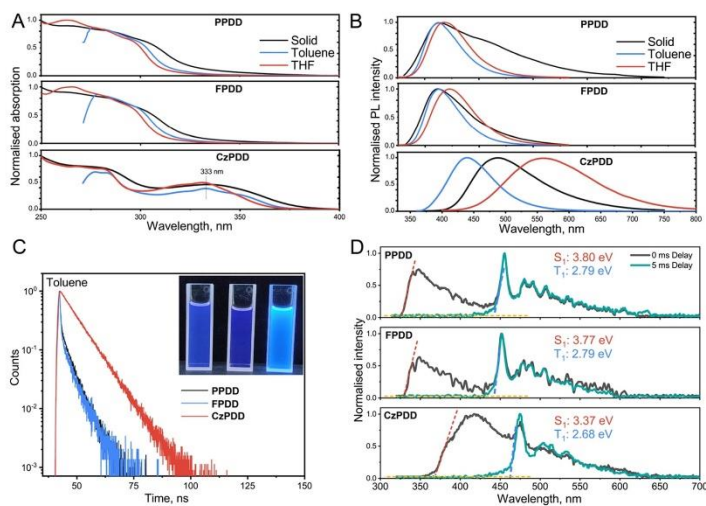


Fig. 4 Normalised UV-VIS (a) and PL (b) spectra of solid films, toluene and THF solutions of **PPDD**, **FPDD**, and **CzPDD** with a concentration of 1×10^{-5} M. PL decay curves (c) of their toluene solutions. The inset shows photos of the samples under UV excitation. PL and phosphorescence spectra (d) of THF solutions of **PPDD**, **FPDD**, and **CzPDD** at 77 K. Excitation of $\lambda_{\text{exc}} = 300$ nm was used for **PPDD**, **FPDD** and $\lambda_{\text{exc}} = 340$ nm for **CzPDD**.

Table 2 Photophysical and photoelectron emission parameters of investigated compounds **PPDD**, **FPDD**, and **CzPDD**

Comp.	λ_{abpp} , nm	λ_{PLE} , nm	FWHM, nm		LM slope, cm^{-1}	S_1^a , eV	T_1^a , eV	IP_{PE}^b , eV	$E_{\text{PC}}^{\text{optc}}$, eV	EA_{PE}^b , eV
	Toluene/film									
PPDD	296*/303*	394/397, 472*	60/139	2851/21 295	3.8	2.79	n/a ^d	3.74	n/a ^d	
FPDD	296*/303*	394/394	62/79	3264/21 749	3.77	2.79	n/a ^d	3.83	n/a ^d	
CzPDD	333/335	439/488	83/121	21 283	3.37	2.68	5.94	3.25	2.69	

^a Singlet and triplet values taken from the intersection with the baseline of high-energy edges of fluorescence and phosphorescence spectra at 77 K. ^b Ionization potentials (IP_{PE}) of the solid samples estimated by photoelectron emission in air; electron affinity (EA_{PE}) was calculated by $\text{IP}_{\text{PE}} - E_{\text{PC}}^{\text{optc}} = \text{EA}_{\text{PE}}$. ^c Optical bandgap taken from onset of the low-energy absorption band. ^d Due to limitations of electron photoemission in air, the instrumentation value was not observed.

noticeable shoulder at ca. 296 nm. Theoretically calculated UV spectra (in toluene) indicate that this band originates from $S_0 \rightarrow S_5$ excitation (Fig. S3, ESI[†]). This transition can be attributed to HOMO \rightarrow LUMO+4 transitions with high and similar oscillator strength values of 1.0775 and 1.0773, respectively. They are dominated by $\pi-\pi^*$ transition of 3,5-dicyanopyridine fragments.

Compound **CzPDD**, containing the phenyl carbazole moiety, exhibited different absorption spectra. The high-energy band peaking at ca. 290 nm shows overlapping of absorption of $\pi-\pi^*$ transitions of both 3,5-dicyanopyridine moieties and the carbazole unit. In the range of ca. 300–340 nm, the less intensive band with the visible maximum at ca. 333 nm was observed (Fig. 4(a), and Fig. S3, ESI[†]). This band originates from the $n-\pi^*$

transitions of the carbazole moiety. At the wavelengths higher than 340 nm, the tail or even shoulder at 352 nm (in the cases of toluene and chloroform solutions of **CzPDD**) can be observed (Fig. 4(a), and Fig. S3, ESI[†]). This observation is mainly associated with the intramolecular charge transfer (ICT) between electron-donating carbazole and electron-accepting 3,5-dicyanopyridine moieties.^{24–27} The theoretical absorption spectra were characterized by the excitation of several excited states including $S_0 \rightarrow S_{16}$, $S_0 \rightarrow S_2$ and $S_0 \rightarrow S_5$ (Fig. S4, ESI[†]). These transitions can be attributed to the transition from the highest occupied to the lowest unoccupied natural transition orbitals (from HONTO to LUNTO) from the phenylcarbazole moiety to the whole molecule. The oscillator strength values of these transitions are 0.3085 and 0.3763, respectively. The quite

high values of oscillator strength indicate no steric hindrance between the molecular fragments, resulting in the increased overlap of the orbitals.

There are no substantial differences in the absorption spectra of different solutions and films of **PPDD**, **FPDD**, and **CzPDD**. However, compounds exhibited an enhanced absorption tail at wavelengths higher than 350 nm. The absence of notable shifts in the absorption maxima as the solvent polarity varies indicates a relatively nonpolar ground state of compound **6**. However, the effect of media polarity is well evident in the excited states. This statement can be proven by the red shifts of PL spectra of the solutions of compound **CzPDD** with the increasing polarity of the solvents (Fig. 4(b)). PL spectra of toluene and tetrahydrofuran (THF) solutions of **CzPDD** peaked at 439 and 560 nm, respectively, due to the different dielectric constants of the solvents (2.38 and 7.58, respectively). As shown in Fig. 4(a), the dilute toluene and THF solutions of **PPDD** and **FPDD** containing phenyl and fluoro-phenyl functional groups, respectively, demonstrate very similar deep-blue emission profiles (395–410 nm). Meanwhile, the emission of the spin-coated thin films is different. The films of both **PPDD** and **FPDD** show PL spectra peaking at 392 nm, but the shapes of the spectra are different. The film of **FPDD** shows a usual emission spectrum of almost a Gaussian shape, while that of **PPDD** shows a broad lower energy shoulder at 480 nm. Such a shoulder can apparently be attributed to the excimer formation. Excimer formation manifests as a broad and structureless long-wavelength band in the photo- or electroluminescence spectra.²⁸ PL decay curves of toluene solutions of **PPDD**, **FPDD**, and **CzPDD** were recorded (Fig. 4(b)) They demonstrate that the emission is fluorescence with lifetimes in the nanosecond range. No long-lived components of PL decay curves were observed.

The triplet energy of organic electroactive compounds is one of the main parameters in case selecting hosts for phosphorescent or TADF OLEDs.²⁹ For the estimation of singlet and

triplet energies of **PPDD**, **FPDD**, and **CzPDD**, fluorescence and phosphorescence spectra of their solutions in THF were recorded at 77 K. Phosphorescence spectra were separated from fluorescence spectra using a delay of 5 ms. The singlet and triplet energies were taken from the intersection with the baseline of high-energy edges of fluorescence and phosphorescence spectra (Fig. 4(c)). As is seen previously with steady-state photophysics, compounds **PPDD** and **FPDD** showed the same triplet energy of 2.79 eV. This observation is consistent with the results of steady-state PL spectrometry measurements, which revealed comparable properties of singlet and triplet states. Compound **CzPDD** also showed a relatively high triplet energy of 2.68 eV, whereas its singlet (3.37 eV) was lower than those of compounds **PPDD** and **FPDD**. Considering high triplet energies of **PPDD**, **FPDD**, and **CzPDD**, it can be presumed that these compounds can be applied as hosts for different OLED emitters. As is mentioned above, PL spectra of dilute solutions of compound **CzPDD** are characterised by the strong bathochromic shift from 439 nm for the low-polarity toluene solution to 560 nm for THF solution. The wavelength of emission intensity maximum of the solid sample of compound **CzPDD** was detected in the middle of those of toluene and THF solutions, that is, at 487 nm. This observation encouraged us to investigate solvatochromic properties in more detail. The absorption spectra of the compounds demonstrated a relatively small dependence on solvent polarity (Fig. S4, ESI†), while the wavelengths of emissions and their profiles were strongly dependent on the polarity of media. The solutions of compounds **PPDD** and **FPDD** containing phenyl and fluoro-phenyl groups in low-polarity solvents exhibited only slight differences in emission energy in low-polarity solvents. However, for the solutions in highly polar solvents such as dimethylformamide (DMF) and acetonitrile, the considerable bathochromic shifts together with the widening of spectra were observed (Fig. 5(a)). The emission

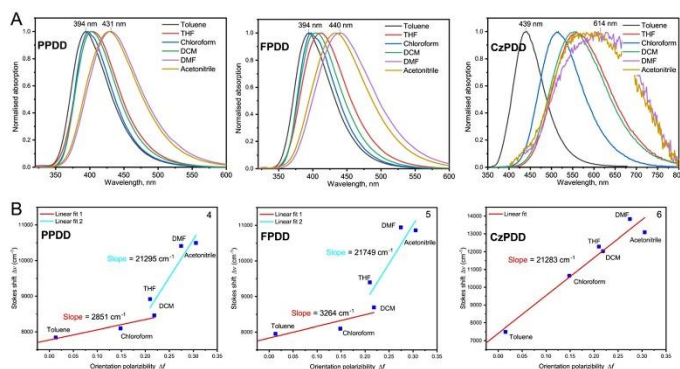


Fig. 5 Normalised PL spectra (a) of the solutions (1×10^{-5} M) of **PPDD**, **FPDD**, and **CzPDD** in the solvents of different polarities and the corresponding Lippert–Mataga plots (b) of dependencies of the Stokes shifts $\Delta\nu$ on solvent orientation polarizability function Δf .

intensity maxima of the solutions of **PPDD** and **FPDD** in toluene were observed at 394 nm, while those of the solutions in DMF appeared at 431 and 440 nm, respectively. The full width at half maxima (FWHM) for the solutions of compounds **PPDD** and **FPDD** in toluene was found to be 60 and 62 nm, respectively, while those of the solution in DMF reached 91 and 93 nm, respectively (Table 2). This observation indicates the possible charge-transfer (CT) emission. Compound **CzPPDD**, having a phenyl-carbazole moiety, showed a linear dependence on solvent polarity, which is typical for CT emission (Fig. 5(a)). The emission intensity maximum of the solution of **CzPPDD** in toluene was observed at 439 nm, while that of the solution in DMF was detected at 614 nm. The FWHM also increased dramatically from 83 nm for the solution in low-polarity toluene to 225 nm for the solution in polar DMF. This observation confirms intensive CT which occurs due to well-balanced donor and acceptor interactions. The plots of Stokes shifts $\Delta(\nu)$ versus orientation polarizability $\Delta(f)$ and the fittings by the Lippert–Mataga equation are plotted in Fig. 5(b).³⁰

Compounds **PPDD** and **FPDD** exhibit non-linear plots. They can be fitted by two linear functions for low- and high-polarity solvents. Such a double-sloped dependence indicates the nature of hybridized local and charge-transfer (HLCT) states.³⁰ The relatively small slopes of 2851 and 3264 cm^{-1} were obtained for compounds **PPDD** and **FPDD**, respectively, in the range of low orientation polarizabilities of ca. 0.001–0.22. This fitting result indicates that the emission is dominated by the relaxation of locally excited states of **PPDD** and **FPDD** molecularly dispersed in low-polarity media. At orientation polarizabilities higher than 0.2, the fitting result shows high slopes of 21295 and 21749 cm^{-1} . This observation can be attributed to CT emission of the solutions of **PPDD** and **FPDD** in highly polar solvents. The HLCT excited state character of emission is predominant for the solutions of **PPDD** and **FPDD** in the solvents of intermediate polarity such as THF and dichloromethane (DCM). For the solutions of compound **CzPPDD**, the linear dependence of Stokes shift on orientation polarizability with a high slope of ca. 21 000 cm^{-1} is observed, suggesting CT emission.

The dominant “hole” – “particle” contributions of the NTOs of the first three excited states for **PPDD**, **FPDD** and **CzPPDD** were theoretically calculated and are illustrated in Fig. 6. The methodology of theoretical calculations corresponds to that of the previously published theoretical investigation of the HLCT state of the electroactive material.³¹

PPDD and **FPDD** exhibit similar transition characters from “hole” to “particle” in the S1 and S2 states as a degree of balance between spatial separation and partial overlap of NTOs is attained, indicating the existence of HLCT. However, **CzPPDD** displays much stronger CT transition in the S1 and S3 states, differing from the aforementioned compounds. Additionally, the energy level diagram is presented (Fig. S5, ESI†). The large energy gap between the S1 and S2 states is observed for all three compounds, preventing efficient exciton relaxation. The energy gap between the T1 and S1 states of **PPDD** and **FPDD** is still too large and may prevent the triplet excitons from relaxing to the S1 state by internal conversion. These results of the calculation of the three excited states basically show the consistent

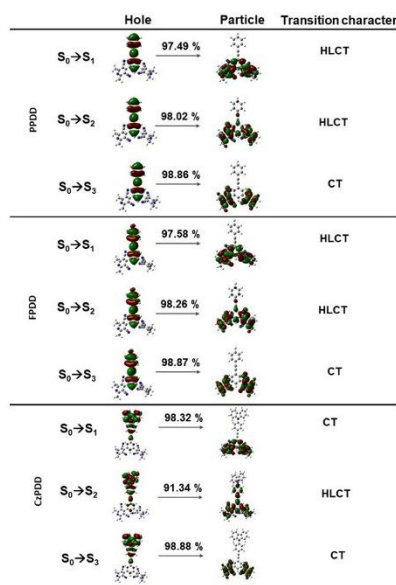


Fig. 6 Natural transition orbitals (NTOs) of the first three singlet excited states for **PPDD**, **FPDD** and **CzPPDD**.

tendency with the experimental Lippert–Mataga plots obtained for the studied compounds (Fig. 5(b)).

In addition, the PL spectra of the solid molecular dispersions of compound 5 in the mixtures of hosts of different polarities were recorded. Poly(methyl methacrylate) (PMMA) and bis[2-(diphenylphosphino)phenyl] ether oxide (DPEPO) were used for the preparation of the mixtures of hosts of the different polarities (Fig. S6, ESI†). Their dielectric constants are 3.0 (PMMA)³² and 6.12 (DPEPO).³³ PL spectra of the spin-coated films were characterized by two bands (Fig. S6b, ESI†). The high-energy and low-energy bands can be attributed to LE and CT emissions of compound 5, respectively. The observed bands could be explained by some heterogeneity of the mixture of hosts DPEPO and PMMA. In contrast, PL spectra of compound 5 were characterized by a single band in the homogeneous mixture of DPEPO and PMMA obtained after annealing at 120 °C for 5 min (Fig. S6b, ESI†). The slight red shifts of PL spectra of the dispersions of compound 5 in more polar host mixtures of DPEPO and PMMA (with a high ratio of DPEPO) are the additional sign of manifestation of HLCT emission of compound 5.

Hosting properties

It is widely known that the efficiency of emission of TADF emitters is very sensitive to the nature of hosts used.^{34,35} To test

the hosting properties of **PPDD**, **FPDD**, and **CzPDD**, the efficient TADF emitter DAcIPN was selected, mainly taking into account the overlapping of the absorption spectrum of DAcIPN and emission spectra of **PPDD**, **FPDD**, and **CzPDD** in the solid state (Fig. 4(a)).³⁶ In addition, high triplet energies of **PPDD**, **FPDD**, and **CzPDD** are expected to restrict loss of triplet energy of DAcIPN *via* triplet levels of the hosts. The hosting properties of **PPDD**, **FPDD**, and **CzPDD** were compared with those of the reference host mCBP.^{37,38} PL spectra and PL decay curves of DAcIPN (10 wt%) molecularly dispersed in different hosts **PPDD**, **FPDD**, and **CzPDD** were recorded in air and vacuum (Fig. 7(a), (b), and Fig. S7, ESI[†]). Slightly different positions of PL spectra of the films that hosted DAcIPN were observed. This observation indicates the effects of conformational and static dielectric disorders of hosts on the emission properties of TADF emitter DAcIPN, as was previously discussed in more detail.³⁹ The different intensities of delayed fluorescence of DAcIPN molecularly dispersed in hosts **PPDD**, **FPDD**, and **CzPDD** and mCBP were observed, indicating different TADF efficiencies. The lowest intensity of delayed fluorescence of DAcIPN was detected when it was dispersed in host **PPDD** (Fig. 7(b)). The different TADF efficiencies of DAcIPN can be explained by the different singlet-triplet gaps (ΔE_{ST}) of DAcIPN when it is dispersed in the different hosts. However, the ΔE_{ST} value of DAcIPN is practically zero, as is seen from the PL and phosphorescence spectra of DAcIPN recorded at 77 K (Fig. 8(a) and Fig. S8, ESI[†]). For the estimation of the hosting effects of compounds **PPDD** and **FPDD** on the TADF efficiency of DAcIPN in more detail, PL spectra and PL decay curves of the solid solutions of DAcIPN (10 wt%) in the different hosts (**PPDD**, **FPDD**, and **CzPDD** and mCBP) were recorded at different temperatures (Fig. 7(c), (d), and Fig. S9, ESI[†]). The results of these measurements were used for the calculation of the rates

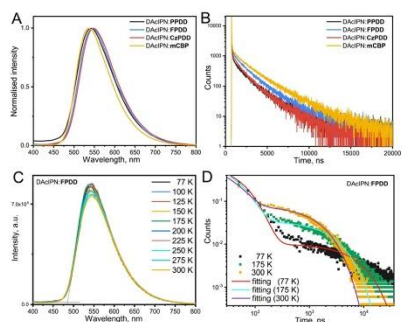


Fig. 7 PL spectra (a) and PL decay curves (b) of the solid solutions of DAcIPN (10 wt%) in the different hosts (**PPDD**, **FPDD**, and **CzPDD** and mCBP) recorded in vacuum. PL spectra (c) and PL decay curves (d) of the solid solution of DAcIPN (10 wt%) in host **5** recorded at the different temperatures.

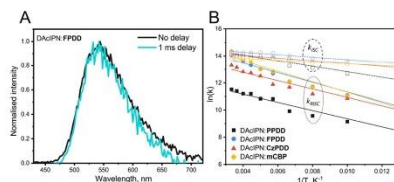


Fig. 8 PL and phosphorescence spectra (a) of the solid solution of DAcIPN (10 wt%) in host **FPDD** at 77 K and plots of $\ln(k_{RISC}/k_{ISC})$ versus temperature for DAcIPN (10 wt%) molecularly dispersed in hosts **PPDD**, **FPDD**, and **CzPDD** and mCBP.

of reverse intersystem crossing (k_{RISC}) of DAcIPN exploiting previously published formulas.⁴⁰ The details of calculations and additional data (e.g., lifetimes of prompt (τ_{PF}) and delayed (τ_{DF}) fluorescence, rates of prompt (k_{PF}) and delayed (k_{DF}) fluorescence, and intersystem crossing rates (k_{ISC})) are listed in Tables S1–S4 (ESI[†]). The TADF emitter (DAcIPN) was characterized by very different k_{RISC} values when it was molecularly dispersed in the different hosts (**PPDD**, **FPDD**, and **CzPDD**, mCBP), that is, by $1 \times 10^5 \text{ s}^{-1}$ for **PPDD**, $1.3 \times 10^6 \text{ s}^{-1}$ for **FPDD**, $6 \times 10^5 \text{ s}^{-1}$ for **6**, and $1.7 \times 10^6 \text{ s}^{-1}$ for mCBP (Tables S1–S4, ESI[†]). The trend of k_{RISC} values is the same as that of the delayed fluorescence intensities of the solid solutions of DAcIPN (10 wt%) in the different hosts (**PPDD**, **FPDD**, and **CzPDD** and mCBP) (Fig. 7(b)). This observation additionally highlights the best hosting properties of host **FPDD**, which are close to those of mCBP. The k_{RISC} and k_{RISC} dependences on temperature are plotted in Fig. 8(b). These dependencies were used for the determination of activation energies of ISC and RISC (E_a^{ISC} and E_a^{RISC}) according to the Arrhenius formula $k = A \times \exp(-E_a/k_B T)$, where A is the frequency factor involving the spin-orbit coupling constant, E_a is the activation energy, and k_B is the Boltzmann constant.⁴¹ The small E_a^{RISC} values of 26–34 meV were obtained for DAcIPN molecularly dispersed in the different hosts (**PPDD**, **FPDD**, and **CzPDD** and mCBP) (Table S5, ESI[†]). Such E_a^{RISC} values of DAcIPN are in excellent agreement with the ΔE_{ST} data (Fig. S8, ESI[†]). The ΔE_{ST} of 20 meV was also published for DAcIPN.³⁶ Considering the higher k_{RISC} values of the molecular mixtures of DAcIPN with **FPDD** and **CzPDD**, it can be presumed that compounds **FPDD** and **CzPDD** are more promising as OLED hosts than compound **PPDD**.

Charge-transporting properties

Considering the potentially good hosting properties of **FPDD** and **CzPDD**, charge-transporting and electroluminescent properties were further studied for the samples of these compounds. Charge-transporting properties of **FPDD** and **CzPDD** were studied at room temperature by TOF and CELIV methods using a diode-like structure ITO/film/Al with different thicknesses (d) of the layers of the compounds.⁴² TOF photocurrent transients were recorded for micrometres-thick vacuum-deposited films applying

negative voltages to the ITO electrode (Fig. S10, ESI[†]). The TOF photocurrent transients were found to be shorter at higher voltages than at lower voltages, indicating the transport of electrons. However, it was impossible to obtain transit times at any voltages from the TOF photocurrent transients because of the high dispersivity of electron transport in the studied films. Fortunately, the CELIV method is less sensitive to charge transport dispersivity.⁴² Dark-CELIV and photo-CELIV photocurrent transients were recorded at different slopes of the voltage ramp ($A = dU/dt$) for the 100 nm-thick vacuum-deposited films (Fig. S11, ESI[†]). Subtracting dark-CELIV from photo-CELIV current transients at the exact duration of pulses (Fig. S11, ESI[†]), the maximum for current transients resulting from photo-generated charges extracted by the linear increasing voltage can be recognised at times (t_{peak}), which is needed for the calculation of charge mobility in CELIV measurements. Using the formula $\mu_e = 2/3 \cdot d^2 / (t_{\text{peak}} \cdot A)$,⁴³ electron mobility (μ_e) values were calculated at the different electric fields for the layers of FPDD ($d = 150$ nm) and CzPDD ($d = 200$ nm) (Fig. S12, ESI[†]). The compounds demonstrated close μ_e values exceeding $1 \times 10^{-7} \text{ cm}^2 \text{ V}^{-1} \text{ s}^{-1}$ at the electric fields higher than 10^6 V cm^{-1} . The relatively low μ_e values are apparently caused by very twisted molecular structures of the compounds, which may prevent LUMO-LUMO overlapping of the neighbouring molecules (Fig. 2).

Fabrication and characterization of OLEDs

OLEDs were fabricated as the final experimental study. The performances of hosts FPDD and CzPDD were investigated in OLEDs with the following configuration: ITO/HAT-CN (5 nm)/NPB (40 nm)/TCTA (10 nm)/mCBP (10 nm)/DAcIPN:Host (50 nm)/NBPhen (30 nm)/Liq (2 nm)/Al. The energetical structure of OLEDs is shown in Fig. 9(a). The composition of the emissive layer was 90 wt% of the host (compound FPDD in device A, compound CzPDD in device B or mCBP in device C) and 10 wt% of the emitter DAcIPN (Fig. 9(b)). The abbreviations HAT-CN, NPB, TCTA, mCBP, NBPhen and Liq are used for 1,4,5,8,9,11-hexaazatriphenylenehexacarbonitrile, *N,N'*-di(1-naphthyl)-*N,N'*-diphenyl-(1,1'-biphenyl)-4,4'-diamine, tris(4-carbazoyl-9-ylphenyl)amine, 3,3'-di(9*H*-carbazol-9-yl)-1,1'-biphenyl, 2,9-dinaphthalen-2-yl-4,7-diphenyl-1,10-phenanthroline and

8-hydroxyquinolinolato-lithium, respectively. The vacuum-deposited film HAT-CN was used as the hole injection layer, NPB and TCTA were used as the hole-transporting materials and the layer of mCBP was used as the electron-blocking layer. NBPhen and Liq were used as the electron-transporting and electron injection materials, respectively.

The electroluminescence (EL) spectra, EQE *versus* brightness plots and current density–voltage–luminescence characteristics for OLEDs with the investigated materials are given in Fig. 10. The data are listed in Table 3. The EL spectra of devices A–B are very similar with a peak at ca. 540 nm. The PL spectrum of the reference OLED with mCBP as a host was blue-shifted and peaked at 526 nm. Since the emitter DAcIPN exhibits strong solvatochromic properties,³⁶ such a slight shift of EL is mainly related to a different polarity of mCBP matrix compared to the polarities of dicyanopyridine derivatives FPDD and CzPDD. EL spectra of devices A–C are in good agreement with the PL spectra of the corresponding light-emitting films (Fig. 6(a)). The fabricated devices A–C were characterized by green EL with slightly different CIE 1931 RGB colour space coordinates, which are listed in Table 3 (Fig. 10(A)–(C), insets). The EL colours are stable under different external voltages, demonstrating efficient host-guest energy transfer.

Devices A–C demonstrated rather high maximum EQEs of 21.9, 8.6 and 12.2%, respectively (Fig. 10(b) and Table 3). Furthermore, devices A and B with newly synthesized compounds as hosts exhibited low turn-on voltages (V_{ON}) of less than 4 V.

Only device C, with commercial host mCBP, showed V_{ON} slightly higher than 4 V (Fig. 10(c)). Such low V_{ON} suggests that the overall OLED energetical structure was chosen correctly and there were no apparent barriers for charges to overcome. Interestingly, device A with FPDD as the host showed almost twice higher efficiency than reference device C with mCBP (*cf.* EQE_{max} of 21.9% vs. EQE_{max} of 12.2%). Such different EQE values of devices A–C most probably can be explained by the better hosting properties of FPDD compared to those of CzPDD or mCBP. Apparently, triplets can be more efficiently harvested by emitter DAcIPN when it is dispersed in host FPDD than in host CzPDD or mCBP. More intensive long-lived components of EL decay curves can be expected for device A than

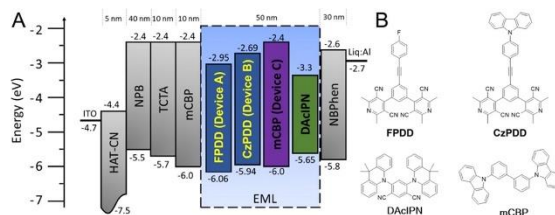


Fig. 9 Energy level diagram of devices A–C and molecular structures (b) of the compounds used for the preparation of light-emitting layers of the devices.

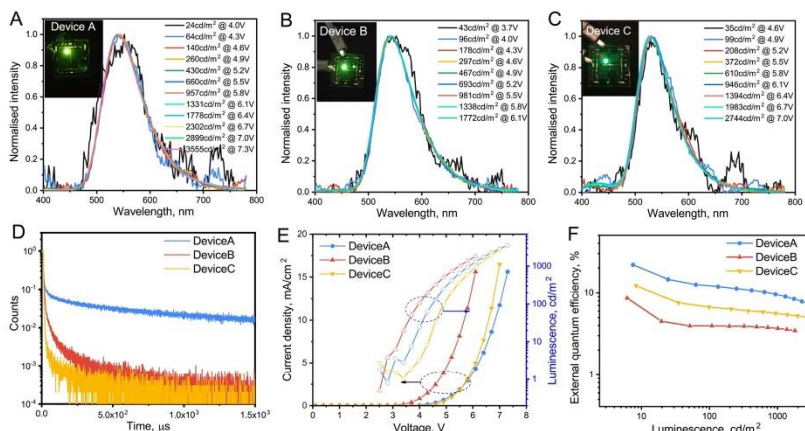


Fig. 10 Normalised EL spectra (A)–(C) at ca. different voltages and EL decay curves (D) of devices A–C; current density and luminescence versus voltage (E) and EQE versus luminescence (F) plots for devices A–C.

Table 3 Electroluminescence characteristics of OLEDs based on the synthesized hosts

Device	A	B	C
Emissive layer	DAcIPN (10 wt%): FPDD	DAcIPN (10 wt%): CzPDD	DAcIPN (10 wt%): mCBP
V_{on} (V) @ 10 cd m^{-2} ^a	3.76	3.2	4.3
CE_{max} , CF_{1000} , CF_{1000}^b (cd A^{-1})	43.2, 39.7, 31.7	14.6, 13.1, 12.4	23.9, 22.4, 18.8
PE_{max} , PE_{100} , PE_{1000}^c (lm W^{-1})	36.7, 27.8, 17.0	14.8, 10.4, 7.1	17.5, 14.4, 9.6
EQE_{max} , EQE_{100} , EQE_{1000}^d (%)	21.9, 12.1, 9.5	8.6, 4.0, 3.7	12.2, 6.7, 5.6
Peak (nm)@ 1000^e cd m^{-2}	540	542	526
FWHM (nm)@ 1000^e cd m^{-2}	88	86	78
CIE (x,y)@ 1000^e cd m^{-2}	(0.38, 0.58)	(0.38, 0.57)	(0.33, 0.58)

^a Turn-on voltage measured at an initial brightness of 10 cd m^{-2} . ^b Current efficiency. ^c Power efficiency. ^d External quantum efficiency taken at maximum brightness, at 100 and at 1000 cd m^{-2} . ^e Wavelengths of peaks of electroluminescence spectra. ^f Full width at half maxima. ^g CIE 1931 RGB colour space coordinates taken at 1000 cd m^{-2} of brightness.

for devices B or C. The trend of recorded EL decay curves of devices A–C perfectly supports this presumption (Fig. 10(d)). These results suggest that the newly synthesized dicyanopyridine derivative with the fluorophenyl group (**FPDD**) has significant potential for the increase of efficiency of green TADF OLEDs. In addition, the usage of host 5 is not limited to the green emitters. Taking into account its high triplet level of 2.79 eV, host **FPDD** can be applied for blue emitters with emission wavelengths higher than ca. 450 nm. Considering its values of HOMO/LUMO (6.06/2.95 eV), host **FPDD** can be used for emitters with band gaps narrower than 3.11 eV. However, the usage of host **FPDD** for deep-blue OLEDs should be excluded due to its values of the lowest triplet level and HOMO/LUMO energy levels. Furthermore, the next molecular design of hosts based on the 3,5-dicyanopyridine motifs should be attributed to further improvements in their electron mobility values.

Conclusions

Three derivatives of (1,3-phenylene)bis(2,6-dimethylpyridine-3,5-dicarbonitrile) with the different substituents attached to the phenylene moiety were designed and synthesized. They are characterized by HLCT or CT emissions. Practically, identical triplet energies of 2.68–2.79 eV were observed for the studied compounds from the onsets of phosphorescence spectra of the frozen THF solutions. The compounds form molecular glasses with high glass-transition temperatures of 123–185 °C. The compounds are characterized by high ionization potentials (5.7–6.06 eV), comparable electron affinities of ca. 3.0 eV, and similar electron mobility values exceeding $1 \times 10^{-7} \text{ cm}^2 \text{ V}^{-1} \text{ s}^{-1}$. The compounds were used as hosts for emitting layers of TADF-based OLEDs. The best performance was observed for OLED containing 4,4'-(5-(4-fluorophenyl)ethynyl)-1,3-phenylene)bis(2,6-dimethylpyridine-3,5-dicarbonitrile) as a

host. The device showed a maximum external quantum efficiency of 21.9%.

Author contributions

P. A. and J. V. G. performed studies included in the current article. P. A., J. V. G., and D. V. designed the research. B. V. and P. D. performed synthesis. D. V., K. L., A. B., and T.-L. C. were responsible for the photophysical studies and OLED fabrication. R. K. performed DFT calculations. J. V. G., P. A. and D. V. wrote the manuscript with support and contributions from all authors.

Conflicts of interest

There are no conflicts to declare.

Acknowledgements

This work was supported by the project of scientific co-operation program between Latvia, Lithuania and Taiwan, "Synthesis and study of deep-blue TTF fluorescent emitters to exceed theoretical OLED external quantum efficiency reaching 15%" (grant LV-LT-TW/2023) and Research Council of Lithuania (LMTLT), agreement no. S-LLT-22-4.

Notes and references

- 1 S. Pimputkar, J. S. Speck, S. P. DenBaars and S. Nakamura, *Nat. Photonics*, 2009, **3**, 180–182.
- 2 G. M. Phelan, *Inf. Disp.*, 2018, **34**, 10–15.
- 3 C. W. Tang and S. A. VanSlyke, *Appl. Phys. Lett.*, 1987, **51**, 913–915.
- 4 D. F. O'Brien, M. A. Baldo, M. E. Thompson and S. R. Forrest, *Appl. Phys. Lett.*, 1999, **74**, 442–444.
- 5 C. Adachi, M. A. Baldo, S. R. Forrest and M. E. Thompson, *Appl. Phys. Lett.*, 2000, **77**, 904–906.
- 6 T.-A. Lin, T. Chatterjee, W.-L. Tsai, W.-K. Lee, M.-J. Wu, M. Jiao, K.-C. Pan, C.-L. Yi, C.-L. Chung, K.-T. Wong and C.-C. Wu, *Adv. Mater.*, 2016, **28**, 6976–6983.
- 7 T. Fleetham, G. Li and J. Li, *Adv. Mater.*, 2017, **29**, 1601861.
- 8 H. Uoyama, K. Goushi, K. Shizu, H. Nomura and C. Adachi, *Nature*, 2012, **492**, 234–238.
- 9 Y. X. Hu, J. Miao, T. Hua, Z. Huang, Y. Qi, Y. Zou, Y. Qiu, H. Xia, H. Liu, X. Cao and C. Yang, *Nat. Photonics*, 2022, **16**, 803–810.
- 10 N. Li, F. Ni, X. Lv, Z. Huang, X. Cao and C. Yang, *Adv. Opt. Mater.*, 2022, **10**, 2101343.
- 11 T. Chatterjee and K.-T. Wong, *Adv. Opt. Mater.*, 2019, **7**, 1800565.
- 12 Y. Tao, C. Yang and J. Qin, *Chem. Soc. Rev.*, 2011, **40**, 2943.
- 13 J. H. Lee, C. H. Chen, B. Y. Lin, Y. H. Lan, Y. M. Huang, N. J. Chen, J. J. Huang, D. Volyniuk, R. Keruckiene, J. V. Grazulevicius, Y. R. Wu, M. K. Leung and T. L. Chiu, *ACS Appl. Mater. Interfaces*, 2020, **12**, 49895–49904.
- 14 M. T. Cocco, C. Congiu, V. Lilliu and V. Onnis, *Eur. J. Med. Chem.*, 2005, **40**, 1365–1372.
- 15 M. T. Cocco, C. Congiu, V. Lilliu and V. Onnis, *Bioorg. Med. Chem.*, 2007, **15**, 1859–1867.
- 16 J. R. Horton, S. Pathuri, K. Wong, R. Ren, L. Rueda, D. T. Fosbenner, D. A. Heerding, M. T. McCabe, M. B. Pappalardi, X. Zhang, B. W. King and X. Cheng, *Structure*, 2022, **30**, 793–802.e5.
- 17 D. Catarzi, F. Varano, E. Vigiiani, S. Calenda, F. Melani, K. Varani, F. Vincenzi, S. Pasquini, N. Mennini, G. Nerli, D. Dal Ben, R. Volpini and V. Colotta, *Pharmaceuticals*, 2022, **15**, 478.
- 18 M. Luo, B. Huang, Z. Xu, S. Liu, Z. Zhu, J. Zhang and X. Meng, *J. Mol. Struct.*, 2021, **1228**, 129748.
- 19 N. A. Macias-Ruvalcaba and D. H. Evans, *J. Electroanal. Chem.*, 2011, **660**, 243–246.
- 20 H. Liu, J. Li, W.-C. Chen, X. Lv, C. Zhou, C.-S. Lee and C. Yang, *J. Phys. Chem. C*, 2020, **124**, 25489–25498.
- 21 A. D. Becke, *Phys. Rev. A: At., Mol., Opt. Phys.*, 1988, **38**, 3098–3100.
- 22 M. J. Frisch, G. W. Trucks, H. B. Schlegel, G. E. Scuseria, M. A. Robb, J. R. Cheeseman, G. Scalmani, V. Barone, G. A. Petersson, H. Nakatsuji, X. Li, M. Caricato, A. V. Marenich, J. Bloino, B. G. Janesko, R. Gomperts, B. Mennucci, H. P. Hratchian, J. V. Ortiz, A. F. Izmaylov, J. L. Sonnenberg, D. Williams-Young, F. Ding, F. Lipparini, F. Egidi, J. Goings, B. Peng, A. Petrone, T. Henderson, D. Ranasinghe, V. G. Zakrzewski, J. Gao, N. Rega, G. Zheng, W. Liang, M. Hada, M. Ehara, K. Toyota, R. Fukuda, J. Hasegawa, M. Ishida, T. Nakajima, Y. Honda, O. Kitao, H. Nakai, T. Vreven, K. Throssell, J. A. Jr. Montgomery, J. E. Peralta, F. Ogliaro, M. J. Bearpark, J. J. Heyd, E. N. Brothers, K. N. Kudin, V. N. Staroverov, T. A. Keith, R. Kobayashi, J. Normand, K. Raghavachari, A. P. Rendell, J. C. Burant, S. S. Iyengar, J. Tomasi, M. Cossi, J. M. Millam, M. Klene, C. Adamo, R. Cammi, J. W. Ochterski, R. L. Martin, K. Morokuma, O. Farkas, J. B. Foresman and D. J. Fox, 2016.
- 23 K. Karon and M. Lapkowski, *J. Solid State Electrochem.*, 2015, **19**, 2601–2610.
- 24 L.-S. Cui, A. J. Gillett, S.-F. Zhang, H. Ye, Y. Liu, X.-K. Chen, Z.-S. Lin, E. W. Evans, W. K. Myers, T. K. Ronson, H. Nakanotani, S. Reineke, J.-L. Bredas, C. Adachi and R. H. Friend, *Nat. Photonics*, 2020, **14**, 636–642.
- 25 Z. Xie, T. Yu, J. Chen, E. Ubbal, L. Wang, Z. Mao, T. Su, Y. Zhang, M. P. Aldred and Z. Chi, *Chem. Sci.*, 2018, **9**, 5787–5794.
- 26 Z. Xie, C. Chen, S. Xu, J. Li, Y. Zhang, S. Liu, J. Xu and Z. Chi, *Angew. Chem., Int. Ed.*, 2015, **54**, 7181–7184.
- 27 A. Khan, X. Tang, C. Zhong, Q. Wang, S. Yang, F. Kong, S. Yuan, A. S. D. Sandanayaka, C. Adachi, Z. Jiang and L. Liao, *Adv. Funct. Mater.*, 2021, **31**, 2009488.
- 28 G. Baryshnikov, P. Gawrys, K. Ivaniuk, B. Witulski, R. J. Whitby, A. Al-Muhammad, B. Minaev, V. Cherpak, P. Stakhira, D. Volyniuk, G. Wiosna-Salyga, B. Luszczynska, A. Lazauskas, S. Tamulevicius and J. V. Grazulevicius, *J. Mater. Chem. C*, 2016, **4**, 5795–5805.

- 29 Y. Tao, C. Yang and J. Qin, *Chem. Soc. Rev.*, 2011, **40**, 2943.
- 30 W. Li, D. Liu, F. Shen, D. Ma, Z. Wang, T. Feng, Y. Xu, B. Yang and Y. Ma, *Adv. Funct. Mater.*, 2012, **22**, 2797–2803.
- 31 Y. Pan, J. Huang, W. Li, Y. Gao, Z. Wang, D. Yu, B. Yang and Y. Ma, *RSC Adv.*, 2017, **7**, 19576–19583.
- 32 Dielectric Constant, <https://polymerdatabase.com/polymer%20physics/Epsilon%20Table.html>, (accessed 25 May 2023).
- 33 E. Skuodis, O. Bezikonny, A. Tomkeviciene, D. Volyniuk, V. Mimaite, A. Lazauskas, A. Bucinskas, R. Keruckiene, G. Sini and J. V. Grazulevicius, *Org. Electron.*, 2018, **63**, 29–40.
- 34 M. K. Etherington, J. Gibson, H. F. Higginbotham, T. J. Penfold and A. P. Monkman, *Nat. Commun.*, 2016, **7**, 13680.
- 35 T. Serevičius, R. Skaisgiris, J. Dodonova, I. Fiodorova, K. Genevičius, S. Tumkevičius, K. Kazlauskas and S. Juršėnas, *J. Phys. Chem. Lett.*, 2022, **13**, 1839–1844.
- 36 E. Skuodis, O. Bezikonny, A. Tomkeviciene, D. Volyniuk, V. Mimaite, A. Lazauskas, A. Bucinskas, R. Keruckiene, G. Sini and J. V. Grazulevicius, *Org. Electron.*, 2018, **63**, 29–40.
- 37 P. Schrögel, N. Langer, C. Schildknecht, G. Wagenblast, C. Lennartz and P. Strohrig, *Org. Electron.*, 2011, **12**, 2047–2055.
- 38 H. Nakanotani, K. Masui, J. Nishide, T. Shibata and C. Adachi, *Sci. Rep.*, 2013, **3**, 2127.
- 39 D. K. A. Phan Huu, S. Saseendran, R. Dhali, L. G. Franca, K. Stavrou, A. Monkman and A. Painelli, *J. Am. Chem. Soc.*, 2022, **144**, 15211–15222.
- 40 K. Goushi, K. Yoshida, K. Sato and C. Adachi, *Nat. Photonics*, 2012, **6**, 253–258.
- 41 A. E. Nikolaenko, M. Cass, F. Bourcet, D. Mohamad and M. Roberts, *Adv. Mater.*, 2015, **27**, 7236–7240.
- 42 O. Semeniuk, G. Juska, J.-O. Oelerich, M. Wiemer, S. D. Baranovskii and A. Reznik, *Sci. Rep.*, 2016, **6**, 33359.
- 43 G. Juška, K. Arlauskas, M. Viliūnas and J. Kočka, *Phys. Rev. Lett.*, 2000, **84**, 4946–4949.

8. CURRICULUM VITAE

Karolis Leitonas

karolis.leitonas@ktu.lt

Education:

- 2002 – 2014 Rokiškis, Juozo Tumo-Vaižganto Gymnasium
2014 – 2018 Kaunas University of Technology, Bachelor's degree
in Materials Science
2018 – 2020 Kaunas University of Technology, Master's degree
in Materials Science
2020 – 2024 Kaunas University of Technology, PhD in Materials
Engineering

Work experience:

- 2018 – 2024 Kaunas University of Technology, Laboratory technician/
Junior Researcher
2024 – present Dresden University of Technology, Postdoc researcher

Scientific work:

- 2018, 2019 3 times participant of the Research Council of Lithuania
project *Students' Scientific Practice*
2017 – 2024 Research work in Prof. Dr. Juozas Vidas Gražulevičius
scientific group *Materials Chemistry*: photophysical and
electrooptical investigation of newly synthesised organic
semiconductors
2024 – present Research work in Prof. Dr. Sebastian Reineke scientific
group *LEXOS* at Dresden Integrated Center for Applied
Physics and Photonic Materials (IAPP), Dresden University
of Technology, Germany

Participation in scientific projects:

- 2017 – 2019 *Synthesis and research of substances with high triplet state
energy for blue organic LEDs (BLUEOLEDs)*, project No.
TAP LLT-2/2017
2019 – 2021 *Synthesis, studies and applications of organic bipolar
semiconductors exhibiting high luminescence quantum yields
in the solid state*, project No. 09.3.3-LMT-K-712-01-0140
2019 – 2021 *Polymeric emitters with controllable thermally activated
delayed fluorescence for solution-processable OLEDs*,
project No. P-LLT-19-8
2020 – 2023 *Self-assembling donor-acceptor materials for efficient
electroluminescent devices*, project No. 01.2.2-LMT-K-718-
03-0019

- 2021 – 2024 *Development of organic emitters with long persistent luminescence towards optical sensors (ELOS), project No. P-MIP-21-30*
- 2022 – 2024 *Donor-acceptor type organic semiconductors exhibiting close to infrared absorption for efficient photodetectors (OSDEP), project No. S-MIP-22-78*
- 2024 – 2024 *Strong-coupling-enhanced nanoparticle array organic light emitting diode (SCOLED), project No. 101098813*

Internships:

- 2020.06 – 12 Guest researcher at GmbH Cynora, Bruchsal, Germany
 Research supervisor: Dr Harald Flügge
 Project *Heavy metal free emitters for new-generation light – “MEGA”*
 Project No. 823720
- 2021.07 – 08 Guest researcher at Lviv Polytechnic National University, Ukraine
 Research supervisor: Prof Dr Habil. Pavlo Stakhira
 Project *Development of highly efficient white light-emitting diodes utilizing organic emitters with exciplex and thermally-assisted fluorescence for lighting applications*
 Project No. P-LU-20-42
- 2022.05 – 08 Guest researcher at National Taiwan University, Taipei, Taiwan
 Research supervisor: Prof Dr Jiun-Haw Lee
 Project *Heavy metal free emitters for new-generation light – “MEGA”*
 Project No. 823720
- 2023.09 – 12 Guest researcher at Dresden Integrated Center for Applied Physics and Photonic Materials (IAPP), Dresden University of Technology, Germany
 Research supervisor: Prof Dr Sebastian Reineke
 Project *Heavy metal free emitters for new-generation light – “MEGA”*
 Project No. 823720

Scholarships:

- 2019 – 2020 University talent scholarship for outstanding academic and study results, 3 times
- 2020 – 2023 KTU most active PhD student’s scholarship, 4 times
- 2020 – 2024 Lithuanian Research Council PhD student’s scholarship for academic achievements, 3 times

Languages:

Lithuanian (native), English (C1)

9. LIST OF AUTHOR'S PUBLICATIONS AND CONFERENCES

List of publications on the subject of thesis:

1. **Leitonas, Karolis**; Guzauskas, Matas; Tsiko, Uliana; Simokaitiene, Jurate; Volyniuk, Dmytro; Grazulevicius, Juozas Vidas. White vertical organic permeable-base light-emitting transistors obtained by mixing of blue exciton and orange interface exciplex emissions // *Journal of Materials Chemistry C*. Cambridge: Royal Society of Chemistry. ISSN 2050-7534. eISSN 2050-7526. 2022, Vol. 10, iss. 26, p. 9786–9793. DOI: 10.1039/d2tc01326f. [Science Citation Index Expanded (Web of Science); Scopus] [IF: 6.400; AIF: 5.750; IF/AIF: 1.113; Q1 (2022, Clarivate JCR SCIE)]

2. Andruleviciene, Viktorija; **Leitonas, Karolis**; Volyniuk, Dmytro; Sini, Gjergji; Grazulevicius, Juozas Vidas; Getautis, Vytautas. TADF versus TTA emission mechanisms in acridan and carbazole-substituted dibenzo[a,c]phenazines: towards triplet harvesting emitters and hosts // *Chemical Engineering Journal*. Amsterdam: Elsevier. ISSN 1385-8947. eISSN 1873-3212. 2021, Vol. 417, art. No. 127902, p. 1–14. DOI: 10.1016/j.cej.2020.127902. [Science Citation Index Expanded (Web of Science); Scopus] [IF: 16.744; AIF: 8.626; IF/AIF: 1.941; Q1 (2021, Clarivate JCR SCIE)]

3. Arsenyan, Pavel; Vigante, Brigita; **Leitonas, Karolis**; Volyniuk, Dmytro; Andruleviciene, Viktorija; Skhirtladze, Levani; Belyakov, Sergey; Grazulevicius, Juozas Vidas. Dual versus normal TADF of pyridines ornamented with multiple donor moieties and their performance in OLEDs // *Journal of Materials Chemistry C*. Cambridge: Royal Society of Chemistry. ISSN 2050-7526. eISSN 2050-7534. 2021, Vol. 9, iss. 11, p. 3928–3938. DOI: 10.1039/d0tc05745b. [Science Citation Index Expanded (Web of Science); Scopus] [IF: 8.067; AIF: 6.018; IF/AIF: 1.340; Q1 (2021, Clarivate JCR SCIE)]

4. **Leitonas, Karolis**; Vigante, Brigita; Volyniuk, Dmytro; Bucinskas, Audrius; Keruckiene, Rasa; Dimitrijevs, Pavels; Chiu, Tien-Lung; Grazulevicius, Juozas Vidas; Arsenyan, Pavel. 3,5-Dicyanopyridine motifs for electron-transporting semiconductors: from design and synthesis to efficient organic light-emitting diodes // *Journal of Materials Chemistry C*. Cambridge: Royal Society of Chemistry. ISSN 2050-7526. eISSN 2050-7534. 2023, Vol. 11, iss. 28, p. 9514–9526. DOI: 10.1039/d3tc00841j. [Science Citation Index Expanded (Web of Science); Scopus] [IF: 6.400; AIF: 5.750; IF/AIF: 1.113; Q1 (2022, Clarivate JCR SCIE)]

List of other publications:

1. Butkute, Rita; Masiulyte, Ausrine; Rashid, Ehsan Ullah; Sargsyan, Svetlana; Moudgalya, Neelalohith Satish; **Leitonas, Karolis**; Volyniuk, Dmytro; Grazulevicius, Juozas V. Ultralow dark current density of organic photodetectors and organic light-emitting diodes endowed by highly thermally stable derivatives of 2,7-Di-tert-butyl-9,9-dimethyl-9,10-dihydroacridine and phenanthroimidazole exhibiting balanced bipolar charge transport // *ACS Applied Electronic Materials*. Washington: American Chemical Society. eISSN 2637-6113. 2024, Vol. 6, iss. 6, p. 4735–4745.

DOI: 10.1021/acsaelm.4c00746. [Science Citation Index Expanded (Web of Science); Scopus] [IF: 4.300; AIF: 4.900; IF/AIF: 0.877; Q1 (2023, Clarivate JCR SCIE)] [CiteScore: 7.20; SNIP: 0.929; SJR: 1.058; Q1 (2023, Scopus Sources)]

2. Dabuliene, Asta; Shi, Zhong-En; **Leitonas, Karolis**; Lung, Chien-Yu; Volyniuk, Dmytro; Kaur, Khushdeep; Matulis, Vitaly; Lyakhov, Dmitry; Michels, Dominik; Chen, Chih-Ping; Grazulevicius, Juozas Vidas. Enhancement of efficiency of perovskite solar cells with hole-selective layers of rationally designed thiazolo[5,4-d]thiazole derivatives // *ACS Applied Materials and Interfaces*. Washington: American Chemical Society. ISSN 1944-8244. eISSN 1944-8252. 2024, Vol. 16, iss. 23, p. 30239-30254. DOI: 10.1021/acсами.4c04105. [Science Citation Index Expanded (Web of Science); Scopus; MEDLINE] [IF: 8.300; AIF: 7.000; IF/AIF: 1.185; Q1 (2023, Clarivate JCR SCIE)]

3. Starykov, Hryhorii; Bezikonnyi, Oleksandr; **Leitonas, Karolis**; Simokaitiene, Jurate; Volyniuk, Dmytro; Skuodis, Eigirdas; Keruckiene, Rasa; Grazulevicius, Juozas Vidas. Derivatives of phenyl pyrimidine and of the different donor moieties as emitters for OLEDs // *Materials*. Basel: MDPI. ISSN 1996-1944. 2024, Vol. 17, iss. 6, art. No. 1357, p. 1–18. DOI: 10.3390/ma17061357. [Science Citation Index Expanded (Web of Science); Scopus; MEDLINE] [IF: 3.400; AIF: 6.020; IF/AIF: 0.564; Q2 (2022, Clarivate JCR SCIE)]

4. Skhirtladze, Levani; Keruckiene, Rasa; Bezikonnyi, Oleksandr; Mahmoudi, Malek; Volyniuk, Dmytro; **Leitonas, Karolis**; Ghasemi, Melika; Simokaitiene, Jurate; Nasir, Farah Hannan Abd; Ariffin, Azhar; Grazulevicius, Juozas V. Switching thermally activated delayed fluorescence to room temperature phosphorescence for oxygen sensing: effect of donor substituents of trifluoromethylphenyl // *Spectrochimica acta Part A: Molecular and Biomolecular Spectroscopy*. Kidlington: Elsevier. ISSN 1386-1425. eISSN 1873-3557. 2024, Vol. 306, art. No. 123531, p. 1–11. DOI: 10.1016/j.saa.2023.123531. [Science Citation Index Expanded (Web of Science); Scopus; MEDLINE] [IF: 4.400; AIF: 2.700; IF/AIF: 1.629; Q1 (2022, Clarivate JCR SCIE)] [CiteScore: 7.90; SNIP: 1.037; SJR: 0.635; Q1 (2022, Scopus Sources)]

5. Ghasemi, Melika; Mahmoudi, Malek; Gudeika, Dalius; **Leitonas, Karolis**; Simokaitiene, Jurate; Dabuliene, Asta; Panchenko, Alexander; Minaev, Boris F.; Volyniuk, Dmytro; Grazulevicius, Juozas Vidas. Effects of the change of isomers on room-temperature phosphorescence, thermally activated delayed fluorescence, and long persistent luminescence of organic hole-transporting materials with the selective potential for the application in electronic devices and optical sensors of oxygen // *Chemical Engineering Journal*. Lausanne: Elsevier. ISSN 1385-8947. eISSN 1873-3212. 2023, Vol. 473, art. No. 145004, p. 234–238. DOI: 10.1016/j.cej.2023.145004. [Science Citation Index Expanded (Web of Science); Scopus] [IF: 15.100; AIF: 8.550; IF/AIF: 1.766; Q1 (2022, Clarivate JCR SCIE)]

6. **Leitonas, Karolis**; Vigante, Brigita; Volyniuk, Dmytro; Bučinskas, Audrius; Dimitrijevs, Pavels; Lapcinska, Sindija; Arsenyan, Pavel; Gražulevičius, Juozas Vidas. Aromatic systems with two and three pyridine-2,6-dicarbazolyl-3,5-dicarbonitrile fragments as electron-transporting organic semiconductors exhibiting

long-lived emissions // *Beilstein Journal of Organic Chemistry*. Frankfurt am Main : Beilstein-Institut. ISSN 1860-5397. 2023, Vol. 19, p. 1867–1880. DOI: 10.3762/bjoc.19.139. [Science Citation Index Expanded (Web of Science); Scopus; MEDLINE] [IF: 2.700; AIF: 3.900; IF/AIF: 0.692; Q2 (2022, Clarivate JCR SCIE)]

7. Mahmoudi, Malek; Urbonas, Ervinas; Volyniuk, Dmytro; Gudeika, Dalius; Dabrovskas, Kęstutis; Simokaitienė, Jūratė; Dabulienė, Asta; Keruckienė, Rasa; **Leitonas, Karolis**; Gužauskas, Matas; Skhirtladze, Levani; Stanitska, Mariia; Gražulevičius, Juozas Vidas. Indolocarbazoles with sterically unrestricted electron-accepting anchors showcasing aggregation-induced thermally activated delayed mechanoluminescence for host-free organic light-emitting diodes // *Molecules*. Basel: MDPI. ISSN 1420-3049. 2023, Vol. 28, iss. 16, art. No. 5999, p. 1–17. DOI: 10.3390/molecules28165999. [Science Citation Index Expanded (Web of Science); Scopus; MEDLINE] [IF: 4.600; AIF: 6.400; IF/AIF: 0.718; Q2 (2022, Clarivate JCR SCIE)]

8. Skhirtladze, Levani; **Leitonas, Karolis**; Bucinskas, Audrius; Woon, Kai Lin; Volyniuk, Dmytro; Keruckiene, Rasa; Mahmoudi, Malek; Lapkowski, Mieczyslaw; Ariffin, Azhar; Gražulevičius, Juozas V. Turn on of room temperature phosphorescence of donor-acceptor-donor type compounds via transformation of excited states by rigid hosts for oxygen sensing // *Sensors and Actuators B: Chemical*. Lausanne: Elsevier. ISSN 0925-4005. 2023, Vol. 380, art. No. 133295, p. 1–10. DOI: 10.1016/j.snb.2023.133295. [Science Citation Index Expanded (Web of Science); Scopus] [IF: 8.400; AIF: 5.066; IF/AIF: 1.658; Q1 (2022, Clarivate JCR SCIE)]

9. Skuodis, Eigirdas; **Leitonas, Karolis**; Panchenko, Alexander; Volyniuk, Lesia; Simokaitienė, Jūratė; Keruckienė, Rasa; Volyniuk, Dmytro; Minaev, Boris F.; Gražulevičius, Juozas V. Very sensitive probes for quantitative and organoleptic detection of oxygen based on conformer-induced room-temperature phosphorescence enhancement of the derivative of triazatruxene and phenothiazine // *Sensors and Actuators B: Chemical*. Lausanne: Elsevier. ISSN 0925-4005. eISSN 1873-3077. 2022, Vol. 373, art. No. 132727, p. 1–13. DOI: 10.1016/j.snb.2022.132727. [Science Citation Index Expanded (Web of Science); Scopus; Dimensions] [IF: 8.400; AIF: 5.066; IF/AIF: 1.658; Q1 (2022, Clarivate JCR SCIE)]

10. Tsiko, U.; Volyniuk, D.; Andrulevičienė, V.; **Leitonas, Karolis**; Sych, G.; Bezikonny, O.; Jašinskas, V.; Gulbinas, V.; Stakhira, P.; Gražulevičius, J.V. Triphenylamino or 9-phenyl carbazoyl-substituted pyrimidine-5-carbonitriles as bipolar emitters and hosts with triplet harvesting abilities // *Materials Today Chemistry*. Oxford: Elsevier. ISSN 2468-5194. 2022, Vol. 25, art. No. 100955, p. 1–13. DOI: 10.1016/j.mtchem.2022.100955. [Science Citation Index Expanded (Web of Science); Scopus; Dimensions] [IF: 7.300; AIF: 6.550; IF/AIF: 1.114; Q1 (2022, Clarivate JCR SCIE)]

11. Skhirtladze, Levani; **Leitonas, Karolis**; Bucinskas, Audrius; Volyniuk, Dmytro; Mahmoudi, Malek; Mukbaniani, Omar; Woon, Kai Lin; Ariffin, Azhar; Gražulevičius, Juozas V. 1,4-Bis(trifluoromethyl)benzene as a new acceptor for the design and synthesis of emitters exhibiting efficient thermally activated delayed

fluorescence and electroluminescence: experimental and computational guidance // *Journal of Materials Chemistry C*. Cambridge: Royal Society of Chemistry. ISSN 2050-7526. eISSN 2050-7534. 2022, Vol. 10, iss. 12, p. 4929–4940. DOI: 10.1039/d1tc05420a. [Science Citation Index Expanded (Web of Science); Scopus] [IF: 6.400; AIF: 5.750; IF/AIF: 1.113; Q1 (2022, Clarivate JCR SCIE)]

12. **Leitonas, Karolis**; Tomkeviciene, Ausra; Baratte, Gabriel; Dabulienė, Asta; Punniyakoti, Sanjay Madhuran; Volyniuk, Dmytro; Grazulevicius, Juozas Vidas. Oxygen sensing properties of thianthrene and phenothiazine derivatives exhibiting room temperature phosphorescence: effect of substitution of phenothiazine moieties // *Sensors and Actuators B: Chemical*. Lausanne: Elsevier. ISSN 0925-4005. 2021, Vol. 345, art. No. 130369, p. 1–12. DOI: 10.1016/j.snb.2021.130369. [Science Citation Index Expanded (Web of Science); Scopus] [IF: 9.221; AIF: 5.220; IF/AIF: 1.766; Q1 (2021, Clarivate JCR SCIE)]

13. Mahmoudi, Malek; Gudeika, Dalius; Volyniuk, Dmytro; **Leitonas, Karolis**; Butkute, Rita; Danyliv, Iryna; Grazulevicius, Juozas V. Tuning of spin-flip efficiency of blue emitting multicarbazolyl-substituted benzonitriles by exploitation of the different additional electron accepting moieties // *Chemical Engineering Journal*. Amsterdam: Elsevier. ISSN 1385-8947. eISSN 1873-3212. 2021, Vol. 423, art. No. 130236, p. 1–12. DOI: 10.1016/j.cej.2021.130236. [Science Citation Index Expanded (Web of Science); Scopus] [IF: 16.744; AIF: 8.626; IF/AIF: 1.941; Q1 (2021, Clarivate JCR SCIE)]

14. Mahmoudi, Malek; Keruckas, Jonas; **Leitonas, Karolis**; Kutsiy, Stepan; Volyniuk, Dmytro; Gražulevičius, Juozas V. Exciplex-forming systems with extremely high RISC rates exceeding 107 s^{-1} for oxygen probing and white hybrid OLEDs // *Journal of Materials Research and Technology*. Amsterdam: Elsevier. ISSN 2238-7854. eISSN 2214-0697. 2021, Vol. 10, p. 711–721. DOI: 10.1016/j.jmrt.2020.12.058. [Science Citation Index Expanded (Web of Science); Scopus] [IF: 6.267; AIF: 5.342; IF/AIF: 1.173; Q1 (2021, Clarivate JCR SCIE)]

15. Keruckiene, Rasa; Volyniuk, Dmytro; **Leitonas, Karolis**; Grazulevicius, Juozas Vidas. Dual emission fluorescence/room-temperature phosphorescence of phenothiazine and benzotrifluoride derivatives and its application for optical sensing of oxygen // *Sensors and Actuators B: Chemical*. Amsterdam: Elsevier. ISSN 0925-4005. 2020, Vol. 321, art. No. 128533, p. 1–10. DOI: 10.1016/j.snb.2020.128533. [Science Citation Index Expanded (Web of Science); Scopus] [IF: 7.460; AIF: 4.780; IF/AIF: 1.560; Q1 (2020, Clarivate JCR SCIE)]

16. Pashazadeh, Ramin; Sych, Galyna; Nasiri, Sohrab; **Leitonas, Karolis**; Lazauskas, Algirdas; Volyniuk, Dmytro; Skabara, Peter J.; Grazulevicius, Juozas Vidas. Multifunctional asymmetric D-A-D' compounds: mechanochromic luminescence, thermally activated delayed fluorescence and aggregation enhanced emission // *Chemical Engineering Journal*. Amsterdam: Elsevier. ISSN 1385-8947. 2020, Vol. 401, art. No. 125962, p. 1–9. DOI: 10.1016/j.cej.2020.125962. [Science Citation Index Expanded (Web of Science); Scopus] [IF: 13.273; AIF: 7.015; IF/AIF: 1.892; Q1 (2020, Clarivate JCR SCIE)]

17. Petrenko, Alla; **Leitonas, Karolis**; Volyniuk, Dmytro; Baryshnikov, Gleb V.; Belyakov, Sergey; Minaev, Boris F.; Ågren, Hans; Durgaryan, Ranush; Gražulevičius, Juozas Vidas; Arsenyan, Pavel. Benzosenophenylpyridine platinum complexes: green versus red phosphorescence towards hybrid OLEDs // *Dalton Transactions*. Cambridge: Royal Society of Chemistry. ISSN 1477-9226. eISSN 1477-9234. 2020, Vol. 49, iss. 11, p. 3393–3397. DOI: 10.1039/d0dt00214c. [Science Citation Index Expanded (Web of Science); Scopus; MEDLINE] [IF: 4.390; AIF: 3.569; IF/AIF: 1.230; Q1 (2020, Clarivate JCR SCIE)]

18. Thiyagarajan, Manojkumar Dhanthala; Balijapalli, Umamahesh; **Leitonas, Karolis**; Volyniuk, Dmytro; Simokaitiene, Jurate; Keruckas, Jonas; Jatautiene, Egle; Pathak, Madhvesh; Iyer, Sathiyarayanan Kulathu; Gražulevičius, Juozas Vidas. Human-eyes-friendly white electroluminescence from solution-processable hybrid OLEDs exploiting new iridium (III) complex containing benzoimidazophenanthridine ligand // *Dyes and Pigments*. Oxford: Elsevier. ISSN 0143-7208. eISSN 1873-3743. 2020, Vol. 174, art. No. 108068, p. 1–8. DOI: 10.1016/j.dyepig.2019.108068. [Science Citation Index Expanded (Web of Science); Scopus] [IF: 4.889; AIF: 4.712; IF/AIF: 1.037; Q1 (2020, Clarivate JCR SCIE)]

19. Arsenyan, Pavel; Petrenko, Alla; **Leitonas, Karolis**; Volyniuk, Dmytro; Simokaitiene, Jurate; Klinavičius, Tomas; Skuodis, Eigirdas; Lee, Jiun-Haw; Gražulevičius, Juozas Vidas. Synthesis and performance in OLEDs of selenium-containing phosphorescent emitters with red emission color deeper than the corresponding NTSC standard // *Inorganic Chemistry*. Washington, DC: American Chemical Society. ISSN 0020-1669. eISSN 1520-510X. 2019, Vol. 58, iss. 15, p. 10174–10183. DOI: 10.1021/acs.inorgchem.9b01283. [Science Citation Index Expanded (Web of Science); Scopus; MEDLINE] [IF: 4.825; AIF: 3.001; IF/AIF: 1.607; Q1 (2019, Clarivate JCR SCIE)]

20. Vigante, Brigita; **Leitonas, Karolis**; Volyniuk, Dmytro; Andruleviciene, Viktorija; Simokaitiene, Jurate; Ivanova, Anna; Bucinskas, Audrius; Gražulevičius, Juozas Vidas; Arsenyan, Pavel. Synthesis of linear and V-shaped carbazolyl-substituted pyridine-3,5-dicarbonitriles exhibiting efficient bipolar charge transport and E-type fluorescence // *Chemistry – A European Journal*. Weinheim: Wiley-VCH. ISSN 0947-6539. eISSN 1521-3765. 2019, Vol. 25, iss. 13, p. 3325–3336. DOI: 10.1002/chem.201805323. [Science Citation Index Expanded (Web of Science); Scopus; MEDLINE] [IF: 4.857; AIF: 6.158; IF/AIF: 0.788; Q1 (2019, Clarivate JCR SCIE)]

21. Eltan, T.; Lapienyte, Liveta; Keruckienė, Rasa; **Leitonas, Karolis**; Simokaitienė, Jūratė; Buika, Gintaras; Gražulevičius, Juozas Vidas. Electroactive D-A derivatives bearing 2,3-dimethylindole and tetrafluorostyrene moieties: synthesis, polymerization, DFT calculations and photophysical properties // *Molecular Crystals and Liquid Crystals*. Abingdon: Taylor & Francis. ISSN 1542-1406. eISSN 1563-5287. 2018, Vol. 671, iss. 1, p. 24–32. DOI: 10.1080/15421406.2018.1542082. [Science Citation Index Expanded (Web of Science); Scopus] [IF: 0.559; AIF: 4.366; IF/AIF: 0.128; Q4 (2018, Clarivate JCR SCIE)]

List of conferences:

1. **Leitonas, Karolis**; Skhirtladze, Levani; Bucinskas, Audrius; Volyniuk, Dmytro; Keruckiene, Rasa; Mahmoudi, Malek; Woon, Kai Lin; Ariffin, Azhar; Grazulevicius, Juozas Vidas. Glowing guardians of air quality: room-temperature phosphorescent organic semiconductors for oxygen sensing // Advanced materials and technologies: book of abstracts of 25th international conference-school, 21–25 August 2023, Palanga, Lithuania. Kaunas: Kaunas University of Technology. ISSN 2669-1930. 2023, P42, p. 79

2. **Leitonas, Karolis**; Andruleviciene, Viktorija; Volyniuk, Dmytro; Grazulevicius, Juozas V. Carbazole derivatives with cyano groups for photodetector applications // ICOE2023: 16th international conference on organic electronics, Madrid, 2023, July 3–7: book of abstracts.

3. **Leitonas, Karolis**; Skhirtladze, Levani; Bucinskas, Audrius; Volyniuk, Dmytro; Mahmoudi, Malek; Woon, Kai Lin; Ariffin, Azhar; Grazulevicius, Juozas V. Unlocking cyan electroluminescence: exploring intramolecular interactions for concentration-insensitive TADF emitters // Multidisciplinary international school of nanobiomaterials engineering: workshop on bionanomaterial and nanomaterial engineering, 18–23 June 2023: poster session abstract book. Lodz, Poland

4. **Leitonas, Karolis**; Skhirtladze, Levani; Bucinskas, Audrius; Volyniuk, Dmytro; Mahmoudi, Malek; Woon, Kai Lin; Ariffin, Azhar; Butkute, R.; Grazulevicius, Juozas V. Insensitive to concentration cyan color electroluminescence based on derivatives of 1,4-bis(trifluoromethyl)benzene acceptor // Baltic polymer symposium 2022, Tallinn, Estonia, September 21–23, 2022: programme and abstracts. Tallinn: Tallinn University of Technology. 2022, p. 59.

5. **Leitonas, Karolis**; Volyniuk, Dmytro; Grazulevicius, Juozas Vidas. Room temperature phosphorescence for oxygen sensing // Chemistry and chemical technology: proceedings of international scientific conference, Kaunas, 2022. Kaunas: Kaunas University of Technology.

6. **Leitonas, Karolis**; Skhirtladze, Levani; Bucinskas, Audrius; Volyniuk, Dmytro; Mahmoudi, Malek; Woon, Kai Lin; Ariffin, Azhar; Grazulevicius, Juozas V. Characterisation of new TADF emitters based on 1,4-bis(trifluoromethyl)benzene as an acceptor moiety // Advanced materials and technologies: book of abstracts of 24th international conference-school, 22–26 August 2022, Palanga, Lithuania. Kaunas: Kaunas University of Technology. ISSN 2669-1930. 2022, B-P50, p. 87.

7. **Leitonas, Karolis**; Andruleviciene, Viktorija; Volyniuk, Dmytro; Grazulevicius, Juozas. Investigation of dibenzo[a,c]phenazine derivatives substituted by acridan or carbazole moieties as efficient OLED hosts or emitters // 63rd electronic materials conference (EMC 2021), June 23–25, 2021, Columbus, USA. Columbus: Ohio State University. 2021, PS2.16, p. 73–74.

8. **Leitonas, Karolis**; Bezvikonny, Oleksandr; Gudeika, Dalius; Volyniuk, Dmytro; Rutkins, Martins; Gražulevičius, Juozas V. Investigation of diphenylsulfone derivatives as hosts for TADF based OLEDs // Advanced materials and technologies: book of abstracts of 23rd international conference-school, 23–27 August 2021,

Palanga, Lithuania. Kaunas: Kaunas University of Technology. ISSN 2669-1930. 2021, A-P64, p. 95.

9. **Leitonas, Karolis**; Volyniuk, Dmytro; Andruleviciene, Viktorija; Arsenyan, Pavel; Vigante, Brigita; Grazulevicius, Juozas Vidas. TADF behaviour of carbazole and phenothiazine substituted pyridines towards OLED applications // Open readings 2021: 64th international conference for students of physics and natural sciences, March 16–19, Vilnius, Lithuania: abstract book / editors: Š. Mickus, R. Platakytė, S. Pūkienė. Vilnius: Vilnius University Press, 2021, P3-9. ISBN 9786090705902. p. 228.

10. **Leitonas, Karolis**; Keruckienė, R.; Volyniuk, D.; Gražulevičius, J. V. Benzotrifluorido ir fentiazino darinių kambario temperatūros fosforencijos jautrumo deguoniui tyrimas // Studentų moksliniai tyrimai 2019/2020: konferencijos pranešimų santraukos. Vilnius: Lietuvos mokslo taryba. ISSN 2669-2074. 2020, p. 268–269

11. **Leitonas, Karolis**; Keruckiene, Rasa; Volyniuk, Dmytro; Grazulevicius, Juozas Vidas. Investigation of room-temperature phosphorescence sensitivity to oxygen using benzotrifluoride and phenothiazine derivatives // Open readings 2020: 63rd international conference for students of physics and natural sciences, March 17–20, Vilnius, Lithuania: abstract book. Vilnius: Vilnius University, 2020, P3-5. ISBN 9786090703779

12. **Leitonas, Karolis**; Tomkevičienė, Aušra; Gražulevičius, Juozas Vidas. Metal-free room temperature phosphorescent organic materials: poster // Open readings 2019: 62nd international conference for students of physics and natural sciences, March 19–22, Vilnius, Lithuania: abstract book. Vilnius: Vilnius University, 2019, P1-90. ISBN 9786090701379. p. 168.

10. ACKNOWLEDGEMENTS

Completing this PhD thesis has been a profound journey, and it would not have been possible without the strong support and guidance of many remarkable individuals.

First and foremost, I would like to express my deepest gratitude to my supervisor, Dr. Hab. Dmytro Volyniuk. His expertise, patience, and constant encouragement have been the foundation of my research. His insightful feedback and steady support have guided me through the most challenging moments of this journey.

I would also like to thank the leader of our scientific group Prof. Dr. Juozas Vidas Gražulevičius, scientific advisor Dr. Asta Dabulienė and Dr. Jūratė Simokaitienė for their thoughtful guidance and constructive criticism. Their diverse perspectives greatly enriched my work and broadened my understanding of the field.

I am grateful to my research collaborators and colleagues, particularly Dr. Rasa Keruckienė, Dr. Rita Butkutė, Dr. Viktorija Andrulėvičienė, Dr. Eigirdas Skuodis, Dr. Audrius Bučinskas, Dr. Aušra Tomkevičienė, for their collaborative spirit and intellectual contributions. Your insights and discussions were influential in shaping this research.

I acknowledge the financial support from Research Council of Lithuania, whose funding made this research possible. I am also thankful to Kaunas University of Technology for providing the necessary resources and facilities.

On a personal note, I would like to thank my family and friends for their firm support and encouragement. To my parents, Jonas and Jolanta, for unconditional support. To my wife, Judita, your patience, love, and understanding have been vital throughout this journey. I also want to give a huge thanks to my best friend and colleague, Matas Gužauskas. We've been through it all together, from our Bachelor's to Master's and now PhD studies, always pushing each other to keep going when things got tough. We've not only grown academically but also grown up as people along the way. Your support and friendship have meant the world to me, and I'm grateful we could share this crazy journey. BING BONG!

I would also like to extend my gratitude to my high school teachers of Physics (Zigmantas Meškauskas), Chemistry (Danutė Ramanauskienė), and Mathematics (Jolanta Bernienė). Their passion and expertise ignited my interest in the natural sciences, laying a solid foundation for my academic pursuits. Their encouragement and mentorship have been important in shaping my career path.

Lastly, I dedicate this thesis to all those who have supported me, directly and indirectly, in this academic endeavor. Your contributions, big and small, have been greatly appreciated.

UDK 621.383.52(043.3)

SL344. 20xx-xx-xx, xx leidyb. apsk. I. Tiražas 14 egz. Užsakymas xxx.
Išleido Kauno technologijos universitetas, K. Donelaičio g. 73, 44249 Kaunas
Spausdino leidyklos „Technologija“ spaustuvė, Studentų g. 54, 51424 Kaunas